Can Restoration of Endothelial Insulin Sensitivity Rescue Vascular Function and Repair in Systemic Insulin Resistance?

Dr Anshuman Sengupta

Submitted in accordance with the requirements for the degree of Doctor of Philosophy

University of Leeds

School of Medicine

August 2015

Intellectual Property and Publication Statements

The candidate confirms that the work submitted is his own and that appropriate credit has been given where reference has been made to the work of others.

This copy has been supplied on the understanding that it is copyright material and that no quotation from the thesis may be published without proper acknowledgement.

Author Contribution

The majority of the work in this thesis is my own. The animals used in these experiments were derived from established breeding colonies but I took subsequent responsibility for the animals as a personal licence holder. I am grateful for the assistance of Dr Nadira Yuldasheva, Miss Anna Skromna and Mrs Natallia Makava in helping with decisions regarding breeding, and to the animal unit technicians at the University of Leeds for weaning, feeding and ear notching. I performed gross phenotyping, metabolic testing and genotyping.

For vascular injury work, I am indebted to Dr Nadira Yuldasheva for performing both the surgery and the imaging. In the aortic vasomotion experiments, I dissected the aortae and passed them to Mrs Stacey Galloway, who cleaned the tissue and operated the organ bath, after which I analysed the data. For the Western blot from endothelial cell lysates, I derived primary cells, passaged them to confluence and lysed them before passing them to Dr Romana Mughal for the immunoblot.

I performed the remainder of this work. This includes: sample acquisition by dissection or venepuncture; endothelial progenitor cell culture, enumeration and flow cytometry; the progenitor cell function assay; primary endothelial cell culture; quantitative PCR on cells and organs; insulin ELISAs; and all the assays of endothelial cell proliferation, migration and superoxide production. I also performed all the data analysis, with the exception of the quantitative imaging of vascular injury tissue; I did, however, perform the summary statistical analysis of these data.

At each stage of experimental design, planning and data analysis, I received guidance from my primary supervisor.

Presentations

None of this work has been published, but it has been presented in poster format at three national and two international conferences. The abstract details are as follows:

British Cardiovascular Society (London, 2013)

- <u>Sengupta A</u>, Viswambharan H, Yuldasheva N, Mercer B, Aziz A, Imrie H, Gage M, Gatenby V, Skromna A, Wheatcroft S, Kearney M, Cubbon R. Vascular endothelial insulin sensitisation reduces blood pressure and promotes endothelial repair in the context of global insulin resistance. *Heart* 2013; 99 (Suppl. 2): A95 [Abstract no. 163].

Academy of Medical Sciences (London, 2014)

- <u>Sengupta A</u>, Yuldasheva N, Gage M, Viswambharan H, Aziz A, Ali N, Galloway S, Mercer B, Kearney M, Cubbon R. Role of vascular endothelial insulin sensitisation in vascular repair in systemic insulin resistance. *Lancet* 2014; Spring Meeting for Clinician Scientists Supplement: 97 [Poster 41].

British Cardiovascular Society (Manchester, 2014)

- <u>Sengupta A</u>, Viswambharan H, Yuldasheva N, Ali N, Mercer B, Walker A, Galloway S, Aziz A, Gage M, Imrie H, Gatenby VK, Skromna A, Wheatcroft S, Kearney M, Mughal R, Cubbon R. Endothelial insulin sensitisation enhances vascular repair and aortic vasomotor function in systemic insulin resistance. *Heart* 2014; 100: Suppl 3 A96-A97 [Abstract no. 169].

American Heart Association Scientific Sessions (Chicago, 2014)

- <u>Sengupta A</u>, Viswambharan H, Yuldasheva N, Mercer B, Galloway S, Ali N, Walker A, Aziz A, Gage M, Skromna A, Wheatcroft S, Kearney M, Cubbon R. Endothelial insulin sensitisation enhances vascular repair in systemic insulin resistance and improves endothelial function by restoring nitric oxide bioavailability. *Circulation* 2014; 130: A13829.

American Heart Association Scientific Sessions (Orlando, 2015)

- <u>Sengupta A</u>, Yuldasheva N, Viswambharan H, Galloway S, Mughal R, Mercer B, Ali N, Walker A, Aziz A, Smith J, Skromna A, Makava N, Kearney M, Cubbon R. Increasing endothelial insulin sensitivity rescues vascular function and repair by restoring nitric oxide bioavailability and improving endothelial cell migration. *Circulation* 2015; 132: A13492.

Acknowledgements

Abstract

Diabetes and insulin resistance are prominent cardiovascular risk factors and are projected to affect more than 500 million individuals worldwide in the next few decades. Managing hyperglycaemia is not sufficient to reduce the cardiovascular risk that these diseases confer, and there is increasing awareness of insulin resistance as an independent predictor of morbidity and mortality. Animal models partially recapitulate this profile: mice with insulin receptor knockout (IRKO) show elements of human metabolic syndrome, such as hypertension and endothelial dysfunction. These mice also exhibit impaired vascular repair after arterial injury and associated defects in the number and function of endothelial progenitor cells and mature endothelial cells. These impairments appear to relate to reduced nitric oxide bioavailability and oxidative stress. Loss of intact endothelial insulin signalling seems to play a key pathogenetic role.

In this work, we describe a murine model with global insulin receptor knockout and concomitant rescue of endothelial insulin receptor expression (HIRECOxIRKO). In order to achieve this, we have targeted expression of a human insulin receptor transgene to vascular endothelial cells using a Tie-2 promoter. This manipulation results in a viable mouse with preserved glucoregulation. We have confirmed endothelium-specific expression of the human insulin receptor transgene in HIRECOxIRKO mice. These animals display restoration of normal blood pressure, endothelial function and vascular repair after arterial injury, as compared with IRKO littermates, often with recovery to wild-type levels. We have observed augmented endothelial cell migration and, perhaps, proliferation, which may mediate increased vascular repair. We also present evidence of increased nitric oxide bioavailability, which may underpin the rescue of vasomotor function. Much work remains, but this project supports the pursuit of endothelial insulin sensitisation as a potential therapeutic target in insulin resistance.

Contents

List of Figures

Abbreviations

ACh	Acetylcholine
AcLDL	Acetylated low density lipoprotein
Akt	Protein kinase B
APC	Allophycocyanin
AS	Atherosclerosis
AUC	Area under curve
BCA	Bicinchoninic acid
BH_4	Tetrahydrobiopterin
BM	Bone marrow
BP	Blood pressure
BSA	Bovine serum albumin
CAD	Coronary artery disease
CBG	Capillary blood glucose
CD	Cluster of differentiation
CFU	Colony forming unit
cGMP	Cyclic guanosine monophosphate
CPC	Circulating progenitor cell
CRP	C-reactive protein
Ct	Cycle threshold
CV	Coefficient of variation
CVD	Cardiovascular disease
C57BL/6	C57 black 6
DAF	Diaminofluorescein
DHE	Dihydroethidium
DiI	1,1'-dioctadecyl-3,3,3'3'-tetramethylindocarbocyanine perchlorate
DM	Diabetes mellitus

DMEM	Dulbecco's modified Eagle's medium
DMSO	Dimethysulfoxide
DNA	Deoxyribonucleic acid
dNTP	Deoxynucleotide phosphate
eNOS	Endothelial nitric oxide synthase
EC_{50}	Concentration for 50% vasomotion
EDTA	Ethylene diamine tetra-acetate
EdU	5-ethynyl-2'-deoxyuridine
EEPC	Early outgrowth endothelial progenitor cell
EGM	Endothelial growth media
ELISA	Enzyme linked immunosorbent assay
EPC	Endothelial progenitor cell
ES	Embryonic stem (cell)
ET-1	Endothelin 1
ESMIRO	Endothelium specific mutant insulin receptor over-expression
FACS	Fluorescence activated cell sorting
FCS	Foetal calf serum
Fc	Crystallisable fragment
FFA	Free fatty acid
FITC	Fluorescein isothiocyanate
Flk1	Foetal liver kinase 1
FMD	Flow-mediated dilatation
FOXO	Forkhead box class O
GLUT-4	Glucose transporter type 4
GTP	Guanosine triphosphate
GTT	Glucose tolerance test
HAT	Hypoxanthine, aminopterin and thymidine
HbA_{1c}	Glycosylated haemoglobin

HBSS	Hank's balanced salt solution
HDL	High density lipoprotein
HEPES	2-[4-(2-hydroxyethyl)piperazin-1-yl]ethanesulfonic acid
HIRECO	Human insulin receptor endothelial cell over-expression
Hprt	Hypoxanthine phosphoribosyl transferase
HRP	Horseradish peroxidase
HUVEC	Human umbilical vein endothelial cell
IC	Isotype control
ICAM-1/2	Intercellular adhesion molecule 1/2
IFG	Impaired fasting glucose
IGF-1	Insulin-like growth factor 1
IGT	Impaired glucose tolerance
IHD	Ischaemic heart disease
iNOS	Inducible nitric oxide synthase
IP	Intraperitoneal
IR	Insulin receptor
IRS	Insulin receptor substrate
IRKO	Insulin receptor knock out
ITT	Insulin tolerance test
IU	International units
IVC	Inferior vena cava
kDa	kiloDalton
KDR	Kinase domain receptor (or VEGF receptor 2)
LDL	Low density lipoprotein
LEPC	Late outgrowth endothelial progenitor cell
L-NMMA	Levo-N-monomethyl arginine
MAPK	Mitogen activated protein kinase
MCP-1	Monocyte chemoattractant protein 1

MnTMPyP	Manganese(III) tetrakis(1-methyl-4-pyridyl)porphyrin
MPC	Magnetic particle concentrator
mRNA	Messenger ribonucleic acid
mTORC2	Mammalian target of rapamycin complex 2
NADPH	Nicotinamide adenine dinucleotide phosphate
NFκB	Nuclear factor kappa B
NO	Nitric oxide
nNOS	Neuronal nitric oxide synthase
NOS	Nitric oxide synthase
NOX	NADPH oxidase
PBMC	Peripheral blood mononuclear cell
PCI	Percutaneous coronary intervention
PDGF	Platelet-derived growth factor
PBS	Phosphate-buffered saline
PCR	Polymerase chain reaction
PE	Phenylephrine (in context of organ bath)
PE	R-phycoerythrin (in context of flow cytometry)
PEC	Pulmonary endothelial cell
PECAM-1	Platelet endothelial cell adhesion molecule 1
PIP$_{(2/3)}$	Phosphatidyl inositol (bis/tris)phosphate
PI3K	Phosphatidyl inositol-3-kinase
PPAR	Peroxisome proliferator activated receptor
RIPA	Radio immunoprecipitation assay
RNA	Ribonucleic acid
ROS	Reactive oxygen species
rpm	Revolutions per minute
Sca1	Stem-cell antigen 1
SDS	Sodium dodecyl sulphate

SEM	Standard error of the mean
SNP	Sodium nitroprusside
SOD	Superoxide dismutase
SOS	Son of sevenless
T2DM	Type II diabetes mellitus
TAE	Tris-acetate-EDTA
Taq	*Thermophilus aquaticus*
TBS-T	Tris-buffered saline-tween
TE	Tris-EDTA
TK	Tyrosine kinase
TNF-α	Tumour necrosis factor alpha
UV	Ultraviolet
VCAM-1	Vascular cell adhesion molecule 1
VEGF	Vascular endothelial growth factor
VEGFR	Vascular endothelial growth factor receptor
VENIRKO	Vascular endothelial insulin receptor knockout
VLDL	Very low density lipoprotein
VSMC	Vascular smooth muscle cell
WT	Wild Type

Chapter 1 **Introduction**

1.1 Diabetes Mellitus, Insulin Resistance and Cardiovascular Risk

1.1.1 Background Epidemiology

Diabetes mellitus (DM) is a multi-system metabolic disorder which is rising in prevalence within an ageing and increasingly overweight global population [1]. It is implicated in 28-38% of mortality in North America and Europe, with a higher proportion seen in developing countries, and is responsible for healthcare expenditure of US$ 548 billion worldwide [2]. Moreover, the prevalence of DM is forecast to rise to over 500 million people worldwide by 2035 [2]. Type I DM, which accounts for 10% of all diabetes, is characterised by autoimmune destruction and failure of pancreatic beta-cells, resulting in absolute insulin deficiency, often from a young age [2]. Most of the remainder is type II DM, in which beta-cells become progressively less responsive to the presence of glucose but retain a degree of capacity to produce insulin. However, co-existing insulin resistance in peripheral target tissues results in progressive hyperinsulinaemia despite hyperglycaemia [3].

Patients with T2DM have demonstrably higher rates of all-cause mortality than individuals with normal glucose metabolism, resulting in an additional mortality risk equivalent to that of 15 years of ageing [4]. The Framingham study was the first large epidemiological paper to report a link with cardiovascular disease (CVD): it showed a two-fold increase in cardiovascular complications in diabetic compared with non-diabetic men, and the increase was three-fold in women [5]. This association with cardiovascular risk has been demonstrated recurrently since, and this includes patients with established cardiovascular disease [6].

1.1.2 Impact of Insulin Resistance in Humans

Hyperglycaemia *per se* is closely linked to microvascular complications of diabetes, such as retinopathy, neuropathy and nephropathy [7]. It is also associated with CVD, as demonstrated by a 2004 meta-analysis that showed an increase of 1.18 in relative risk for every 1% increment in glycosylated haemoglobin (HbA$_{1c}$) [8]. Indeed, pooled evidence from large prospective studies of non-diabetic subjects has implicated glycaemia as an independent risk factor for mortality [9].

However, sustained hyperglycaemia alone is not sufficient to explain the excess of CVD seen in individuals with disturbed glucose homoeostasis, and is in fact likely to account for only a minority of cardiovascular events [10]. This has been surmised in theory since the early 1990s [11], with an accumulating portfolio of supporting data subsequently. The Helsinki Policemen Study, one of the contributors to the above pooled analysis [9], showed that in 970 healthy middle-aged men, hyperinsulinaemia was an independent risk factor for heart disease after 22 years of follow-up [12]. Similarly, Hu *et al* performed a prospective twenty-year follow-up study on 117,000 nurses, and noted that in those who eventually became diabetic, there was a higher CVD risk than in healthy subjects even in the period before diagnosis [13]. Finally, the AusDiab study showed that impaired fasting glucose (IFG) was an independent cardiovascular risk factor [14]. These findings have raised the possibility of a "ticking clock" phenomenon in which the beginnings of CVD risk pre-date biochemically detectable glycaemic derangements [10].

Pathophysiologically, this "pre-diabetes" period is characterised by a chronic reduction in end-organ insulin sensitivity, resulting in a requirement for increased pancreatic insulin secretion: compensatory hyperinsulinaemia [11]. Whilst early metabolic testing may unmask IFG or impaired glucose tolerance (IGT) after oral glucose challenge, the rising insulin concentration

can help maintain broadly normal plasma glucose levels for decades, such that the condition evades formal diagnosis [3]. This phase of insulin resistance is associated with elevation in plasma free fatty acid concentration and hypertension, resulting in many pre-diabetic individuals suffering from a constellation of cardiovascular risk factors, as first described in Reaven's 1988 Banting lecture [15]. Importantly, this risk occurs in the absence of total beta-cell failure and hyperglycaemia [10]. Our understanding of this disturbance has subsequently been refined and it has been named "metabolic syndrome" or "syndrome X", a combination of three or more of the following insults: abdominal obesity, hypertension, raised plasma glucose concentration, raised triglycerides and low high density lipoprotein (HDL) cholesterol [11] (Figure 1-1). Thus, by the time frank diabetes has developed, many patients have already been exposed to a high risk of cardiovascular illness, the exact pathogenetic mechanisms of which are incompletely understood. This may, in part, explain the modest reduction in macrovascular events noted in clinical trials of strict glycaemic control [7]. Clearly, insulin resistance merits attention as a window of opportunity for early intervention and cardiovascular risk reduction.
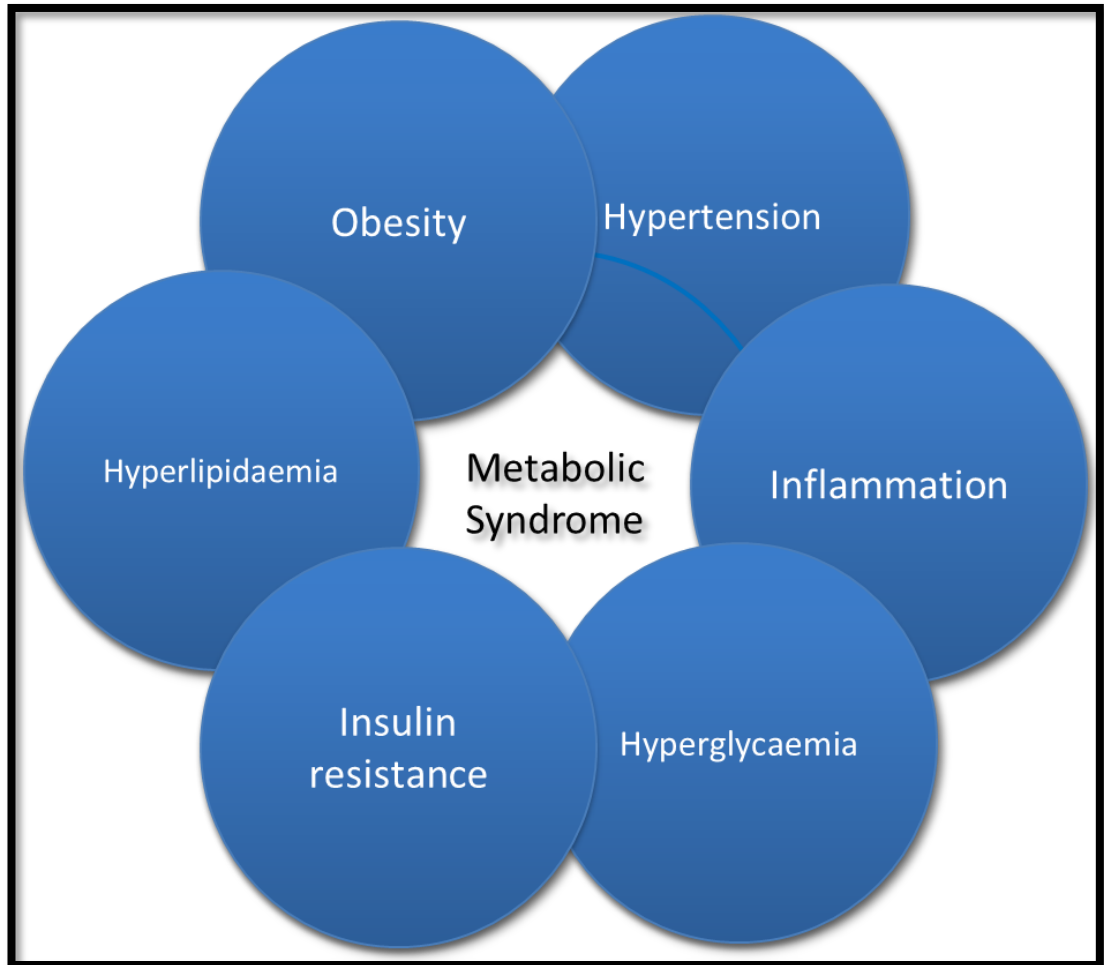
Figure 1-1   The Metabolic Syndrome

Adapted from Cubbon *et al*, 2012 [16]

1.1.3 Treatment of Insulin Resistance

One of the cornerstones of diabetes therapy in general is strict glycaemic control, mainly driven by the observation that this yields significant reductions in microvascular disease; this was demonstrated convincingly in the United Kingdom Prospective Diabetes Study, in which patients were randomised either to intensive or conventional glucose lowering strategies [7]. This seminal study failed to show a significant risk reduction for macrovascular outcomes, although a modest benefit was seen in these end-points in a ten-year follow up study published in 2008 [17]. Similarly, the large Action to Control Cardiovascular Risk in Diabetes (ACCORD) study was terminated prematurely when an interim analysis revealed a higher

mortality rate in the intensive treatment arm, without any beneficial effects on cardiovascular end-points [18]. This suggestion has been borne out in a meta-analysis of several large randomised controlled trials, which failed to show a significant reduction in short- to medium-term mortality [19]. One must balance these data with the results of the Diabetes Control and Complications Trial (DCCT), which showed reduced microvascular and macrovascular end points with intensive glycaemic control in type I diabetes [20]. It appears that longer follow-up does reveal some benefits in macrovascular outcomes with tight glycaemic control [17], but clearly other aspects of the insulin resistant phenotype could be targeted therapeutically.

It is tempting to surmise that the slightly disappointing findings in some of the above studies could be explained by the propensity for intensive glycaemic control to cause problematic hypoglycaemia; alternatively, it may lend support to the suggestion that glycaemia is not as potent a risk factor for macrovascular disease as one may initially suspect. If so, a potential explanation for the paradoxical finding of greater mortality in the ACCORD study is that strategies that increase circulating insulin levels may exacerbate the portion of biological damage that is attributable to insulin resistance and thus augment overall cardiovascular risk.

Drug agents that improve insulin sensitivity in target organs appear attractive, but the evidence for improvements in cardiovascular end points to date has been relatively unconvincing. Metformin is a key agent used to help maintain glucose levels within a healthy range, and there are some data to show reduced rates of myocardial infarction in obese patients with T2DM taking metformin [21]. Another class that has so far yielded largely disappointing results is the thiazolidinediones [22]. In fact, there has been a link with an increase in symptoms compatible with heart failure in patients treated with rosiglitazone, one such agent [22]. Meta-analysis of safety data for rosiglitazone showed a paradoxical increase in non-fatal myocardial infarction as well [23], resulting in the temporary withdrawal of the drug from

the market. These findings were not recaptured in a more recent study, suggesting that this class of agents may not be as harmful as once thought [24]. Equally, adverse events may reflect the pleiotropic effects of agonism of the thiazolidinedione target, the peroxisome profilerator activated receptor-gamma (PPAR-ɣ), and the phenomenon may not be a class effect [25]. Indeed, the ProACTIVE study highlighted a possible CVD risk reduction with pioglitazone, a different member of this drug class [26]. This must be interpreted with caution as the quoted benefits here were based on a non-prespecified secondary end point. However, both metformin and the thiazolidinediones carry some promise and therefore insulin sensitisation may still be a valid therapeutic strategy. Overall, ongoing drug development in this class has implications for patient safety and may prompt wider financial concerns, leaving us with a pharmacopeia that does not include adequate provision for cardiovascular risk reduction in insulin resistance.

This caveat notwithstanding, it is not necessarily wise to exclude insulin sensitisation as a way of reducing macrovascular risk in diabetes and pre-diabetes. Instead, the thiazolidinedione experience provides a case for developing alternative and more refined methods of achieving greater tissue insulin sensitivity. The insulin receptor may present a more precise target for rational drug design, and in order to investigate this possibility, this project will focus on the interplay between insulin receptor physiology, its manipulation and the effects this has on cardiovascular risk.

1.2 Physiology and Pathophysiology of Insulin Signalling

1.2.1 Physiological Action of Insulin

Human insulin is a 5.8 kiloDalton (kDa) polypeptide comprising 51 amino acids, and is synthesised in pancreatic beta-cells. It is encoded on chromosome 11p15 in a precursor form known as preproinsulin, which undergoes post-translational modification by way of cleavage of a signal peptide sequence [27, 28]. The resulting molecule, proinsulin, consists of an A-chain and a B-chain, joined by a third connecting subunit known as C-peptide. Within the Golgi apparatus, C-peptide is cleaved, allowing the remaining A- and B-chain subunits of the resulting dimer to link by forming disulphide bonds; this is the form in which insulin is released systemically in response to glucose ingestion [27] (Figure 1-2).
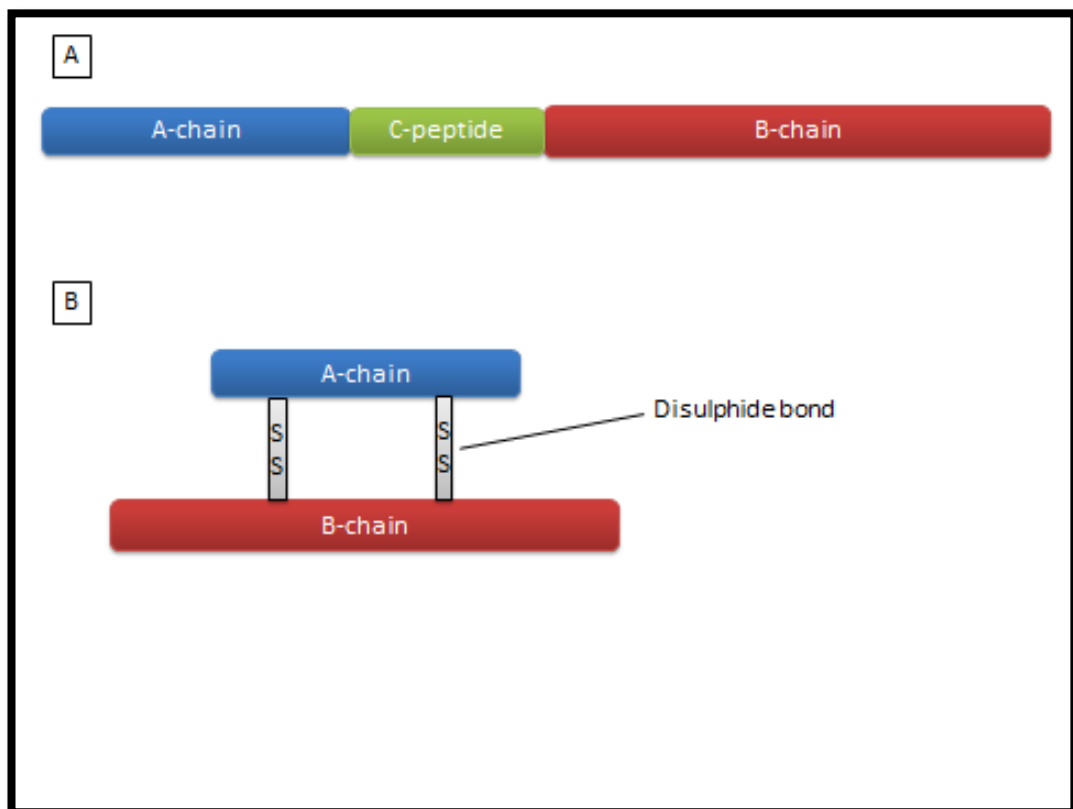
Figure 1-2   Schema demonstrating structure of proinsulin (A) and insulin (B)

SS = disulphide bond.

Cellular glucose uptake is mediated by a group of glucose transporters (GLUT); most are basally expressed on target-cell membranes, and allow transport of glucose from the blood to the intracellular environment for use in metabolism [29]. GLUT-4 channels are the predominant isoform in cells that store energy in the form of glycogen or lipids, such as skeletal myocytes and adipocytes. GLUT-4 is stored in intracellular vesicles under basal conditions, and re-localisation of the transporter to the plasma membrane is an inducible process triggered by the binding of insulin to its cell surface receptor [30]. In storage tissues, glucose is converted to glycogen or lipids, following which it can be broken down again when blood glucose levels drop. As the translocation of GLUT-4 to the plasma membrane relies on intact insulin receptor binding and intracellular signalling, defects in this process can result in glucoregulatory derangements in the insulin-resistant state [30].

1.2.2 Structure of the Insulin Receptor

The insulin receptor belongs to the receptor tyrosine kinase family and is a 320 kDa heterodimeric protein encoded, in humans, on chromosome 19p13 [31, 32]. The tetramer comprises two alpha and two beta subunits, linked with disulphide bonds [33, 34]. The alpha subunits, which are predominantly extracellular, appear to form the majority of the hormone-binding domain [35]. However, the beta subunits also comprise a small extracellular portion, thus presenting an additional ligand binding site; these act synergistically and encourage cross-linking, which has the overall effect of allowing high-affinity binding of insulin to the receptor structure [36]. The beta subunit on either side then spans the plasma membrane and contains a tyrosine kinase (TK) domain in its intracellular portion [35] (Figure 1-3).
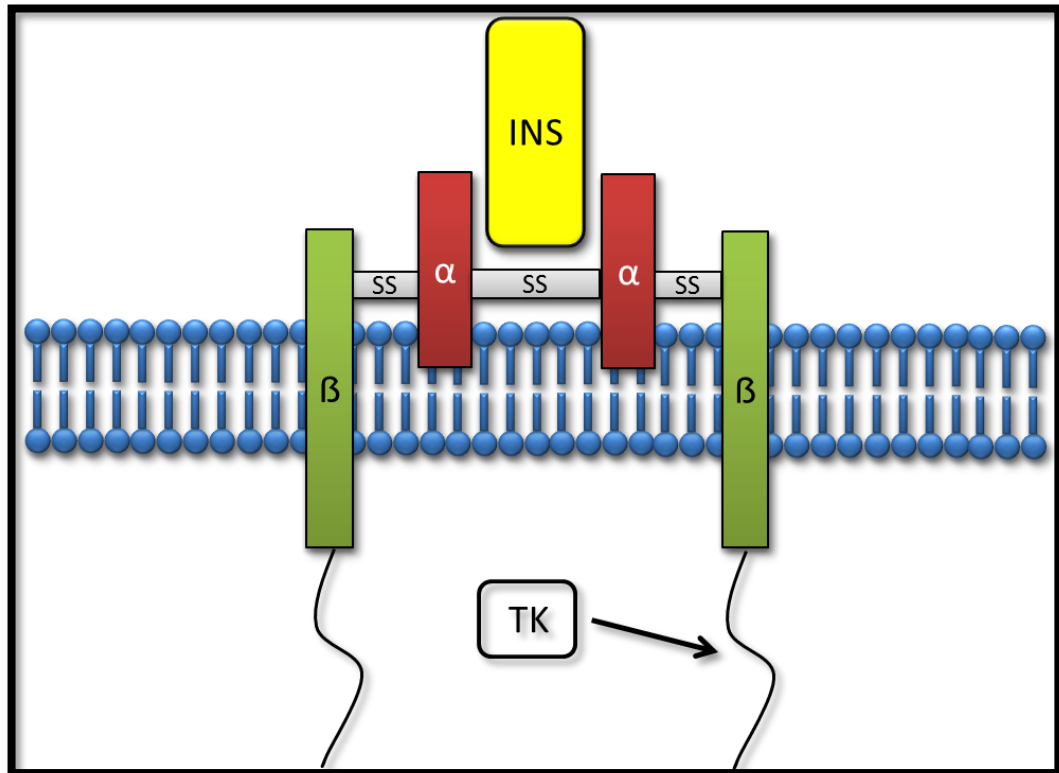
Figure 1-3   Structure of the Insulin Receptor

INS = Insulin; α = Alpha subunit; ß= Beta subunit; SS = disulphide bond; TK = tyrosine kinase domain.

1.2.3 Insulin Signalling in Health

In the resting state, the alpha subunit of the insulin receptor inhibits the beta subunit's tyrosine kinase activity. Following the binding of insulin (or an alternative ligand such as the insulin-like growth factor-1) to the alpha subunit, de-repression of the beta subunit's kinase activity occurs, triggering a cascade of autophosphorylation of tyrosine residues in the TK domain [37]. This induces a conformational change in the beta subunit and results in increasingly potent kinase activity, the first of many steps in a complex intracellular cascade of phosphorylation [38]. After activation, the whole receptor is internalised and degraded by receptor-mediated endocytosis [35] but only after the above process of autophosphorylation has triggered intracellular signalling. Initially, a variety of multi-site "docking" proteins such

as insulin receptor substrates (IRS) and Shc are phosphorylated and activated. These substrates help to propagate the insulin signal to target effectors deeper within the intracellular pool [39]. These result in the formation of complex, divergent and tissue-specific intracellular signalling pathways, summarised in Figure 1-4 [40]. The downstream effects of insulin receptor activation are tightly regulated in order to optimise metabolic function: for example, tyrosine phosphatase activity and inhibitory serine phosphorylation can downregulate signalling [37]. Similarly, the internalisation of the insulin receptor after ligand binding can act as a negative regulator of signalling and limit excessive activation of downstream nodes.

These tyrosine-phosphorylated substrates interact with intracellular proteins: in the case of Shc, the first interaction is with growth factor receptor bound protein 2 (Grb-2) and son-of-sevenless (SOS), the latter of which is an exchange factor for guanosine triphosphate (GTP). By inducing further activity in proteins such as Ras and Raf, this pathway results in the activation of mitogen-activated protein kinases (MAPK), which mediate insulin's effects as a growth factor and promoter of mitosis and cellular differentiation in some target cell types [40]. In vascular endothelial cells, however, a further downstream result of the MAPK pathway is the production of endothelin-1 (ET-1), a vasoconstrictor which helps maintain blood pressure homoeostasis by augmenting vascular tone [40].

Parallel with the MAPK pathway is a cascade triggered by tyrosine phosphorylation of insulin receptor substrates [41]. The IRS proteins are expressed as various isoforms, of which IRS-1 and IRS-2 are the most commonly encountered; IRS-3 is mainly found in adipocytes and neural tissue and the expression of IRS-4 is largely limited to embryonic cells [37]. IRS proteins contain phosphotyrosine-binding domains at their N-termini, which allow close interaction with the intracellular portion of the insulin receptor. The central portion and C-terminus of IRS contain tyrosine

residues that can be phosphorylated in response to insulin receptor activation and thus bind downstream "adaptor" molecules [37]. In the case of IRS-1, one key adaptor is phosphatidylinositol-3-kinase (PI3K), an enzyme with a regulatory (p85) and a catalytic (p110) portion. The latter portion is highly unstable in isolation and is thus usually found bound to p85 to prevent premature degradation [37]. When IRS-1 binds the regulatory p85 subunit, this frees and activates the catalytic p110 portion of PI3K [40], allowing the phosphorylation and conversion of the lipid second messenger phosphatidylinositol-4,5-bisphosphate (PIP2) to phosphatidylinositol-3,4,5-trisphosphate (PIP3) and propagation of the insulin signalling cascade. PI3K may also exert an inherent negative feedback effect on insulin signalling by promoting inhibitory serine phosphorylation of IRS-1 by downstream effectors, such as Akt [42].
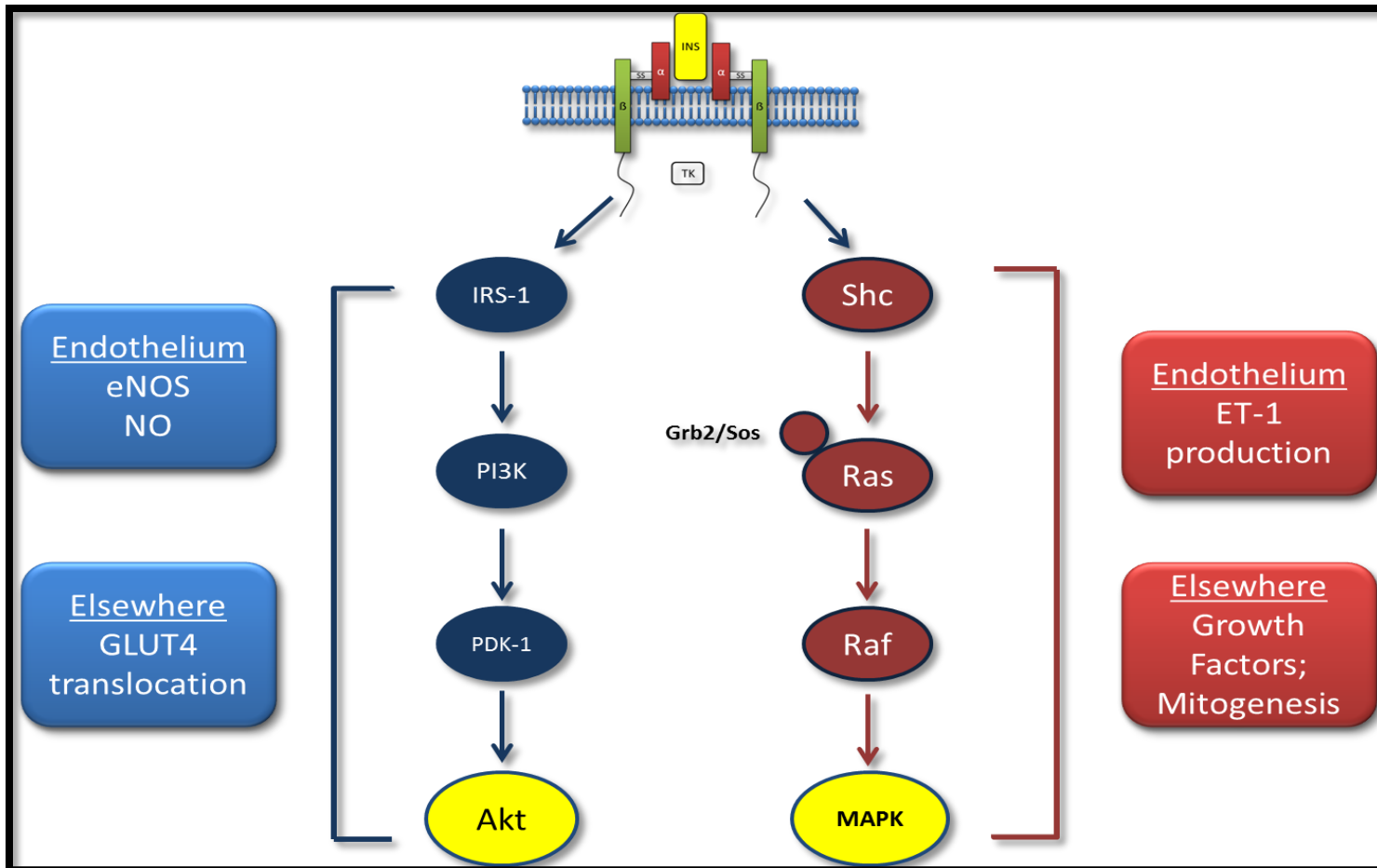
Figure 1-4   Parallel and Tissue-Specific Pathways of Insulin Signalling

INS = insulin; TK = tyrosine kinase; IRS-1 = insulin receptor substrate-1; PI3K = phosphatidylinositol-3-kinase; PDK-1 = phosphoinositide-dependent kinase-1; eNOS = endothelial nitric oxide synthase; NO = nitric oxide; GLUT4 = glucose transporter 4; Grb2 = growth factor receptor bound protein 2; Sos = son of sevenless; MAPK = mitogen activated protein kinase; ET-1 = endothelin-1. Adapted from Kim et al *[40].*

PIP3 binds to the pleckstrin homology domain of cytosolic protein kinase B (otherwise known as Akt), triggering an alteration in the latter's morphology [43]. Akt is then able to translocate from the cytoplasm to the plasma membrane, a process shown to rely on PI3K and its interaction with the pleckstrin homology domain of Akt [44]. This brings Akt into closer proximity with phosphoinositide-dependent kinase-1 (PDK-1), which phosphorylates the Threonine-308 site on Akt [37]. Together with serine phosphorylation (serine 473) by mammalian target of rapamycin complex 2 (mTORC2), this results in full activation of Akt and thus propagates the insulin signalling cascade. The downstream effects of Akt phosphorylation in this pathway are dependent on the nature of the target cell. In vascular endothelium, one effect is to phosphorylate and activate endothelial nitric oxide synthase (eNOS) [45], thus generating nitric oxide (NO) and promoting a variety of anti-atherogenic effects that will be discussed in more depth below. A second pathway distal to Akt involves phosphorylation and inactivation of the transcription factor Forkhead box class O (FoxO), resulting in it moving out of the nucleus [46]. Thus, by repressing the expression of vascular cell adhesion molecule 1 (VCAM-1), Akt-mediated actions on FoxO protect against atherosclerosis, as demonstrated in LDL receptor knockout mice with endothelium-specific deletion of FoxO [46, 47]. For a diagrammatic summary of the PI3K/Akt signalling pathway in endothelial cells, see

Figure **1-5**. Conversely, in skeletal muscle cells and adipocytes, both PI3K [48] and Akt [43] have been demonstrated to cause translocation of GLUT-4 to the plasma membrane by inducing cytoskeletal reconfigurations via action on Rab small GTPases. This facilitates cellular glucose uptake in these tissues [37]. In keeping with the paradigm of pathway-specific effectors, it has been demonstrated that blocking the MAPK pathway has no effect on GLUT-4 translocation [48, 49]. Insulin-induced Akt activation also leads to phosphorylation of glycogen synthase kinase 3-beta, and therefore loss of its inhibition of glycogen synthetase, allowing skeletal muscle cells and hepatocytes to synthesise glycogen for storage.
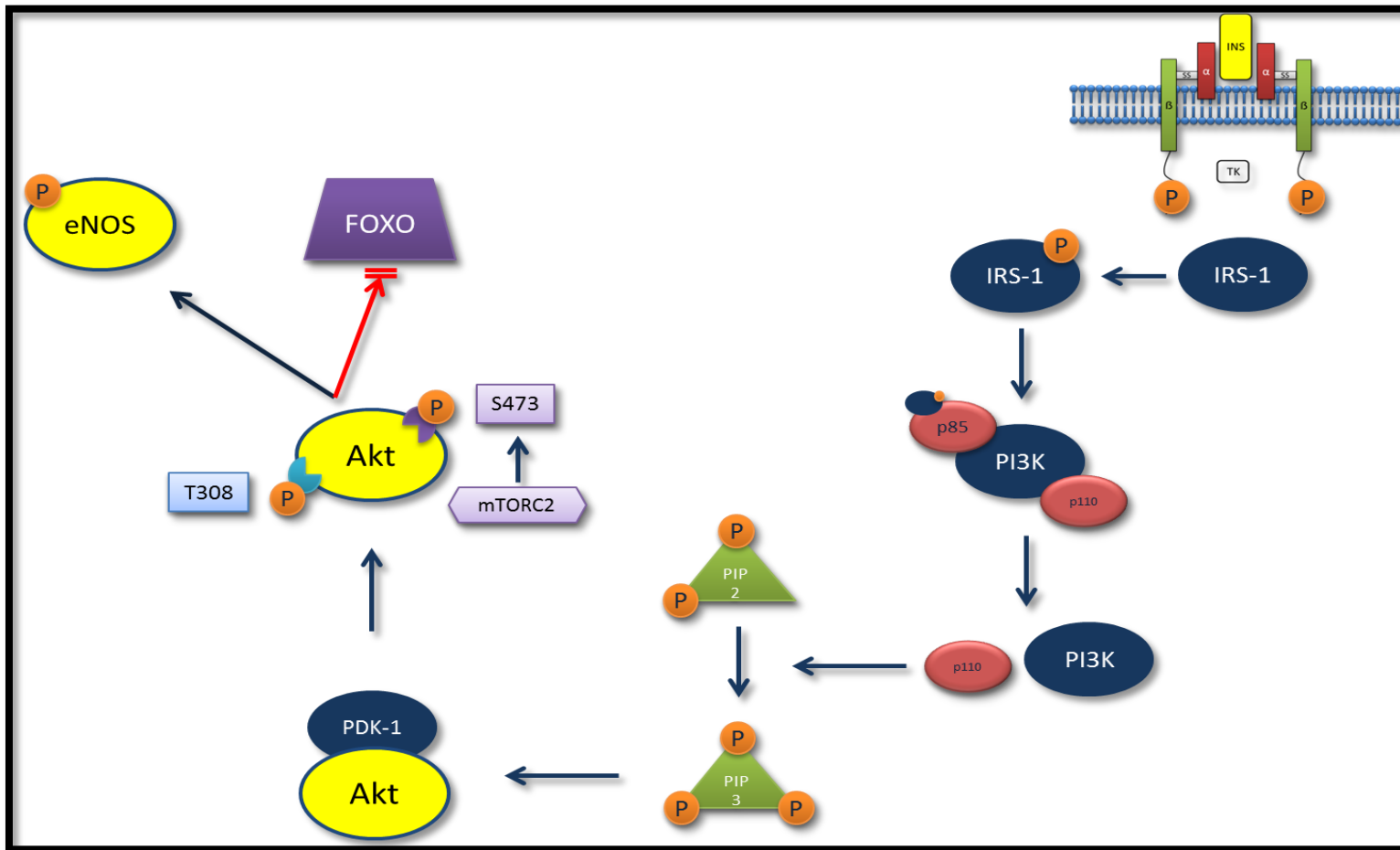
Figure 1-5   Cell Membrane Changes Resulting from Activation of the PI3K/Akt Pathway of Endothelial Insulin Signalling

P (in orange circle) represents phosphorylation; IRS-1 = insulin receptor substrate 1; PI3K = phosphatidylinositol-3-kinase; PIP = phosphatidylinositol bis/trisphosphate; PDK-1 = phosphoinositide dependent kinase 1; T308 = threonine-308; S473 = serine-473; mTORC2 = mammalian target of rapamycin complex 2; eNOS = endothelial nitric oxide synthase; FOXO = Forkhead box class O. Adapted from Gatenby et al *[50].*

1.2.4 **Molecular Mechanisms of Insulin Resistance**

The concept of insulin resistance is complex and its development and progression are multifactorial. Many putative mechanisms exist, including diminished quantity of insulin receptors and intracellular signalling proteins, structural aberrations of key mediators such as IRS or PI3K, and inhibitory post-translational modification of these proteins, leading to reduced propagation of insulin signalling [3].

Structural anomalies in the receptor itself are rare in man, and are not postulated to be important in the majority of human insulin resistance [51]. In fact, case series describing patients who lack functioning insulin receptors reveal a variable, but often markedly abnormal, phenotype with severe growth failure and predominant hypoglycaemia [52]. However, missense mutations of crucial tyrosine residues within the insulin receptor, such as tyrosine 960, have been reported: these are associated with complete absence of downstream signalling and biological effects of insulin [53]. A specific point mutation in the human insulin receptor gene has also been reported to result in insulin resistance due to ineffective maturation of the receptor's precursor into mature alpha and beta subunits, markedly interfering with the receptor's ability to bind insulin [54]. Diminished receptor abundance has also been noted in skeletal muscle and adipocytes from obese humans, as well as muscle and liver from type 2 diabetics, although genetic variants were not implicated in this work [32]. Indeed, it appears that the majority of human insulin resistance is a multifactorial phenomenon, with a significant contribution from modifiable environmental factors such as diet and exercise [55]. Whilst weight loss can thus improve insulin sensitivity in people with diabetes, some data suggest this is not the case in obese, insulin-resistant subjects without frank diabetes, suggesting that other mechanisms are involved in the pathophysiology of pre-diabetes [56].

Murine models of insulin receptor knockout are similarly complex. Homozygous insufficiency of the insulin receptor (IR) leads to a consistent lethal phenotype comprising normal *in utero* development but rapid neonatal deterioration. In two sets of reports, IR^{-/-} mice have been shown not to differ morphologically from healthy littermates but quickly develop profound hyperglycaemia, hyperinsulinaemia and eventual death from diabetic ketoacidosis within 72 hours [57, 58]. However, mice with whole-body haploinsufficiency of the insulin receptor (IRKO) show a much milder phenotype that survives to adulthood [59]. The IRKO model will be discussed in greater depth in subsequent sections, although in summary, these mice are glucocompetent but display post-prandial hyperinsulinaemia and hypertension, akin to human metabolic syndrome [59, 60].

Aberrances downstream from the insulin receptor are also well-described: for example, several naturally-occurring genetic polymorphisms of IRS-1 have been documented [32]. The most commonly seen in Caucasians, G972R, involves the substitution of glycine 972 for arginine and is seen almost twice as commonly in diabetics as it is in healthy individuals. Obese Caucasian carriers are relatively insulin resistant after oral glucose challenge [32]. Transfection studies were used to show that this variant results in reduced binding of PI3K to IRS-1, with concomitantly reduced PI3K activity [61]. Similarly, Goodyear *et al* observed diminished insulin-induced phosphorylation of the insulin receptor and IRS-1, along with blunted PI3K activity, in rectus abdominis muscle biopsy specimens from lean and obese human subjects with this polymorphism [62]. Knockout models of IRS proteins also aid understanding of their role in insulin sensitivity. For example, murine models of IRS-1 knockout show a phenotype of insulin resistance with growth retardation, but do not develop frank diabetes due to compensatory hyperinsulinaemia [63], while those with IRS-2 knockout display localised perturbations in insulin signalling (hepatic and beta-cell) and growth disturbance (neuronal) with frank type II diabetes due to the negative impact on pancreatic beta-cell function [64]. Combined insulin

receptor and IRS-1 and/or IRS-2 insufficiency result in varying degrees of insulin resistance, ranging from mild tissue-specific insulin resistance to frank diabetes [65, 66]. Furthermore, inhibitory serine phosphorylation of IRS-1 is also more commonly seen in insulin resistance, suggesting an additional pathophysiological mechanism of interference with IRS-1 function [37]. This notion is controversial: a knock-in study replacing the implicated serine 307 residue on IRS-1 with alanine showed more marked insulin resistance in the knock-in mice than in controls, questioning the inhibitory impact of phosphorylation at this residue *in vivo* [67]. Similarly, the entire role of IRS protein post-translational modification is called into question by a study showing that platelet derived growth factor (PDGF) signalling, which acts independently of IRS, is also impaired in the setting of insulin resistance [68].

Similar principles apply to dysfunction of nodes further down the signalling cascade. For example, deletion of the Akt-2 isoform, in particular, results in insulin resistance and diabetes in mice [69]. This has a correlate in humans, as evidenced by the reporting of severe insulin resistance and diabetes in a family with an autosomal dominant mutation in the kinase portion of Akt-2 [70]. These data imply that aberrant function at a node distal to the insulin receptor and its immediate substrates can also contribute to the pathogenesis of the insulin resistant state.

Factors external to the insulin signalling axis can also modulate insulin signalling: for example, tumour necrosis factor-alpha (TNF-α) is an inflammatory cytokine that is produced in multiple body sites, including adipose tissue [32]. Local TNF-α concentrations correlate with body mass index and rise in hyperinsulinaemic states, and raised levels can impair insulin signalling by increasing serine phosphorylation of IRS-1, which is deleterious to downstream signal transduction [71]. Leptin, a fat-derived hormone with central nervous system effects on feeding, has also been implicated in insulin resistance: its circulating concentrations mirror those of

insulin. However, no definitive consensus exists as to its relevance in the pathophysiology of insulin resistance [32].

1.2.5 **Tissue-specific Insulin Resistance**

Various models of tissue-specific insulin receptor manipulation have begun to shed light on a multi-system mechanism for the pathological effects of whole body insulin resistance and its interplay with the metabolic syndrome. For example, insulin-receptor knockout targeted to murine pancreatic beta-cells (betaIRKO) is associated with lower levels of DNA and protein synthesis, which prevents the augmentation of beta-cell mass required to mount compensatory hyperinsulinaemia in response to insulin resistance [72]. This contributes to hyperglycaemia and can hasten progression from insulin resistance to frank diabetes [46]. Hyperglycaemia may be potentiated by hypothalamic insulin resistance: in health, insulin acts on the arcuate nucleus to suppress appetite, so impairments in central nervous insulin signalling may result in increased food intake, hyperglycaemia and obesity [46].

Similarly, insulin receptor dysfunction in hepatocytes, as seen in the liver insulin receptor knockout (LIRKO) mouse, can have wide-ranging metabolic effects [73]. As well as reducing global insulin sensitivity, the loss of insulin-mediated suppression of hepatic gluconeogenesis release worsens hyperglycaemia. Meanwhile, disruption of the liver's critical role in insulin clearance further augments hyperinsulinaemia, thus resulting in profound insulin resistance in this model. The hepatic insulin receptor also appears to have a role in lipid metabolism, and its knockout results in diminished low density lipoprotein (LDL) receptor abundance, a consequent reduction in LDL clearance from blood, and also increased secretion of apolipoprotein B, a key component of LDL and very low density lipoprotein (VLDL) [74]. These abnormalities may have implications in terms of cardiovascular risk.

Lipid-related consequences can result from insulin receptor dysfunction in other organs too. Adipose tissue-specific insulin receptor knockout (FIRKO) mice exhibit normal glucoregulation but impaired suppression of lipolysis, resulting in increased concentrations of free fatty acids (FFA) [75]. A similar phenotype is seen in murine models of Cre-Lox-driven muscle-specific knockout (MIRKO), which display normal glucocompetence but high body fat stores and raised triglycerides, reminiscent of human metabolic syndrome [76]. Mice with dual-site insulin receptor knockout, affecting both skeletal muscle and adipocytes, show a more severe insulin-resistant phenotype, suggesting that normal IR function in one tissue can partially compensate for a mutation in the other unless both are disrupted together [59, 77]. These findings suggest that perturbations of the insulin receptor in traditional target tissues can encourage elements of the metabolic syndrome without necessarily disrupting glucoregulation. Despite normal glycaemic parameters, raised circulating FFA can interfere with insulin signalling, potentially instigating a "vicious cycle" of impaired glucoregulation and disturbed lipid homoeostasis. Additionally, FIRKO mice show increased expression of monocyte chemoattractant protein-1 (MCP-1), which results in an influx of macrophages into adipose tissue and consequent induction of a chronic pro-inflammatory state [46]. These effects are compounded in obesity, where body fat expansion occurs due to adipocyte hypertrophy; enlarged adipocytes lack full functional capacity and further promote an inflammatory cell infiltrate into areas of white fat [46]. Thus, insulin receptor dysfunction at multiple organ sites can act synergistically to create both systemic insulin resistance and a wider constellation of increased vascular risk with or without dysglycaemia [59].

Clearly, insulin receptors are widespread and disturbance in their number, function and downstream mediators can have wide-ranging effects on glucose metabolism, lipid clearance and inflammation. These derangements are closely tied in with cardiovascular risk and are worthy of attention. Of particular relevance to vascular health is the endothelium, which is insulin-

responsive and thus subject to dysfunction in insulin resistance. This will be the focus of this research, and a discussion of the interplay between endothelial health and the insulin signalling axis follows.

1.3 The Vascular Endothelium

1.3.1 Physiological Role of the Endothelium

The endothelium is a cellular monolayer that lines the arteries, capillaries and veins that make up the mammalian circulatory system. Vascular endothelial cells provide an essential physical barrier between blood and tissue, controlling the diffusion of oxygen and nutrients to the extravascular environment. An intact endothelium also acts as an interface between blood constituents and deeper tissue, reducing the risk of inappropriate coagulation [78]. However, the traditional view that the endothelium is simply a mechanical barrier has been challenged in recent years, with increasing recognition that it is a complex and dynamic organ involved in mediating vascular tone and integrity [3, 79]. Complex cytoskeletal arrangements and signal transduction mechanisms involving actin fibres, intermediate filaments and caveolae (plasma membrane invaginations) allow endothelial cells to sense subtle alterations in vessel tension, thus rendering them sensitive and responsive to shear stress and cyclic strain [80].

By regulating the balance between vasoconstriction and vasodilatation, the endothelium helps to optimise blood pressure and maintain undisturbed laminar flow. This is achieved by a fine balance between the release of substances that encourage vasoconstriction, such as endothelin 1 (ET-1), angiotensin II (AngII) and some reactive oxygen species (ROS) and those that do the opposite, such as nitric oxide (NO) [79]. These, and other mediators, also modulate platelet function, cell adhesion, inflammation and smooth muscle function, thus influencing the processes of atherosclerosis and plaque maturation, which underlie the majority of cardiovascular disease. Given that the endothelium is insulin-responsive, the interplay between the insulin signalling axis and wider endothelial biology may influence cardiovascular risk, rendering this a subject of significant interest.

1.3.2 **Nitric Oxide (NO) Generation**

Nitric oxide (NO) is arguably the most important mediator of vascular health, and achieves this by a variety of actions that are anti-atherogenic, anti-thrombotic and anti-inflammatory. In 1980, Furchgott and Zawadski concluded from seminal *in vitro* experiments that acetylcholine-mediated vasodilatation of mammalian vasculature depended on the presence of an intact endothelium, by virtue of an unknown substance that caused smooth muscle relaxation [81]. This "endothelium-derived relaxing factor" was later noted to be nitric oxide, a volatile gas [82, 83].

NO is produced by the action of three nitric oxide synthase (NOS) enzymes: endothelial (e)NOS, inducible (i)NOS and neuronal (n)NOS [84]. These share a dimeric structure with C-terminal reductase domains that bind nicotinamide adenine dinucleotide phosphate (NADPH) and N-terminal oxygenase domains that bind the main substrate (L-arginine) as well as haem and tetrahydrobiopterin (BH_4) [84]. In between these domains lies a calmodulin-binding domain, common to all three isoforms. However, subtle differences in structure and function distinguish the three isoforms from one another.

The most relevant isoform in the context of cardiovascular physiology is eNOS, which is upregulated in response to various stimuli including hypoxia, alterations in shear stress, insulin, vascular endothelial growth factor (VEGF) and oxidative stress. eNOS is encoded on the NOS3 gene [85] and is composed of two identical 134kDa monomers which form a biologically active dimer under the influence of haem [84]; it is thought that the dimer is rendered more stable by BH_4 [80]. Thus dimerised, eNOS is able to bind and hydroxylate a urea cycle product called L-arginine, ultimately converting it to L-citrulline and NO in a complex redox reaction. Initially, NADPH binds to the reductase domain, causing flavin-dependent electron transfer from the former to a hydroxylated intermediate of L-arginine; this is then oxidised in

the N-terminal domain using BH$_4$ as an essential co-factor, generating L-citrulline and NO [84]. Additionally, the calmodulin-binding domain and presence of free calcium ions both appear critical in enzyme activation [80]. Similarly, Akt-mediated phosphorylation of serine 1177 on eNOS has been shown to augment enzyme activity [86], even at sub-physiological concentrations of calcium, suggesting a calcium-independent pathway for eNOS activation in addition to the calmodulin-mediated, calcium-dependent pathway described above [87]. The process of NO generation is presented diagrammatically in Figure 1-6.
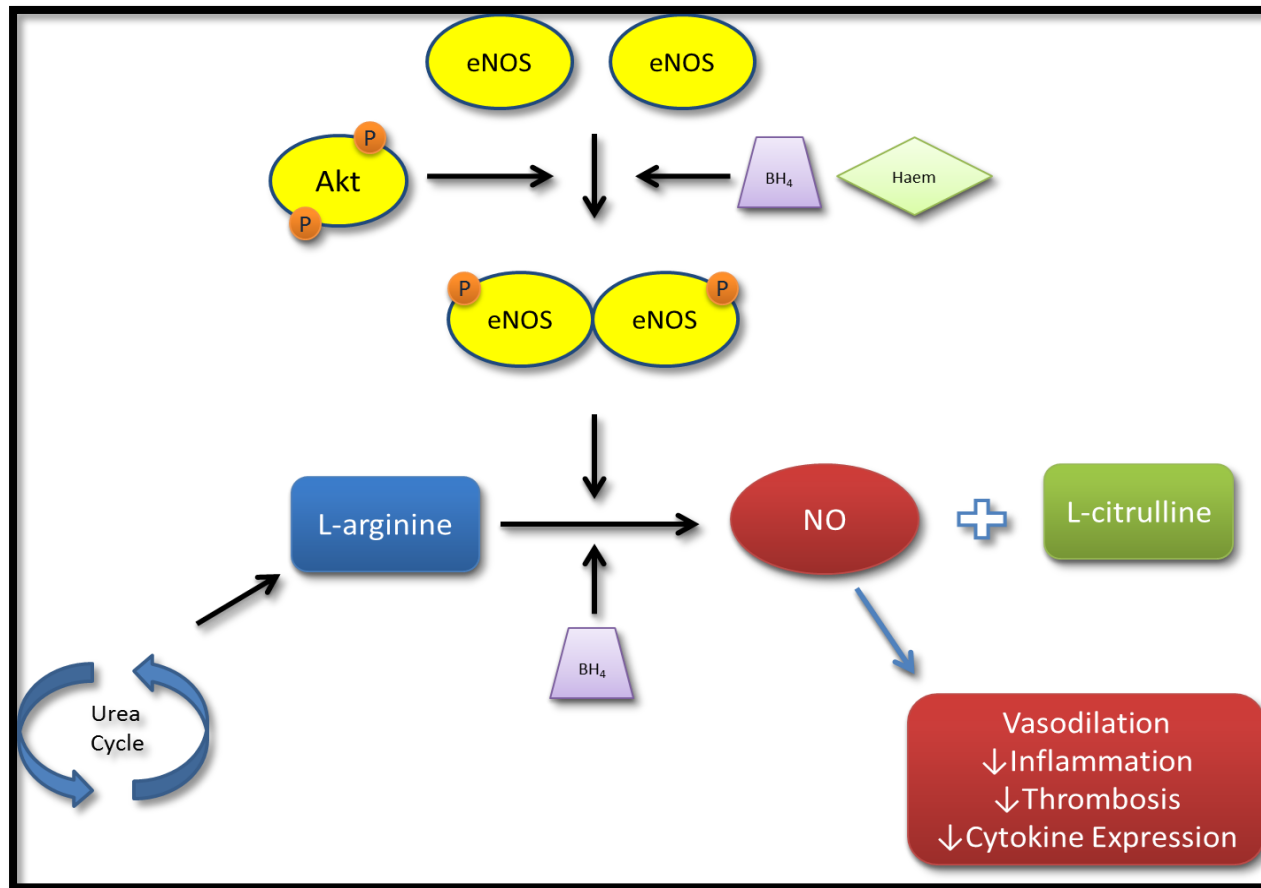
Figure 1-6   Nitric Oxide Generation

P (orange circle) represents phosphorylation; eNOS = endothelial nitric oxide synthase; BH₄ = tetrahydrobiopterin; NO = nitric oxide.

Endothelial NOS possesses certain properties that are distinct from the other two isoforms of NOS and allow it to respond to a variety of environmental stimuli that are relevant to the cardiovascular system. For example, experiments using bovine endothelial cells have shown increased eNOS activity in response to hypoxia [88], and after 24 hours of shear stress [89] *in vitro*. Post-translational modifications at the enzyme's N-terminus direct eNOS to a subcellular location where it can interact with plasma membrane phospholipids [80, 90]. It is thought that palmitoylation of eNOS allows it to interact with caveolin-1 and thus aids trafficking of the enzyme towards caveolae, as demonstrated in human umbilical vein endothelial cells (HUVECs) [91]. This location brings eNOS into the same cellular microenvironment as proteins downstream of G-protein-coupled receptors and the insulin receptor, allowing it to be released in response to triggers transduced by these receptors [91, 92]. Experiments using bovine eNOS have shown that it binds caveolin-1 directly, diminishing synthase activity; once free of the caveolae, catalytic activity is regained, allowing the generation of NO [93].

1.3.3 Physiological Action of NO

NO is a gaseous, lipophilic molecule with low molecular weight, properties which allow it to diffuse easily across plasma membranes [78] to adjacent target cells such as vascular smooth muscle cells (VSMC) and blood constituents like platelets. In these effectors, it exerts a variety of anti-atherosclerotic actions [84] via activation of soluble guanylate cyclase and production of cyclic guanosine monophosphate (cGMP) [94]. In VSMCs, NO regulates cytoplasmic calcium concentrations, encouraging VSMC relaxation and therefore vasodilatation. Consequent alterations in vessel diameter can affect vascular flow and shear stress. This mechanism is thought to be of particular physiological importance as the infusion of levo-N-monomethyl arginine (L-NMMA; an inhibitor of NOS) results in raised systolic blood pressure in a rabbit model, with reversal of vasoconstriction after exposing *ex vivo* aortic segments to L-arginine [95]. In human studies, forearm

infusion of L-NMMA has been found to result in blunted flow-mediated vasodilatation in healthy volunteers [96]. NO also has an antiproliferative effect on VSMCs [85].

NO has been repeatedly demonstrated to be upregulated in response to haemodynamic triggers: for example, eNOS expression is increased in response to shear stress in bovine aortic endothelial cells [89] and eNOS mRNA and protein expression were noted to rise after vacuum-induced deformation of flexible membranes, mimicking cyclic strain [97]. These features become important in the maintenance of vascular tone and permeability. For example, in conditions of undisturbed laminar flow, the unopposed movement of blood within vasculature results in a physiological level of shear stress, which allows endothelial cells to flatten and assume a conformation that places them in line with the direction of blood flow. In areas of low shear stress, blood flow can become erratic or even assume a retrograde direction, resulting in misalignment of cells. This, along with subtle alterations in cytoskeletal integrity, can result in widening of spaces between individual endothelial cells, thus disrupting the physical barrier to permeation of blood-borne substances across the monolayer. Relative blood stasis, along with a concomitant inflammatory reaction, increases the chances of atherosclerosis and thrombosis [78]. Conversely, supra-physiological shear stress can result from turbulence caused by atherosclerotic plaque. This can hasten plaque maturation and eventually lead to damage, as well as exposure of the endothelium to erosive forces, thus increasing the chance of plaque rupture and subsequent thrombotic occlusion of the vessel lumen [78]. The production of NO in these situations triggers beneficial vasodilatation and inhibits the inflammatory infiltrate, thus resulting in attempted normalisation of flow, blood constituents and vascular tone.

NO is also protective against thrombosis. It inhibits platelet adhesion to the endothelium [98] and reduces platelet aggregation [99], thus reducing the

risk of thrombus formation on vulnerable plaques. For example, mice with knockout of the NOS3 gene (and thus reduced eNOS activity) lack the physiological inhibition of secondary platelet recruitment into evolving thrombi, suggesting a role for NO in limiting thrombus propagation in health [100]. When platelets derived from these mice were transfused into thrombocytopenic eNOS-deficient mice, haemostasis was improved compared with wild-type platelet infusion, suggesting specifically that platelet-derived NO reduces platelet activation [99, 100]. Additionally, by interfering with platelet activation, NO indirectly leads to reduced concentrations of trophic factors such as platelet-derived growth factor (PDGF), which ordinarily promotes proliferation in VSMCs [99]. Similarly, NO is a negative regulator of cell adhesion molecule and cytokine expression, thus reducing the recruitment of inflammatory [101] and pro-thrombotic cells to areas of atheroma [78]. Specific cell surface molecules that are downregulated in response to NO include P-selectin, vascular cell adhesion molecule-1 (VCAM-1) and intercellular adhesion molecule-1 (ICAM-1) [99].

Taken together, these descriptions show that NO has wide-ranging effects on vascular tone, cytokine release, monocyte recruitment into maturing atheroma and acute thrombosis after plaque rupture. Thus, any deficiency in its bioactivity can negatively impact on all stages of atherosclerosis and eventually promote myocardial infarction or stroke. Reduced NO bioavailability is thus a key contributor to the pathogenesis of vascular disease and can occur as a result of reduced generation, which is directly relevant to the insulin signalling axis, or due to increased sequestration by reactive oxygen species (ROS), which will be discussed in more depth later.

1.3.4 Endothelial Dysfunction and Insulin Resistance

As previously mentioned, the endothelium maintains a delicate balance between vasoconstrictive and pro-thrombotic mediators such as ET-1 and angiotensin and molecules like nitric oxide, which have a portfolio of anti-

coagulant and vasodilatory properties [40]. A disturbance of this balance is referred to as endothelial dysfunction. This is a key initiating step in atherosclerosis [102] and has been shown to be an independent predictor of cardiovascular disease in studies using both human forearm flow-mediated vasodilatation and invasive measures of coronary artery dilation responses [103, 104].

The endothelium is an insulin-responsive tissue: once insulin binds with its cell surface receptor, parallel intracellular signalling pathways are activated, in turn stimulating NO and ET-1 release [40] (Figure 1-4). Conditions of high glucose can, *in vitro*, reduce signalling in the PI3K pathway in human aortic endothelial cells, potentially implicating this pathway in the pathogenesis of endothelial dysfunction in the setting of diabetes [105]. In insulin resistance, there is selective downregulation of the PI3K pathway, resulting in reduced eNOS activation, and therefore NO production, as demonstrated in both rat [106] and human [107] experiments. This appears to be physiologically important in man: insulin resistant human subjects display blunted endothelium-dependent vasodilatation in response to both insulin [108] and acetylcholine [109]. At the same time, flux through the MAPK pathway is undisturbed or even augmented due to compensatory hyperinsulinaemia; therefore, ET-1 synthesis is not diminished [106, 107]. It has been observed that humans with metabolic syndrome in fact have higher concentrations of ET-1 than healthy controls, suggesting a potential link, albeit not necessarily a causal one, with upregulated ET-1 synthesis [110]. Physiologically, studies in rats have shown that ET-1 antagonism improves endothelium-dependent vasodilatation in both *ex vivo* aortic segments and after chronic pharmacological blockade using bosentan, suggesting that at least in animal models, this mechanism may be a relevant contributor to altered vascular tone [111]. Furthermore, ET-1 can inhibit PI3K signalling and accentuate the reduction in NO production [112]. Finally, the MAPK pathway promotes expression of cell adhesion molecules such as VCAM-1, which can encourage leukocyte infiltration, and thus promote atherosclerosis [40].

Collectively, one may surmise that the pathway-specific nature of insulin resistance encourages endothelial dysfunction via a two-fold mechanism: firstly, by reducing NO, and secondly, via the concomitant deleterious effects of raised ET-1 and leukocyte adhesion. Whilst the applicability of MAPK pathway overactivation in man is not entirely established, there seems to be circumstantial evidence that ET-1 levels are raised in insulin resistant humans, and it is feasible that this contributes to a disruption in the balance of vasoactive mediators, favouring vasoconstriction and atherogenesis.

Much can be inferred from work focussing on the interplay between insulin resistance and endothelial function using murine models. As previously discussed, homozygous loss of the insulin receptor results in early post-natal death, limiting the use of this model for studies of adult physiology [57, 58]. However, mice with heterozygous insulin receptor knockout (IRKO) display a milder phenotype, with normal weight gain and only post-prandial (as opposed to basal) hyperinsulinaemia [60]. These features make the IRKO mouse a useful model for pre-diabetes without the potential confounding influences of hyperglycaemia and obesity. Interestingly, this modest disturbance in parameters is accompanied by a convincingly deranged vascular phenotype: IRKO mice are hypertensive compared with wild-type (WT) controls and display marked endothelial dysfunction in *ex vivo* assays of aortic vasomotor responses in organ bath apparatus [60]. Six month-old IRKO aortic rings pre-exposed to phenylephrine, an endothelium-independent vasoconstrictor, showed a reduced dilation response to acetylcholine after insulin incubation compared with rings from WT littermates. Crucially, this vasomotor dysfunction was shown to be related to reduced NO bioavailability as evidenced by a diminished incremental constriction response after incubation with the NOS inhibitor L-NMMA [60]. Examination of downstream intracellular signalling in this study showed equivalent eNOS mRNA expression in IRKO and WT but reduced insulin-induced eNOS phosphorylation in IRKO [60].

IRKO mice display the above vascular phenotype in association with whole body haploinsufficiency for the insulin receptor; the specific role of the endothelium within this has been studied using two separate murine modelling approaches. In 2003, one group used Cre-lox recombination to knock out the insulin receptor from vascular endothelial cells in the VENIRKO model [113]. These mice showed no difference from WT in terms of glucocompetence, but reduced eNOS mRNA expression was observed in endothelialised organs such as heart and aorta in the VENIRKO mice. This interference at mRNA level was in contrast to the findings in the IRKO study above [60]. Our laboratory employed a different approach to study a similar theme by generating a transgenic mouse with endothelium-specific mutant insulin receptor overexpression (ESMIRO). This model utilised a Tie-2 promoter-enhancer in order to express a mutant kinase-defective human insulin receptor within endothelial cells [114]. ESMIRO mice behaved similarly to IRKO mice: they exhibited preserved glucoregulation, but showed a blunted vasodilator response to acetylcholine, reduced insulin-mediated vasorelaxation and diminished insulin-induced eNOS phosphorylation [114]. As with IRKO mice, there was no difference in eNOS mRNA expression between ESMIRO and WT. In this study, raised levels of reactive oxygen species (ROS) were noted in endothelial cells from ESMIRO mice, and the endothelial dysfunction seen in aortic ring experiments could be reversed using anti-oxidants [114].

Taken together, these studies imply a key role for endothelial insulin receptor function and signalling in maintaining vascular function. Whilst the exact mechanism appears to differ between the above models, they all suggest a defect at the level of eNOS, which may be a direct consequence of reduced signalling through the insulin receptor. However, as previously mentioned, another possible explanation for reduced NO bioavailability is sequestration by ROS, which may be relevant given the results of previous work in ESMIRO mice and older IRKO mice [114, 115]. A discussion of the role of ROS in endothelial function and cardiovascular health follows.

1.3.5 **Reactive Oxygen Species**

Reactive oxygen species are a group of molecules generated in redox reactions either in mitochondrial electron transport chains or via the activity of endogenous enzymes such as NADPH oxidase (or NOX), lipoxygenase, xanthine oxidase, and even eNOS. In these reactions, electrons are transferred sequentially to molecular oxygen, generating molecules such as the superoxide anion (O_2^-), hydrogen peroxide (H_2O_2) and hydroxyl radicals (OH^-) [116] (Figure 1-7). Some types of ROS contain unpaired electrons and can thus act as free radicals, with damaging effects on mammalian cells; others are not strictly free radicals but can still exert deleterious but perhaps milder pro-oxidant effects [117]. ROS are traditionally viewed as harmful, but work done in recent years has yielded increasing recognition of a beneficial and necessary role for ROS in intracellular redox signalling and vascular health at physiological concentrations [118]. However, in the context of insulin resistance, various mechanisms can lead to enhanced production or reduced breakdown of ROS, and their resultant accumulation to harmful concentrations (oxidative stress) [116].
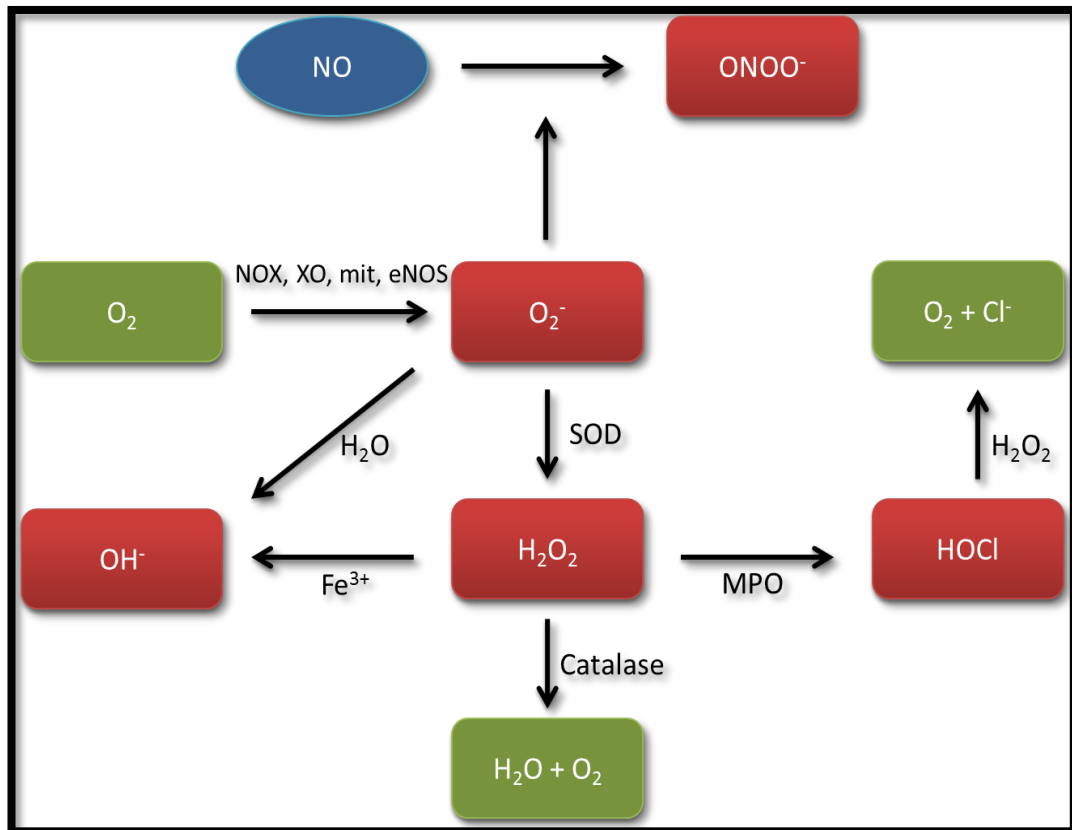
Figure 1-7   Generation of Reactive Oxygen Species

NO = nitric oxide; ONOO = peroxynitrite; O_2 = oxygen; O_2^- = superoxide anion; Cl^- = chloride ion; OH^- = hydroxyl radical; H_2O_2 = hydrogen peroxide; HOCl = hypochlorous acid; H_2O = water; NOX = nicotinamide adenine dinucleotide phosphate oxidase; XO = xanthine oxidase; mit = mitochondria; eNOS = endothelial nitric oxide synthase (in this case, uncoupled); SOD = superoxide dismutase; Fe^{3+} = iron (III) ion; MPO = myeloperoxidase. Red boxes denote reactive oxygen species, green boxes and blue oval denote less toxic sources and metabolites.

The primary source of vascular ROS is the family of NOX enzymes, which use NADPH as the substrate and source of electrons for transfer to oxygen molecules [118]. Whilst there are several NOX isoforms, it appears that NOX1, NOX2 and NOX4 are of particular importance in vascular and endothelial cell biology [79]. The action of these enzymes is to generate hydrogen peroxide and superoxide anions which, in supra-physiological

quantities, can result in vascular damage through a variety of mechanisms. Superoxide reacts with NO to form peroxynitrite, another pro-oxidant which can nitrosylate proteins and thus interfere with phosphorylation, cell signalling and function [99]. Thus, the effect of this is two-fold, as it causes sequestration of bioavailable NO and reduction of its beneficial vascular effects, while the direct effects of peroxynitrite on endothelial cells can be harmful in themselves [119]. Superoxide can also interfere with normal function of BH_4, a key component of eNOS. Not only does this reduce NO generation, but modifying BH_4 can cause uncoupling of eNOS into monomers, which preferentially generate more superoxide, further potentiating the effect [120]. It can also promote oxidation of the zinc-thiollate core of eNOS, with similar reduction in enzyme activity and therefore diminished NO generation [79]. Finally, NOX-derived ROS can enhance mitochondrial ROS generation [121], resulting in a 'vicious cycle' of ROS overproduction to the point where endogenous antioxidants are unable to compensate and harmful concentrations are reached [79].

Appraisal of animal models lends validity to the suggestion that these effects are pathophysiologically relevant in insulin resistance. For example, Duncan *et al* described the phenotype of a transgenic mouse in which a mutated human insulin receptor (at threonine 1134) was targeted to the vascular endothelium using a Tie-2 promoter-enhancer sequence [114]. These ESMIRO mice exhibited diminished vasorelaxation of explanted aortic rings to acetylcholine, with associated blunting of insulin-induced eNOS phosphorylation. Aortic relaxation could be restored to wild-type levels with the administration of the superoxide dismutase mimetic manganese(III)tetrakis(1-methyl-4-pyridyl) porphyrin pentachloride (MnTMPyP), implicating oxidative stress as a causative factor in endothelial dysfunction. In this study, NOX2 and NOX4 were demonstrated to be key sources of ROS in both aortic samples and in cultured microvascular endothelial cells [114]. Elevated superoxide concentrations have also been shown in aortae and cultured endothelial cells from IRKO mice; in the same

study, endothelial dysfunction in aortic vasorelaxation experiments could be reversed using MnTMPyP [115].

The relevance of this manipulation has been explored in further detail using existing murine models of vascular disease. In our laboratory, ESMIRO were crossed with atherosclerosis-prone apolipoprotein E knockout mice (ApoE$^{-/-}$); in addition to endothelial dysfunction, these animals displayed significantly higher atherosclerotic burden at the aortic sinuses and arch than ApoE knockout controls [122]. These findings suggest that, as well as manifesting as endothelial dysfunction in *ex vivo* experiments, the increase in oxidative stress is relevant to an *in vivo* marker of adverse vascular risk. Again, a convincing elevation in superoxide concentrations was observed, though this time, multiple enzyme sources were implicated: the heightened superoxide signal could be suppressed using gptat (which inhibits NOX enzymes), rotenone (which quenches mitochondrial ROS production) and L-NMMA (which abrogates the effects of uncoupled eNOS) [122]. In a further study from our group, the use of gptat was found to reverse the endothelial dysfunction and raised superoxide concentrations seen in both ESMIRO and IRKO mice when administered acutely *in vitro* [123]. In IRKO aortic rings, this was associated with increased NO bioavailability. This 'rescue' was recapitulated with chronic administration of gptat into ESMIRO mice via a subcutaneously implanted 'minipump', which gradually released the antioxidant over a 28-day period [123]. Finally, chronic ROS inhibition was modelled genetically by crossing ESMIRO with mice with NOX2 inactivation (ESMIROxNOX2$^{y/-}$), yielding the same beneficial effects on aortic vasomotor function [123]. This study therefore utilised acute and chronic pharmacological inhibition as well as genetic deletion to demonstrate the relevance of NOX-derived ROS on vascular function [123].

A similar adverse vascular phenotype has also been induced with high fat feeding in mice [124]. This group showed that high-fat fed mice had features akin to the human metabolic syndrome, accompanied by increased levels of

ROS, NOX2 expression and endothelial dysfunction, all of which was abrogated both with pharmacological antioxidant therapy using apocynin, as well as in NOX2 knockout mice subjected to the same high-fat diet [124]. Similar work in cholesterol-fed, atherosclerotic rabbits has shown that acetylcholine-induced vasorelaxation can be rescued by infusing polyethylene-glycated superoxide dismutase (SOD) [125]. Importantly, this was not found with sodium nitroprusside-induced vasorelaxation, implying a key role for specifically endothelium-derived superoxide.

Human studies appear to support the presence of increased vascular ROS in insulin-resistant states: for example, it has been shown that arteries and veins from patients with diabetes contain more superoxide and uncoupled eNOS than tissue from matched controls, with restoration of superoxide concentrations to physiological levels after exposure to supplemental BH_4 [126]. Similarly, human subjects with metabolic syndrome show increased NADPH oxidase activity and superoxide production in peripheral blood mononuclear cells compared with healthy controls, correlating with plasma insulin levels [127]. Similar findings of increased NOX activity in obese humans and those with heart failure lend further validity to the implication of ROS in cardiovascular and metabolic disease states [79]. Whilst these studies do not specifically demonstrate a dysfunctional human vascular phenotype, there is a strong suggestion that such a disturbance exists; increased ROS is linked with reduced NO bioactivity, which has been shown to be a crucial contributor to endothelial dysfunction and thus hypertension and atherosclerosis in humans.

1.3.6 **Atherosclerosis**

The key reason for studying oxidative stress, nitric oxide bioavailability and endothelial dysfunction is that these are key events in the development of atherosclerosis. Whilst hypercholesterolaemia has long been recognised as a risk factor for atherosclerosis and subsequent cardiovascular events,

research over the last few decades has shown that the development of plaques is more complex than simply the laying down of layers of lipid in the arterial wall [102, 128]. An overview of the pathogenesis of atherosclerotic plaque development will now be presented.

Atherosclerosis is a process that can begin in an individual's childhood or teenage years with the development of fatty streaks [129]. These are predominantly inflammatory lesions that begin with a monocyte infiltrate but mature over time to become more complex entities which gradually protrude into the vessel lumen and disturb the flow of blood to distal structures. As plaques evolve, they can also undergo erosion and become unstable and prone to rupture; this exposes circulating clotting factors and platelets to highly thrombogenic plaque contents and can result in acute thrombotic occlusion of vessels, leading to distal ischaemia and infarction [130].

The initiating event in atherosclerosis is often disturbance of laminar flow at specific sites within an artery, such as bifurcations or areas of curvature or tortuosity. In these areas, turbulence can rise and shear stress can be altered, and it is thought that these stimuli can increase the expression of genes for several cell surface molecules that modulate the local immune response. For example, genes for ICAM-1 and platelet-derived growth factor-B can be induced in endothelial cells [102, 131] in response to low shear stress. The collective action of a variety of such molecules is to encourage an inflammatory cell infiltrate and to promote the docking of monocytes in particular onto the endothelium. Cell adhesion molecules such as ICAM-1 and VCAM-1 facilitate rolling and adhesion of monocytes, which eventually undergo diapedesis and are incorporated into subendothelial locations. As in other anatomical locations, monocytes are able to reside in these plaques and the receptor-ligand interactions discussed above allow them to become activated and to differentiate into macrophages [102]. Furthermore, production of chemokines such as monocyte chemoattractant protein (MCP) leads to propagation of the influx of inflammatory cells,

initiating and maintaining a cycle of ongoing cell accumulation. Immunohistology of surgically obtained arterial specimens from humans has confirmed the presence of a marked inflammatory infiltrate rich in macrophages in areas of atheroma, with fewer of these cells noted in adjacent healthy endothelium [132].

Alongside this cellular infiltrate, low density lipoprotein (LDL) can also accumulate in early plaques after interaction with the LDL receptor on the endothelial surface [133]. With endothelial dysfunction and inflammation, vascular permeability is increased, leading to excessive internalisation of LDL. Once this has accumulated, it can be oxidised by ROS derived from activated macrophages. Oxidised LDL is a profound chemotactic stimulus for inflammatory cells; for example, modified LDL can stimulate gene expression for macrophage colony stimulating factor and MCP and thus propagate the cellular infiltrate [130]. Furthermore, inflammatory mediators such as tumour necrosis factor-alpha (TNF-α) and interleukin-1 (IL-1) have been shown to increase LDL receptor gene expression and promote binding of LDL to endothelial cells, which could maintain a spiral of increasing inflammation and lipid deposition [134].

As LDL accumulates in the subendothelial space, it can also become internalised by resident macrophages, which contain cell-surface scavenger receptors for lipoproteins. This encourages the formation of cholesterol esters, which accumulate within the macrophages and cause them to develop into foam cells. These can undergo necrosis, which causes further release of pro-inflammatory and chemotactic mediators into the circulation [133]. Thus, the combination of lipid deposition, lipoprotein modification and chronic inflammation appears to induce the development of metabolically active lesions which can interfere with normal vascular anatomy and physiology. Consistent with a role for ROS in the harmful oxidation of LDL, antioxidant treatment has also been shown to reduce atherosclerotic burden

in hypercholesterolaemic macaques [135], though clinical trials have failed to reproduce these encouraging findings in humans [136].

Another downstream effect of the early inflammatory response is the production of growth factors and vasoactive cytokines. This can stimulate local vascular smooth muscle cells to migrate and proliferate at the site of damage, which often leads to development of fibrosis around affected areas. Thus, the potentially thrombogenic and toxic core of an atheromatous plaque can be separated mechanically from the blood by a "fibrous cap", which can lend stability to the lesion, at least in the early stages of plaque development [130]. Human atheromatous lesions have been noted to be more rich in smooth muscle cells than neighbouring healthy endothelium, suggesting an important role for these cells in plaque maturation [132]. Fibrosis in the arterial wall can also be promoted by sustained hypertension, potentially due to the trophic effects of chronic exposure to angiotensin II on VSMCs [137]. Interestingly, angiotensin II can also augment lipoxygenase activity in VSMCs, which in turn stimulates inflammation and can result in further oxidation of LDL [102]. The initial response of arteries to this degree of fibrosis is to undergo a period of remodelling and compensatory vasodilatation in an attempt to preserve luminal morphology and thus distal blood flow [130]. However, with increasing inflammation and fibrosis, there comes a point at which remodelling can no longer preserve an adequate luminal diameter and the thickened arterial wall encroaches into the lumen [102]. At this stage, provided that the fibrous cap maintains its integrity, necrotic plaque contents are not exposed to blood and platelets so the risk of thrombus formation remains low; however, the stenosed artery may not be of sufficient calibre for adequate tissue perfusion at times of stress, leading to phenomena such as stable angina and intermittent claudication.

With further plaque maturation, macrophages and foam cells can undergo apoptosis or necrosis, with consequent release of multiple inflammatory mediators and, importantly, proteolytic enzymes. A wider inflammatory

response can also ensue due to the antigen presentation by major histocompatibility complexes on macrophages; this causes local recruitment of T-lymphocytes, which stimulate collagenase and matrix metalloproteinase release from viable macrophages [128]. The result of this enhanced proteolytic activity is gradual degradation of the fibrous cap, rendering it unstable and vulnerable to erosion and ulceration in the face of ongoing disturbed blood flow [128]. The long-term action of locally-secreted collagenase can also induce structural reconfiguration in the tunica media of atheromatous arterial segments. In these areas, extracellular matrix composition can therefore change from an organised collagen matrix to a pathological one, predominantly containing proteoglycans interspersed with chaotically-distributed collagen fibrils [102]. The weakened and complicated plaque is therefore at high risk of rupture, with exposure of its internal thrombogenic core to circulating platelets and coagulation factors. This is the underlying basis of acute coronary syndrome and cerebrovascular events, wherein thrombus formation on a ruptured plaque can quickly propagate, leading to acute vascular occlusion and distal infarction.

Atherosclerosis is a multifactorial and complex phenomenon, which is clearly influenced by endothelial dysfunction and consequent reduction in NO bioavailability at every stage in the disease process. Thus, studying the interaction between insulin resistance and endothelial dysfunction is of crucial importance in understanding and developing treatments for cardiovascular risk in this group of patients. Vascular injury is both a causative factor in atherogenesis and a consequence of plaque rupture, and so the next section of this project will consider vascular regeneration and repair and their interplay with diabetes and insulin resistance.

1.4 Vascular Injury and Regeneration

1.4.1 Vascular Regeneration in Health

Diabetes and insulin resistance both lead to accelerated atherosclerosis, and it is therefore important to understand the impact of these conditions on the processes of vascular injury and endogenous endothelial repair. In order to appreciate the complexities of vascular regeneration and identify targets for therapeutic manipulation, it is important to have knowledge of the processes involved in blood vessel formation in physiological circumstances.

1.4.1.1 Vasculogenesis

In mammalian development, the earliest example of normal vascular development this is the *de novo* synthesis of blood vessels *in utero*, a process known as vasculogenesis [138]. This involves the maturation of angioblasts, sometimes referred to as endothelial progenitor cells (EPCs), which share an origin with haematopoietic cells [139]. These EPCs form primitive capillary networks that eventually coalesce to form the primordial vasculature [140]. There is little doubt that this process is relevant to embryonic development, but studies published in the last 15 years have raised discussion as to the possibility of a novel role for post-natal vasculogenesis in the response to endothelial injury in adulthood [141, 142]. This is a controversial subject and will be discussed in more depth later.

1.4.1.2 Angiogenesis and Arteriogenesis

Quite distinct from *de novo* vessel formation, angiogenesis is strictly defined as the extension of vasculature by new blood vessels sprouting from an existing vascular network [138, 139]. There is confusion in the wider biomedical literature about this, as angiogenesis is often incorrectly used to refer indiscriminately to new vessel formation in any context [138]. In this thesis the term will be used solely with reference to the first definition. In

adult life, most vascular beds are in a quiescent state; however, in the setting of vascular insults such as myocardial infarction or stroke, the resultant hypoxic and inflammatory milieu can drive angiogenesis and thus aid recovery [139]. Equally, disorders such as diabetic retinopathy and age-related macular degeneration demonstrate that aberrant angiogenesis can also be harmful as it can encourage formation of vascular networks that do not perfuse appropriately despite increased quantity [139]. Similarly, "unwanted" angiogenesis can aid tumour metastasis by way of vascular invasion of neoplastic lesions, providing a route for distant spread. In the context of diabetes and insulin resistance, angiogenesis is relatively ineffective [143] and therefore study of its intricate mechanisms may yield therapeutic targets for reduction of cardiovascular risk in these conditions.

Arteriogenesis is the third process that occurs during the generation of blood vessels, and refers to the maturation of new capillary networks within conduit vessels. These neovessels must assimilate with perivascular mesenchymal cells in order to transform into mature vascular tissue with lumina capable of accommodating and transporting blood and a vessel wall that is able to withstand haemodynamic stress [139]. Arteriogenesis is therefore an important contributor to eventual vascular development but remains incompletely understood and will not form a significant consideration in this project.

1.4.2 Vascular Repair

In contrast to vascular regeneration, the term "vascular repair" refers to re-endothelialisation in a pathological setting in which established and mature conduit vessels undergo injury. This can occur endogenously as a consequence of recurrent biochemical insult: for example, in diabetes, the accumulation of advanced glycation end products can lead to oxidative stress and endothelial cell loss [144]. Chronic hyperglycaemia can also induce senescence and apoptosis in endothelial cells [145]. Dead

endothelial cells then detach, either as whole cells or as endothelial microparticles, leaving behind a denuded endothelium that triggers an inflammatory response in an attempt to induce repair and regain structural integrity [144]. Whilst a degree of inflammation is helpful for repair, the overactivation of this cascade can also encourage the development of atheroma in the denuded area. Conversely, a similar process of endothelial denudation can occur after acute vascular events in areas of established atherosclerosis, such as plaque rupture. Iatrogenic causes are also relevant in human disease: therapeutic balloon angioplasty and stent implantation into stenosed arteries can both induce a degree of endothelial injury [138, 146]. Whilst sustained hyperglycaemia is likely to be restricted to frank diabetes, several other mechanisms outlined above, such as plaque rupture and oxidative stress, are likely to be relevant in the context of insulin resistance as well.

The process of vascular repair can be modelled in mice in various ways [146]. An electrical current can be applied to exposed femoral arteries, resulting in total endothelial denudation as well as removal of smooth muscle cells in the tunica media, and also the formation of mural thrombosis due to local platelet activation [147]. Whilst this method is attractive due its relatively low technical difficulty, one could argue that the mechanism of injury and the significant damage incurred to non-endothelial structures here reduce the clinical relevance of this model and induce a more severe phenotype than that usually encountered in man. Other researchers have described slightly more targeted endothelial injury following unilateral carotid artery ligation, which offers the advantage of a lack of thrombosis, thus allowing assessment of the response to injury without the confounding influence of local platelet biology [148]. More recently, Roque *et al* described a model of arterial injury utilising an angioplasty guide wire to denude the femoral artery endothelium [149]. This model, whilst challenging to perform in animals as small as mice, could be argued to induce more selective endothelial damage than in the previous models, and in a manner

that is perhaps more likely to simulate a realistic disease process in man. Similarly, balloon injury can also be induced in small animals, with several studies reported in rats using this technique [150, 151].

Such models have allowed us to employ genetically modified mice in the study of the pathophysiological mechanisms involved in the response to injury. Traditionally, it has been believed that regeneration of injured endothelium principally depends on mitosis and migration of adjacent healthy endothelial cells, which simply bridge the gap. Murine studies using the femoral arterial injury model support this, with evidence of a specific role for VEGF in driving endothelial cell proliferation and angiogenic inhibitors such as endostatin in promoting endothelial cell apoptosis [152, 153]. However, endothelial cells are terminally differentiated and retain only limited capacity for proliferation, suggesting that other mechanisms may contribute to repair. Much work in the last 15 years has challenged the traditional view of solely endothelial cell-mediated repair, highlighting a potential role for circulating bone-marrow derived cells (i.e. EPCs) in a process akin to post-natal vasculogenesis [154, 155]. This has in turn been disputed recently by other authors, who have concluded from murine experiments that EPCs do not permanently incorporate into injured endothelium and that the aforementioned traditional mechanism is the sole contributor to healing [156]. Whilst the overall suggestion is that EPCs are probably not directly involved in repair, these findings do not rule out a "bystander" role by way of paracrine stimulation of local endothelial regenerative mechanisms.

Vascular repair is an important area of study in the specific context of the cardiovascular risk associated with diabetes and insulin resistance [157]. In humans with diabetes, percutaneous coronary intervention (PCI) is associated with less promising outcomes due to re-endothelialisation in the stented segment: a study using intravascular ultrasound demonstrated that exaggerated intimal hyperplasia can contribute to this phenomenon [158]. This may be related to insulin resistance: obese Zucker rats exhibit

increased neointimal hyperplasia after balloon arterial injury compared with lean counterparts [151]. Importantly, two separate studies failed to recreate the same phenotype in rats rendered diabetic in an insulin-deficient fashion with streptozotocin, implicating hyperinsulinaemia (rather than hyperglycaemia) as a possible aetiological factor in the process [151, 159]. Similarly, Sprague Dawley rats (with no inherent metabolic derangements) infused with subcutaneous insulin developed pathological remodelling after balloon injury to the aorta and carotid arteries, unlike control animals who received no insulin [150]. These findings are in contrast to those of Breen *et al*, who instead propose a protective role for insulin in various studies of arterial injury in rats [160-162]; in their experiments, neointimal hyperplasia was reduced in rats exposed to more insulin, while re-endothelialisation of injured segments was augmented. In the last of these three studies, the beneficial effect of insulin was shown to be dependent on eNOS and nitric oxide through infusion of the NOS inhibitor L-NMMA [162]. The discrepancies between this group's work and the studies implicating insulin in pathological remodelling may arise from differential techniques for inducing hyperinsulinaemia, and the fact that circulating insulin concentrations in the animals concerned may not have been consistent between experiments.

Studies of carotid arterial injury in diabetic mice demonstrate that vascular repair mechanisms can be impaired in this pathological setting; importantly, the insulin resistant spectrum also appears to result in *in vitro* and *in vivo* EPC dysfunction [163]. Similarly, our laboratory's work has shown diminished re-endothelialisation after femoral artery wire injury in IRKO mice compared with WT littermates, demonstrating that even relatively mild insulin resistance can be associated with a significantly impaired repair phenotype in the context of essentially normal glucoregulation [164]. Interestingly, numbers of circulating and culture-derived EPCs (which will be defined in more detail below) were reduced in IRKO mice in this study, and the mobilisation of these cells to intraperitoneal VEGF administration was also

blunted. Finally, transfusion of c-kit-positive cells (with a putative EPC phenotype) from WT mice restored IRKO vascular healing to WT levels, whilst IRKO-derived c-kit-positive cells provided partial recovery. These findings suggest that, even if EPCs are not of crucial importance in health, their dysfunction is prominent in the setting of insulin resistance and contributes to diminished endothelial repair. Our group's work in insulin resistant (but otherwise healthy) South Asian men has also shown impaired progenitor cell mobilisation compared with white European control males [165]. Taking these studies together, it is tempting to speculate that insulin resistance, even at the milder end of the spectrum, is associated with impaired endothelial repair which is likely to involve, at least in part, a defect in EPC quantity and function. These issues will now be discussed in more depth.

1.4.3 **Endothelial Progenitor Cells**

In 1997, a group from Boston hypothesised that haematopoietic and endothelial cells shared a common stem cell precursor that could differentiate into either cell type [141]. They selected a shared cell surface antigen [cluster of differentiation (CD)34 or VEGF receptor 2 (VEGFR2)] that would be typical of mature endothelial cells but that would disappear on maturation to haematopoietic lineage. Cells with this phenotype could be isolated from human peripheral blood using magnetic bead separation and, when cultured *in vitro*, developed an antigen profile overlapping with human umbilical vein endothelial cells (HUVEC). Furthermore, the cells could form tube-like structures on fibronectin-coated culture plates. Finally, these cells were labelled and injected into athymic mice that had undergone hind-limb ischaemia after unilateral femoral artery excision. It was found that labelled cells had incorporated into new vessel walls, identifying a potential role in angiogenesis both *in vitro* and *in vivo*. These cultured cells were later termed EPCs and it was postulated by other authors that they were able to promote vascular repair and/or regeneration in humans [142]. Clinical studies have also shown that reduced numbers of circulating cells bearing
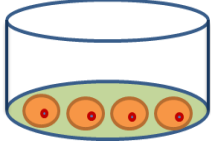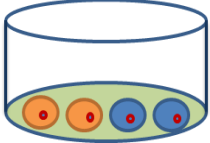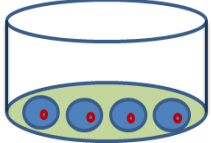
the progenitor markers the Boston group selected for (determined using flow cytometry) correlate with cardiovascular death [166]. The definition of these circulating entities has evolved over time and current understanding is that they co-express CD34, CD133 and VEGF receptor 2, or kinase domain receptor (KDR); an antigen profile that may distinguish them from both haematopoietic cells and from mature endothelial cells [138]. Their biology is also altered in insulin resistance: in the aforementioned study of femoral artery injury in IRKO mice, a murine equivalent of these cells (Sca1$^+$Flk1$^+$) was reduced in abundance and mobilisation potential in the IRKO group [164]. For the remainder of this thesis, this particular EPC subset, as defined by flow cytometry, will be referred to as circulating progenitor cells (CPC).

Various subsets of EPCs have also been described *in vitro* using variants of the originally described cell culture conditions [138]. Using density-gradient centrifugation of whole blood, homogenised spleen or bone marrow, a mononuclear cell fraction can be isolated and cultured in endothelial growth medium [167]. Over four to seven days, these cells differentiate into early-outgrowth EPCs (EEPCs) that retain a monocyte/macrophage phenotype and have limited capacity for proliferation or incorporation into neovessels [167]. However, they do express some endothelial cell markers such as CD31 and VEGFR2. It is now recognised that these cells were described in the seminal report of Asahara *et al* above [141]. A role for EEPCs in the paracrine modulation of angiogenesis has been suggested: for example, endothelial growth medium conditioned in spleen-derived EEPCs has been shown to augment tube formation in human umbilical vein endothelial cells (HUVECs), with a reduction in this angiogenic capacity seen in IRKO-derived EEPC medium [164]. With a subtle alteration in initial cell culture, a different subset of circulating mononuclear cells differentiates into colony forming units (EPC-CFUs, or CFU-Hill cells), which show characteristics typical of T-lymphocytes [138]. These behave similarly to EEPCs in that they may indirectly exert positive paracrine effects on vascular repair but appear not to incorporate themselves into new endothelium. Human studies have

shown that the abundance of these EPC-CFUs inversely correlates with Framingham risk score and endothelial vasomotor function [168].

After prolonged culture (up to twenty-one days), a third EPC phenotype is observed: the late-outgrowth EPC (LEPC) [138]. These are morphologically similar to mature endothelial cells, expressing essentially the same antigen profile, while they do not ingest bacteria, suggesting a divergence from the monocyte/macrophage phenotype seen in earlier EPCs. LEPC have the capacity to form capillaries in a VEGF-dependent manner when infused *in vivo*, and display significant proliferative potential with a clear progenitor hierarchy. An important caveat in the study of these cells is that they are a culture-derived entity that may or may not bear resemblance to circulating progenitor cells that have been studied in whole blood; as with all EPCs, this brings their endogenous relevance into question. However, LEPCs are of particular interest because they offer a model for *in vitro* study of neovascularisation and may represent a future autologous cell-based cardiovascular repair therapy.

The different subsets of EPC can be easily confused and nomenclature in the literature is inconsistent. For this reason, their characteristics are compared and contrasted in Table 1-1.

	CPC	CFU-Hill	Early Outgrowth EPC	Late Outgrowth EPC
Isolation Technique				
Derivation Technique	Flow cytometry			
Morphology in Culture	N/A	Spindle shaped cells cluster at day 4-9	No colony formation	Cobblestone shaped colonies at day 7-21
Defining Features	Cell surface expression of CD34, CD133, VEGFR2	Ability to form colonies in culture	Uptake of acetylated LDL and *Ulex europeaus* lectin	Classical endothelial cell surface markers and progenitor hierarchy in single cells
Angiogenic Potential	Form capillary-like structures *in vitro* with unclear role *in vivo*	No spontaneous neovessels formation; may have paracrine effects	No spontaneous neovessels formation; may have paracrine effects	Can form capillary-like structures *in vitro* and aid vascular repair *in vivo*

Table 1-1   Comparison of Endothelial Progenitor Cell Subsets

Not to scale. Blue-topped tube with antibody/fluorochrome denotes flow cytometric cell isolation, while orange-topped tubes denote density gradient centrifugation as isolation method, with culture of cells in buffy layer (in grey). Orange cells represent selection of non-adherent population after

seeding on fibronectin-coated plates; blue cells denote those that remain adherent. EPC = endothelial progenitor cell; CFU = colony forming unit; CPC = circulating progenitor cell; CD = cluster of differentiation; VEGFR = vascular endothelial growth factor receptor; LDL = low density lipoprotein. Data assimilated from Hirschi et al *[167] and Cubbon* et al *[138].*

1.4.4 Endothelial Progenitor Cells in Insulin Resistance

Several studies have assessed the role of progenitor cells in the response to vascular injury, in addition to work from our laboratory group described above [164]. Working on the basic paradigm that these cells are manufactured in the bone marrow and mobilise to sites of injury, there are various steps during which the multiple deleterious effects of insulin resistance can influence indices of EPC behaviour.

Hyperglycaemia in itself can hinder EPC function, as evidenced by *in vitro* experiments and assays using umbilical cord blood from human diabetic pregnancies [169]. Furthermore, exposing peripheral blood from healthy volunteers, patients with diabetes and those with coronary artery disease to high glucose concentrations affects EPC abundance in a manner related to increased MAPK pathway activation [170]. Similarly, cultured early and late outgrowth EPCs from healthy volunteers have been demonstrated to undergo senescence and display reduced proliferative and migratory capacity after exposure to glucose *in vitro*, with concomitant reductions in phosphorylated Akt, FOXO and eNOS, implicating the PI3K insulin signalling pathway [171]. Patients with type I diabetes also show reduced abundance of CPCs, as determined by flow cytometry, than healthy counterparts [172], with concomitant reductions in flow-mediated vasodilation. Although these studies vary widely in methodology, they attempt to separate the effects of hyperglycaemia from those of insulin resistance and, in doing so, provide some evidence to suggest a contributory role for elevated glucose concentrations in EPC dysfunction.

Work from our laboratory has provided some evidence implicating insulin resistance, in the absence of frank hyperglycaemia, in EPC dysfunction, as previously discussed [164, 165, 173]. In brief, murine insulin resistance results in diminished vascular repair associated with reduced abundance of both CPCs and culture-derived blood EPCs compared with WT mice; in

these experiments, there was reduced CPC mobilisation to parenteral VEGF administration, as well as an absence of eNOS in bone marrow lysates, potentially highlighting a mechanism underlying the failure to mobilise progenitors to sites of injury [164]. Human studies involving insulin-resistant (but otherwise healthy) South Asian men showed that NO is critical in the mobilisation of CPCs in the response to exercise [165], and that cultured LEPCs from a similar population display impaired vascular repair potential related to reduced Akt signalling [173]. In the latter study, re-endothelialisation after femoral artery wire injury in mice could be enhanced with transfusion of EPCs from healthy white Europeans but not from South Asians, a deficit which could be reversed by expressing a constitutively active form of Akt in the South Asian EPCs [173]. The PI3K insulin signalling cascade, again, appears to be critical in the dysfunction noted in insulin resistant states. In addition to the above studies, work in obese and insulin-resistant Zucker rats has shown diminished Akt phosphorylation in EEPCs exposed to tumour necrosis factor-alpha (TNF-α), with an increased propensity to apoptosis in these cells [174]. Interestingly, these authors were able to correlate this defect with vascular repair: when the poorly functioning EPCs were treated with a nuclear factor kappa B (NF-κB) inhibitor and transfused into rats post-angioplasty, they were able to reduce pathological neointimal hyperplasia in the injured segments.

The involvement of TNF-α and NF-κB in EPC dysfunction is not entirely surprising, considering that insulin resistance is closely linked with chronically overactivated indices of inflammation [138]. Other acute phase proteins, such as C-reactive protein (CRP), have also been implicated: EPCs incubated with CRP *in vitro* were shown to become prone to oxidative stress and apoptosis, with impaired endogenous antioxidant activity [175]. A similar study found increased EPC apoptosis when these cells were cultured in the presence of CRP; in keeping with previous findings regarding the PI3K pathway, this phenomenon was eNOS dependent. Interestingly, this exposure to CRP was also associated with reduced expression of

endothelial markers like VE-cadherin and Tie-2, suggesting a relative failure of differentiation towards an endothelial cell-like phenotype [176]. This group also found impaired EPC-induced angiogenesis in Matrigel assays, suggesting that the phenotypic changes observed are likely to be relevant to vascular regeneration.

Other features of the insulin resistant syndrome may be relevant in EPC function. For example, insulin resistance is associated with lower serum levels of adiponectin, a cytokine derived from adipose tissue (or adipokine) in health. Adiponectin can stimulate EEPC differentiation towards an endothelial phenotype and inhibit EPC senescence, as well as augmenting Akt and eNOS activation in a hyperglycaemic environment, suggesting a protective effect on progenitor function that may be blunted or lost in insulin resistance [138]. Conversely, leptin and visfatin are examples of adipokines found in higher concentrations in insulin resistant states and which may have deleterious effects on EPC function; in the case of the latter, the mechanism may be NF-κB-dependent, again hinting at an overlapping role for inflammation [177]. Finally, the hypertension and dyslipidaemia that form part of the metabolic syndrome can also contribute. For example, oxidised LDL can promote EPC apoptosis by interfering with Akt signalling, and CPC abundance has been shown to correlate directly with HDL and inversely with LDL cholesterol levels in serum [138]. Equally, angiotensin II disturbs EPC function *in vitro* and can inhibit arterial repair in mice after carotid injury, a deficit that was shown to be rescued by transfusing EEPCs with angiotensin receptor 1 knockout [178].

Despite all the above data, it is still not entirely clear how much EPCs contribute to vascular repair after endothelial injury, if at all. The culture-derived entities described may not exist in identical form *in vivo* and, whilst the flow cytometric definitions of CPCs do represent cells that are present in mammalian blood, their exact physiological role is yet to be ascertained. Some convincing evidence exists to suggest that endothelial cells are the

predominant contributors to vascular repair after injury [156]; however, even if EPCs do not directly incorporate themselves into injured vasculature, they may play a role in paracrine stimulation of endothelial cell-mediated healing and thus remain of interest. Their dysfunction has been recurrently demonstrated in insulin resistant humans and animal models and they may therefore represent a novel therapeutic target for vascular health in insulin resistance. Given the promising results seen in murine studies of EPC transfusion, it may be feasible for EPCs to be developed as an autologous cell-based therapy in the future.

1.4.5 Role of Endothelial Insulin Sensitivity in Vascular Repair

Studies of endothelial function and vascular repair using the IRKO model are of great interest as they allow us to differentiate between the effects of insulin resistance *per se* and hyperglycaemia. However, given that the endothelium is an insulin-responsive organ, one of the limitations of whole-body insulin receptor knockout is the potential for the observed effects to be mediated by dysfunction in other tissues.

To date, models such as the VENIRKO and ESMIRO, which are endothelium-specific, have suggested that dysfunction of this tissue alone can result in a similar phenotype to whole-body insulin resistant models [113, 114]. This has led to interest in the possibility that enhancing insulin sensitivity specifically within the endothelium may be beneficial in addressing the cardiovascular sequelae of global insulin resistance. To address the value of this therapeutic paradigm, our laboratory has generated a murine model that overexpresses a human insulin receptor specifically on endothelial cells: the HIRECO mouse. This model makes use of the Tie-2 promoter-enhancer, which codes for an angiopoietin tyrosine kinase receptor that shows relative specificity for endothelial cells (expression is also noted in a subset of myeloid cells) and a degree of asymmetry for arterial over venous endothelium [179]. Unpublished data from our laboratory have

confirmed the nature of endothelium-specific overexpression of the human insulin receptor but, interestingly, we have demonstrated that this results in reduced NO bioavailability, endothelial dysfunction and accelerated atherosclerosis. HIRECO mice display increased expression of the NOX2 isoform of NADPH oxidase, and also elevated superoxide generation, versus wild-type controls; additionally, expression of proline-rich tyrosine kinase (PYK2) was higher in HIRECO endothelial cells, with concomitant inhibitory phosphorylation of eNOS [180].

Whilst these data suggest endothelial insulin sensitisation in the context of otherwise undisturbed whole-body insulin signalling is deleterious, there remains a possibility that this manipulation could rescue the vascular phenotype associated with systemic insulin resistance. In order to investigate this, we have crossed the HIRECO mouse with IRKO to generate offspring with systemic insulin resistance, but rescue of endothelial insulin sensitivity. This work will form the basis of this PhD thesis.

Chapter 2 **Aims and Hypotheses**

The aim of this project was to expand on data from existing animal models of insulin resistance by ascertaining whether endothelial insulin sensitisation is a valid therapeutic target. In order to address this, our laboratory generated a colony of mice that includes the HIRECOxIRKO cross, which we anticipate to be globally insulin resistant, but with selective restoration of endothelial insulin signalling due to the targeted expression of a human insulin receptor transgene in endothelial cells.

Specifically, I aimed to assess the impact of this manipulation by:

1. Investigating the morphological and metabolic characteristics of HIRECOxIRKO mice as compared with IRKO littermates.

2. Interrogating murine and human insulin receptor expression in endothelial cells from both groups.

3. Assessing whether HIRECOxIRKO mice display improved vascular repair after denuding endothelial injury.

4. Comparing the numbers and function of endothelial progenitor cells across genotypes.

5. Studying endothelial function in the HIRECOxIRKO cross using organ bath assays of aortic vasomotor function and nitric oxide bioavailability.

6. Using assays of eNOS activity, reactive oxygen species, intracellular signalling and markers of endothelial cell function *in vitro* to ascertain a mechanism for any differences that are observed.

Using these methods, I sought to examine the following hypotheses:

1. Selective restoration of endothelial insulin signalling can result in normalisation of blood pressure and vasomotor function.

2. HIRECOxIRKO mice exhibit improved vascular repair after denuding femoral artery injury.

Chapter 3 **Materials**

3.1 Animal Husbandry

- Chow feed   B&K Universal Ltd.; Hull, UK

3.2 Genotyping

- Sodium hydroxide   Fisher; Loughborough, UK
- Tris-HCl   Fisher; Loughborough, UK
- Molecular grade H_2O BD Biosciences; Nottingham, UK

- Biomix Red "Mastermix"   Bioline; London, UK
- Primers (see Methods)   Invitrogen; Carlsbad, CA
- Tris base   Fisher; Loughborough, UK
- EDTA   Sigma-Aldrich; St Louis, MO
- PCR reaction tubes/lids   Thermo Scientific; Rockford, IL

- PTC-200 Thermal Cycler   MJ Research; Ramsey, MN
- Agarose   Bioline; London, UK
- Glacial acetic acid   Fisher; Loughborough, UK
- Ethidium bromide   Sigma-Aldrich; St Louis, MO
- 100 base pair ladder   Thermo Scientific; Rockford
- Syngene G-box imaging system   Syngene; Cambridge, UK

3.3 Gross Morphological Measurements

- Microcentrifuge tubes   Eppendorf; Stevenage, UK

3.4 Glucocompetence Testing

- Accucheck glucometer/test strips   Aviva; Mannheim, Germany
- D-glucose   Sigma; St Louis, MO
- Actrapid insulin   Novo Nordisk; Bagsvaerd, Denmark
- Dulbecco's phosphate-buffered Saline (PBS)   Sigma; St Louis, MO

3.5 Blood Pressure Measurement

- Coda Non-invasive Tail BP system   Kent Scientific; Torrington, CT

3.6 Blood Sampling from Saphenous Vein Puncture

- Veet hair removal cream   Reckitt-Benckiser; Slough, UK
- Vaseline® Paraffin-based ointment   Unilever; Leatherhead, UK
- 14G needle   Terumo; Bagshot, UK
- Microvette tubes (powdered lithium heparin)   Sarstedt; Numbrecht, Germany
- Microvette (EDTA-tripotassium)   Sarstedt; Numbrecht
- Liquid heparin sodium   Wockhardt; Wrexham, UK

3.7 Plasma Insulin Measurement (ELISA)

- Ultrasensitive mouse insulin ELISA kit (#90080)   Crystal Chem; Downers Grove, IL
- Dynex MRX plate reader and Revelation v4.21   Dynex Technologies, Chantilly, VA

3.8 Quantitative PCR

•	Tissue Lyser	Qiagen; Venlo, Netherlands
•	6mm cone balls (RS.22.455.0003C)	Retsch; Castleford, UK
•	RNAse Away spray	Molecular Bio Products; San Diego
•	TRIzol® (Tri reagent)	Sigma; St Louis, MO
•	Phenol chloroform	Sigma; St Louis, MO
•	Isopropanol	Sigma; St Louis, MO
•	Ethanol	Fisher; Loughborough, UK
•	RNAse free H_2O	Life Technologies; Paisley
•	NanoDrop® ND1000 Spectrophotometer	Thermo Scientific; Rockford
•	ND-1000 v3.1 software	Thermo Scientific; Rockford
•	High capacity cDNA reverse transcription kit	Applied Biosystems; Warrington, UK
•	96 well optical reaction plate	Applied Biosystems
•	ABI Prism 7900 HT PCR cycler	Applied Biosystems
•	SDS v2.2 software	Applied Biosystems
•	RT-PCR primers (SYBR green)	Invitrogen; Carlsbad, CA
•	Power SYBR® green PCR Mastermix	Applied Biosystems
•	Taqman® Gene Expression Mastermix	Applied Biosystems
•	RT-PCR primers (Taqman®)	Applied Biosystems
•	Molecular grade H_2O	BD Biosciences; Nottingham

3.9 Vascular Injury

•	Buprenorphine	Alsatoe Animal Health; York, UK
•	Isoflurane	Abbott Logistics BV; Short

	Hills, NJ
• Irripod (sterile 0.9% saline)	Unither; Paris, France
• Lignol (1% lignocaine + adrenaline)	Arnolds; Harlescott, UK
• Dissecting microscope OPMI 1-FC	Zeiss; Livingston, UK
• Veet hair removal cream	Reckitt-Benckiser; Slough
• 0.75% providone-iodine	Animal Care; York, UK
• Vicryl absorbable 8.0/6.0 suture	Ethicon; Somerville, NJ
• Iris Scissors and needle holder	World Precision Instruments; Sarasota, FL
• Dry sterilizer #500121	World Precision Instruments
• Lubrital #31329	Dechra; Northwich, UK
• Vannas spring scissors	Fine Science Tools; Heidelberg, Germany
• Dumont micro-blunted, atraumatic tipped forceps #11253-25	Fine Science Tools
• Round handled suture tying forceps	Fine Science Tools
• Hitorque Cross-it 200XT guide wire	Abbott Vascular; IL
• Evans Blue #195550050	Acros Organics; Geel, Belgium
• 4% paraformaldehyde	Fisher; Loughborough, UK
• 30% hydrogen peroxide	Sigma; St Louis, MO
• Insulin syringe / 27Gx13mm needle	Terumo; Bagshot, UK
• Olympus Dissecting Stereo Microscope SZ61	Olympus; Southend-on-Sea, UK
• QiCam Olympus digital camera	Olympus; Southend-on-Sea
• ImagePro Plus 7.2	Media Cybernetics; Bethesda, MD

3.10 Enumeration of Circulating Progenitor Cells (CPCs)

• Heparin 1000IU/mL	Wockhardt; Wrexham, UK

• Microvette (EDTA-tripotassium)	Sarstedt; Numbrecht
• Pharmlyse red cell lysis buffer	BD Biosciences; Nottingham
• Syringe filter (0.2µm membrane)	Pall Life Science; Portsmouth, UK
• Corning centrifuge tubes	Sigma; St Louis, MO
• Foetal bovine serum (FBS)	Biosera; Boussens, France
• Bovine serum albumin (BSA)	Sigma; St Louis, MO
• Fc block (CD16/CD32 rat anti-mouse; 553142)	BD Biosciences; Nottingham
• FITC (rat IgG2a Isotype Control; 553929)	BD Biosciences; Nottingham
• Sca1-FITC (rat IgG2a κ Ly6A/E; 557405)	BD Biosciences; Nottingham
• PE rat (IgG2a κ Isotype Control; 553930)	BD Biosciences; Nottingham
• Flk1-PE (Flk1 VEGFR2; 555308)	BD Biosciences; Nottingham
• APC (rat IgG2b κ Isotype Control; 553991)	BD Biosciences; Nottingham
• APC (rat anti-mouse CD117; 553356)	BD Biosciences; Nottingham
• Fortessa Flow Cytometer	BD Biosciences; Nottingham

3.11 Isolation and Enumeration of Early Outgrowth EPCs

• Insulin syringe / 29Gx13mm needle	Terumo; Bagshot, UK
• Sodium citrate from 4mL blood collection tubes	Greiner Bio-One; Kremsmünster, Austria
• 4mL EDTA blood tube	Greiner Bio-one
• 23G needle	Terumo; Bagshot, UK
• 70µm nylon cell strainer	Greiner Bio-one
• 5cm Petri dish	BD Falcon; Oxford, UK
• Histopaque-1083	Sigma; St Louis, MO

- EGM-2 basal medium/bullet kit — Lonza; Blackley, UK
- Foetal bovine serum — Biosera; Boussens, France
- Antibiotic/antimycotic supplement — Invitrogen; Carlsbad, CA
- Trypan blue — Sigma; St Louis, MO
- Neubauer Counting Chamber — Hawksley; Lancing, UK
- 24-well/6-well fibronectin coated cell culture plates — BD Biocoat; Redford, MA
- Dil-ac-LDL — Life Technologies; Paisley, UK
- FITC-lectin — Sigma; St Louis, MO
- CKX-41 fluorescent microscope — Olympus; Southend-on-Sea
- Cell B software — Olympus; Southend-on-Sea
- Image J v1.46r — National Institutes of Health

3.12 Isolation and Culture of Pulmonary Endothelial Cells

- Scalpel blades size 22 — Swann-Morton; Sheffield, UK
- Dulbecco's Modified Eagle's Medium (31966-021) — Life Technologies; Paisley
- Hank's Balanced Salt Solution (with calcium/magnesium; H9269) — Sigma; St Louis, MO
- Collagenase/Dispase #11097113001 — Roche; Basel, Switzerland
- Bovine skin gelatin — Sigma; St Louis, MO
- Bovine serum albumin 7.5% — Sigma; St Louis, MO
- MACSmix^{TM} tube rotator — Miltenyi Biotec; Cologne, Germany
- 14G Cannula — BD Biosciences; Nottingham
- 10mL syringe — BD Biosciences; Nottingham
- Endothelial cell growth medium MV2 plus endothelial supplements — PromoCell; Heidelberg, Germany
- Foetal bovine serum — Biosera; Boussens, France

- Antibiotic/antimycotic supplement   Invitrogen; Carlsbad, CA
- Rat anti-mouse CD31 (553369)   BD Biosciences; Nottingham
- Rat anti-mouse CD102 (553326)   BD Biosciences; Nottingham
- Sheep anti-rat IgG Dynabeads   Life Technologies; Paisley
- Magnetic particle concentrator   BD Biosciences; Nottingham
- T25 Corning® cell culture flask   Sigma; St Louis, MO
- Trypsin-EDTA 0.25%   Sigma; St Louis, MO
- 35mm imaging μ-dish   Ibidi; Martinsried, Germany
- Triton X-100   Sigma; St Louis, MO
- 4% paraformaldehyde   Fisher; Loughborough, UK
- Isolectin B4-Alexa Fluor 488 (I21411)   Invitrogen; Carlsbad, CA
- Hoechst 33342 (#H1399)   Invitrogen; Carlsbad, CA
- LSM700 confocal microscope   Zeiss; Livingston, UK

3.13 Endothelial Cell Proliferation Assay

- Click-iT® EdU Alexa Fluor® 488   Life Technologies; Paisley
  Imaging Kit (#C10337)
- Propidium iodide/RNAse   Cell Signaling; Danvers, MA

3.14 Endothelial Cell Migration Assay (Boyden Chamber)

- Recombinant murine vascular   Peprotech; London, UK
  endothelial growth factor A 165
- Polycarbonate Boyden chamber   Scientific Lab Supplies;
  inserts (8μm pore size)   Hessle, UK
- 24 well plastic culture vessels   BD Falcon; Oxford, UK
- Haematoxylin/Eosin   Sigma; St Louis, MO

3.15 Endothelial Cell Migration Assay (Scratch Wound)

- ImageLock 96 well plate   Essen Biosciences; Ann Arbor, MI
- Woundmaker^{TM} 96-pin tool   Essen Biosciences
- Integrated Cell Migration Analysis Module (9600-0012)   Essen Biosciences
- IncuCyte^{TM} Imaging System   Essen Biosciences
- Alconox/Vircon cleaning solutions   Sigma; St Louis, MO

3.16 Vasomotor Studies of Aortic Rings

- 8-chamber organ bath system   Panlab; San Diego, CA
- LabChart Pro Software   Panlab; San Diego, CA
- Light microscope Olympus SZ61   Olympus; Southend-on-Sea,
- Sodium chloride   Fisher; Loughborough, UK
- Potassium chloride   Fisher; Loughborough, UK
- Monopotassium phosphate   Fisher; Loughborough, UK
- Sodium hydrogen carbonate   Fisher; Loughborough, UK
- Magnesium sulphate heptahydrate   VWR®; Lutterworth, UK
- Calcium chloride   Fisher; Loughborough, UK
- D-glucose   Sigma; St Louis, MO
- Phenylephrine   Sigma; St Louis, MO
- Acetylcholine   Sigma; St Louis, MO
- Sodium nitroprusside   Sigma; St Louis, MO
- Actrapid insulin (100mU/L)   Novo Nordisk; Bagsvaerd
- L-NMMA   Merck Millipore; Darmstadt, Germany

3.17 Superoxide Assay

- Clear 96 well cell culture plate   Thermo Scientific; Rockford
- Dihydroethidium D11347   Life Technologies; Paisley
- HEPES sodium salt   Sigma; St Louis, MO
- Flex Station 3 Multi-mode   Molecular Devices;
  Microplate Reader   Sunnyvale, CA
- SoftMax® Pro v5.4.5   Molecular Devices

3.18 Western Blotting

- Tris-HCl   Fisher; Loughborough, UK
- Glycerol   Sigma; St Louis, MO
- EDTA   Sigma; St Louis, MO
- Sodium dodecyl sulphate   Sigma; St Louis, MO

- Phosphatase inhibitors 2&3   Sigma; St Louis, MO
- Tween®-20   Sigma; St Louis, MO
- Bovine serum albumin (BSA)   Sigma; St Louis, MO
- Pierce® BCA protein assay kit   Thermo Scientific; Rockford
- 96 well clear microplate   Greiner Bio-One
- Micro-amp® optical adhesive film   Life Technologies; Paisley
- NuPAGE® LDS sample buffer   Invitrogen; Carlsbad, CA
- NuPAGE® sample reducing agent   Invitrogen; Carlsbad, CA
- NuPAGE® MES SDS running buffer   Invitrogen; Carlsbad, CA
- Criterion XT 4-12% Bis-Tris Gel   Bio-Rad Laboratories;
                                          Hercules, CA
- Criterion Cell Tank   Bio-Rad Laboratories

- Amersham Tracker Tape (#RPN2050)   GE Healthcare; Little
                                          Chalfont, UK

- Primary antibodies (Table 4-12)   Cell Signaling; Danvers, MA

  BD Biosciences; Nottingham

- Secondary antibodies (Table 4-12)   Dako; Ely, UK

- Immobilon Western Chemiluminescent   Merck Millipore; Darmstadt
  HRP Substrate

- Immobilon®-P transfer membrane   Merck Millipore; Darmstadt

- Syngene G-box imaging system   Syngene; Cambridge, UK

- Restore^{TM} PLUS Western Blot   Thermo Scientific; Rockford
  stripping buffer

- Dynex MRX plate reader and   Dynex Technologies
  Revelation v4.21

- Image J v1.46r   National Institutes of Health

Chapter 4 **Methods**

4.1 Animal Husbandry

4.1.1 General

All murine work was undertaken under the auspices of the Experimental Animals (Scientific Procedures) Act 1988 as per United Kingdom Home Office regulations. This was performed under personal licence 40/10387 and project licence 40/3523. Mice were housed at the University of Leeds animal facility, under standard laboratory temperature and humidity conditions and a 12-hour light-dark cycle. They were fed standard chow diet and normal drinking water, both unrestricted. Mice were weaned and underwent ear notching 2-3 weeks after birth to provide a means of identification and also to provide tissue with which to perform genotyping. Males and females were split at this stage and generally females were sacrificed after weaning, unless required for the establishment of new breeding colonies. Females were not used in experiments for a number of reasons: for example, the use of females may introduce confounding effects from cyclical variation in female sex hormones. More importantly, the Hprt locus (see below) used in this model is on the X chromosome and so the effects of Lyonisation in heterozygotes and double transgene expression in homozygotes could cause variability in the data. Male littermates were split into cages of up to five mice each. Mice aged 2-6 months were used for the majority of experiments and work was planned to avoid leaving animals alone in cages.

4.1.2 Insulin receptor knockout (IRKO) mice

Mice with haploinsufficiency of the insulin receptor were used as the principal control group for this project as their phenotype with respect to endothelial function and vascular repair and regeneration has previously been studied extensively [60, 123, 164].

IRKO mice were initially developed at the National Institutes of Health, Bethesda, USA [57]. Briefly, the insulin receptor gene was targeted using a vector that incorporated a premature chain termination at exon 4, in association with a cassette encoding neomycin resistance. Embryonic stem (ES) cells were transfected with this mutant allele using electroporation and the gene incorporated using homologous recombination. ES cells were grown in the presence of neomycin, allowing selection for the mutated allele; surviving cells were expanded prior to injection into mouse embryos at day 3.5. See Figure 4-1 for a diagrammatic summary of this process.
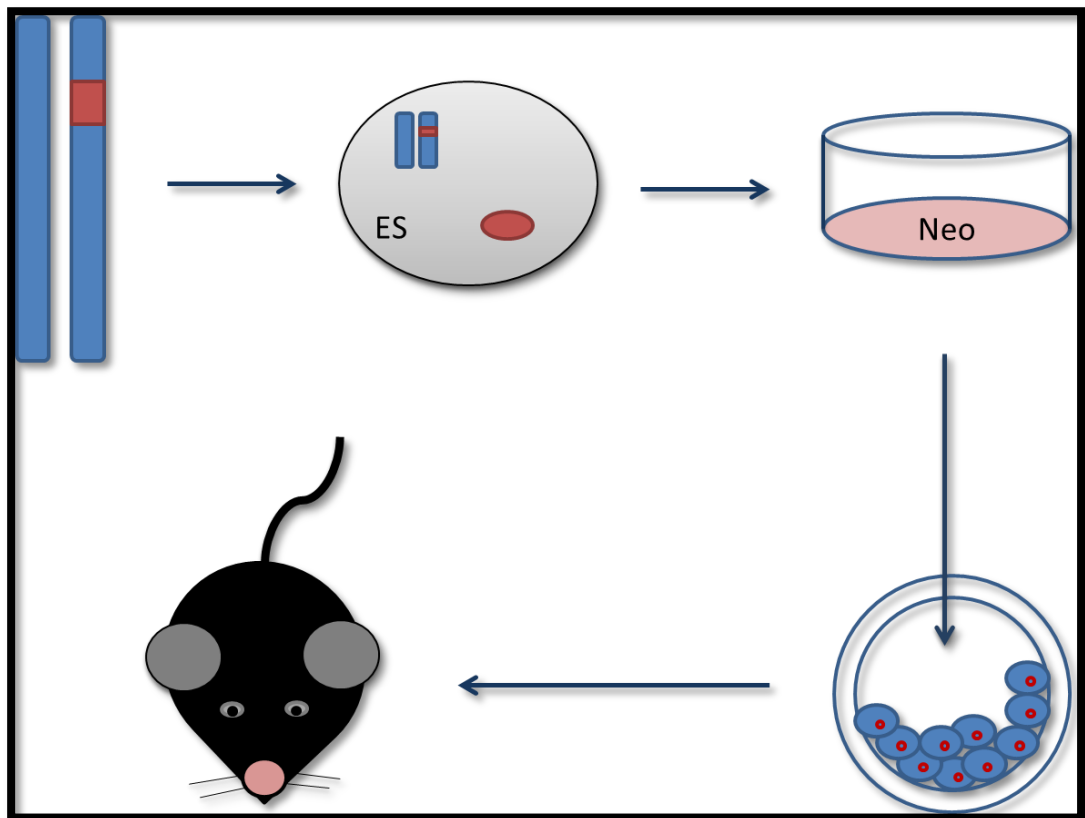
Figure 4-1   Technique for Introducing Mutant Insulin Receptor Allele
The red allele represents the null insulin receptor allele and neomycin (Neo) resistance cassette introduced into chromosome 8. This is transfected into embryonic stem (ES) cells which are selected using neomycin (Neo) before injection into a blastocyst for implantation into a C57 black 6 female.

These embryos were implanted into dark-coated female C57 black 6 (C57BL/6) mice, resulting in chimaeric progeny that could be identified using coat colour. Resulting chimaeric males expressing the null allele were bred into a C57 black-6 (C57BL/6) background. Mice receiving both null alleles, and thus homozygous for IR deletion, do not survive beyond early neonatal life due to profound diabetic ketoacidosis [57], but heterozygotes are viable and can thus be used for research.

IRKO mice were initially generated externally and purchased from Jackson laboratory stocks, following which they were bred with C57BL/6 females from our own colonies at the University of Leeds for 12 generations. This avoided any need for genetic manipulation at this site. All the mice used in this project were obtained from breeding colonies already established at this site. The local IRKO breeding trios comprise two C57BL/6 females with one transgenic IRKO male.

4.1.3 Human insulin receptor endothelial cell over-expression (HIRECO)

In order to enhance endothelial insulin sensitivity, the type A isoform of the human insulin receptor was overexpressed selectively in endothelial cells under transcriptional control of the Tie-2 promoter-enhancer sequence, which is regarded as being relatively specific for endothelial cell lineage [179]. Human insulin receptor complementary DNA was obtained from the National Institutes of Health (Bethesda, USA) and this gene, along with the Tie-2 promoter, a polyadenylation site and a core enhancer, was inserted into the hypoxanthine phosphoribosyl transferase (Hprt) locus in embryonic stem cells using a specific homologous recombination technology known as "Quick Knock-in[TM]" (GenOway; Lyon, France) [181]. The Hprt protein that the target gene encodes is an enzyme that synthesises purines from degraded nucleotides in what is known as the "salvage pathway". ES cells containing the Hprt locus can be selected from a wider population using

growth medium containing aminopterin as Hprt-deleted cell lines rely on the alternative "*de novo*" purine synthesis pathway in the presence of this drug. For this reason, ES cells were cultured in hypoxanthine, aminopterin and thymidine (HAT) medium and therefore only those cells expressing the human insulin receptor construct in the Hprt locus survived. Appropriate transgene expression was confirmed using Southern blotting and surviving ES cells expressing the transgene were then injected into blastocysts that were implanted into C57BL/6 surrogate mothers prior to breeding in a similar manner to that described for IRKO mice. For a summary, see Figure 4-2.

By virtue of the Hprt approach utilised, male mice exhibiting expression of the transgene were hemizygous for the manipulaton. Females expressing the HIRECO transgene were bred with wild-type males in trios comprising one female and two males. Established colonies at the University of Leeds were used for all experiments in this project, obviating the need for genetic manipulation by the author.
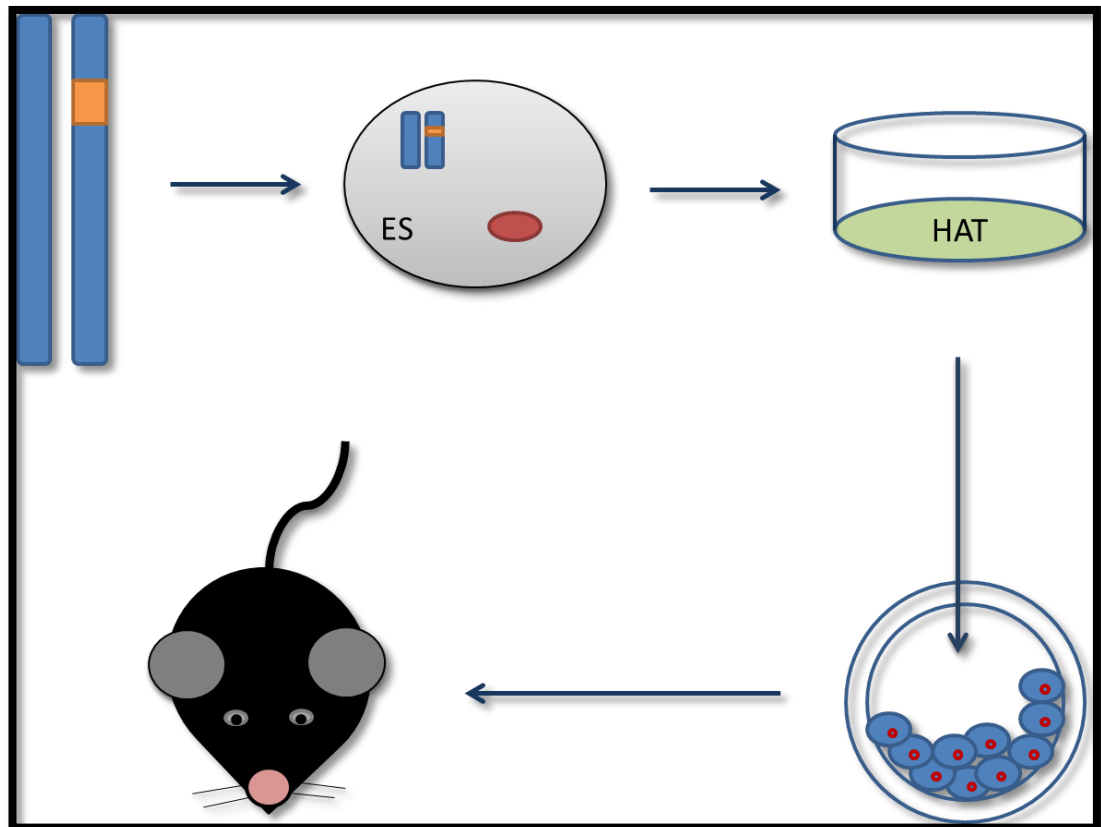
Figure 4-2   Technique for Introducing Human Insulin Receptor Transgene

The orange gene represents the transgene in association with the Tie2 promoter, introduced into chromosome X. This is transfected into embryonic stem (ES) cells which are selected using media containing hypoxanthine, aminopterin and thymidine (HAT) before injection into a blastocyst for implantation into a C57 black 6 female.

4.1.4 Generation of a HIRECOxIRKO colony

Male IRKO mice were bred with female HIRECO mice from established colonies at the University's animal unit. This gave rise to either WT, IRKO, HIRECO or HIRECOxIRKO progeny. Genotyping was performed on ear notches as described below, and HIRECOxIRKO mice were compared with IRKO for all experiments, and additionally with WT in some in order to ensure reproducibility of the key phenotypic changes seen previously in IRKO mice. HIRECO mice were not used in this project as a separate

project was being used to characterise their phenotype. A schematic diagram illustrating the various tissue sensitivities to insulin in these progeny is presented in Figure 4-3.
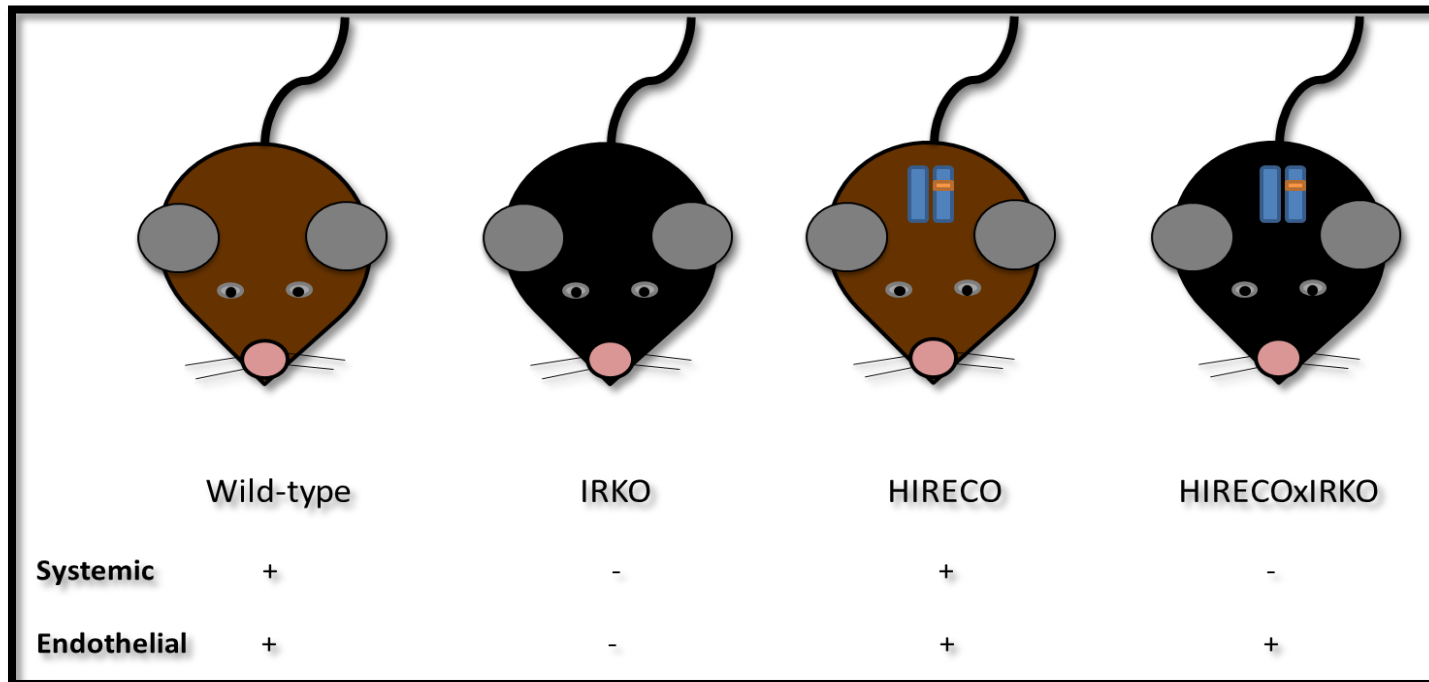
Figure 4-3   Offspring from HIRECO x IRKO Colony

Brown mice = systemic insulin sensitivity, i.e. wild-type and HIRECO (human insulin receptor endothelial cell overexpression). Black mice = systemic insulin resistance, i.e. IRKO (insulin receptor knockout) and HIRECOxIRKO. The blue and orange genes denote the insertion of a human insulin receptor targeted to the endothelium. Note that these colours do not correlate with coat colour and are simply used to illustrate tissue-specific insulin sensitivity; all mice are on a C57 background and have black coats.

4.1.5 **Animal euthanasia**

Animals were sacrificed using one of two Home Office approved techniques, depending on the specific tissue requirements. Prior to obtaining solid organs, or when mice were sacrificed without removing tissue, mice were exposed to rising concentrations of carbon dioxide in a 12 minute cycle, which rendered them unconscious. Subsequently, death was confirmed using blunt cervical dislocation, allowing the subsequent dissection of tissues as required.

For EPC isolation experiments, 1mL of blood was required and the 12 minute cycle in the carbon dioxide chamber resulted in widespread intravascular thrombosis, making blood collection very difficult from either the inferior vena cava (IVC) or via intracardiac puncture. These mice therefore underwent terminal inhalation anaesthesia with isoflurane, after which exsanguination was performed and any necessary tissue was obtained and stored on ice, or "snap-frozen" in liquid nitrogen, for transfer back to the laboratory. The technique for general anaesthesia is described in detail in Chapter 4.9 below.

4.2 Genotyping

4.2.1 DNA Extraction

Ear notches were incubated in 100µL of 25mM NaOH/EDTA (pH 12) and heated to 95°C in 0.5mL microcentrifuge tubes for 25 minutes. Following this, 100µL of 40mM Tris-HCl (pH 5) were added and the sample was vortexed thoroughly to disperse deoxyribonucleic acid (DNA). Samples were kept refrigerated to allow repeat genotyping if required.

4.2.2 Polymerase Chain Reaction (PCR)

4.2.2.1 General

A stock solution comprising a commercially obtained pre-made Biomix Red "Mastermix" and variable volumes of primers and distilled water was prepared for each PCR; details are presented below. This was done in a laminar flow hood to minimise the risk of contamination, and DNA was added using dedicated pipettes. The pre-made Mastermix contained PCR buffer, Magnesium chloride, a deoxynucleotide triphosphate (dNTP) mixture and *Thermophilus aquaticus* (Taq)-derived DNA polymerase.

Primer stocks were obtained commercially from Invitrogen, reconstituted in TE buffer (10mM Tris, 1mM EDTA; pH 8) and diluted 1:10 using distilled water. All components were mixed and 24µL reaction volumes were measured into PCR tubes. 1µL of DNA was added to each, along with positive and negative controls. Specific programmes for IRKO and HIRECO DNA were performed in thermal cyclers with heated lids and the results of both reactions combined to determine the final genotype.

4.2.2.2 IRKO PCR

The IRKO PCR protocol had previously been optimised in our laboratory and incorporated three primer sequences specific for the gene targeting cassette:

- TTA AGG GCC AGC TCA TTC CTCC (forward)
- AGC TGT GCA CTT CCC TGC TCAC (forward)
- TCT TTG CCT GTG CTC CAC TCT CA (reverse).

0.5μL of each primer (in a 1:10 dilution with TE buffer) was added to 10μL of Mastermix and 12.5μL of distilled water. The PCR comprised the following cycles:

- One denaturation cycle: 94°C for four minutes
- 31 amplification cycles: 94°C for one minute, 62°C for one minute and 72°C for one minute
- One completion cycle: 72°C for four minutes.

Following this, PCR products were refrigerated at 4°C until they were ready to be loaded onto agarose gels for electrophoresis (see below). On ultraviolet (UV) imaging, WT DNA fluoresced as a single band at 232 base pairs and IRKO DNA comprised a double band with the WT band and an extra band at 255 base pairs.

4.2.2.3 HIRECO PCR

For HIRECO PCR, two primers were used to detect the transgene:

- ACG TCA GTA GTC ATA GGA ACT GCG GTCG (forward)
- TGC CTT GAT TCA CCA GAT GCT GAGG (reverse).

0.5µL of each primer (again at 1:10 dilution) was added to 10µL of Mastermix and 13µL of distilled water. The HIRECO PCR comprised the following cycles:

- One denaturation cycle: 94°C for two minutes
- 35 amplification cycles: 94°C for 30 seconds, 65°C for 30 seconds and 68°C for two minutes
- One completion cycle: 68°C for eight minutes.

As with IRKO, PCR products were stored at 4°C and underwent subsequent gel electrophoresis. WT DNA showed no bands on UV imaging and HIRECO DNA fluoresced as a single band at 762 base pairs.

4.2.2.4 Gel Electrophoresis and Imaging

A 15g/L agarose gel was made in Tris-acetate-EDTA (TAE; 40mM Tris, 20mM glacial acetic acid, 1mM EDTA in distilled water; pH 8.6) buffer and heating at 800W for 90 seconds in a microwave. 3µL of ethidium bromide solution were added to the heated agarose-TAE mixture in order to allow fluorescence of PCR products under ultraviolet (UV) light and the liquid agarose was poured into a gel tray with a comb to allow the formation of wells into which DNA samples could be loaded. After allowing this to set for two hours, the gel was inserted into a tank containing 700mL of TAE buffer. 15µL of a 100 base-pair ladder were loaded as a reference for PCR product size and 20µL samples of PCR product were pipetted into adjacent wells. Electrophoresis was performed at 110V for 60 minutes and imaging was done using the Syngene G-box imaging system.

4.3 Gross Morphological Measurements

4.3.1 Body Weight

Mice of all four genotypes were weighed from weaning until the age of four months, at which point their weights were generally found to plateau.

4.3.2 Wet Organ Weight

Mice were weighed on the day of sacrifice before dissecting and weighing the heart, lungs, spleen, liver and kidney in 1.5mL microcentrifuge tubes. Samples were then stored at -80°C for future protein or RNA extraction. All wet organ weights were normalised to total body weight.

4.4 Metabolic Testing

4.4.1 Glucose tolerance testing (GTT)

Mice were fasted overnight in fresh cages to avoid them consuming chow fragments from cage floors; access to water was maintained throughout. The following morning, mice were consciously restrained in syringe-like devices with free air flow by gently coaxing them in head-first and allowing tails to protrude from the end of the device. Mice had been habituated to these on previous occasions to prevent excessive stress during tolerance tests. Once mice were accustomed to the restrainer, measurements of capillary blood glucose (CBG) were made using 1-2µL droplets of blood from superficial tail incisions using a sterile scalpel and an Accuchek glucometer and test strips. A fasting measurement was made before the intraperitoneal (IP) injection of glucose dissolved in distilled water at a dose of 1mg/g. CBG was measured at 30, 60, 90 and 120 minute time points after glucose challenge. In between, mice were removed from restraint and returned to their cages, where they were able to drink water freely but not given access to chow until after the final time point.

4.4.2 Insulin tolerance testing (ITT)

ITTs were performed a week after GTTs to ensure normalisation of homoeostasis and restoration of circulatory volume. A similar protocol was employed to the GTT as above, but mice were fasted for four hours rather than overnight. After a fasted CBG measurement, IP insulin was administered at a dose of 0.75 International Units (IU)/kg using a stock of 200mIU Actrapid insulin in 5mL Dulbecco's phosphate-buffered saline (PBS). Mice were observed closely in between measurements in case of hypoglycaemia, with a solution of glucose available for immediate intraperitoneal injection in the event of profound or symptomatic hypoglycaemia.

4.5 Blood Pressure Measurement

Mice aged 2-4 months underwent blood pressure (BP) measurement using tail cuff plethysmography using the Coda Non-invasive Tail BP (Kent Scientific, USA) system. Occluder and sensor cuffs were inspected and formally tested for adequate inflation prior to each session, with re-threading of the bladder if the automated test suggested unsatisfactory function of the device. Mice were trained on two separate occasions prior to the day of measurement. Each time, conscious animals were restrained in dedicated tubes as described above, and placed in a heat chamber set at 32°C to encourage tail vasodilatation. The device protocol included ten acclimatisation cycles followed by three sets of six measurement cycles with five seconds of recovery time in between. Data were only recorded from the third session to avoid including artificially high readings prior to habituation to the device and environment. Mean systolic readings were taken from as many recordings as feasible after appraisal of each plethysmography trace for adequacy of tail volume, lack of movement artefact and shape of curve. Agitated mice were removed and re-tested at a later session to avoid excessively high BP measurements related to stress.

4.6 Blood Sampling from Saphenous Vein Puncture

Conscious mice were habituated to restraint prior to the day of venepuncture. Once the restrained mouse grew accustomed to the device, the right leg was gently removed and gripped lightly using the operator's left hand. A hair removal cream (Veet) was applied for no more than 30 seconds to avoid skin burns and the leg was then gently shaved using tissue paper, allowing clear visualisation of the distal saphenous veins. A paraffin-based ointment (Vaseline) was applied over the vein to encourage formation of a blood globule and a fresh 14G needle was used to puncture the vein lightly. Blood for plasma extraction was drawn into Microvette tubes lined with powdered lithium heparin using capillary action. When whole blood was required, Microvette tubes with EDTA-tripotassium were pre-filled with 50µL of sterile liquid heparin (1000 IU/mL) and 100-150µL blood were collected using gravity. The removal of this volume adhered to standard murine welfare guidance from the Home Office. Haemostasis was quick and effective using simple light pressure, and further venepuncture was not performed from the same leg until full healing had occurred and with due delays to allow restoration of circulatory volume.

4.7 Plasma Insulin Measurement (ELISA)

4.7.1 Blood Collection

Mice were fasted overnight prior to collecting blood for this experiment. Whole blood (typically 90-100µL) was obtained using saphenous vein puncture as described above, collecting using capillary action into tubes lined with powdered lithium heparin. Blood was stored on ice and transferred to the laboratory with minimal delay. Samples were centrifuged at 6000 revolutions per minute (rpm) for six minutes to obtain a plasma layer and this was removed and stored at -80°C until enough samples had been obtained for an enzyme-linked immunosorbent assay (ELISA).

4.7.2 ELISA

4.7.2.1 Preparation and First Reaction

Ready-made ELISA kits for mouse insulin (Crystal Chem) were used, using the "low-range" assay conditions (0.1-6.4ng/mL). An antibody-coated microplate was set up by reverse pipetting with 95µL of sample diluent from the ELISA kit into each well. Serial dilutions of a working lyophilised mouse insulin standard (reconstituted in distilled water) were prepared as per manufacturer instructions, diluting in sample diluent. These were measured out in 5µL in duplicate for the first eight pairs of wells allowing a standard curve to be constructed from 0-6.4ng/mL of insulin. Remaining wells were filled with 5µL in duplicate of each plasma sample. These were incubated at 4°C for two hours to allow antibody binding.

4.7.2.2 Washing and Second Reaction

Each well was then washed five times with 300µL of wash buffer provided in the ELISA kit, ensuring full removal of solution using a glass aspirator pipette each time. Before the fifth wash was aspirated, an anti-insulin enzyme conjugate was prepared by mixing together defined quantities of a pre-made stock solution and diluent from the ELISA kit as per manufacturer

instructions. The fifth wash was then aspirated and the conjugate was immediately pipetted into the ELISA wells at 100μL per well. This was incubated at room temperature for 30 minutes.

4.7.2.3 Washing and Third Reaction

This time, wells were washed seven times with 300μL of wash buffer. After full aspiration of wash contents, 100μL of enzyme substrate solution were added to each well. The plate was incubated in the dark at room temperature for 40 minutes, following which the reaction was aborted by adding 100μL of a "stop" solution to each well.

4.7.2.4 Colorimetric Analysis

A Dynex MRX plate reader and Revelation version 4.21 software were used to perform colorimetric analysis at a wavelength of 450nm. The mouse insulin standards were used to construct a standard curve, which was appraised for linearity and correlation co-efficient (r^2), the latter accepted only when > 0.99. Sample insulin concentrations were extrapolated automatically using this curve and values were accepted at a co-efficient of variation (CV) between duplicates of < 10%.

4.8 Quantitative PCR

4.8.1 RNA Extraction

Ribonucleic acid (RNA) extraction was performed with care to avoid DNA contamination and RNA degradation, including the use of laboratory equipment dedicated to RNA work and the prior cleaning of all work surfaces with "RNAse away" spray.

Organ samples were obtained from mice euthanised using rising carbon dioxide concentrations. A laparotomy and/or thoracotomy was performed and organs of interest were carefully dissected and "snap" frozen in liquid nitrogen prior to storage at -80°C. Cell lysates were harvested from pulmonary endothelial cell (PEC) cultures at P2, having been seeded onto 6 well plates coated with 20g/L gelatin. Once these cells reached 95% confluence, 500µL of Tri reagent (Trizol®) were added to each well and the cells removed using a cell scraper. Samples were stored at -80°C prior to RNA extraction.

Organs underwent mechanical homogenisation using a Qiagen tissue lyser. Samples were transferred to 2mL microcentrifuge tubes along with a 6mm stainless steel cone ball and 1mL of Tri reagent. Sample tubes were closed securely and loaded into the homogeniser for three cycles at 30Hz, each lasting two minutes. Following this, the liquidised portions were transferred into fresh 1.5mL microcentrifuge tubes, with any remaining solid debris and the cone ball discarded. This was not done to cell lysates, which were instead gradually defrosted on ice and dispersed thoroughly using a vortex mixer prior to use. Both tissue types were handled in a similar fashion from hereon in.

Samples were centrifuged at 4°C for 10 minutes at 10,000g, following which the supernatants were transferred into fresh microcentrifuge tubes. The

samples were left to dry at room temperature for five minutes before 200µL of phenol chloroform were added to each. All tubes were agitated for 30 seconds to ensure sufficient mixture of the tri reagent and phenol chloroform, then left at room temperature for three minutes before a 15-minute spin at 12,000g, again at 4°C. This resulted in the samples separating into three strata: a clear top layer (RNA-containing aqueous phase), a thin lipid interphase and a protein rich organic phase. The aqueous phase was transferred to a fresh microcentrifuge tube and 500µL of isopropanol were added to each sample. These tubes were gently mixed and then left to rest at room temperature for ten minutes before a 12,000g centrifuge step for ten minutes at 4°C.

At this stage, the supernatants were discarded and 1mL of 750mL/L ethanol was added to each pellet before a further centrifuge step at 7500g (five minutes at 4°C). As much ethanol as possible was removed from the pellet, which was then left to air dry for ten minutes at room temperature. Following this, 20µL of RNAse-free water were added to each tube. Pellets were left on ice for 20 minutes to dissolve. After this, 2µL samples from each sample were tested using NanoDrop® apparatus to measure the RNA concentration, with use of ethanol to clean the probe in between each sample.

4.8.2 **Reverse Transcription**

Reverse transcription of RNA to complementary (c)DNA was performed in a dedicated PCR laboratory with equipment used only for RNA work. A "mastermix" was created using a High Capacity cDNA Reverse Transcription Kit (Applied Biosystems), with constituents as summarised in Table 4-1. The RNA concentrations measured using the NanoDrop® were used to calculate the volume of RNA solution needed to load 2µg per sample into a PCR plate (topped up to 10µL with distilled water). 10µL of the mastermix were added to each sample, resulting in reaction volumes of 20µL. The reverse

transcription was then performed in a thermal cycler using the following conditions:

- 25°C (10 minutes)
- 37°C (2 hours)
- 85°C (5 minutes)
- End

Samples were then frozen at -20°C until real-time PCR was performed.

Constituent	Volume/µL (for 10µL mastermix)
Water	4.2
Buffer	2
Random primers	2
MultiScribe^{TM} RT enzyme	1
dNTPs	0.8

Table 4-1   Constituents of Reverse Transcription mastermix

dNTP = deoxynucleotide triphosphate; RT = reverse transcriptase.

4.8.3 Quantitative (real-time) PCR

Samples were analysed using quantitative PCR with two separate sets of probes, both using murine beta-actin as a housekeeping control. For analysis of human insulin receptor messenger RNA (mRNA), a Synergy Brands (SYBR) Green probe was used, while murine insulin receptor mRNA was detected using a Taqman® probe (Applied Biosystems). Mastermixes were created, containing 24µL in the SYBR green protocol and 19µL for

Taqman®, as per manufacturer instructions (see Table 4-2 and Table 4-3 for Mastermix details and Table 4-4 and Table 4-5 for the sequences of each primer). Taqman probes were commercially purchased, with primers pre-attached; see Chapter 3.8 for details. The reaction volumes were measured into 96 well PCR plates and 1µL of cDNA was added in triplicate for each sample. For the SYBR Green probe, cDNA was diluted 1:20 but was added neat for the Taqman® experiments. A series of "blank" samples, containing distilled water rather than cDNA, was also loaded for each primer, as a negative control to rule out nucleic acid contamination of the mastermixes.

Constituent	Volume/µL (for 24µL mastermix)
Water	8.5
SYBR Green	12.5
Forward primer	1.5
Reverse primer	1.5

Table 4-2   Constituents of SYBR Green Mastermix

Constituent	Volume/µL (for 19µL mastermix)
Water	8
Taqman® mastermix	10
Probe	1

Table 4-3   Constituents of Taqman® Mastermix

Gene	Forward Primer	Reverse Primer
Beta-actin	CGT GAA AAG ATG ACC CAG ATCA	TGG TAC GAC CAG AGG CAT ACAG
Human Insulin Receptor	TGC CAC CAA CCC CTC TGT	CGG AGG GTG GTT TCC ACTT

Table 4-4   SYBR Green Primers for Quantitative PCR

A = adenine; C = cytosine; G = guanine; T = thymine

Gene	Assay Number	Supplier
Beta-actin	Mm 00607939	Applied Biosystems
Murine Insulin Receptor	Mm 01211875_m1	Applied Biosystems

Table 4-5   Taqman® Primers for Quantitative PCR

Quantitative PCR was performed in a thermal cycler (ABI Prism 7900HT). The average cycle threshold (Ct) for the three repeats of each sample was recorded from SDS v2.2 software and compared with the average Ct for beta-actin for the same sample. Samples for which the three replicates were not close together were discarded on the basis of differential cDNA loading and pipette error. The difference in Ct (ΔCt) between the gene of interest and the housekeeping gene was recorded and expressed as a relative quantity (RQ) using the following formula:

$$RQ = 2^{-\Delta Ct} \times 100.$$

4.9 Vascular Injury

Vascular injury experiments were performed by Dr Nadira Yuldasheva, using recovery anaesthesia with inhaled isoflurane. The technique for vascular injury experiments is as follows.

4.9.1 General Anaesthesia

The University of Leeds animal facility contains three operating theatres for murine surgery, each of which has a warmed table and pre-operative area as well as anaesthetic apparatus. An isoflurane vaporiser is connected via a series of tubes to both an anaesthetic induction chamber and a nose cone which acts as a mask for the mouse on the operating table. A valve controls the proportion of isoflurane and oxygen that is diverted to each outlet.

Mice were initially identified, weighed and then placed into the induction chamber. Oxygen was turned on at a rate of 2 litres/minute, which was maintained throughout. Isoflurane was then initiated at a concentration of 4-5% and diverted to the induction chamber, with close observation of the mouse throughout. Adequate anaesthesia could be inferred from loss of consciousness and then slowing of the respiratory rate, at which point flow was diverted to the nose cone and the mouse was secured in position on the operating table using surgical tape. For recovery experiments, the table was warmed to 38°C. Analgesia was initiated at the start of the surgical procedure with the intraperitoneal injection of buprenorphine (0.25mg/kg).

During the operation, the mouse's respiratory rate and response to tail-tip stimuli were used to appraise the depth of anaesthesia, and isoflurane dose was adjusted as required, usually between 1.5-2.5%. In the event of any signs of response, the concentration was adjusted and the mouse's position in the nose cone was gently optimised until full anaesthesia had been achieved, and only at this point was surgery recommenced.

At the point of recovery, mice were switched to inhaled oxygen and had 300μL of 0.9% saline injected intraperitoneally to maintain hydration. They were supervised closely in a post-operative recovery area with warmed tables. Soaked diet was provided for the first 24 hours and mice were checked daily until the end of the experiment.

4.9.2 Arterial Injury

Surgery was performed with the aid of a dissecting microscope (Zeiss OPMI 1-FC). Mice were anaesthetised as described and secured in a supine position to an operating table warmed to 38°C. This position allowed abduction and extension of the lower limbs, exposing them adequately for fur removal using Veet cream. Asepsis was maintained and 0.75% providone-iodine solution was used to sterilise the surgical field. A small mid-thigh incision was used to enter the left femoral canal and subcutaneous tissues and fat pads were gently removed with care not to disturb the epigastric artery, which maintained limb perfusion when the femoral artery was ligated. The femoral artery was then identified and carefully isolated from within the neurovascular bundle, following which it was loosely tied using 8.0 suture material and a proximal clamp was secured onto the neurovascular bundle. A drop of 1% lignocaine was applied on the arterial surface to reduce the chance of arteriospasm and an arteriotomy was then made with iris scissors.

After gaining access into the femoral artery, a 0.014 inch diameter angioplasty guide wire (Hitorque Cross-it 200XT) was introduced and, after clamp removal, the wire was gently advanced 1.5-2.0cm for three passes. The wire was removed and the suture tightened to ligate the vessel proximal to the arteriotomy. The overlying skin was closed with a continuous Vicryl 6.0 suture. The contralateral (right) lower limb was then exposed to a sham operation without wire passage. The mouse then underwent a monitored recovery period with analgesia and thermal support as outlined above.

4.9.3 Assessment of Endothelial Regeneration

Four days after injury, the operating area was prepared for vessel harvest and mice were anaesthetised again as described above. The inferior vena cava was exposed using an incision along the linea alba. Three minutes prior to harvesting, Evans blue (50-75µL of 50g/L in saline) was injected via the inferior vena cava. This dye binds with high affinity to circulating albumin, which cannot cross an intact endothelium, so the dye cannot interact with matrix proteins deep to the endothelium. Thus, only areas of denudation appear blue when perfused with Evans blue stain.

Perfusion fixation was then carried out using 40g/L paraformaldehyde in phosphate-buffered saline (pH 7.2). A 27G needle was used to introduce this into the left ventricle under physiological pressure, following which the animal's muscles began to fasciculate. Once perfusion fixation was confirmed, both femoral arteries and surrounding soft tissue were excised as far as the bifurcation of the aorta and stored in 40g/L paraformaldehyde.

Excised arteries were separated from surrounding fascial layers under microscopy (Olympus Dissecting Stereo Microscope SZ61) and imaging was performed using a QiCam Olympus digital camera. Using a 20x magnification, a 5mm segment of artery was identified at a distance of 5mm from the proximal end (near the aortic bifurcation) of the length of vessel. Figure 4-4 shows an injured and a sham vessel after excision. Areas of endothelial regeneration, i.e. those that did not stain blue, were demarcated on images analysed on ImagePro Plus 7.2 software (Media Cybernetics), and this allowed electronic calculation of percentage regeneration. A representative image showing this analysis is presented in Figure 4-5.

.
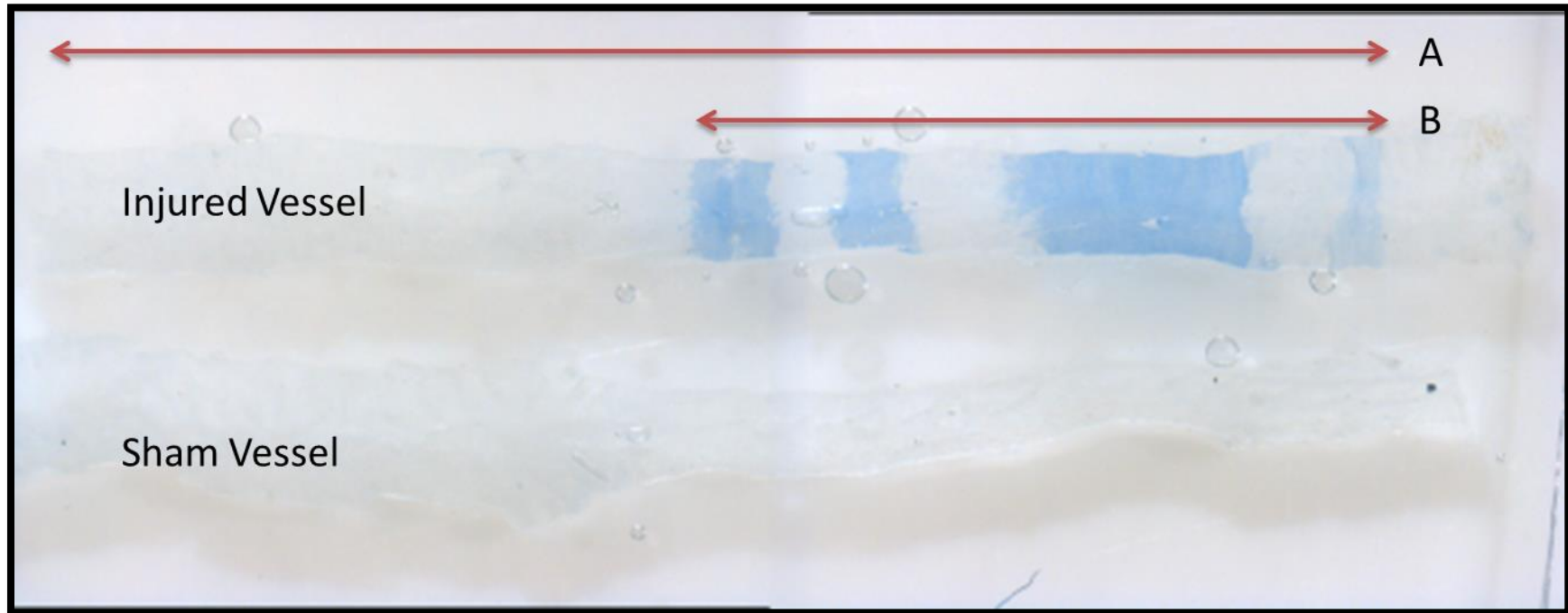
Figure 4-4   Image of Femoral Arteries after Vascular Injury

Image courtesy of Dr Nadira Yuldasheva, from wild-type mouse 210. Magnification: x20. The bottom (sham) vessel is the contralateral artery from the same mouse, which was not injured, showing no staining with Evans Blue and thus an intact endothelium. Distance A denotes the excised vessel, from the origin of the common femoral artery to the femoral artery bifurcation. The injured segment (B) starts 5mm from the origin of the femoral artery and is itself 5mm long. Areas of persistent endothelial denudation stain blue, with areas of recovery appearing white.
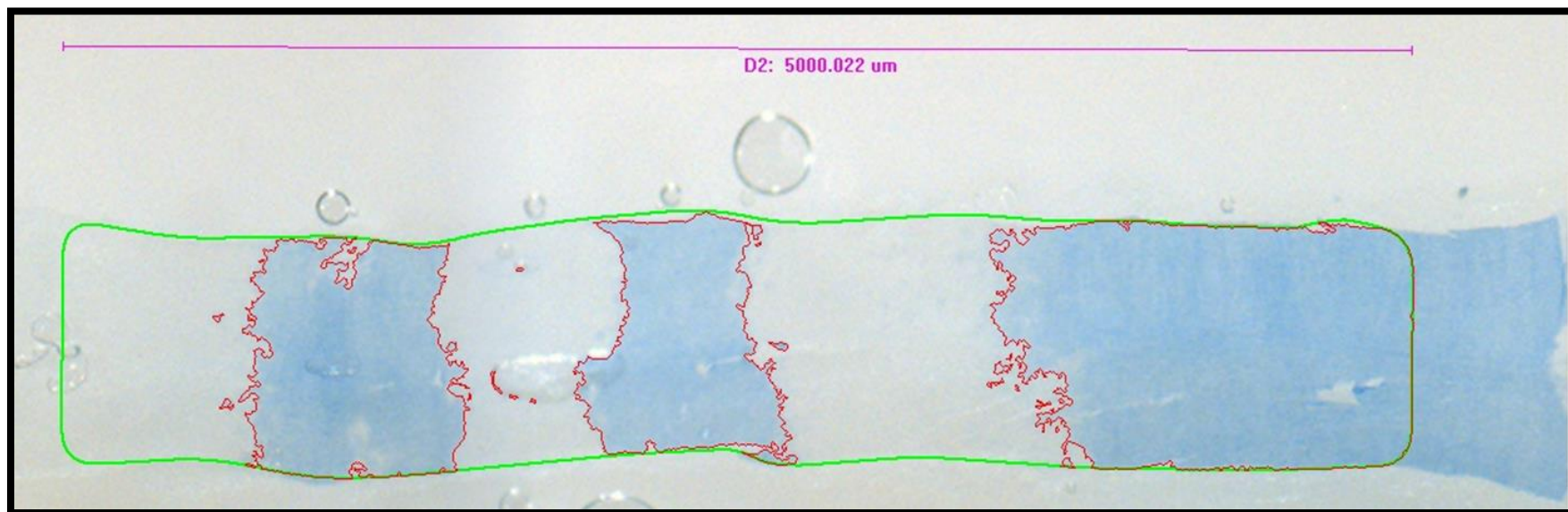
Figure 4-5   Representative Image Showing Quantification of Endothelial Regeneration

Image from WT mouse 210. Magnification: x20. The analysed segment (D2 above) commences 5mm distal to the origin of the common femoral artery (left edge). Areas of persistent denudation, stained blue, were quantified in a 5mm segment of stained artery by Dr Yuldasheva using ImagePro Plus software as shown, and used to calculate the percentage regeneration in each wound.

4.10 Enumeration of Circulating Progenitor Cells (CPCs)

4.10.1 Blood Collection

200µL of sterile heparin (1000 IU/mL) were measured into Microvette tubes lined with EDTA-tripotassium, agitated to encourage adequate lining of the tube, and then 150µL were removed and discarded, leaving a residual 50µL of heparin in the tube. 3mL of 1:10 sterile Pharmlyse^{TM} red cell lysis buffer were measured into 15mL centrifuge tubes, one for each blood sample. This ammonium chloride-based buffer is diluted from a commercially obtained 10x stock solution using distilled water that had undergone syringe filtering; it lyses erythrocytes without affecting viability of the leucocyte population.

These tubes were transported on ice to the animal facility, where habituated mice were consciously restrained for saphenous venepuncture as described previously. 150µL of whole blood were carefully collected into the Microvette tubes with care to avoid thrombus formation. Blood samples were immediately transferred and mixed with the 3mL aliquots of sterile lysis buffer, which were swiftly transferred in ice to the laboratory for processing.

4.10.2 Incubation with Antibodies

Samples in lysis buffer were removed from ice and centrifuged at 300g for 10 minutes, following which the supernatant was aspirated. The peripheral blood mononuclear cell (PBMC) pellet was resuspended in 1mL of fluorescence activated cell sorter (FACS) buffer (50mL/L foetal calf serum, 5g/L bovine serum albumin in PBS; pH 7.4) in fresh 1.5mL microcentrifuge tubes.

Samples were centrifuged again, and a 1:10 dilution of Fc block was prepared in FACS buffer. Cell pellets were resuspended in 100µL of the

Fc/FACS solution to reduce non-specific antibody binding. These were incubated at 4°C in the dark in a refrigerator for 10 minutes.

During this incubation, three separate antibodies (Ab) or corresponding isotype controls (IC) were diluted in FACS buffer from stock solutions (BD Biosciences). The three anti-mouse antibody-fluorochrome combinations were as detailed in Table 4-6.

Antibody	Fluorochrome
Stem cell antigen 1 (Sca1)	Fluorescein isothiocyanate (FITC)
Foetal liver kinase 1 (Flk1)	R-phycoerythrin (PE)
c-kit/CD117	Allophycocyanin (APC)

Table 4-6   Antibody-fluorochrome Combinations used for Flow Cytometry

CD = cluster of differentiation.

Previous work from our laboratory defined CPCs as those expressing both Sca1 and Flk1, but transfusion studies conducted in that project utilised c-kit$^+$ PBMCs. Pilot data obtained in conjunction with Dr Noman Ali (University of Leeds) demonstrated that the population of triple labelled cells is negligible, but that Sca1$^+$Flk1$^+$ cells and c-kit$^+$ cells could be enumerated separately in meaningful quantities using flow cytometry.

After 10 minutes, the samples incubated with Fc block were removed and their volume was doubled by adding 100µL of fresh FACS buffer. This was split evenly between two new microcentrifuge tubes, one to be incubated with 10µL of each IC cocktail and the other with 10µL of the Ab cocktail.

Antibodies were applied in darkness and the samples were again refrigerated for 10 minutes. Following this, 1mL of FACS buffer was added to each tube and they were spun for 10 minutes at 300g to wash off unbound antibody. Pellets were resuspended in 500µL of FACS buffer, transferred into FACS tubes and quickly transferred to the flow cytometer on ice.

4.10.3 Fluorescence Activated Cell Sorting (FACS)

CPC enumeration was performed using a BD-LSR Fortessa flow cytometer. The lymphocyte gate was defined as shown in Figure 4-6 and the number of dual-labelled cells (Sca1$^+$Flk1$^+$;

Figure 4-7) and, separately, c-kit$^+$ cells (Figure 4-8) were counted within 100,000 lymphocyte events. If fewer than 100,000 events were recorded, results were normalised to this event rate. The event number recorded in the IC specimens was subtracted from that obtained in the Ab specimens to control for non-specific fluorescence.
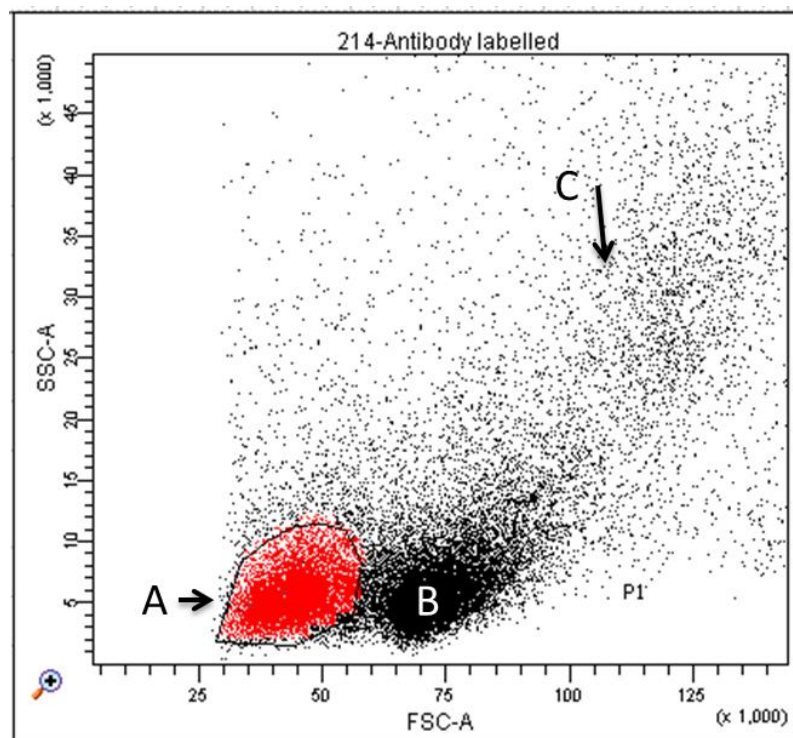
Figure 4-6   Definition of lymphocyte gate on flow cytometry

A = lymphocytes, B = monocytes, C = granulocytes.
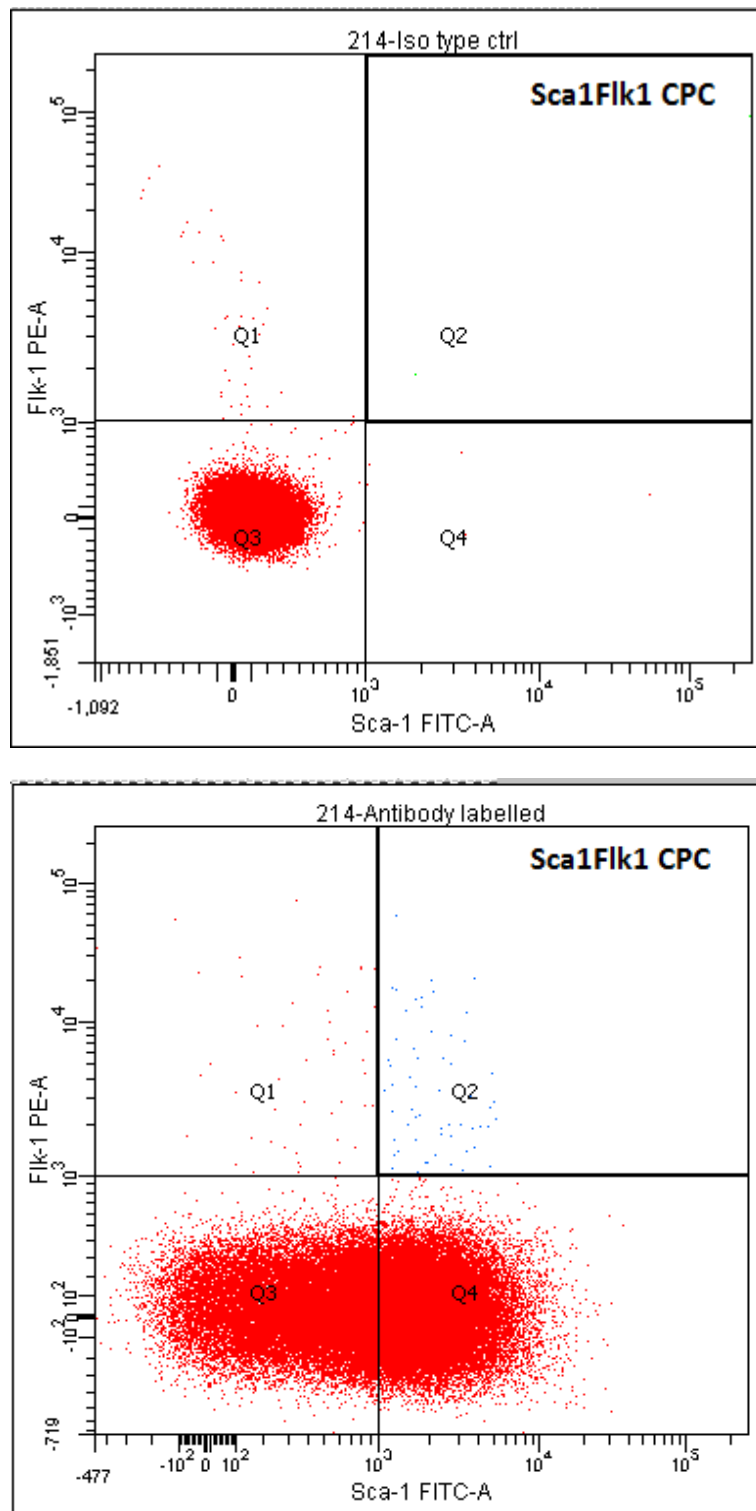
Figure 4-7 Definition of Sca1$^+$Flk1$^+$ circulating progenitor cells (CPC)

Upper panel shows isotype control and lower panel shows antibody-labelled sample. Cells co-labelled with stem cell antigen-1 (Sca1) and foetal liver kinase-1 (Flk1) are presented as Q2 events, in blue.
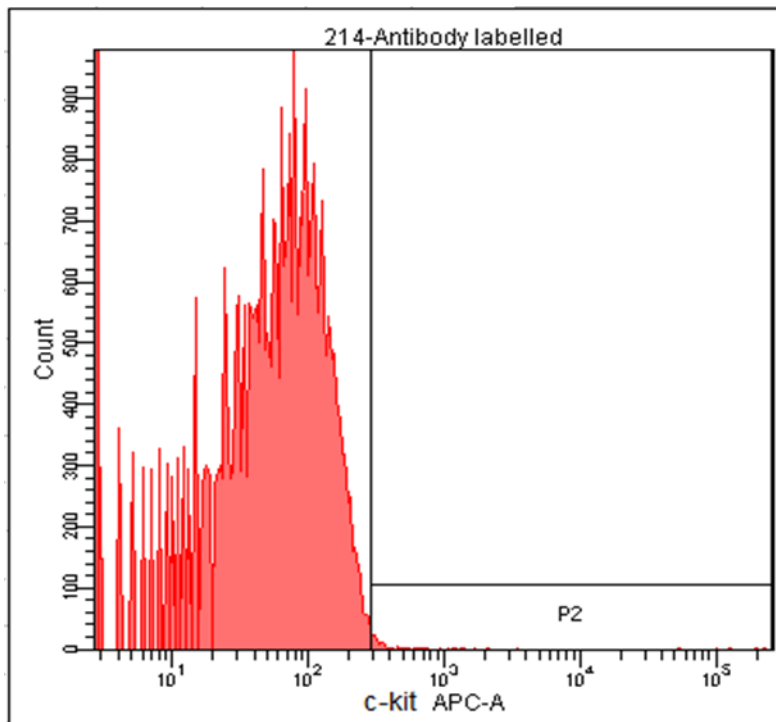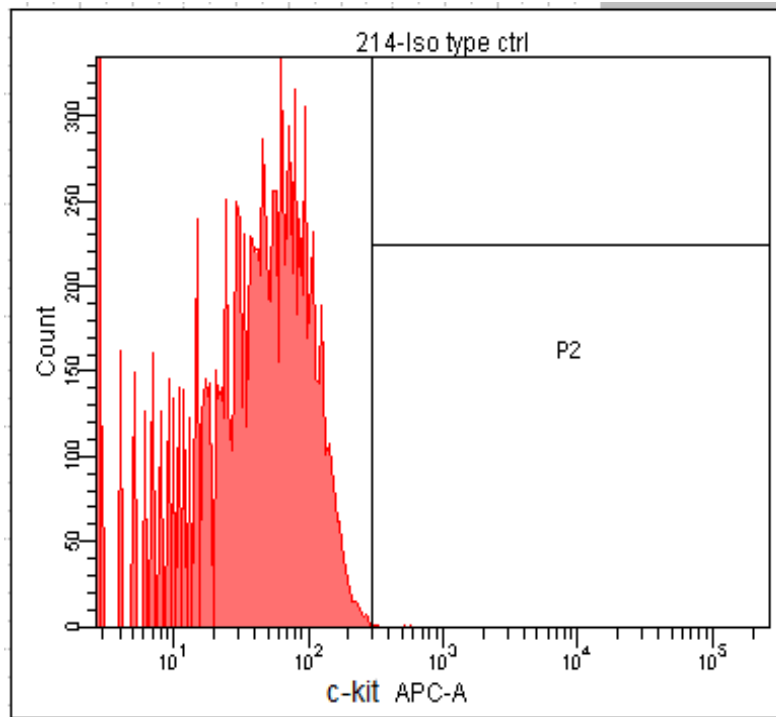
Figure 4-8   Definition of c-kit⁺ circulating progenitor cells (CPC)

Upper panel shows isotype control and lower panel shows antibody-labelled cells. Those expressing c-kit are counted in the P2 region.

4.11 Isolation and Enumeration of Early Outgrowth EPCs

4.11.1   General Anaesthesia

Tissue for EPC culture was obtained under terminal general anaesthesia, as described above. Briefly, mice were identified and anaesthesia was induced in a chamber with oxygen (2L/minute) and isoflurane (3-4%), with peri-operative maintenance at 1-2% isoflurane via a mask on the operating table.

4.11.2   Tissue Harvest (blood, spleen, bone marrow)

Once the mouse was satisfactorily anaesthetised, a midline laparotomy was performed and bowel was moved aside to expose the inferior vena cava (IVC). This was carefully punctured using a 1mL insulin syringe containing 50μL of sterile sodium citrate (obtained from citrated blood collection tubes). 1mL of blood was removed in this manner and immediately expelled into 4mL of sterile PBS, stored on ice in a blood collection tube.

Next, the spleen was identified and carefully dissected out, with removal of any obvious areas of infarction that had developed after IVC puncture. Care was taken to dissect off any adherent adipose tissue. The spleen was then transferred to a 15mL centrifuge tube containing 5mL of sterile PBS and stored on ice.

Finally, the coat, fascial layers and muscle were dissected from each hind limb until the femur and tibia on both sides was exposed. The bones were cleaned of any adherent connective tissue and the fibulae were disconnected from the lower limb and discarded. Scissors were used to make cuts at the metaphyses of the femora and tibiae, after which each long bone was flushed three times with 5mL of sterile PBS using a syringe and a 23G needle into a 15mL centrifuge tube before being stored on ice.

4.11.3 Mononuclear Cell Isolation

All samples were rapidly brought back to the cell culture laboratory on ice and isolation of mononuclear cells was performed in aseptic conditions in a flow-controlled cell culture hood. Blood was expelled into a 50mL centrifuge tube through a 70µm cell strainer to eliminate any thrombus, and washed with 2mL of sterile PBS. Spleens were placed in 3mL of fresh sterile PBS in a Petri dish and mechanically minced through 70µm cell strainers until only non-specific cellular debris remained in the sieve. The filtrate suspension was then injected through the cell strainer into a 50mL centrifuge tube and the Petri dish was washed with a further 2mL of sterile PBS, which was added to the suspension. Similarly, the marrow suspension was mechanically minced and then filtered through a cell strainer with a 2mL PBS wash of the Petri dish.

Each cell suspension was then carefully layered onto 5mL of Histopaque-1083, prior to undergoing density-gradient centrifugation at 400g for 30 minutes with slow deceleration. This resulted in the formation of a buffy layer containing the mononuclear cell fraction, which was carefully aspirated using a 1mL pipette tip and expelled into new centrifuge tubes. The buffy layer was washed twice (for spleen and marrow) and three times (for blood) with 10mL of sterile PBS at 400g for 10 minutes.

4.11.4 Seeding for EPC Culture

The resulting pellets were resuspended in dedicated EPC growth medium, composed of EGM-2 basal medium supplemented with 200mL/L foetal calf serum and EGM-2 bullet kit (Lonza). Blood- and marrow-derived pellets were resuspended in 500µL of medium and those derived from spleen were reconstituted in 2mL of medium. 20µL samples were taken from each and added to equal volumes of trypan blue. These were loaded onto a haemocytometer and viable cells (those that did not take up the trypan blue) were counted. Mononuclear cells were seeded onto 24-well fibronectin-coated cell culture plates at the following densities: 1×10^6 cells/well for

marrow, 5×10^6 cells/well for blood and 8×10^6 cells/well for spleen. EPC growth medium was added to make a total suspension volume of 1mL for blood and marrow and 2mL for spleen. If possible, each sample was seeded in triplicate to reduce data variability.

Cells were kept in a 37°C incubator with 5% CO_2 for seven days such that the resultant cell population was akin to published studies of early outgrowth EPCs. On day 4, wells were washed with sterile PBS in order to remove non-adherent cells and growth medium was refreshed. Imaging was undertaken on day 7.

4.11.5   EPC Imaging

On day 7, each well was washed twice with sterile PBS prior to imaging. Cells were defined as EPCs if they exhibited dual staining with 1,1'-dioctadecy-3,3,3',3'-tetramethyllindocarbocyanine-labelled acetylated low-density lipoprotein (DiI-ac-LDL) and lectin obtained from *Ulex europaeus* conjugated with fluorescein isothiocyanate (FITC). This technique has been used in previous work enumerating EPCs in culture [164]. DiI-ac-LDL was initially added in darkened conditions at a concentration of 10μg/mL (diluted in EPC growth medium). Cells were incubated with this for 3 hours at 37°C prior to further washes with PBS and then fixation with 40g/L paraformaldehyde for 10 minutes. This was washed with PBS again, after which lectin-FITC was added at the same concentration but diluted in PBS. Cells were incubated with lectin in the dark for an hour, following which they underwent a final wash prior to imaging.

Imaging was performed using an Olympus CKX-41 fluorescence microscope. Five images per well were taken at 100x magnification as follows: phase contrast, red fluorescence (DiI), and green fluorescence (lectin-FITC) using Cell B software. Images were saved and then overlain using Image J software (version 1.46r). EPC were denoted as cells staining

yellow on composite images and these were quantified using the Cell Counter tool in Image J. Cell counts were taken from five to ten separate fields chosen at random and mean number of cells per image was calculated. Representative images are shown in Figure 4-9.
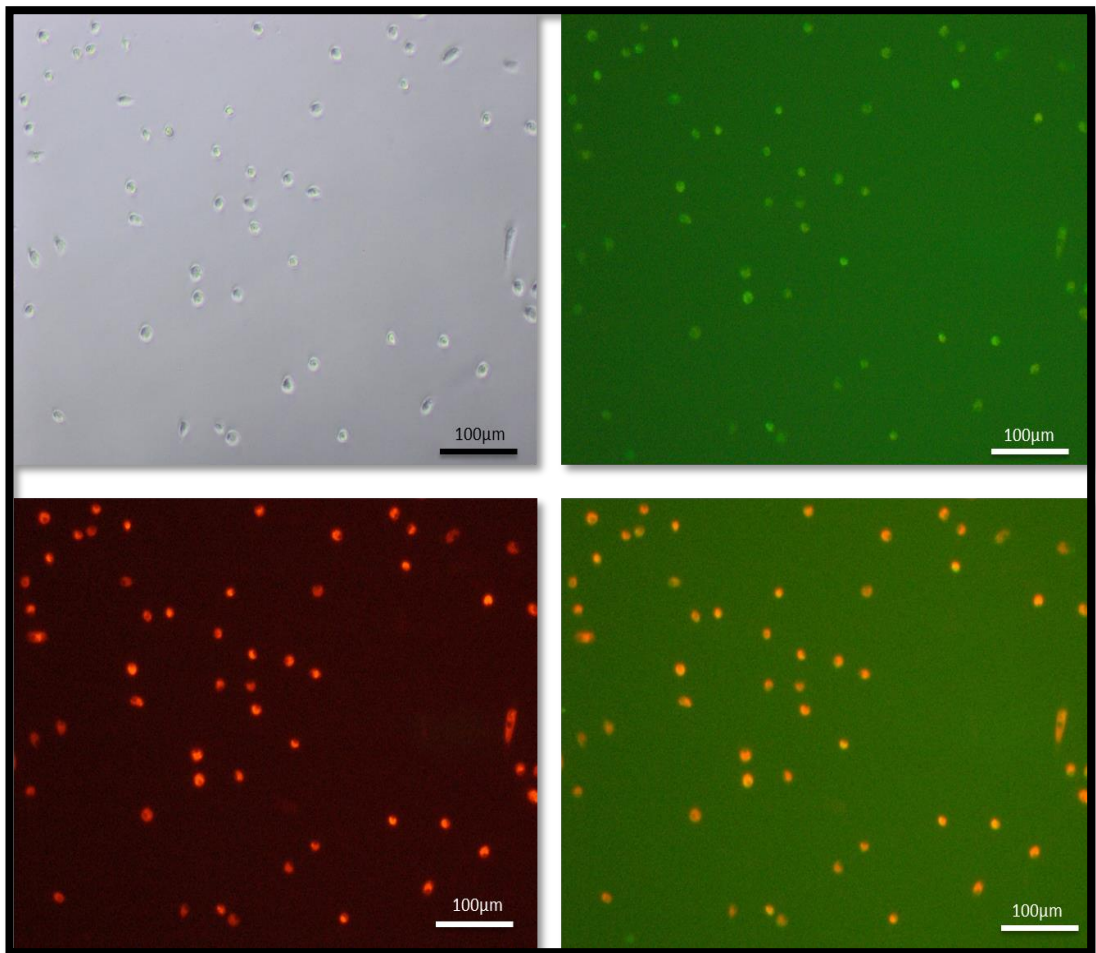
Figure 4-9   Endothelial Progenitor Cells from a Wild-type Spleen

Top left = phase-contrast imaging; top right = fluorescein isothiocyanate-lectin; bottom left = DiI-acetylated-LDL; bottom right = composite image. Yellow-stained cells represent endothelial progenitor cells. Magnification: x100.

4.12 Isolation and Culture of Pulmonary Endothelial Cells

Murine pulmonary endothelial cells (PECs) were isolated using a technique described in detail by Sobczak *et al* [182]. Following a two-step magnetic bead separation using antibody coated microbeads, cells were used in various assays, including studies of proliferation (Chapter 4.12), migration (Chapters 4.14 and 4.15), superoxide production (Chapter 4.18), messenger RNA expression (Chapter 4.8) and Western blotting (Chapter 4.19).

4.12.1 Antibody-coated Microbead Preparation

Commercially purchased sheep anti-rat immunoglobulin (Ig)G Dynabeads were coated with antibodies in advance of cell isolation as follows. For the first bead separation, these beads were incubated with antibodies targeted at platelet endothelial cell adhesion molecule 1 (PECAM-1; also known as CD31). The second enrichment of PECs was done using intercellular cell adhesion molecule (ICAM-2; also known as CD102). Antibodies to both of these agents were acquired from BD Biosciences (details in Chapter 3.12).

A magnetic particle concentrator (MPC) was assembled in a sterile cell culture hood with an autoclaved 1.5mL microcentrifuge tube within the magnetic column. 200µL of Dynabeads were added into the microcentrifuge tube and a solution of sterile PBS supplemented with 1g/L BSA was used as a wash buffer in volumes of 1mL per wash. After each wash, beads were allowed to adhere to the magnet for 30-60 seconds, following which a sterile glass aspirator was used to remove the supernatant; this process was carried out four times. Following this, the beads were resuspended in 500µL of PBS/BSA and 20µL of either anti-PECAM-1 or anti-ICAM-2 antibody solution were added to the tube. This was rotated in a MACSmix^{TM} rotator for two hours at room temperature, following which a further four washes were performed in the MPC in a sterile manner. After the fourth wash, a final volume of 200µL of PBS/BSA was used to reconstitute the beads for

eventual use in PEC enrichment. Beads were refrigerated and used for up to a month.

4.12.2 PEC Growth Medium Preparation

Growth medium was also prepared in advance. Basal MV2 growth medium was purchased along with endothelial growth supplements (Lonza). For every 500mL of basal medium, the growth supplements were added in sterile conditions along with 50mL of batch-tested foetal bovine serum (Biosera) and 10mL of antibiotic-antimycotic solution; these were mixed thoroughly and the medium was used in aliquots for up to a month to avoid alterations in composition and reduce the risk of microbial contamination.

4.12.3 Lung Harvest and PEC Isolation

Mice aged 4-6 weeks were euthanised using rising concentrations of CO_2 and death was confirmed with blunt cervical dislocation, as per Home Office UK regulations. A thoracotomy was performed and lungs were dissected with care to avoid large thrombi or excessive connective tissue. These were stored in ice-cold Hank's Balanced Salt Solution (HBSS) and transferred to the cell culture facility, where they were transferred to 10cm Petri dishes in a cell culture hood. A solution of 1mg/mL collagenase/dispase was prepared in Dulbecco's Modified Eagle Medium supplemented with glucose and pyruvate (DMEM) and a 200μL drop was placed over the lung tissue in the Petri dishes to aid enzymatic digestion during mechanical homogenisation. During this mincing step, 10mL of the 1mg/mL solution of collagenase/dispase in DMEM were warmed to 37°C in a water bath in 15mL centrifuge tubes.

Once lung tissue was adequately homogenised, it was transferred to the collagenase/dispase-DMEM mixture and the Petri dish was washed to collect any remaining cell fragments. Centrifuge tubes were then loaded onto the MACSmix^{TM} rotator for 45 minutes at 37°C. After this, a 14G cannula and

10mL syringe were used to agitate the tissue gently until a single cell suspension was obtained. This suspension was then injected through a 70µm cell strainer into a fresh 50mL centrifuge tube and the collagenase/dispase was neutralised with the addition of 5mL of PEC growth medium. The resulting filtrate was then centrifuged at 800g for ten minutes and the supernatant gently poured off. The pellet was reconstituted in 3mL of PBS/BSA and mixed thoroughly before adding 20µL of PECAM-1-coated microbeads (prepared as per Chapter 4.12.1). Samples were vortexed and rotated on the MACSmix^{TM} rotator for 15 minutes at room temperature.

During this rotation step, 25cm^2 cell culture flasks were coated with 20g/L gelatin (in distilled water) that had been prepared and autoclaved in advance. The magnetic particle concentrator was assembled in the cell culture hood with three autoclaved 1.5mL microcentrifuge tubes per sample. Once the cells had rotated with the antibody-coated beads, the 3mL sample was divided between the three tubes on the MPC. After 30-60 seconds, the supernatant was aspirated using a glass pipette and beads were resuspended in a fresh 1mL of PBS/BSA. Five of these washes were performed, after which the beads were resuspended in 1mL of PEC growth medium. These cells were added to the gelatin-coated T25 flasks and the total volume of PEC growth medium was made up to 5mL per flask. Cells were incubated at 37°C with 5% CO_2.

A complete media refreshment was performed 24 hours after isolation, following which half of the media was changed on alternate days until cells reached 80-90% confluence, typically after 7-10 days. A representative phase-contrast image of P0 cells at the point of confluence is presented in Figure 4-10 (from IRKO mouse 641).
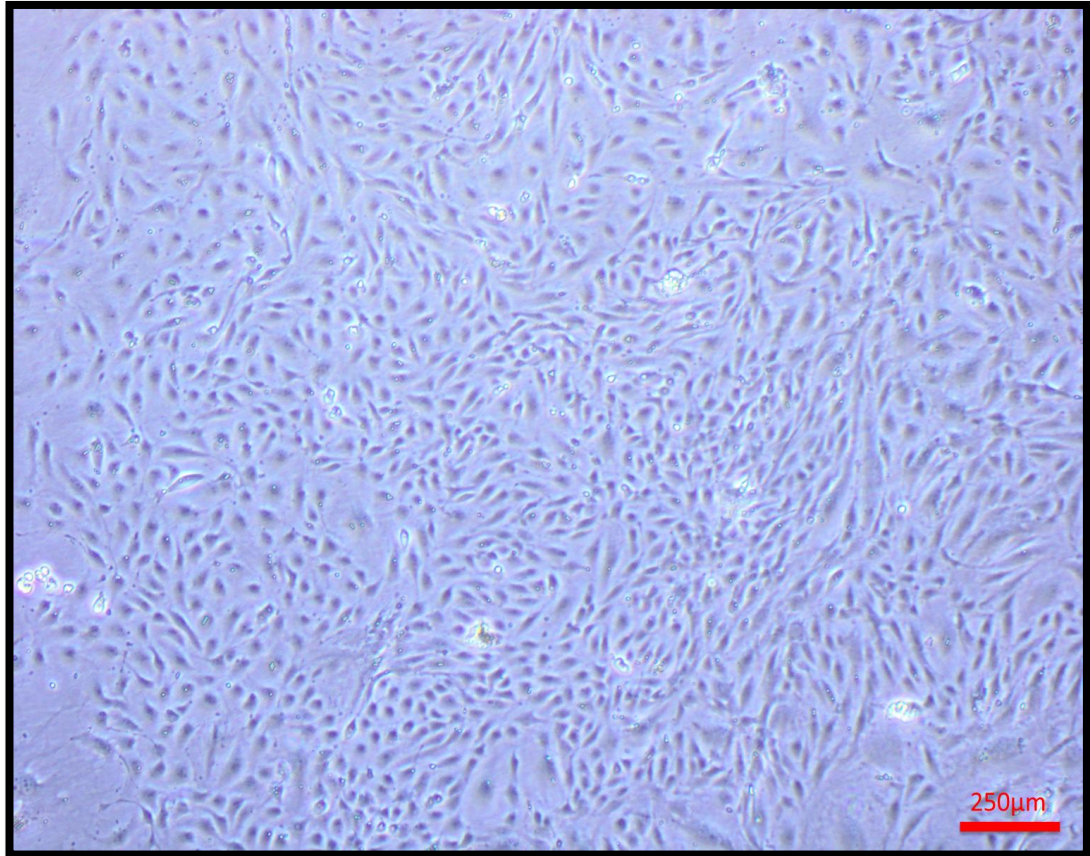
Figure 4-10 Pulmonary Endothelial Cells

Passage 0; magnification x40

4.12.4   Second Antibody-coated Bead Separation

Growth medium was aspirated when cells were sufficiently confluent to contemplate further enrichment, and flasks were washed with warm, sterile PBS to remove all traces of media. 4mL of a pre-warmed 2.5g/L trypsin/EDTA solution were added to each flask and these were incubated at 37°C for up to two minutes, following which cell detachment was confirmed using light microscopy. 8mL of PEC growth medium were added to neutralise the trypsin and the mixture was centrifuged at 400g for eight minutes. Pellets were resuspended in 2mL of PBS/BSA and 10µL of Dynabeads coated with anti-ICAM-2 antibody. In a similar fashion to the first bead separation, these samples were rotated for 15 minutes at room temperature and underwent magnetic bead separation in two 1.5mL microcentrifuge tubes per sample. After this, the beads were resuspended in

PEC medium and transferred to fresh gelatin-coated T25 flasks. Typically, 90% confluence was reached within seven days, at which cells could be detached and re-seeded at various densities for the assays that follow.

In this thesis, cells that have undergone the ICAM-2 separation are referred to as passage number one (P1) and those that are subsequently passaged for assays are referred to as being at P2.

4.12.5   Determination of PEC Purity

Once P1 cells had reached confluence, these were detached using trypsin-EDTA and counted using trypan blue as described in Chapter 4.11.4. 15,000 cells were seeded into 35mm imaging dishes (Ibidi) and incubated at 37°C for 24 hours. At this stage, cells were washed twice in warm PBS and then fixed in 1mL of 40g/L paraformaldehyde in PBS for 15 minutes at 37°C. Immunohistochemistry was performed in conjunction with Dr Richard Cubbon. Following fixation, cells were permeabilised and blocked using a solution of 2.5g/L Triton X-100 and 10g/L BSA in PBS. They were then incubated with an isolectin B4-Alexa Fluor® 488 conjugate at 10μg/mL for two hours at room temperature, after which three PBS washes were performed, for five minutes each. Finally, a nuclear counterstain with 5μg/mL Hoechst 33342 in PBS was applied for ten minutes at room temperature, and another five-minute PBS wash was performed. An LSM700 confocal microscope (Zeiss) was used to image the cells. A representative image of these cells is shown in Figure 4-11.
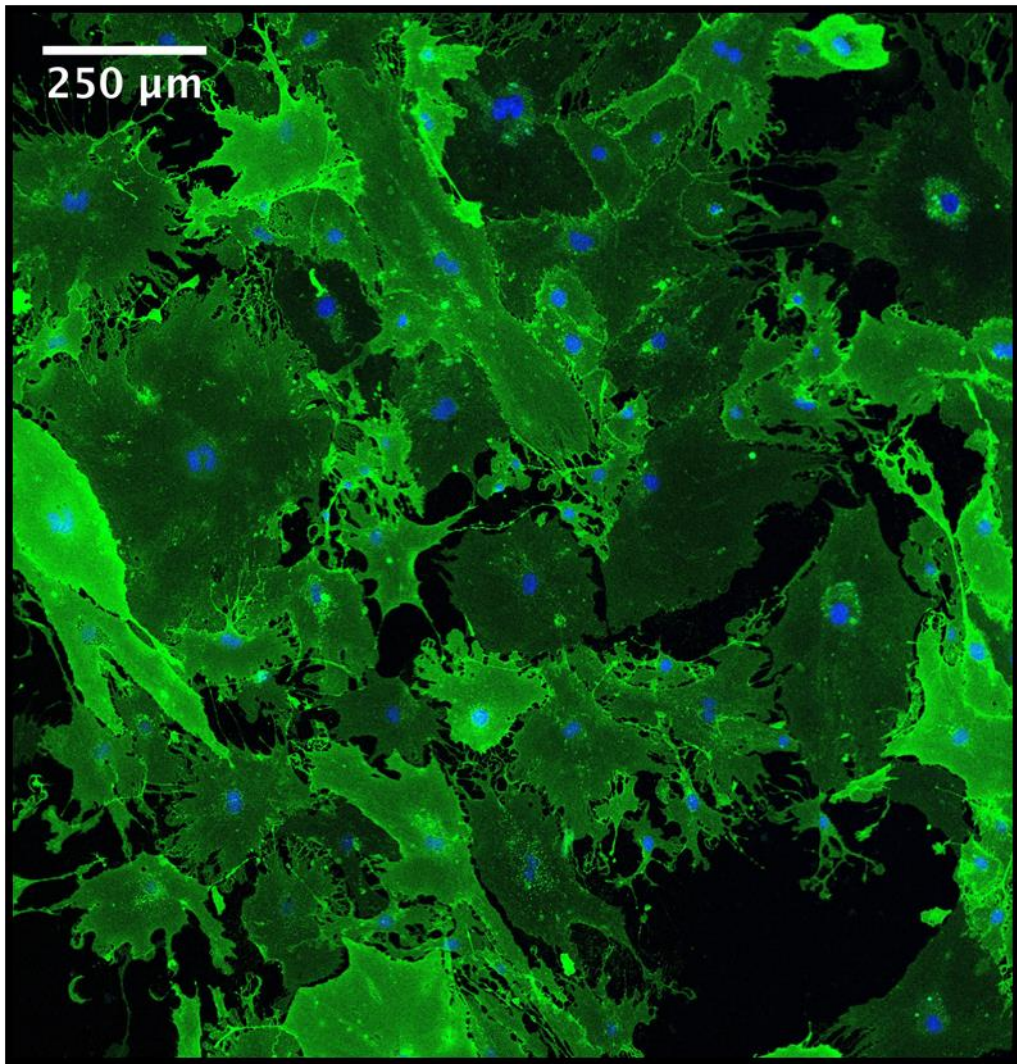
Figure 4-11 Murine pulmonary endothelial cells

Confocal microscope image showing pulmonary endothelial cells (passage 2) stained with isolectin B4 (green) and Hoechst (blue).

4.13 Endothelial Cell Proliferation Assay

Murine PECs were detached from confluent cultures at P1 and counted using trypan blue and a haemocytometer as previously described. 24-well cell culture plates were coated with 20g/L gelatin and cells were seeded onto two wells per mouse, at 20,000 cells per well. These were incubated overnight at 37°C, resulting in 80-90% confluence the following day. At this stage, a commercially available Click-iT® kit (Life Technologies) was used to perform a proliferation assay using 5-ethynyl-2'-deoxyuridine (EdU), a nucleoside analogue that incorporates into the DNA of cells undergoing mitosis. The EdU is conjugated to an alkyne which is detected with an Alexa Fluor® 488-conjugated azide used in the kit.

On first use, the constituents of the kit were prepared and stored as per the manufacturer's instructions, summarised in Table 4-7.

	Reagent	Preparation	Storage
A	EdU	Reconstitute in DMSO and aliquot	-20°C
B	Alexa Fluor® azide	Reconstitute in DMSO	-20°C, dark
C	DMSO	Use to reconstitute A/B	4°C
D	Click-iT® Buffer	Dilute 1:10 in deionised water	4°C
E	Copper sulphate	Use neat	4°C
F	Click-iT® Buffer Additive	Reconstitute in deionised water; freshly dilute 1:10 for each use	-20°C
G	Hoechst	Not used in this project	4°C

Table 4-7   Components of Click-iT® EdU assay kit

EdU = 5-ethynyl-2'-deoxyuridine; DMSO = dimethyl sulfoxide

On the day of the assay, cells were washed twice with warm PBS and replaced with 1mL per well of fresh PEC medium containing EdU at a 1:1000 dilution. This was added for two hours and cells were incubated at 37°C before being washed again with PBS. Cells were then fixed in 40g/L paraformaldehyde in PBS for 15 minutes at room temperature. During this incubation the Click-iT® Buffer Additive (component F) was defrosted and a 1:10 solution was made in deionised water. The paraformaldehyde was washed off with PBS and then cells were permeabilised using 1mL of PBS with 5g/L Triton X-100 per well; this was left for 20 minutes at room temperature. In this time, the Click-iT® cocktail was composed as per manufacturers' instructions, taking care to add the reagents in the specified order. These instructions are summarised in Table 4-8.

Component	Volume (µL)
Click-iT® Buffer	430
Copper sulphate	20
Alexa Fluor® 488 azide	1.2
Click-iT® Buffer Additive	50
Total	*500*

Table 4-8   Composition of Click-iT® cocktail (volumes for one well)

Once permeabilised, cells were washed with PBS and then 500µL of cocktail were measured into each well. The plate was kept protected from light at room temperature for 30 minutes. After this, and a further PBS wash, 500µL of propidium iodide/RNAse were added per well as a nuclear counterstain. The plate was protected from light and kept at room temperature for a 15 minute incubation, following which cells were washed with PBS and then imaged with 500µL of PBS in each well using an Olympus CKX-41

fluorescent microscope. Five images per well were captured at 100x magnification using Cell B software. Images were saved and then proliferating cells (nuclei fluorescing green) and the total number of cells (nuclei fluorescing red) were enumerated using Image J (v1.46r; NIH). Proliferating cells were quantified as a percentage of the total number of cells. Figure 4-12 shows representative images from a wild type mouse (674), including an example of how counting was performed in Image J. For consistency between samples, cells on the edge of the image were counted and any cells that appeared to undergoing cytokinesis were counted as two separate cells; examples of each are shown in the figure.
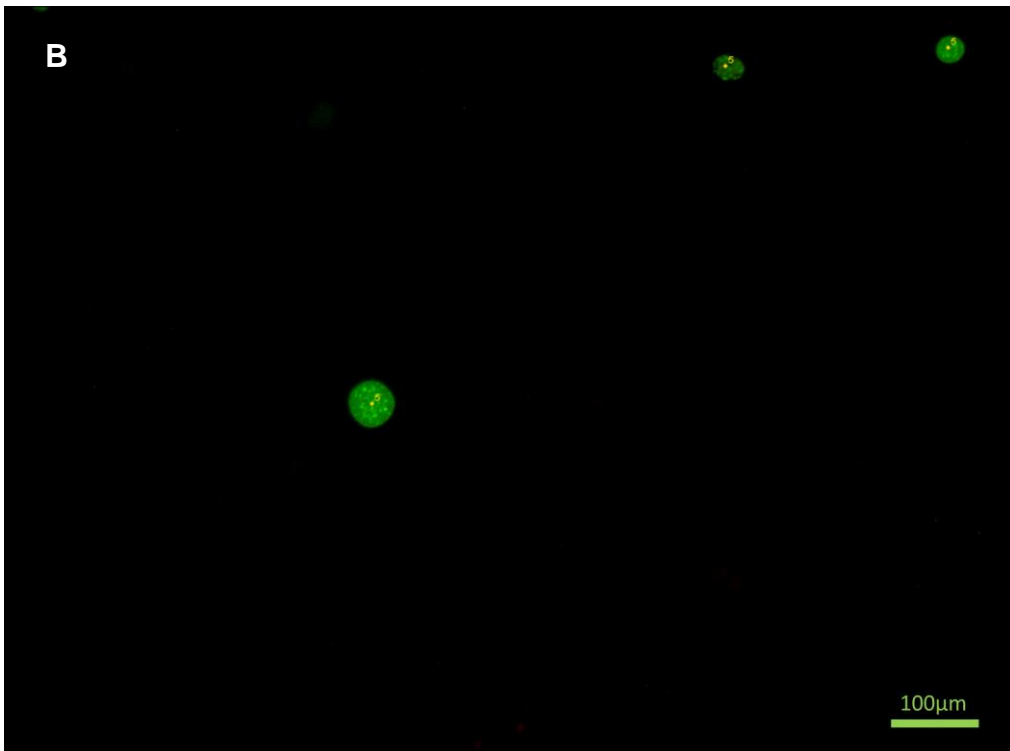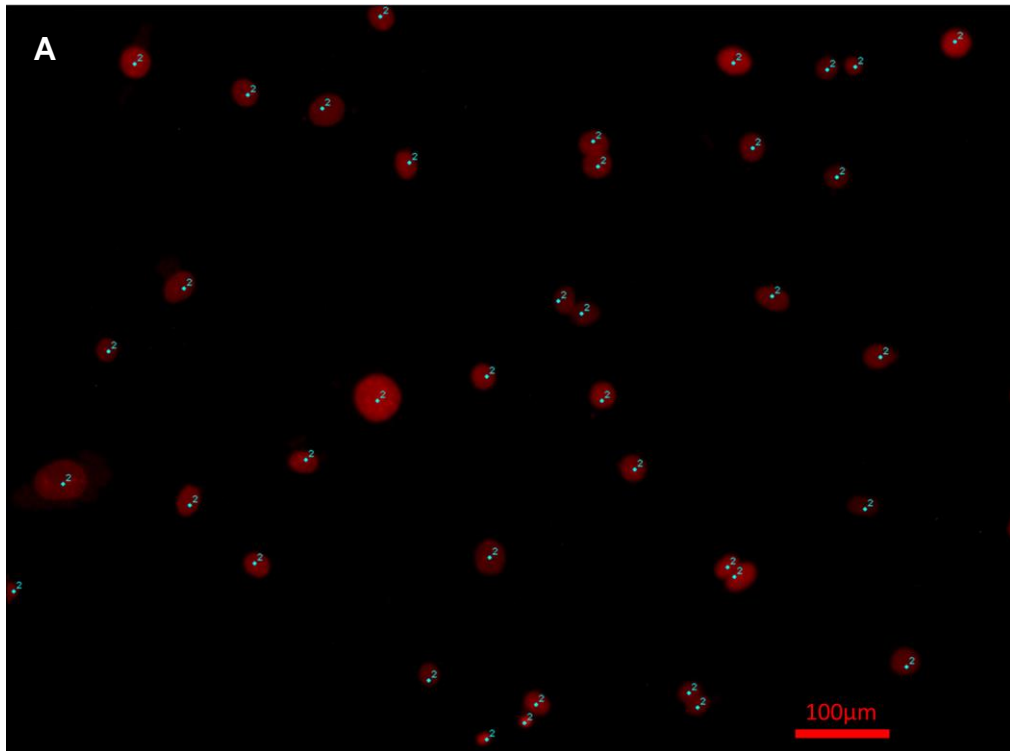
Figure 4-12 Representative Images of EdU Assay

A: Nuclei stained with propidium iodide

B: Proliferating nuclei stained with 5-ethynyl-2'-deoxyuridine (EdU)

Magnification: x100.

4.14 Endothelial Cell Migration Assay (Boyden Chamber)

Confluent cells at P1 were washed in warm PBS and then incubated for four hours in serum-free growth medium (supplemented with an antibiotic/antimycotic solution) on the day of the Boyden chamber assay. Following this, cells were detached using trypsin-EDTA, centrifuged and pellets were reconstituted in 1mL of basal endothelial growth medium (MV2; Lonza) supplemented with 10mL/L FCS. From this 1mL sample, 200,000 cells per mouse were allocated for this assay.

A modified Boyden chamber apparatus was assembled using cell culture inserts with 8µm pores forming the upper compartment and a well of a 24 well cell culture plate forming the lower chamber, as depicted in Figure 4-13. For each animal, two wells were set up as controls containing 750µL of PEC growth medium supplemented with 10mL/L FCS. Two further wells were prepared with vascular endothelial growth factor ($VEGFA_{165}$) at 50ng/mL in the same medium, in order to set up a chemotactic gradient. A cell culture insert was carefully lowered into each well using sterile forceps, ensuring that no large bubbles formed that could hinder cell migration through the pores in the membrane. The cells in suspension were agitated well to ensure even dispersal, and a volume corresponding to 50,000 cells was measured into each insert. The plate was incubated at 37°C for 24 hours.

After 24 hours, the cell culture inserts were carefully lifted out of the wells and fixed in 750μL of 700mL/L ethanol. Once fixed, a clean cotton wool bud was used to remove any non-migrating cells from the upper surface of the membrane and the insert was immersed in water, then stained sequentially in haematoxylin and eosin for 30 seconds each. 500μL of PBS were measured into each insert before imaging using an Olympus CKX-41 microscope. Five images per well were captured at 100x magnification using Cell B software. Images were saved and then stained migrant cells were counted using Image J (v1.46r; NIH). Data were expressed as net migration by subtracting the mean number of migrant cells in the control wells from the mean migration noted in the wells containing VEGF. A representative image is presented in Figure 4-14.
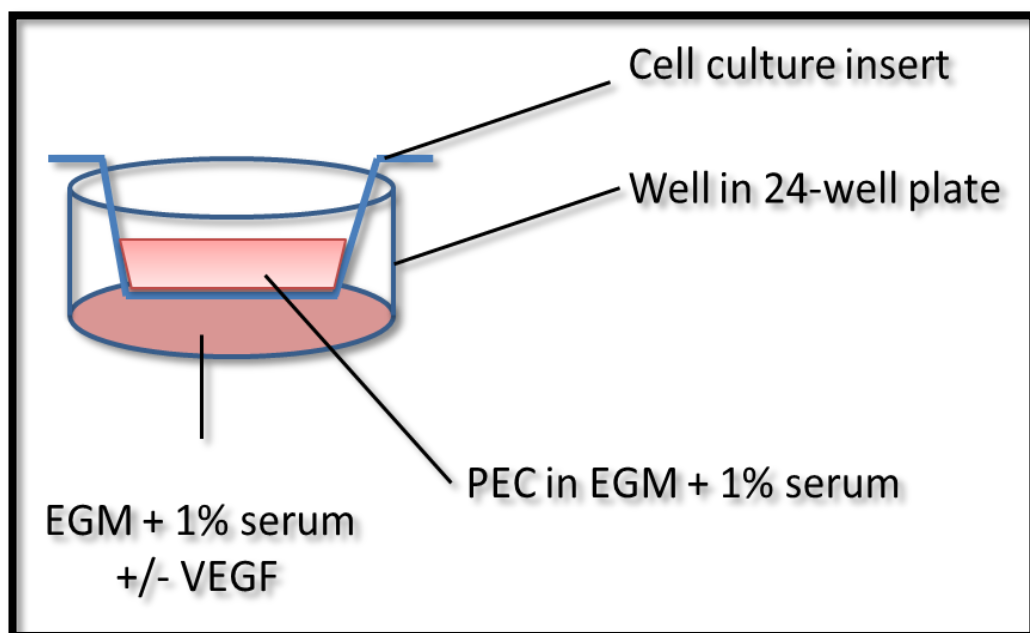
Figure 4-13 Schematic Showing Structure of Boyden Chamber

PEC = pulmonary endothelial cell (50,000 cells/well); EGM = endothelial growth medium; VEGF = vascular endothelial growth factor
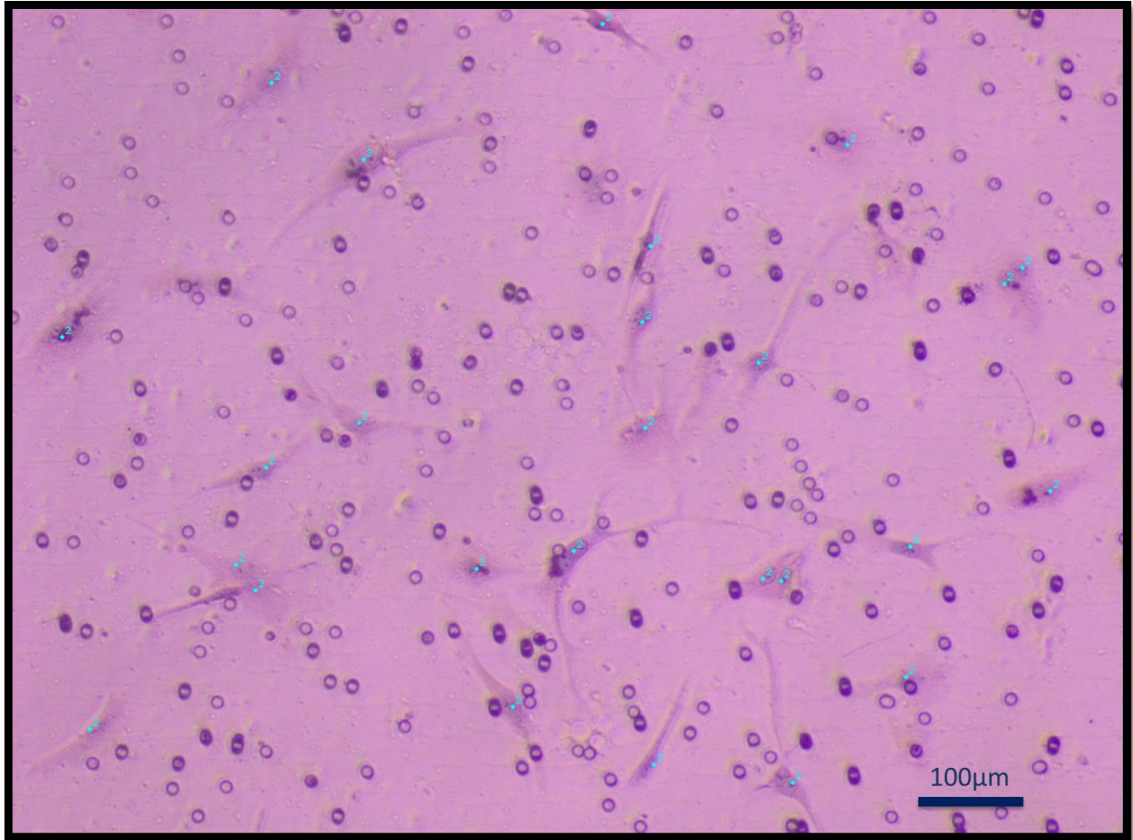
Figure 4-14 Image from Boyden Chamber

Image taken from HIRECOxIRKO mouse 771. Circular pores can be seen in the membrane and migrant cells, stained with haematoxylin and eosin, were counted when both the nucleus and cytoplasm had been clearly visualised. Magnification: x100.

4.15 Endothelial Cell Migration Assay (Scratch Wound)

In addition to the Boyden chamber experiment, PEC migration was studied using an assay of scratch wound closure. A mechanical scratch was made on a confluent layer of PECs at P2 and serial imaging was undertaken using the IncuCyte™ Imaging System (Essen Biosciences) to determine real-time wound closure while cells remained in a 37°C incubator.

Confluent PECs at P1 were trypsinised and counted as previously described. Meanwhile, Essen ImageLock 96 well plates were coated with 20g/L gelatin. From previous experiments undertaken with primary murine PECs in this laboratory, it was determined that the quality of wound creation was optimal at 40,000 cells per well, with gelatin coating and using fully supplemented PEC medium. Cells were therefore seeded at 40,000 cells per well, with three wells per mouse, topped up to 100µL per well with PEC growth medium. Cells were incubated overnight at 37°C and would ordinarily have reached 90% confluence by the following morning.

The next morning, cells were washed in PBS and incubated at 37°C for four hours with serum-free PEC medium. After this, cells were scratched mechanically using the Woundmaker™ 96-pin tool, ensuring that all empty wells contained 100µL PBS to prevent pin damage. This created a longitudinal scratch across the middle of each well, which was appraised under light microscopy to ensure that enough cells had detached to allow appropriate analysis. Each well was washed three times with PBS in order to remove loose cell debris and PEC growth medium was added after the final wash. Cells were placed in the IncuCyte™ and the Woundmaker™ was cleaned as per manufacturer instructions.

Integrated Cell Migration Analysis Module software for use with the IncuCyte™ was used to obtain two images per well, every two hours, for 12 hours; previous experiments had demonstrated a plateau in relative wound

density after this time. An area under the curve (AUC) was calculated and expressed as the mean of all three wells per mouse. Figure 4-15 and Figure 4-16 show representative images of scratch wounds at the time of creation and 12 hours later with partial closure.
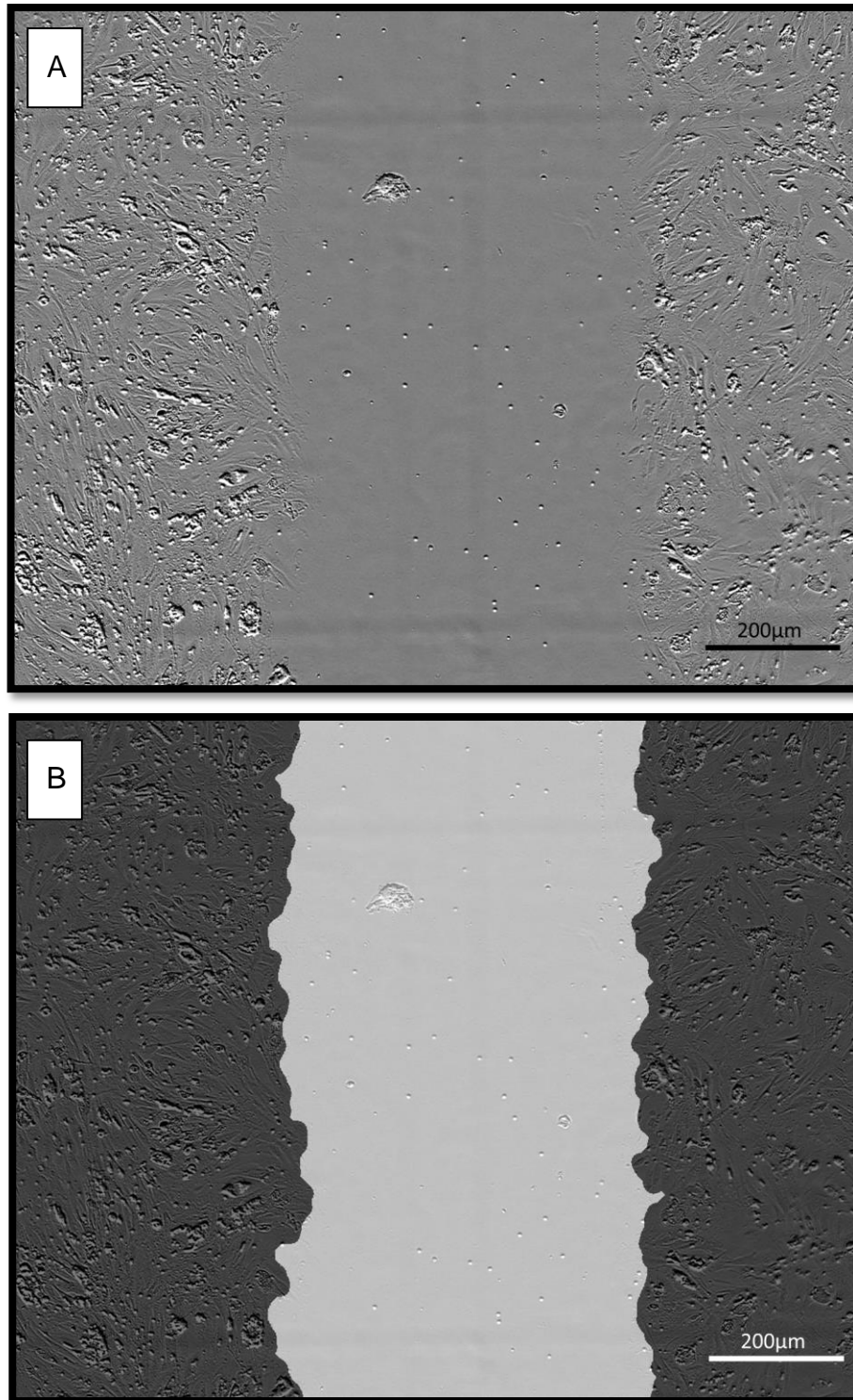
Figure 4-15 Pulmonary Endothelial Cell (PEC) Scratch Wound (t=0)

A = Phase-contrast image showing scratch wound. B = Scratch mask image showing edges of wound as determined by Essen software. From wild-type 909.
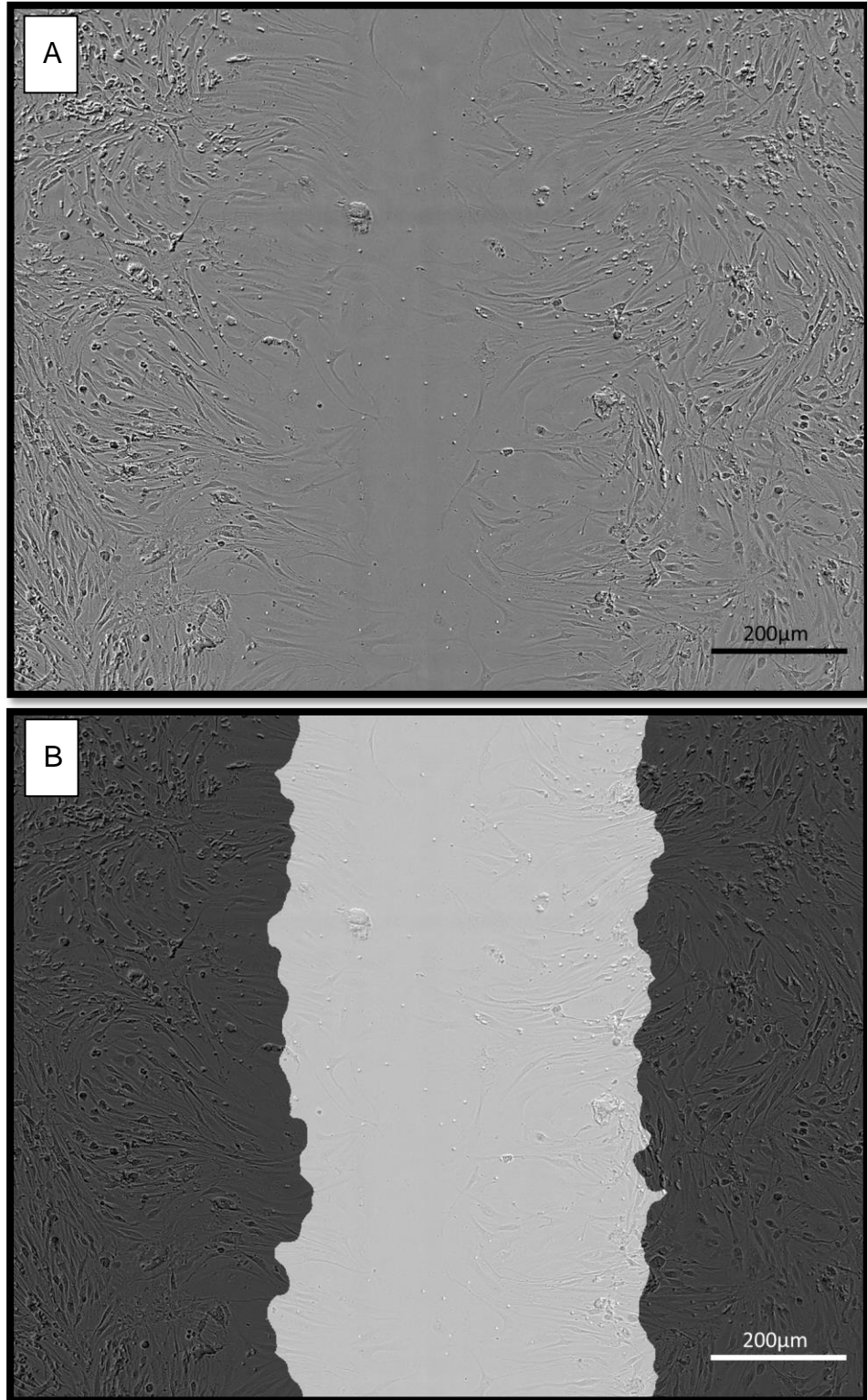
Figure 4-16 Pulmonary Endothelial Cell Scratch Wounds (12 hours)

A = Phase-contrast image showing partially closed wound. B = Scratch mask image showing cell migration beyond original edges of wound. From wild-type 909.

4.16 Endothelial Migration with EPC-Conditioned Media

A similar experiment was undertaken in order to compare the functional effects of EPCs derived from the three genotypes. In this case, human umbilical vein endothelial cells (HUVECs) were used in a scratch wound assay, incubated in conditioned EPC media.

Spleen-derived early outgrowth EPCs were cultured as described in Chapter 4.11; however, cells were seeded at 30 million cells per well on a 6-well fibronectin-coated cell culture plate. After the cells were washed on day four, the EPC growth medium was replaced with 1mL of basal EPC medium supplemented with 10mL/L FCS. This was applied for 24 hours, after which the medium was aspirated and centrifuged at 6000 rpm for six minutes. The supernatant was frozen at -80°C prior to use in the HUVEC scratch assay.

HUVECs were kindly donated by Mrs Jessica Smith at P3 and seeded at 18,000 cells per well into a 96-well Essen ImageLock plate coated with 20g/L gelatin. Three wells were allocated per sample of conditioned medium. The following morning, cells were washed in PBS and incubated at 37°C for four hours with serum-free endothelial growth medium. Cells were then scratched mechanically as described in Chapter 4.15 and washed with PBS. After the final wash, 100µL of conditioned EPC growth media were added to each well, and the plate was placed in the IncuCyte[TM]. One image was obtained per well every two hours for 12 hours; this timing strategy was based on pilot data using WT conditioned media. As with the PEC scratch assay, a mean AUC was calculated for each conditioned media sample, in this case as an average of the three wells per condition.

4.17 Vasomotor Studies of Aortic Rings

Organ bath experiments were performed in conjunction with Mrs Stacey Galloway. I euthanised mice and dissected their aortae, following which Mrs Galloway transported the samples (blinded) to the laboratory and cleaned them before operating the organ bath apparatus. I analysed the data output from these experiments independently and in a blinded fashion.

4.17.1 Dissection of Aortae

Mice were euthanised using rising concentrations of carbon dioxide (unless IVC blood was to be removed concomitantly, in which case terminal anaesthesia was used). Lateral thoracotomies were performed and the heart and lungs removed in order to expose the thoraco-abdominal aorta. The aorta was carefully dissected off the posterior chest wall with efforts to limit stretching or denuding the endothelium in the process. The sample was transported to the laboratory in ice-cold Krebs-Henseleit solution (composed as per Table 4-9), where Stacey Galloway operated the organ bath apparatus to acquire blinded tension data for individual aortic rings.

4.17.2 Preparation of Aortic Rings

The aorta was visualised under direct light microscopy (Olympus SZ61) and any adherent fat or connective tissue was carefully dissected off before separating the aorta into four rings, each measuring 3-5mm in length. These were mounted onto fine opposing triangular wires using the exposed lumen, with care to avoid denuding the endothelium. The wires were then suspended in an organ bath apparatus (PanLabs) and connected to a fixed support at one end and a high sensitivity pressure transducer at the other. Each chamber contained Krebs-Henseleit solution bubbled with 95% oxygen and 5% carbon dioxide at 37°C for the duration of the experiment. Four rings were suspended per mouse (subject to sufficient high-quality tissue being harvested). The organ bath is depicted schematically in Figure 4-17.

Constituent	Concentration (mM)
Sodium chloride	119
Potassium chloride	4.7
Monopotassium phosphate	1.18
Sodium bicarbonate	25
Magnesium sulphate heptahydrate	1.19
Calcium chloride dihydrate	2.5
Glucose	11

Table 4-9   Composition of Krebs-Henseleit solution

4.17.3   Organ Bath Assessment

The organ bath apparatus was set up as above. Each aortic ring was suspended in a chamber with its own micro-environment, allowing exposure of different rings from the same animal to a variety of conditions if necessary.

Rings were initially mechanically stretched to a tension of 3g for two hours. Endothelium-independent vasoconstriction was then assessed using potassium chloride (40 mM KCl; 100μL). If any rings failed to constrict by more than 10% (i.e. to 3.3g or above) then they were excluded from subsequent analyses. KCl was then washed out by multiple refreshments of the Krebs-Henseleit solution in each chamber.
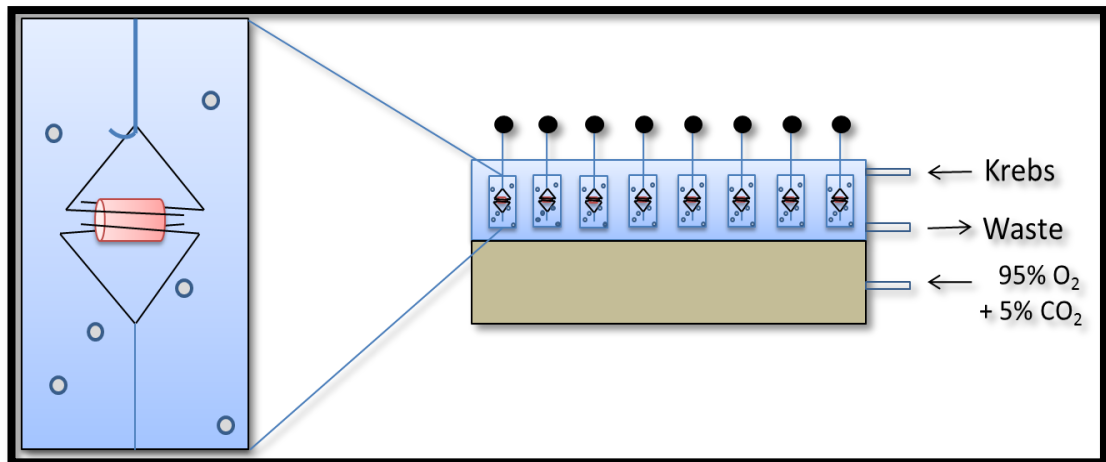
Figure 4-17 Schematic of Organ Bath Apparatus

The organ bath apparatus contains eight chambers, one of which is enlarged on the left. The Krebs-Henseleit buffer (light blue) within the chamber is infused with 95% oxygen (O_2) and 5% carbon dioxide (CO_2) (grey bubbles). Aortic rings (pink) are mounted onto thin triangular wires (black), suspended in buffer as described above.

4.17.4 Endothelium-dependent Vasodilatation

Rings were exposed to the vasoconstrictor phenylephrine used at a specific concentration of 300nM. Again, any rings that did not constrict by 10% or more from baseline were excluded. After pre-constriction, tension was re-equilibrated and incremental concentrations (from 1nM to 10µM) of acetylcholine were added to the chamber. Tension readings were noted and used to create a dose-response curve, from which an EC_{50} (concentration providing 50% of maximum relaxation) was calculated.

4.17.5 Endothelium-independent Vasodilatation

To ensure that any effects seen were related to endothelium-dependent vasodilatation, a similar dose-response curve was created using sodium nitroprusside (SNP; 1nM to 10 µM) after initial phenylephrine pre-constriction. SNP is a NO donor and thus mediates its vasodilatory effects via vascular smooth muscle cells rather than via influences on the

endothelium. Agonists were washed out thoroughly after each part of the experiment.

4.17.6   **Vasoconstriction**

Similarly, cumulative concentrations of phenylephrine (1nM to 10µM) were then used to construct a dose-response curve for constriction. This was performed once at baseline and then repeated after rings were incubated for two hours with 10µL of 0.1M L-NMMA. EC_{50} values were compared for the constriction dose-response curves before and after incubation with L-NMMA to assess the degree of insulin sensitivity and NO bioavailability respectively. Rings that had been exposed to L-NMMA were not used for any further experiments beyond the derivation of post-incubation PE constriction curves.

4.18 Superoxide Assay

In order to measure superoxide concentration in PECs, a Flex Station 3 microplate reader (Molecular Devices) was used to measure dihydroethidium (DHE) fluorescence. DHE, in the presence of superoxide, is oxidised to 2-hydroxyethidium and fluoresces red, allowing indirect quantification of intracellular superoxide generation.

PECs at P1 were enzymatically detached and counted. Based on optimisation experiments, a cell density of 50,000 cells per well on clear, uncoated 96-well cell culture plates was found to be optimal for superoxide detection. Krebs buffer supplemented with 2-[4-(2-hydroxyethyl)piperazin-1-yl]ethanesulfonic acid (HEPES) was the most suitable clear medium in which to incubate the cells during DHE exposure and whilst in the microplate reader; PEC growth medium was found to generate autofluorescence and was not suitable for detection of superoxide. Cells were seeded as such, with two wells for controls and two wells for DHE for each mouse. These were incubated at 37°C overnight in standard PEC media for up to 24 hours, by which time they reached 90% confluence.

Krebs-HEPES buffer was composed as detailed in Table 4-10 and syringe-filtered in a cell culture hood. Once cells were confluent, they were washed in PBS and then incubated either with 100μL of Krebs-HEPES alone (control wells) or with 25μM DHE for 20 minutes at 37°C. Following this, all wells were washed twice with PBS and 100μL of unlabelled Krebs-HEPES medium were added to each well after the final wash. Cells were protected from light and transferred to the Flex Station 3 microplate reader.

Constituent	Concentration (mmol/L)
Sodium chloride	99.01
Potassium chloride	4.69
Dipotassium phosphate	1.03
Sodium bicarbonate	25
Magnesium sulphate	1.2
Calcium chloride dihydrate	2.5
HEPES-sodium salt	20
Glucose	5.6

Table 4-10   Composition of Krebs-HEPES buffer

HEPES = 2-[4-(2-hydroxyethyl)piperazin-1-yl]ethanesulfonic acid.

Using SoftMax® Pro (v5.4.5; Molecular Devices) software, fluorescence was detected using excitation at 500nm and at an emission wavelength of 600nm for two minutes, with readings taken every ten seconds. Prior experiments over longer durations had demonstrated that the fluorescent signal did not decay over this time period. A mean of all the readings taken over the two minutes, in duplicate, was calculated for the DHE-labelled wells and from this was subtracted the mean fluorescence in the unlabelled wells.

4.19 Western Blotting

Western Blots were performed in conjunction with Dr Romana Mughal. I isolated and grew the murine PECs, prepared them for the experiment and performed the insulin stimulation. I lysed the cells and passed them to Dr Mughal, who then performed the protein quantification assay and processed the immunoblots. I then collated the images.

4.19.1   Sample Preparation

Pulmonary endothelial cells were isolated as outlined above and seeded onto 6-well plates coated with 20g/L gelatin. These underwent half media changes every alternate day until the cells reached 95% confluence, at which point they were rendered quiescent with the use of endothelial growth medium supplemented with 10mL/L foetal calf serum (FCS) overnight. The following morning, cells were washed with sterile PBS and then 1mL of basal PEC medium (with no serum) was added to each well. Some cells were stimulated with insulin (100µM working dilution of insulin in 25mM, pH 8.2 HEPES) and others were left in their basal state. After 15 minutes at 37°C, cells were washed in ice-cold PBS twice to ensure cellular processes were arrested. Following this, they were harvested using cell scrapers in 100µL of radio-immunoprecipitation assay (RIPA) buffer (Table 4-11), supplemented with 100µL each of phosphatase inhibitors 2 and 3. Samples were immediately taken for storage at -80°C in 0.5mL microcentrifuge tubes. Samples were then passed to Dr Mughal.

4.19.2   Protein Quantification

Cell lysates were removed from freezer storage and defrosted on ice for 30 minutes. They were then centrifuged at 15,000g for 10 minutes at 4°C before transferring supernatants to fresh microcentrifuge tubes and discarding the pellets. These supernatants were then loaded in a bicinchoninic acid (BCA)

assay for protein quantification using a commercially available assay kit. A sample from each lysate was diluted 1:8 using RIPA buffer (with protease and phosphatase inhibitors) and vortexed. These were measured in duplicate, in volumes of 25µL per well of a 96 well plate, alongside nine standards of bovine serum albumin (BSA) at known concentrations, also in duplicate. The BCA kit contained two reagents for colorimetry: reagent A (sodium carbonate, bicinchoninic acid and sodium tartrate in 0.1M sodium hydroxide) and reagent B (40g/L cupric sulphate). These were mixed in a 50:1 (A:B) ratio and 200µL of the resulting mixture were pipetted into each well. The plate was covered and incubated in a 37°C environment for 30 minutes. A Dynex MRX TC microplate reader and Revelation software (version 4.21) were used to perform colorimetric analysis at a wavelength of 562nm. The BSA standards were used to construct a standard curve, which was appraised for linearity and correlation co-efficient (r^2), the latter accepted only when > 0.99. Sample protein concentrations were inferred using this curve and values accepted at a co-efficient of variation (CV) between duplicates of < 10%. A correction was performed for the 1:8 dilution of the original lysate.

4.19.3   **Gel Electrophoresis**

Using the above protein concentrations, 10-15µg of each sample were diluted in loading dye (1:4) and sample reducing buffer (1:10) and then topped up to a loading volume of 40µL, if necessary, using RIPA buffer. These samples were heated at 95°C for five minutes, following which they were loaded into a pre-cast, commercially purchased polyacrylamide gel along with 6µL of a protein reference ladder. The gel was placed in a Criterion Cell tank (Bio-Rad) containing 500mL of running buffer, composed of 25mL of 2-(N-morpholino)ethanesulfonic acid/sodium dodecyl sulphate (MES SDS) running buffer and 475mL of de-ionised water. Electrophoresis was then performed at 100V for two hours or until the sample dye could be visualised at the bottom of the gel.

4.19.4   **Transfer**

The electrophoresed gel was washed briefly in deionised water to remove traces of running buffer. Dry transfer of proteins to a nitrocellulose membrane was carried out using the iBlot system. The transfer pack was assembled so the membrane was sandwiched between filter paper and an anode and cathode. A plastic roller was used to remove any air bubbles which may hinder transfer to some areas of the membrane. The transfer was complete in seven minutes at the standard manufacturer program setting (P0).

4.19.5   **Immunostaining**

After protein transfer, the membrane was separated from the rest of the contents of the "sandwich" and washed in a blocking solution containing 50g/L BSA in tris-buffered saline (TBST; 50mM Tris, 150mM NaCl, 1g/L Tween; pH 7.4) for five minutes. The membrane was then cut at relevant points with a clean scalpel using the protein ladder as a guide, so as to allow simultaneous immunostaining for more than one protein at different molecular weights. Each membrane was labelled using a pencil. Membranes were then incubated in 15mL of TBST for one hour at room temperature to block any non-specific binding sites.

The primary antibody was prepared in a BSA-TBST solution at a dilution described in Table 4-12. The blocking solution was discarded at the end of the hour incubation, following which the primary antibody was applied and the specimen was incubated overnight at 4°C. The following morning, the antibody solution was recovered for repeat usage (up to three times). The membrane was then washed three times, for five minutes each, in TBST.

The secondary antibody was then prepared (Table 4-12) in BSA-TBST. The membrane was incubated in the secondary antibody for one hour at room temperature. Following this, the antibody solution was discarded and the membrane washed three times in TBST for fifteen minutes each.

Finally, the membrane was removed from the universal container and carefully straightened out onto cling film. Each membrane was covered with 1mL Immobilon Western Chemiluminescent HRP Substrate (500uL peroxide solution, 500uL enhancer solution) before exposure and imaging using the Syngene G imaging system.

4.19.6   Stripping Membranes

When phosphorylated Akt and eNOS were being probed, this could be done on the same membranes as those used for Akt and eNOS blots, by using a Restore PLUS^{TM} Western Blot stripping buffer. Membranes were washed to remove the chemiluminescent substrate solution, then covered with 10mL of stripping buffer and incubated at room temperature under gentle agitation for 10 minutes. Following this, they underwent three washes lasting five minutes each with TBST. They were then incubated in blocking solution (BSA-TBST) for an hour before being re-probed with new antibodies.

Constituent	Volume / /Mass
Tris-hydrochloric acid 500mM	25mL
Glycerol	20mL
Distilled water	43mL
EDTA 100mM	2mL
Sodium dodecyl sulphate	2g

Table 4-11   Constituents of RIPA Lysis Buffer

EDTA = ethylenediamine tetraacetic acid; RIPA = radio-immunoprecipitation assay.

Protein	Dilution	Manufacturer
Primary Antibodies		
Phosphorylated Akt (D9E) XP (Serine 473)	1:2000	Cell Signaling #4060
Total Akt (pan 11E7)	1:1000	Cell Signaling #4685
Phosphorylated eNOS (Serine 1177)	1:1000	BD Biosciences #612393
Total eNOS	1:1000	BD Biosciences #610296
Beta-actin	1:20,000	Cell Signaling #4970
HRP-conjugated Secondary Antibodies		
Polyclonal goat anti-mouse IgG	1:1000	Dako #P0161
Polyclonal goat anti-rabbit IgG	1:1000	Dako #P0217

Table 4-12   Antibodies used in Western Blots

eNOS = endothelial nitric oxide synthase; HRP = horseradish peroxidase

4.20 Statistical Analysis

All continuous data sets are expressed as mean with standard error of mean (SEM) unless otherwise stated. Graphs and statistical analyses were performed using either GraphPad Prism v6 (2012) or Microsoft Excel 2007. For the majority of analyses, two-tailed unpaired or paired Student's t-tests were performed as appropriate. For GTT and ITT analyses, the area under the curve (AUC) function was calculated. A p-value of <0.05 was deemed statistically significant and is represented with a * symbol.

Chapter 5 **Results**

5.1 Genotyping

Typical PCR gels for the HIRECO transgene (Figure 5-1) and IRKO cassette (Figure 5-2) are demonstrated, with a 1000 base pair ladder for reference.

Figure 5-1   HIRECO PCR gel image
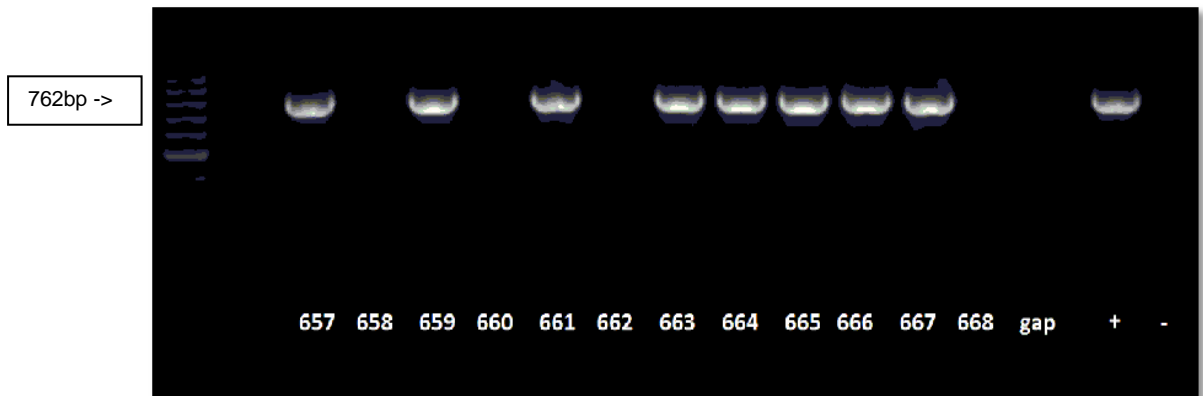
DNA was extracted from ear notches and underwent PCR for the human insulin receptor endothelial cell overexpression (HIRECO) transgene, denoted by a single band at 762 base pairs (bp); wild-type denoted by absence of band. Controls on right. PCR = polymerase chain reaction.
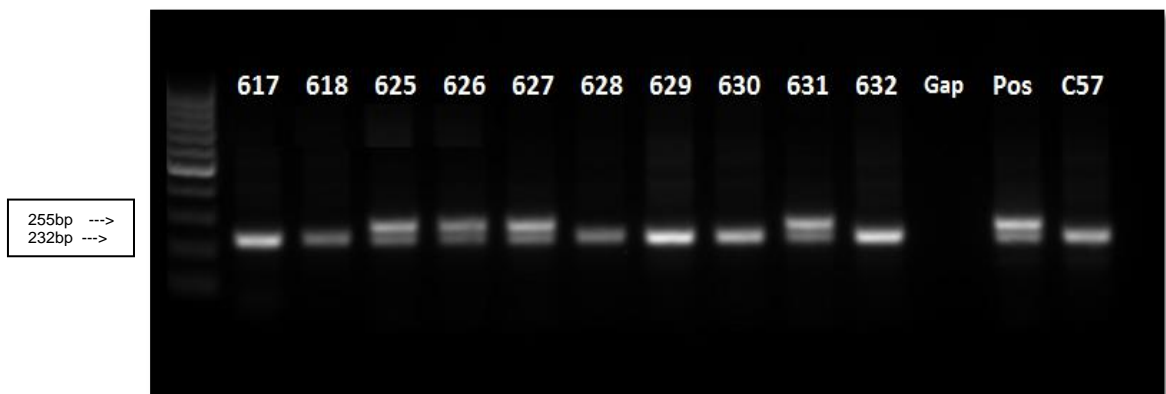
Figure 5-2   IRKO PCR gel image

DNA was extracted from ear notches and underwent PCR for the Insulin receptor knockout (IRKO) gene cassette, denoted by a double band at 232 and 255 base pairs (bp) with a single band at 235 bp for wild-type. Controls on right.

5.2 Viability and Morphology

All mice were born at the expected Mendelian frequency and suffered no propensity towards increased rates of illness or death in adulthood. Total body weight (Figure 5-3) was not found to differ between WT, IRKO and HIRECOxIRKO mice. Despite non-significant differences in mass at an age of two months, weights converged again as the mice matured. Growth was found to plateau at four months, at which point there was no statistically significant difference in total body weight between IRKO [27.4 (0.4) g] and HIRECOxIRKO [28.3 (1.2) g]; p=0.48 (Figure 5-4).

Wet organ weight from selected tissues was also recorded at the time of sacrifice. Again, no significant differences were observed in individual organ weights (normalised to total body weight), as shown in Figure 5-5.
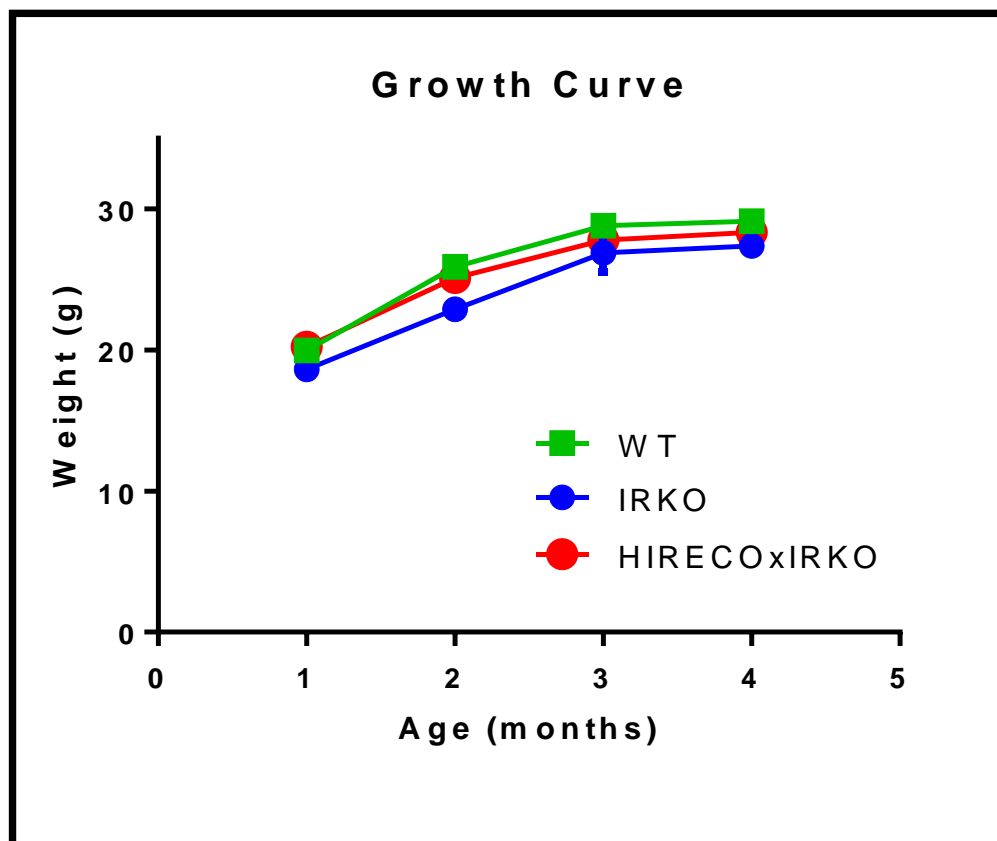
Figure 5-3   Total body weight from 1-4 months

(n=7,6,5)
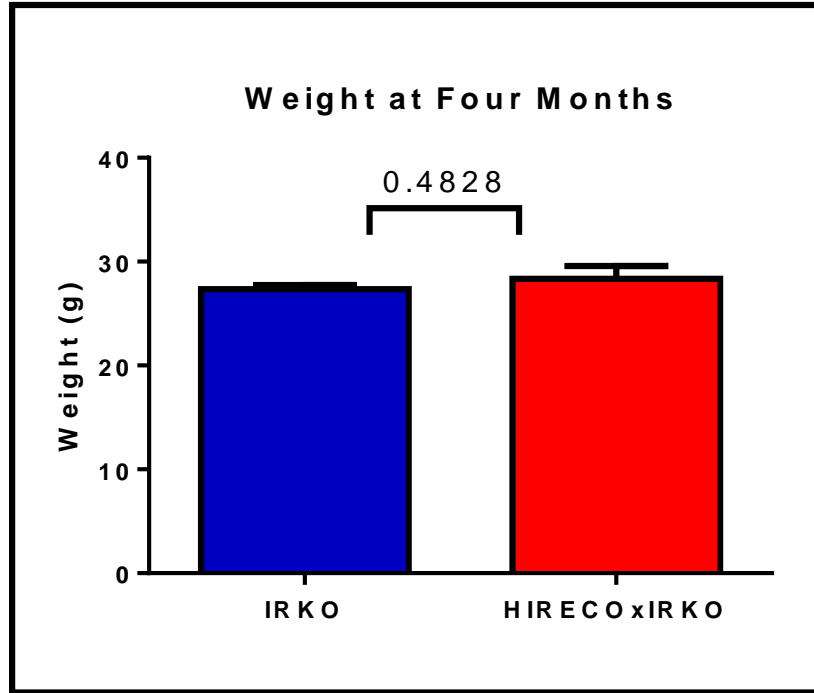
Figure 5-4   Total body weight at four months

(n=6,5)
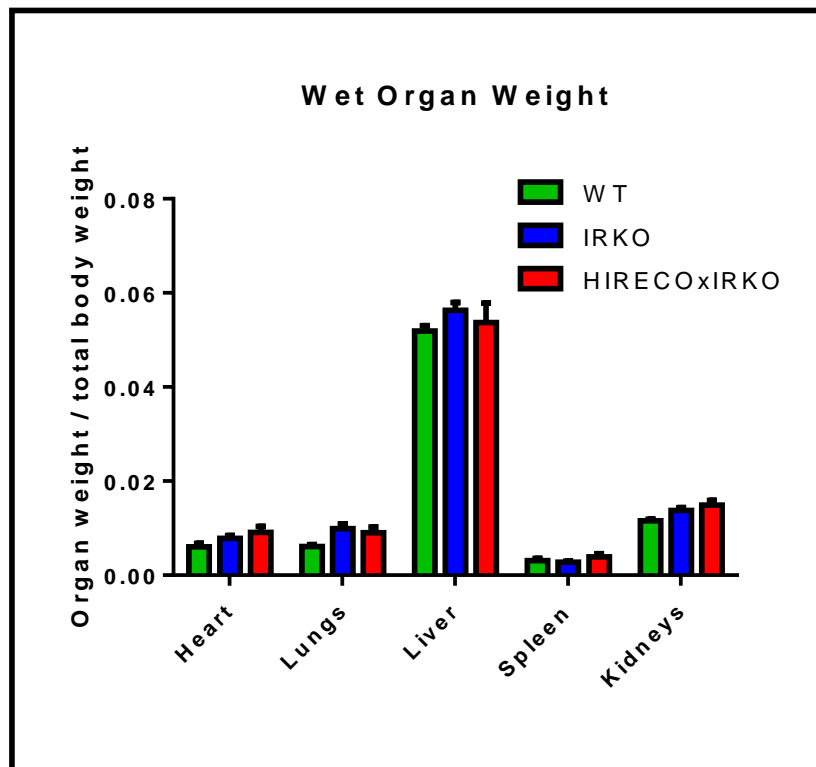
Figure 5-5   Wet organ weight

(n=6,5,6)

5.3 Metabolic Testing

It has previously been demonstrated that IRKO mice have unperturbed glucose handling and insulin tolerance when compared with wild-type (WT) littermates [60]. In the current study, the metabolic parameters of fasted animals in the HIRECOxIRKO colony to glucose was ascertained using periodic capillary blood glucose measurements after the administration of intraperitoneal (IP) glucose or Actrapid insulin.

HIRECOxIRKO mice were found to display a very similar profile to IRKO littermates after IP glucose injection (Figure 5-6), with no statistically significant difference noted in the area under the curve (AUC) analysis. Similar findings were noted in the insulin tolerance test (Figure 5-7). These findings suggest that, like IRKO mice, HIRECOxIRKO animals do not have glucose intolerance or diabetes.

Another method for assessing insulin sensitivity is the measurement of plasma insulin concentration after an overnight fast. For this experiment, saphenous venepuncture was used to obtain whole blood for ELISA. The results (Figure 5-8) suggest no significant difference between IRKO [0.70 (0.18) ng/mL] and HIRECOxIRKO [0.76 (0.14) ng/mL] mice; p=0.78.
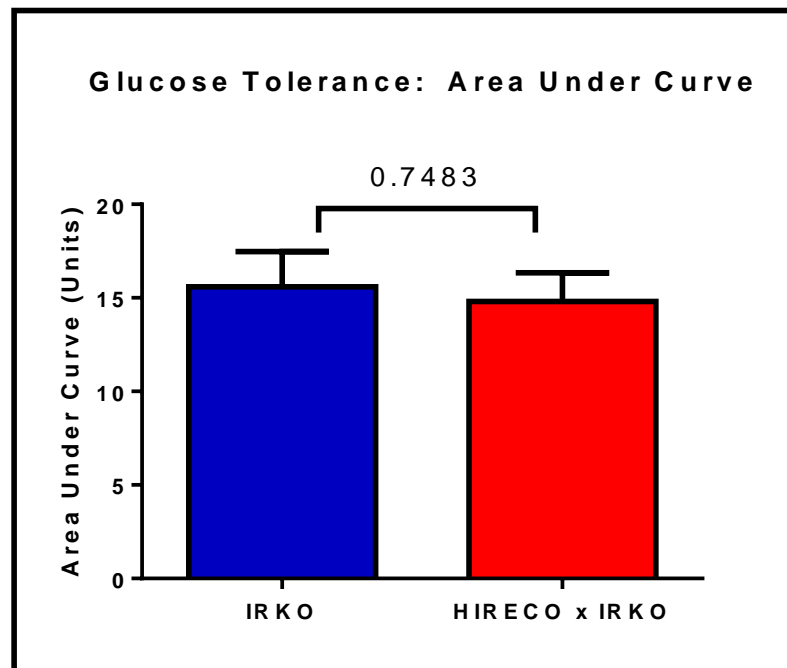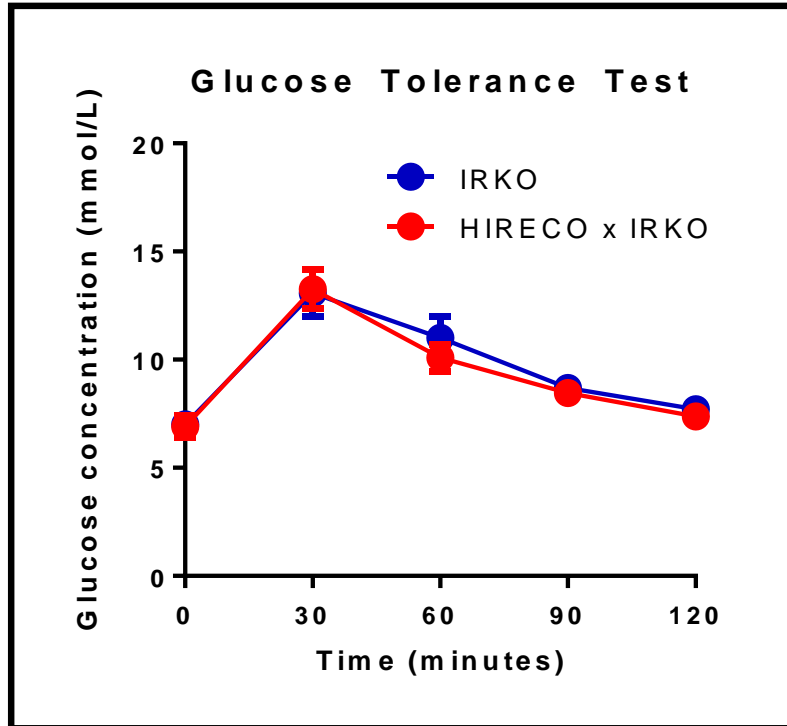
Figure 5-6   Glucose Tolerance Test

Mice were fasted overnight and then given 1mg/g intraperitoneal glucose. Capillary glucose measurements were taken at various time points after glucose challenge. Upper panel: dynamic tolerance test. Lower panel: area under curve. (n=7).
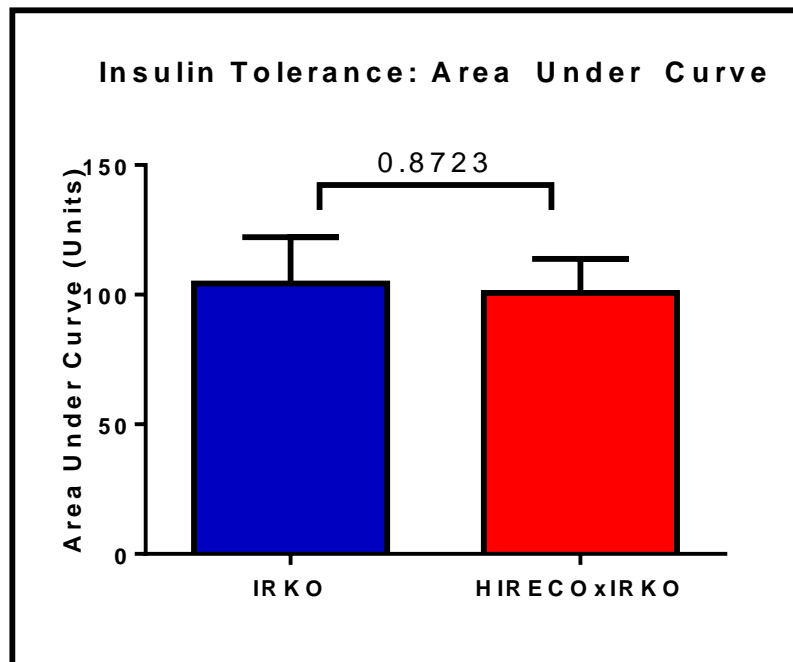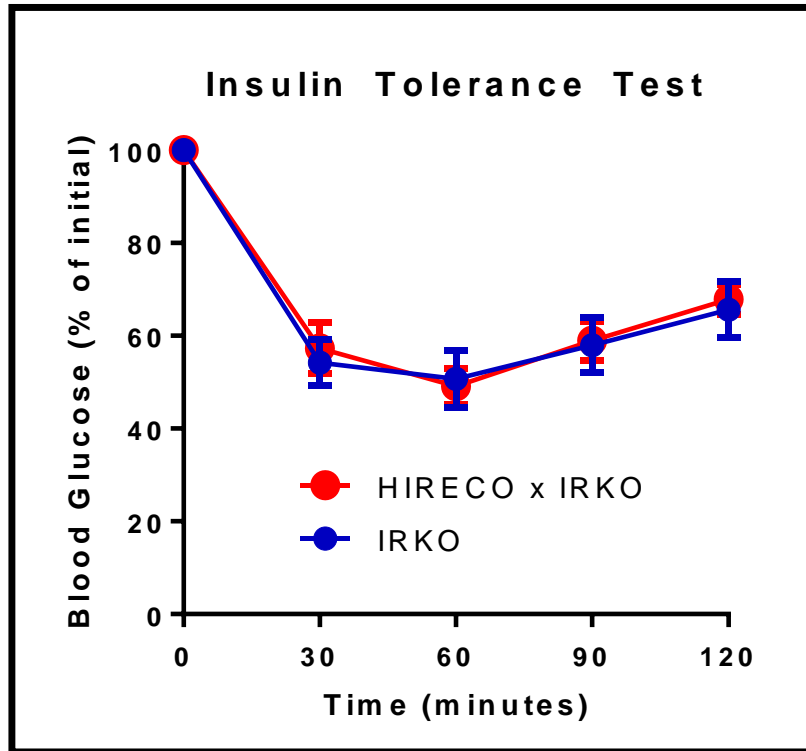
Figure 5-7   Insulin Tolerance Test

Mice were fasted for four hours and then given 0.75 International Units/kg intraperitoneal Actrapid insulin. Capillary glucose measurements were taken at various time points after insulin challenge. Upper panel: dynamic tolerance test. Lower panel: area under curve. (n=10).
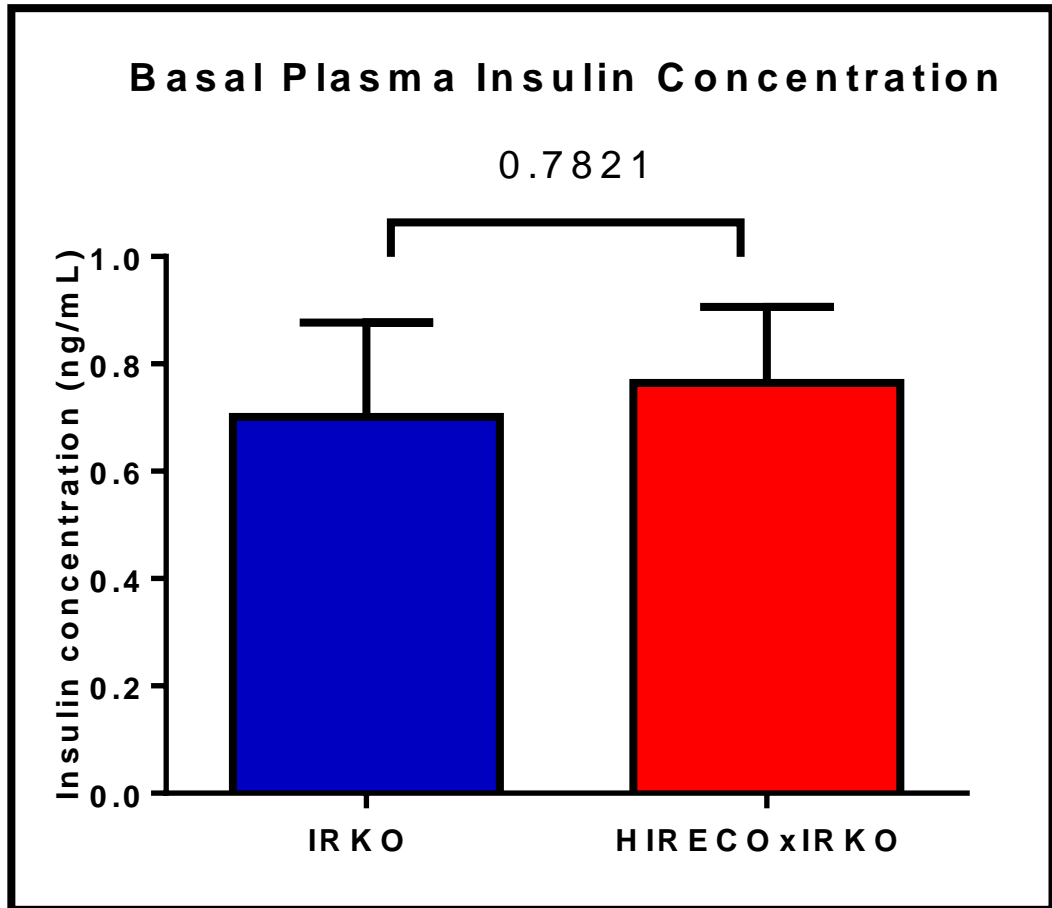
Figure 5-8   Plasma Insulin Concentration

Whole blood was removed using saphenous vein puncture and insulin concentration was measured in plasma using an enzyme linked immunosorbent assay (ELISA) kit. (n=8).

5.4 Blood Pressure

Previous research has demonstrated that systolic blood pressure is raised in IRKO mice compared with WT [60]. The same phenomenon was observed in the HIRECOxIRKO colony in the current project, as shown in Figure 5-9. Mean (SEM) systolic BP in WT was 94.8 (3.0) mmHg, with significantly higher readings in IRKO [105.9 (3.0) mmHg]; p=0.02. Interestingly, the mean systolic BP in HIRECOxIRKO mice was significantly lower than in IRKO [97.3 (2.5) mmHg], p=0.04. Blood pressure in HIRECOxIRKO mice was not significantly different from that in WT; p=0.53.
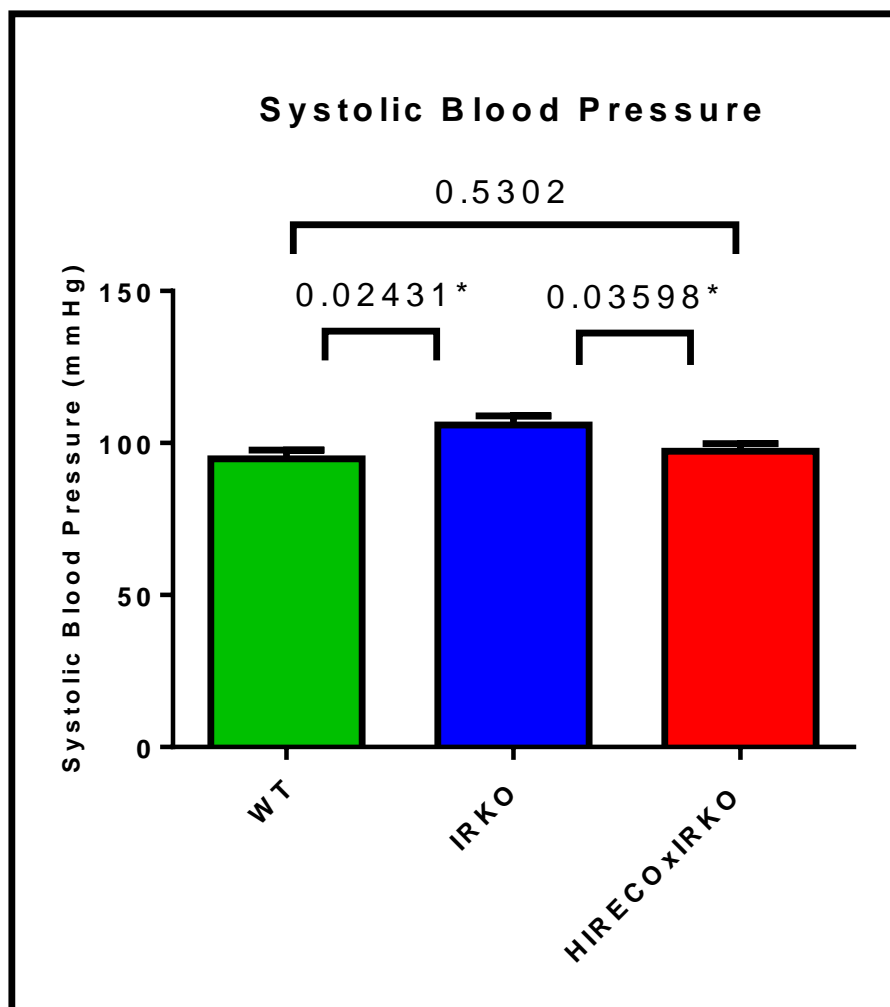
Figure 5-9   Systolic Blood Pressure

Blood pressure was measured using tail-cuff plethysmography in conscious animals after two habituation sessions. (n=10,19,18).

5.5 Quantitative PCR

Having established the viability and gross metabolic and *in vivo* vascular phenotype of the HIRECOxIRKO mouse, we sought to validate the relative expression of murine and human isoforms of the insulin receptor. IRKO are haploinsufficient for the murine isoform (mIR); HIRECOxIRKO have undergone no additional mIR manipulation so these mice were expected to show a similar pattern. Meanwhile, we hypothesised that expression of the human insulin receptor (hIR) would be targeted to endothelial cells in HIRECOxIRKO mice, with no detectable hIR mRNA in WT or IRKO. To examine insulin receptor expression, homogenised solid organs (lungs and aortae) and primary cultured endothelial cell lysates were used to perform quantitative PCR for mIR and hIR mRNA. Figure 5-10 shows that hIR mRNA was undetectable in solid organs harvested from WT and IRKO, confirming that insertion of the hIR transgene only affected HIRECOxIRKO mice.
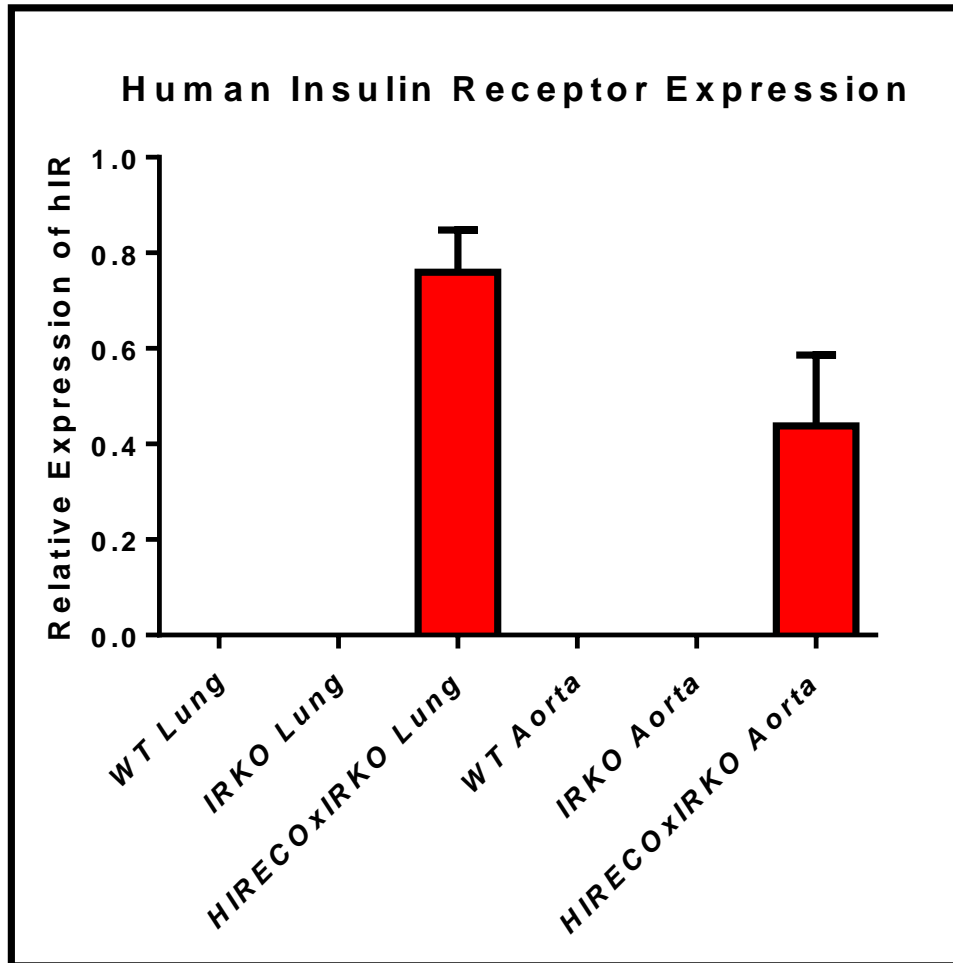
Figure 5-10 Expression of human insulin receptor (hIR) in solid organs

Whole organs were homogenised and RNA extracted. A SYBR Green probe was used to perform quantitative PCR using primers directed to the human insulin receptor. Quantified relative to beta-actin expression. (n=6,5,5 for lung; 3,2,5 for aorta).
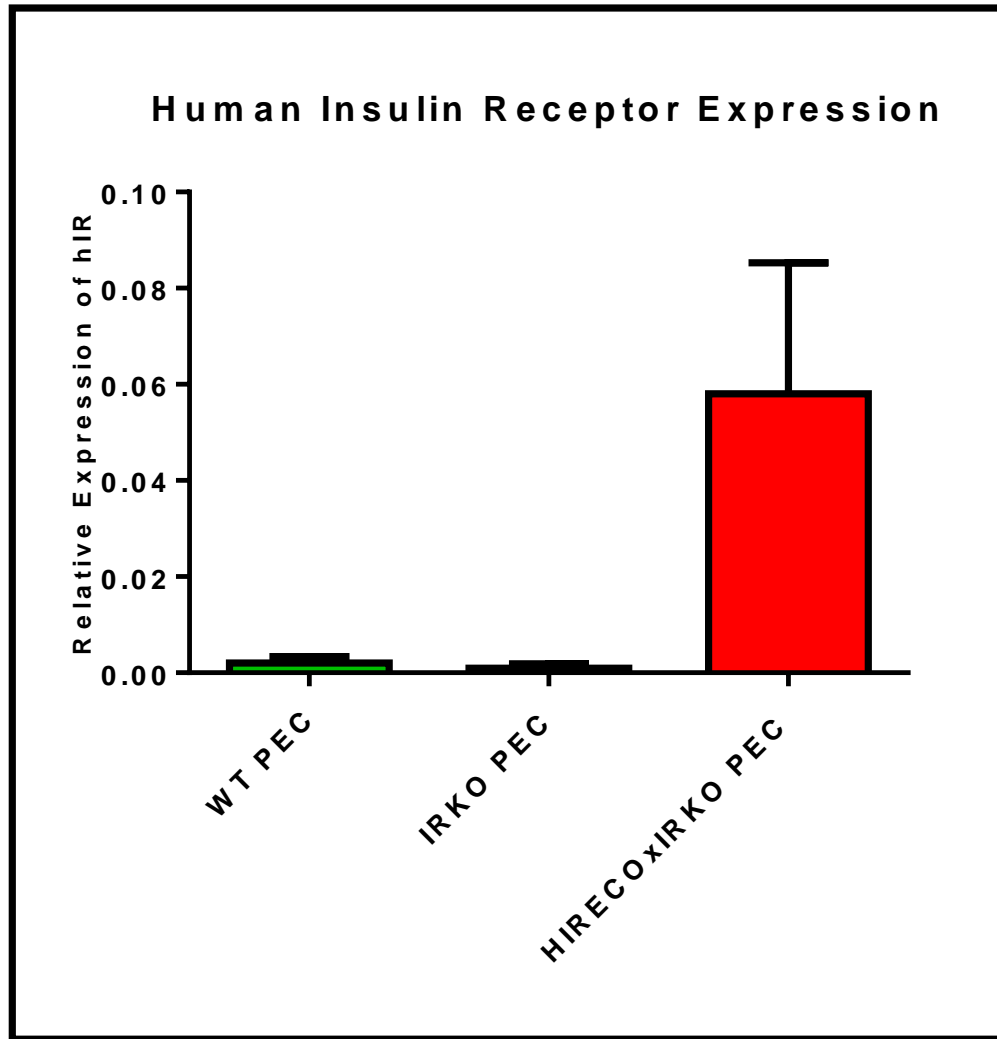
Figure 5-11 Endothelial expression of human insulin receptor (hIR)

Pulmonary endothelial cells (PEC) were cultured from murine lungs and harvested in Tri-reagent at passage 2. RNA was extracted and a SYBR Green probe was used to perform quantitative PCR using primers directed to the human insulin receptor. Quantified relative to beta-actin expression. (n=6,3,4).

Figure 5-11 demonstrates that, as expected, expression of human insulin receptor mRNA in endothelial cells is targeted to HIRECOxIRKO mice, with no significant expression in lysates from WT and IRKO endothelial cells. Additionally, pilot experiments in our laboratory using monocytes from pure HIRECO mice have shown no detectable hIR mRNA, suggesting a lack of overlap with myeloid cells using the Tie-2 promoter strategy.
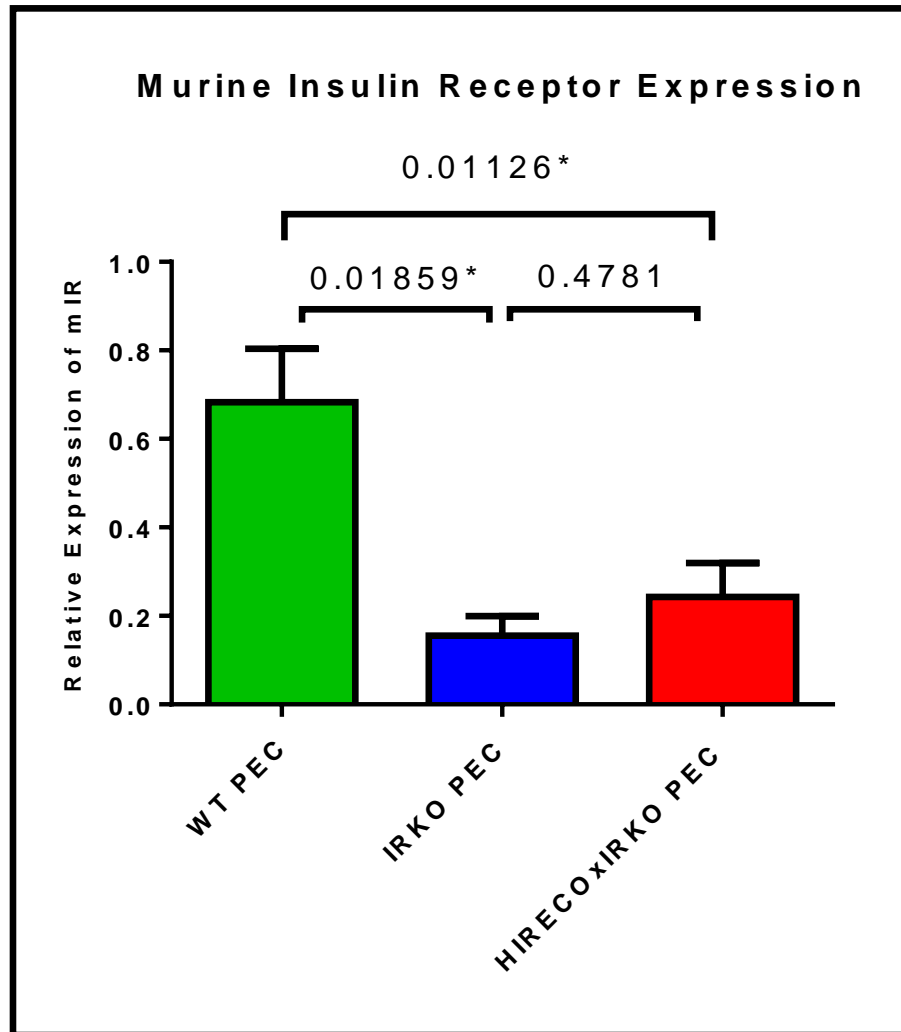
Figure 5-12 Endothelial expression of murine insulin receptor (mIR)

Pulmonary endothelial cells (PEC) were cultured from murine lungs and harvested in Tri-reagent at passage 2. RNA was extracted and a Taqman® probe was used to perform quantitative PCR using primers directed to the murine insulin receptor. Quantified relative to beta-actin expression. (n=5,3,6).

As demonstrated in Figure 5-12, the murine insulin receptor is downregulated in endothelial cells in IRKO mice, as expected. There was no significant recovery in mIR mRNA levels in HIRECOxIRKO endothelial cells. These experiments confirm that the hIR is only expressed in HIRECOxIRKO mice and these animals appear to show similar levels of endothelial mIR expression to IRKO.

5.6 Vascular Injury

IRKO mice exhibit impaired vascular repair after denuding arterial wire injury
[164]. In the current study, HIRECOxIRKO mice appeared to show rescue of
this impairment [57.8 (3.4) % regenerated] compared with IRKO [47.5 (3.3)
%]; p=0.04. This represented a return to the level of repair seen in WT mice
[54.1 (3.3) %]; p=0.50. The summary data are presented in Figure 5-13 and
representative images from each genotype are shown in Figure 5-14.
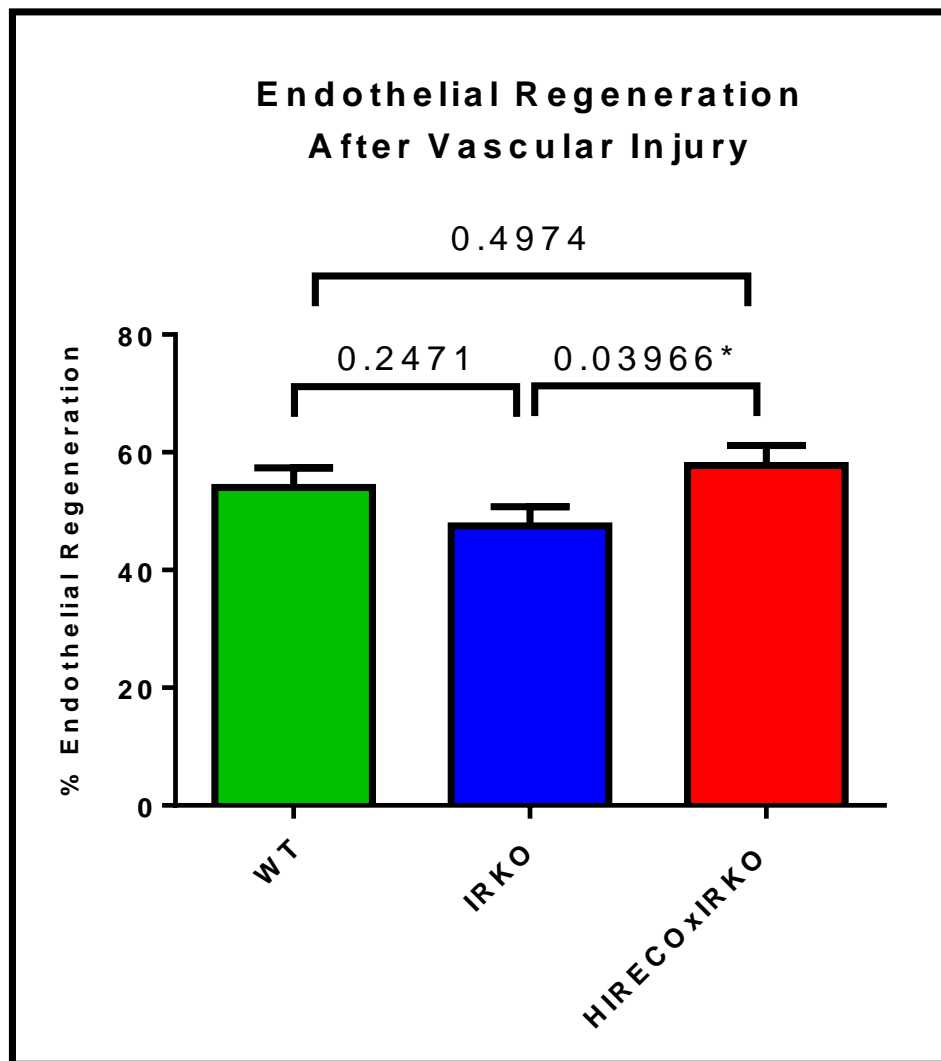
Figure 5-13 Endothelial Regeneration after Vascular Injury

*Mice underwent denuding femoral artery injury and vessels explanted at day
four were stained with Evans Blue dye, allowing measurement of percentage
endothelial regeneration. (n=6,14,12).*
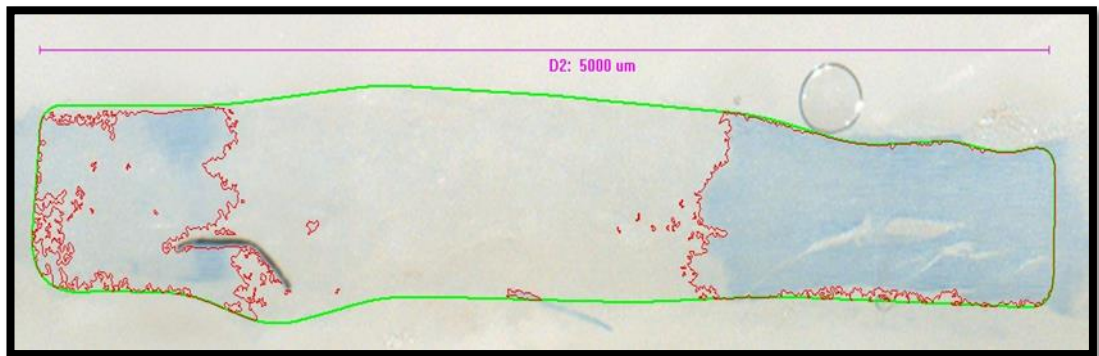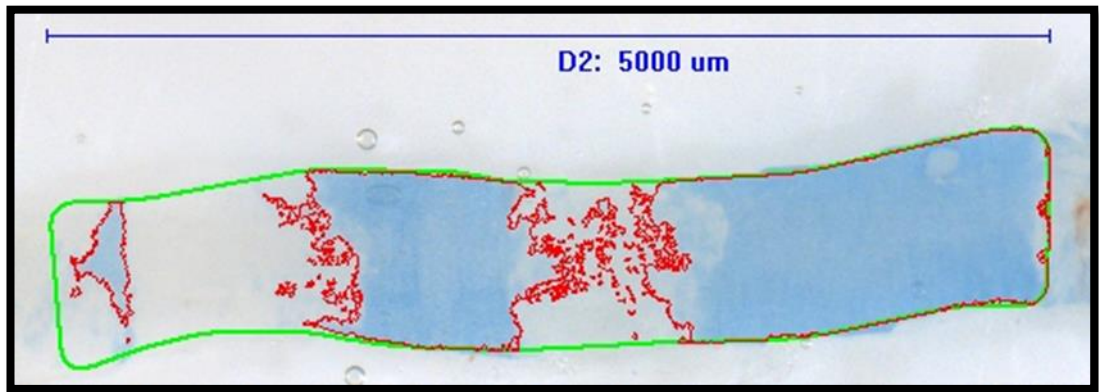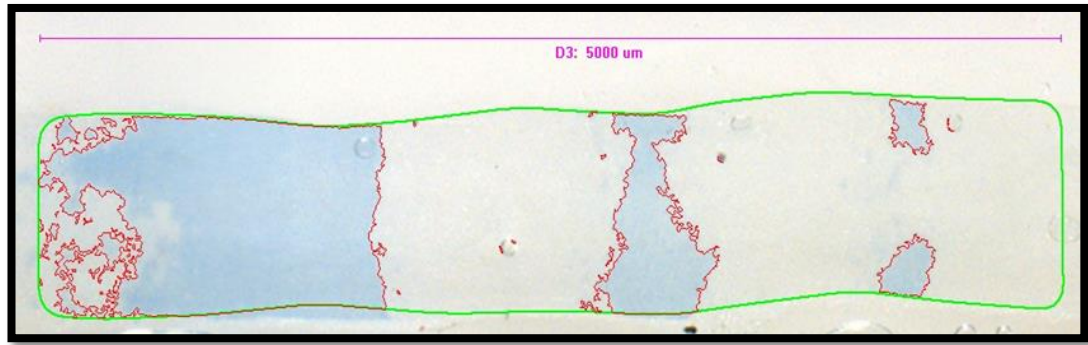
Figure 5-14 Representative images of femoral arterial injury

Magnification: x20. Areas stained with Evans Blue denote ongoing denudation. Red lines demonstrate details of analysis. Upper panel = Wild-type 212. Middle panel = IRKO 647. Lower panel = HIRECOxIRKO 186.

5.7 Circulating EPC enumeration

One of the postulated mechanisms for impaired vascular repair in IRKO mice in the Kahn *et al* study was that IRKO had reduced numbers of circulating progenitor cells (CPC) co-expressing stem cell antigen-1 (Sca1) and foetal liver kinase-1 (Flk1) compared with WT. This was recapitulated in the current study: WT mice had a mean (SEM) of 235.5 (44.4) per 100,000 mononuclear cells compared with a mean (SEM) in IRKO of 104.9 (14.9) per 100,000; p=0.01. However, there was no significant improvement in CPC numbers in HIRECOxIRKO [99.0 (9.8) per 100,000]; p=0.74. These results are presented graphically in Figure 5-15 with representative images in Figure 5-17.
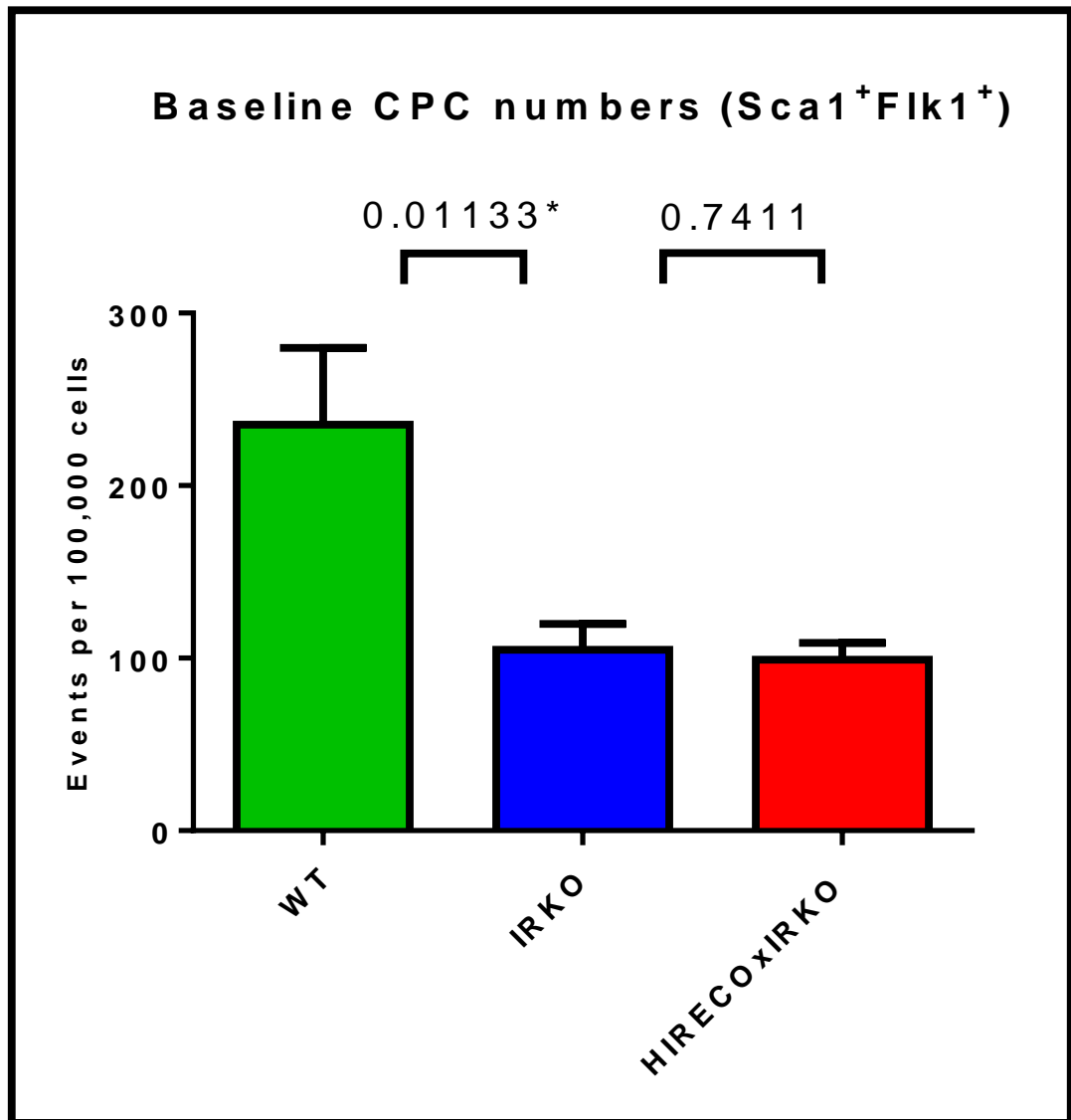
Figure 5-15 Circulating Progenitor Cells (CPC) expressing Sca1 and Flk1

Whole blood was removed from mice using saphenous venepuncture. Samples were labelled with antibodies directed at Stem cell antigen 1 (Sca1) and Foetal liver kinase 1 (Flk1) and underwent fluorescence activated cell sorting. (n=7,8,9).

In the study by Kahn *et al*, vascular repair in IRKO mice could be restored to the level of WT by infusing mononuclear cells expressing the c-kit surface antigen (CD117) derived from WT mice [164]. However, the authors did not look for differences in numbers of these cells between WT and IRKO mice.

For this reason, numbers of mononuclear cells expressing c-kit were appraised in all three genotypes in the current study. No significant difference was seen: WT [229.5 (41.3) per 100,000 cells], IRKO [212.5 (43.9)], HIRECOxIRKO [208.9 (30.0)]. These are presented graphically in Figure 5-16 with representative images in Figure 5-17.
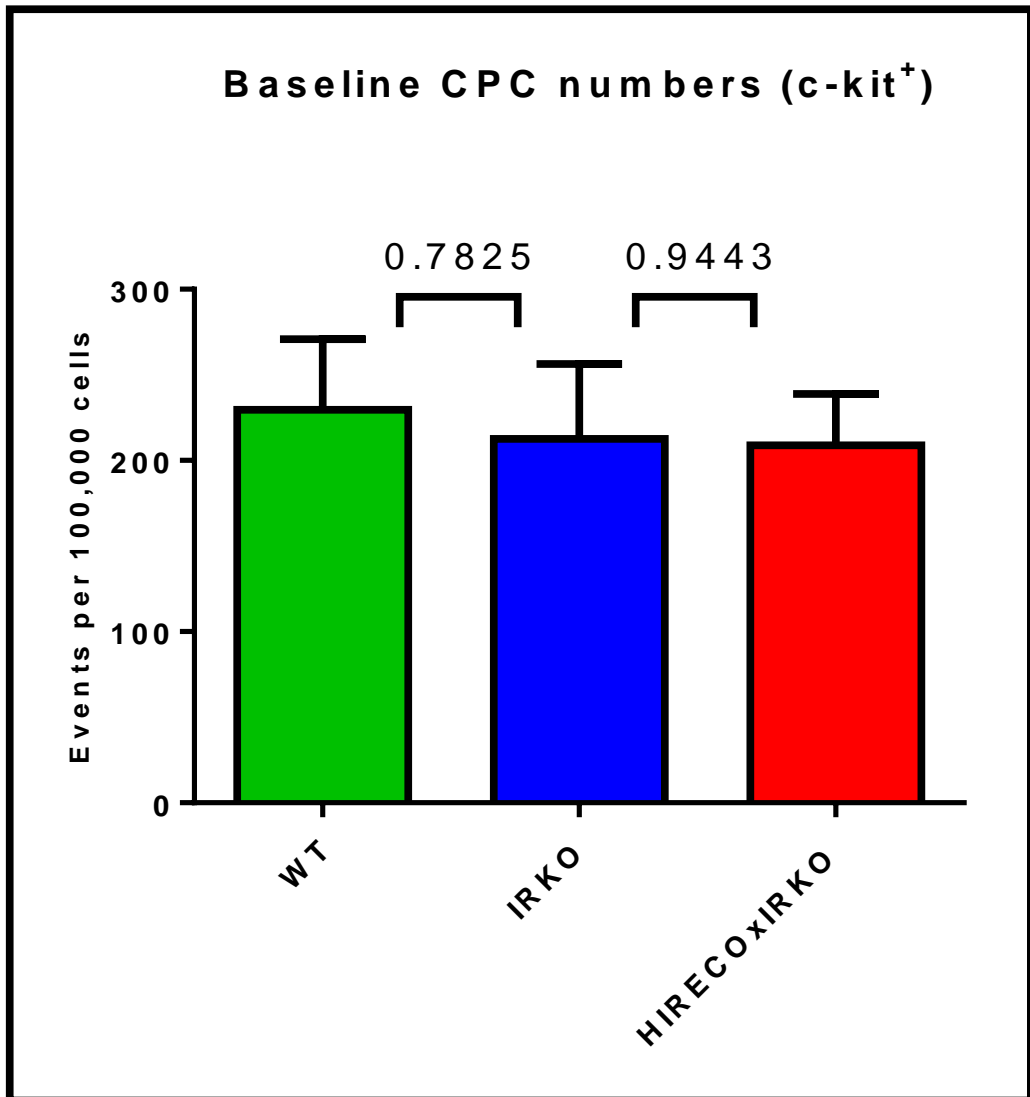
Figure 5-16 Circulating progenitor cells (CPC) expressing c-kit

Whole blood was removed from mice using saphenous venepuncture. Samples were labelled with antibodies directed at c-kit and underwent fluorescence activated cell sorting. (n=8,7,9).
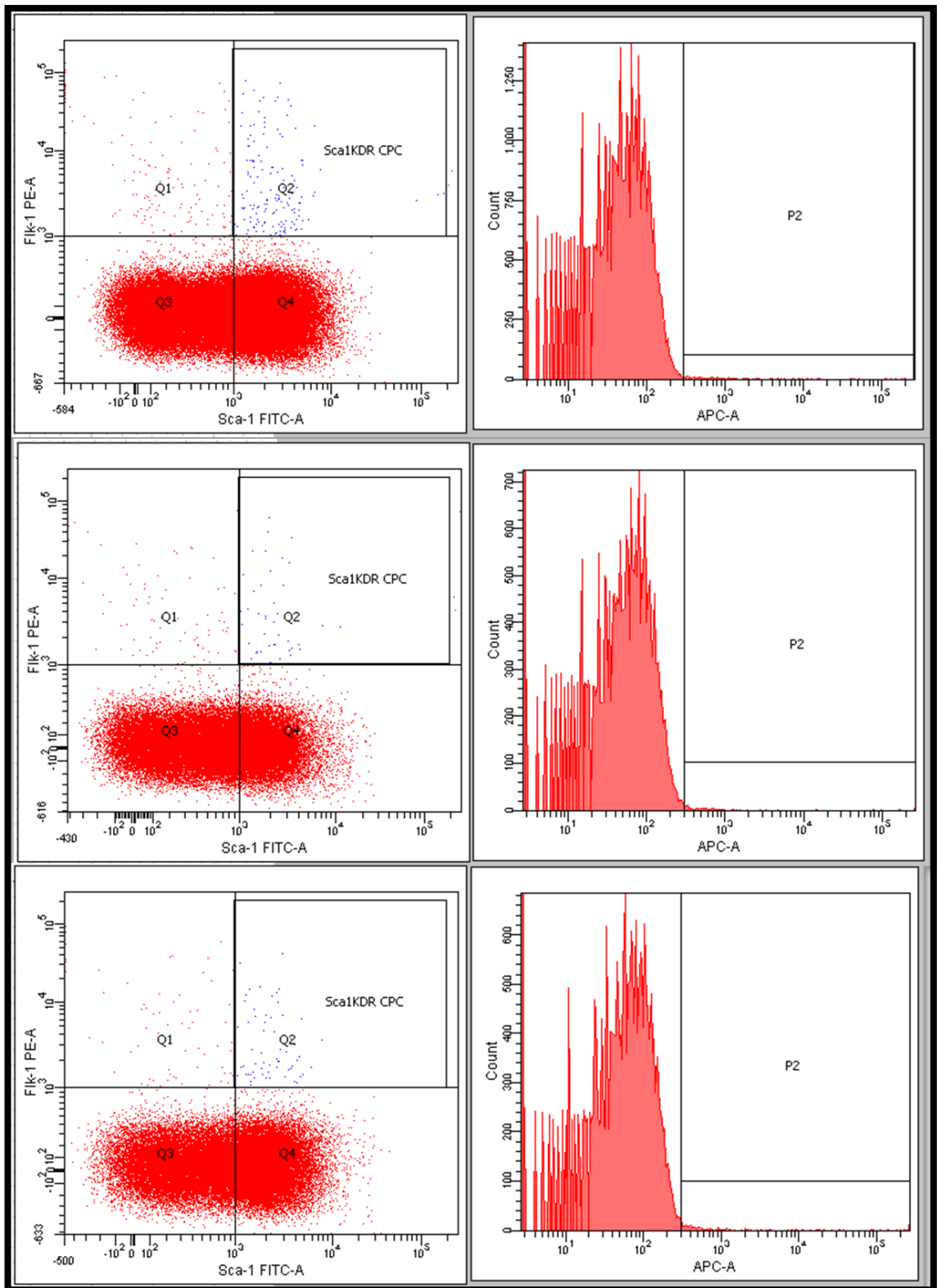
Figure 5-17 Representative FACS images

Left hand panels: labelled for Stem cell antigen 1 (Sca1) and Foetal liver kinase 1 (Flk1). Right hand panels: labelled for c-kit. Upper panels WT, middle panels IRKO, lower panels HIRECOxIRKO.

5.8 Early outgrowth EPC culture and enumeration

As discussed in Chapter 1, EPCs can be isolated using a variety of techniques and the cells derived exhibit different behaviours. For this reason, we sought to quantify and assess early outgrowth EPCs using dual DiI-ac-LDL and lectin-FITC staining as an alternative to simply using flow cytometric definitions in our appraisal of progenitor cells. Previous work has demonstrated that blood-derived EPCs are fewer in number in IRKO mice, despite similar quantities in bone marrow and spleen [164].

In the current study, it was difficult to culture EPCs from the blood of HIRECOxIRKO [0.42 (0.11) EPCs per high-powered field] and IRKO [0.44 (0.16)]; p=0.91. EPCs were more numerous in WT blood [3.82 (1.09)]; p=0.03 for both comparisons with WT (Figure 5-18). The numbers of EPCs cultured from spleen and bone marrow were not significantly different across the three genotypes (Figure 5-19).
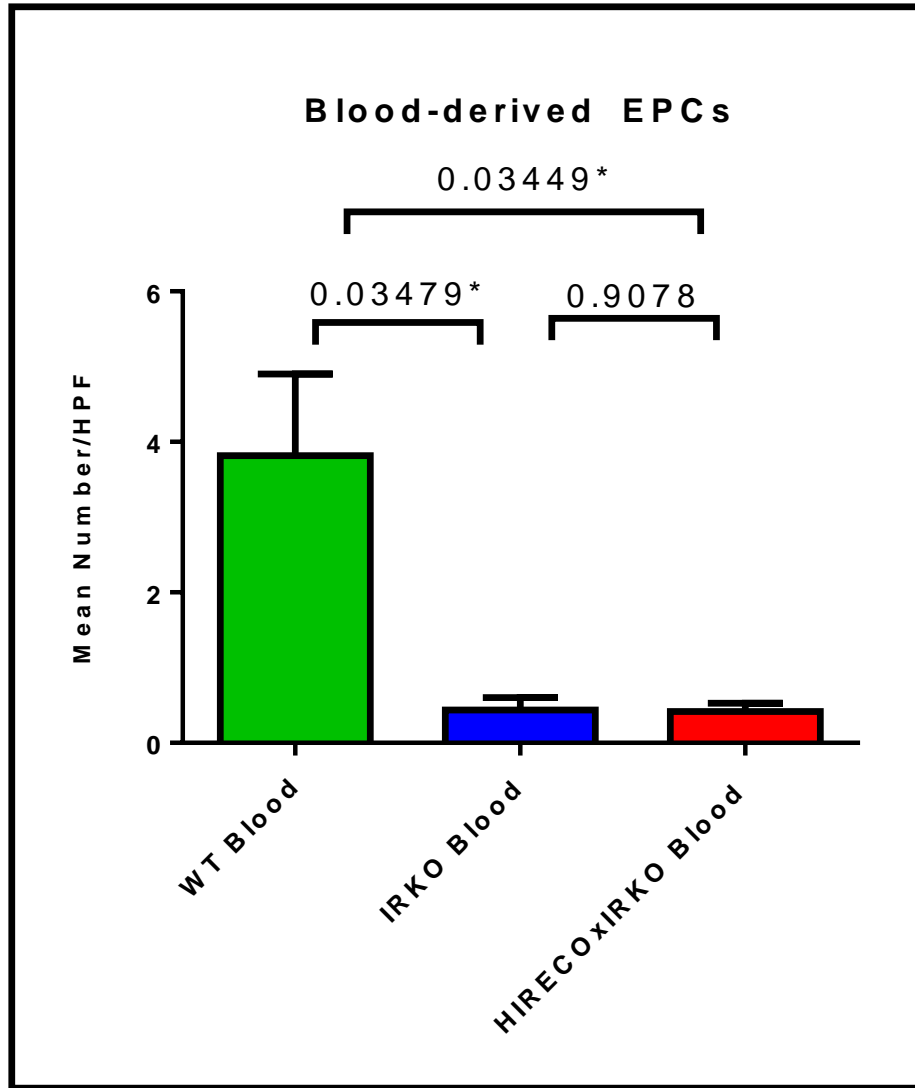
Figure 5-18 Endothelial Progenitor Cell (EPC) enumeration in blood

EPCs were isolated from an inferior vena cava bleed using density gradient centrifugation. After seven days in culture, surviving cells from the mononuclear layer were dual labelled with DiI-acetylated-LDL and FITC-lectin. HPF = high powered field. (n=5,5,6).
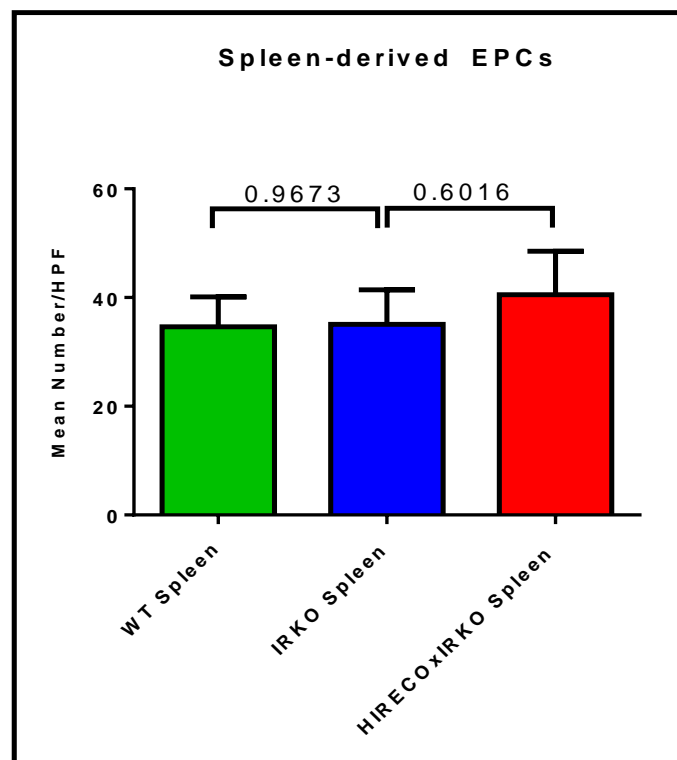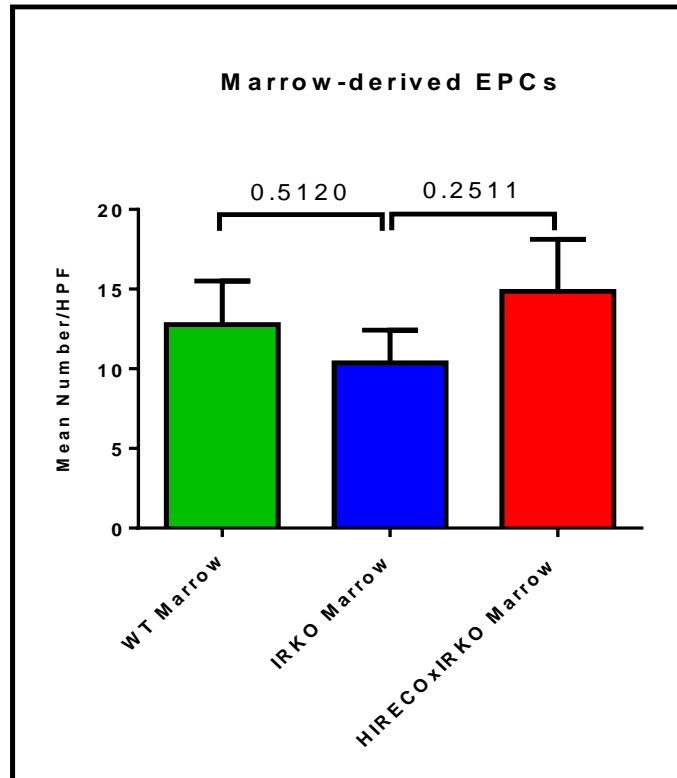
Figure 5-19 EPC enumeration in marrow and spleen

EPCs were isolated from femoral and tibial bone marrow (upper panel; n=5,11,10) and spleens (lower panel; n=5,10,10) as in Figure 5-18.

5.9 EPC function (Scratch Wound Assay)

The above experiments allow an estimation of the impact of endothelial insulin sensitisation on the number of EPCs in culture or in circulation. To extend this, EPC paracrine function was assessed using their ability to influence healing of a scratch wound in endothelial cells. HUVECS exposed to conditioned media from WT, IRKO and HIRECOxIRKO mice showed similar scratch wound closure, suggesting no alterations in this aspect of EPC function. The results are displayed in Figure 5-20.
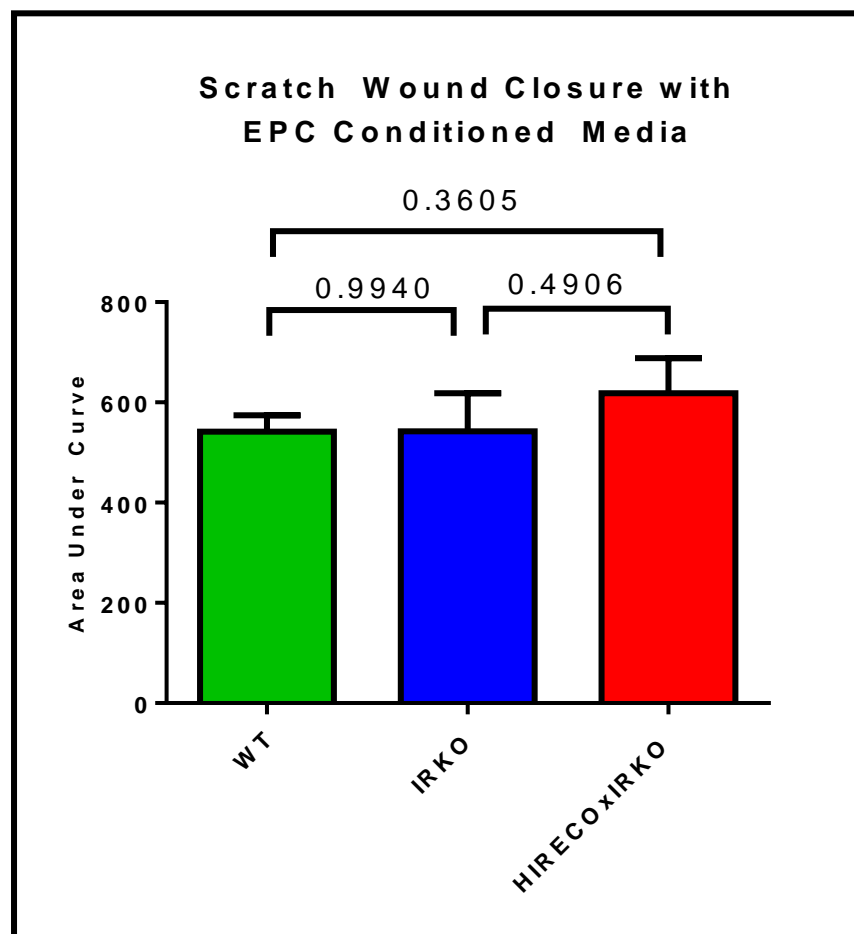
Figure 5-20 Scratch wound closure with EPC conditioned media

Endothelial progenitor cells (EPC) isolated from spleens using density gradient centrifugation were cultured for four days and used to condition basal EPC medium for 24 hours. Conditioned media from each genotype were applied to human umbilical vein endothelial cells subjected to a mechanical scratch wound using the IncuCyte^TM system. The data show the area under curve metric for relative wound density after 12 hours. (n=5,5,6).

5.10 Endothelial Cell Proliferation

HIRECOxIRKO mice show improved vascular repair. The findings in Chapters 5.7 and 5.8 suggest the mechanism is unlikely to relate to increased EPC production. Therefore, we postulated that HIRECOxIRKO endothelial cells may have enhanced proliferative and/or migratory capacity. To assess proliferation, EdU uptake was assessed in PECs. The results are presented in Figure 5-21. The mean (SEM) percentage of proliferating cells seen in WT [6.4 (1.0) %] and IRKO [6.1 (0.6) %] were similar; p=0.79. However, HIRECOxIRKO PECs [10.5 (1.5) %] showed significantly more proliferation than WT (p=0.04) or IRKO (p=0.03).
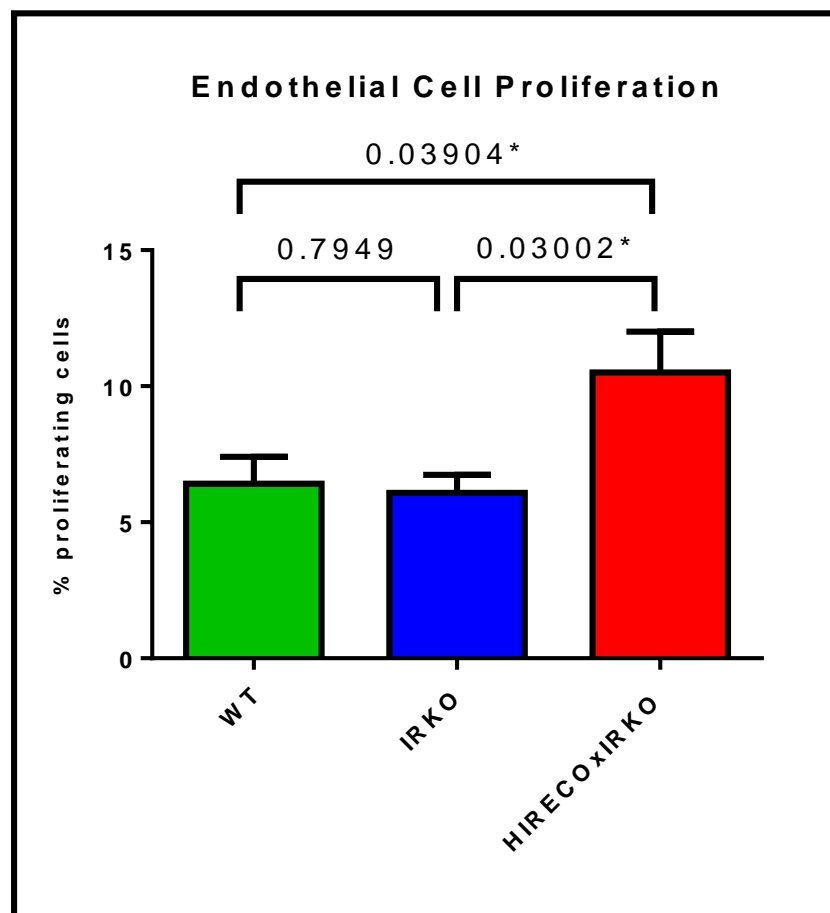
Figure 5-21 Endothelial cell proliferation

Pulmonary endothelial cells (PEC) at passage 2 were incubated with EdU in a Click-iT® kit assay; proliferating cells were counted using fluorescence microscopy. (n=10,8,11).

5.11 Endothelial Cell Migration

5.11.1   Boyden Chamber Assay

An alternative mechanism for improved repair in the HIRECOxIRKO model could be enhanced migration of endothelial cells. This was assessed using the modified Boyden chamber assay described in Chapter 3.14. In WT cells, net migration to VEGF [7.3 (1.8) migrating cells] was significantly higher than in IRKO [1.9 (1.2); p=0.02]. HIRECOxIRKO cells migrated significantly more than IRKO [6.3 (1.3); p=0.03], to levels similar to those seen in WT (p=0.65). The results are presented in Figure 5-22 with sample images in Figure 5-23.
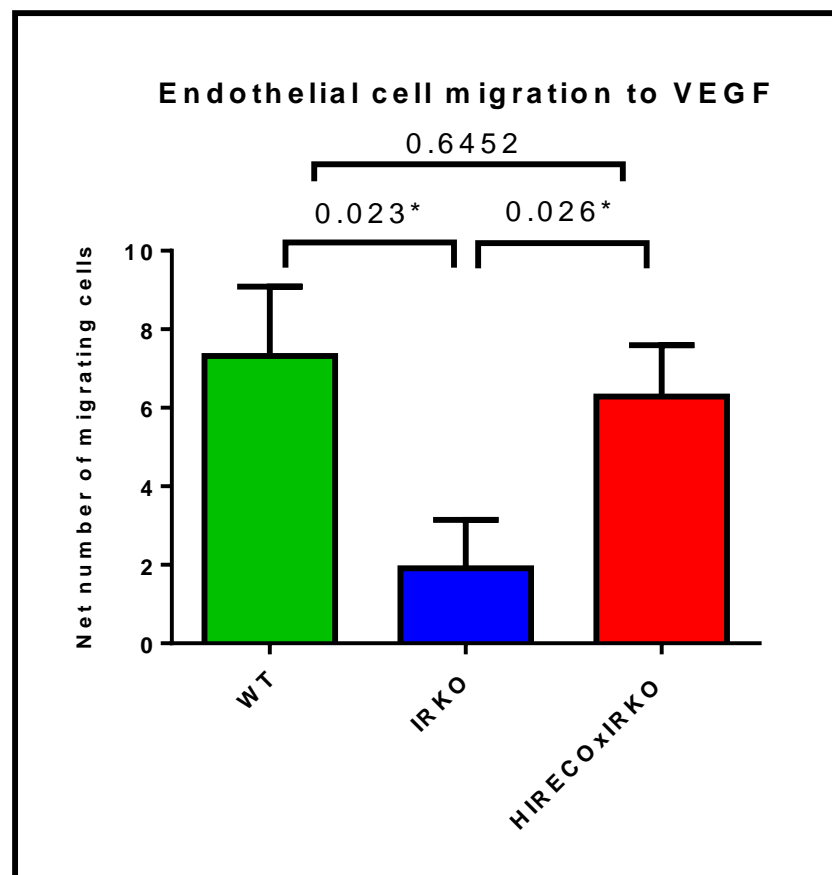
Figure 5-22 Endothelial cell migration (Boyden chamber)

Pulmonary endothelial cells (PEC) at passage 2 were used in modified Boyden chamber assays. Control wells contained low-serum PEC medium and the remainder contained 50ng/mL vascular endothelial growth factor (VEGF). Migrating cells were counted after 24 hours using haematoxylin and eosin; the data show net number of migrating cells (n=9).
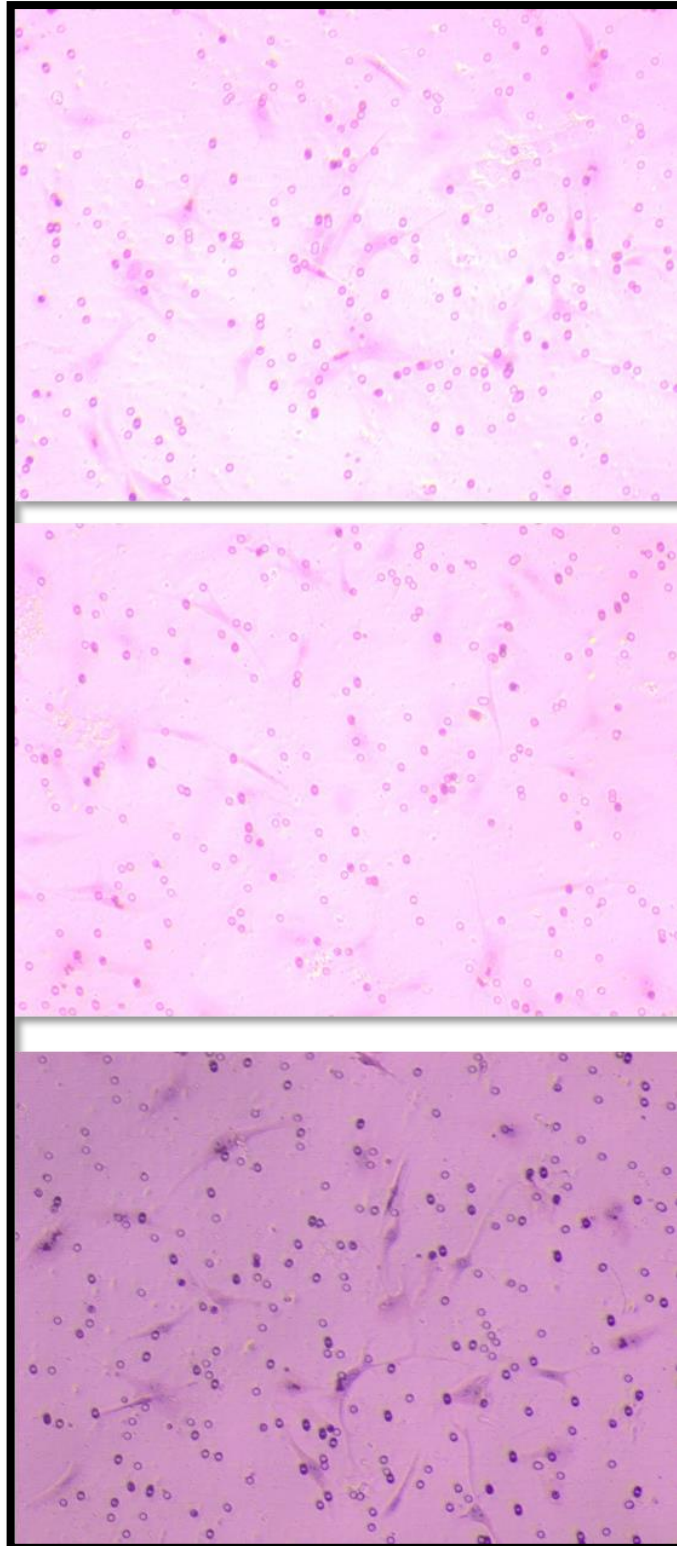
Figure 5-23 Representative Boyden Chamber Images

Images from wells containing vascular endothelial growth factor at 50ng/mL. Upper panel = WT 765, middle panel = IRKO 781, lower panel = HIRECOxIRKO 771.

5.11.2   Scratch Wound assay

An alternative method for assessing cell migration involves measuring relative wound density; in this case, 12 hours after forming a mechanical scratch wound on a confluent cell layer. In this project, the IncuCyte™ was used for incubation and imaging as described in Chapter 5. This experiment was commenced towards the latter end of this project and data remain variable; results to date are presented in Figure 5-24. These data suggest a trend towards a subtle reduction in migration in IRKO PECs with potential recovery in HIRECOxIRKO, though it is difficult to comment with certainty.
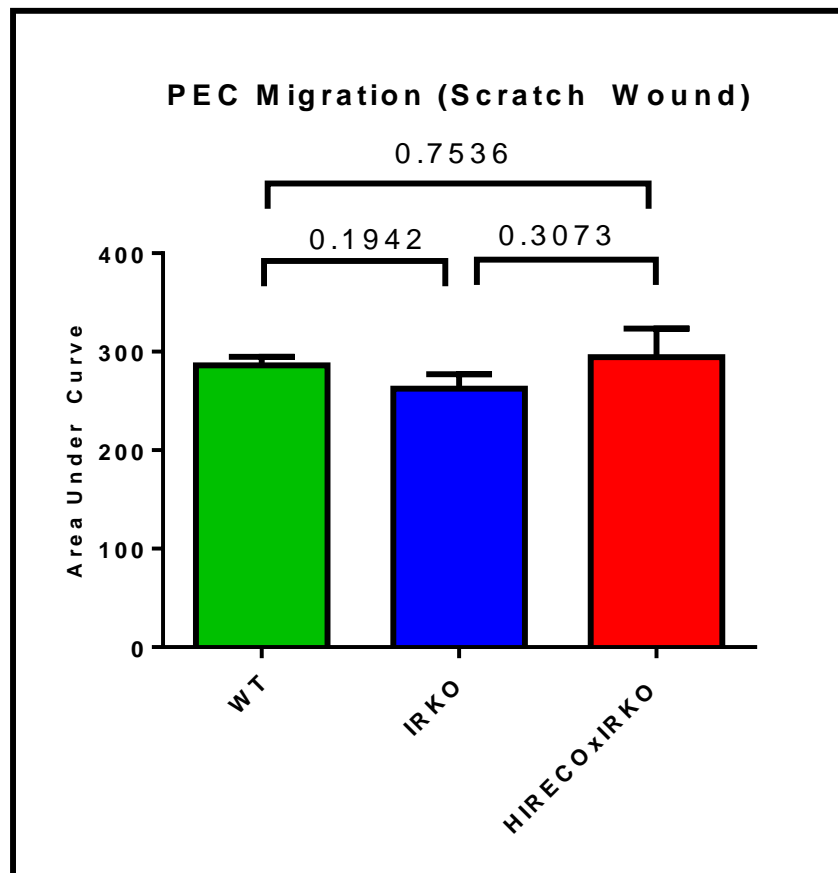
Figure 5-24 Endothelial cell migration (scratch wound)

Pulmonary endothelial cells (PEC) at passage 2 underwent mechanical scratch wound creation and imaging was undertaken using the IncuCyte™ system. The data represent the area under curve metric for relative wound density after 12 hours. (n=8,8,6).

5.12 Aortic vasomotor studies (organ bath)

In a previous study by Wheatcroft *et al* [60], the response of IRKO-derived aortic rings was appraised in depth and it was found that IRKO aortae showed a loss of insulin-induced vasodilatation. Furthermore, rings incubated with L-NMMA, a NOS inhibitor, showed the expected incremental rise in tension in WT but not IRKO aortae, suggesting diminished nitric oxide bioavailability in IRKO mice. In the current study, we sought to assess the same set of responses in HIRECOxIRKO rings.

Initially, rings were exposed to sodium nitroprusside (SNP), a NO donor that exerts vasodilator effects by releasing NO and causing vascular smooth muscle relaxation in an endothelium-independent manner. As expected, there were no differences in SNP-mediated vasodilatation between WT, IRKO and HIRECOxIRKO rings (Figure 5-25). However, IRKO rings showed increased tension when pre-constricted with phenylephrine (PE; Figure 5-26) and blunted vasodilatation when exposed to acetylcholine (ACh;

Figure 5-27) in comparison with WT and HIRECOxIRKO.
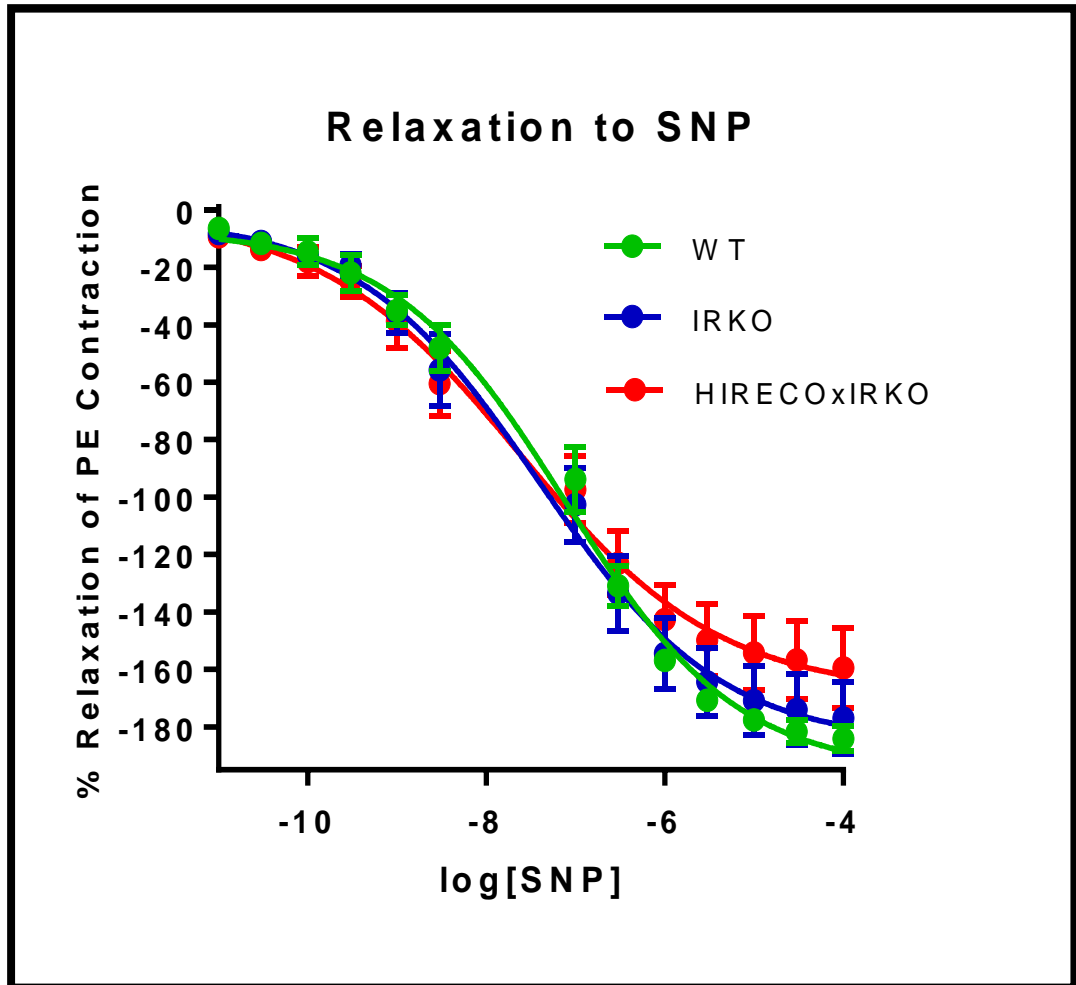
Figure 5-25 Cumulative relaxation of aortic rings to sodium nitroprusside (SNP)

Aortae were excised from mice and transported to the laboratory in Krebs-Henseleit medium. These were stripped of adipose tissue and four rings per mouse mounted in an organ bath apparatus. Rings were pre-constricted with incremental doses of phenylephrine (PE) and then tension was measured at various concentrations of SNP. (n=4,7,6).
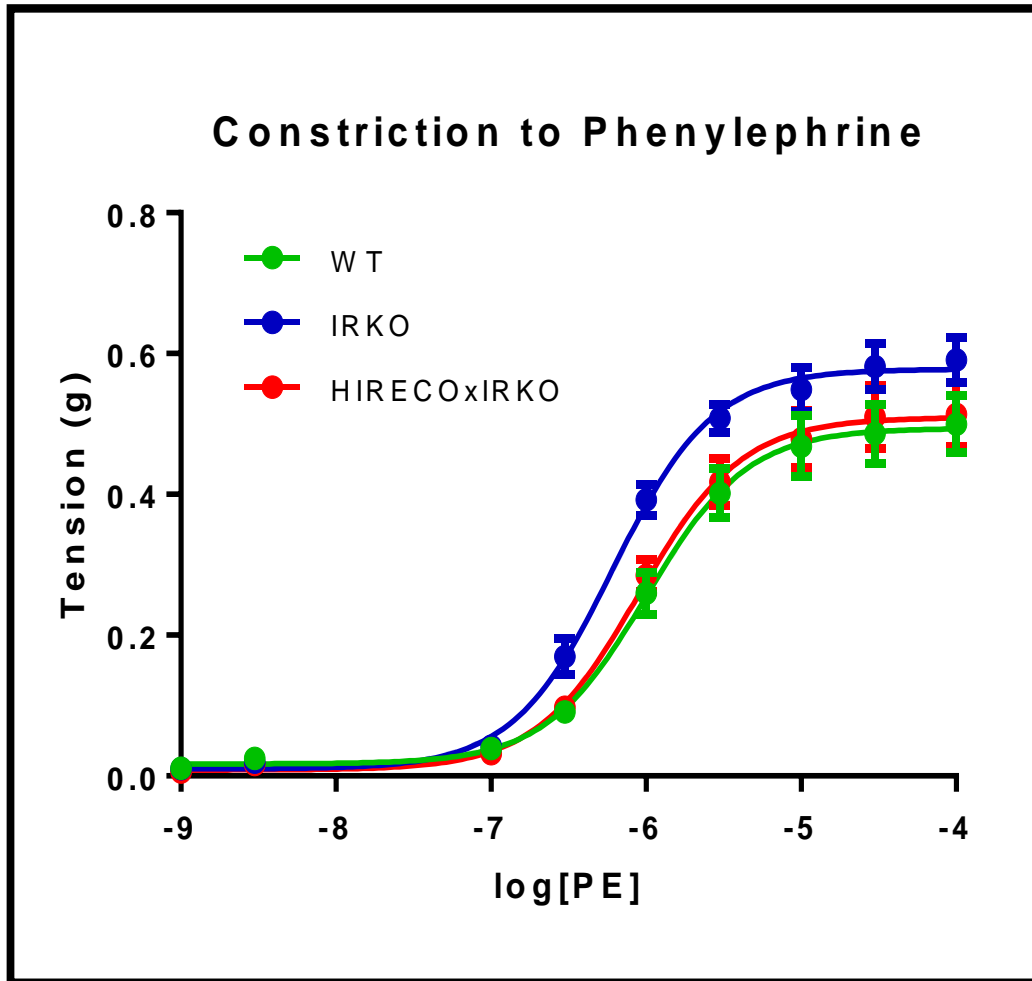
Figure 5-26 Cumulative constriction of aortic rings to phenylephrine

Aortic rings were prepared as in Figure 5-25*. This figure represents the constriction response to incremental doses of phenylephrine (PE). (n=7,10,8).*
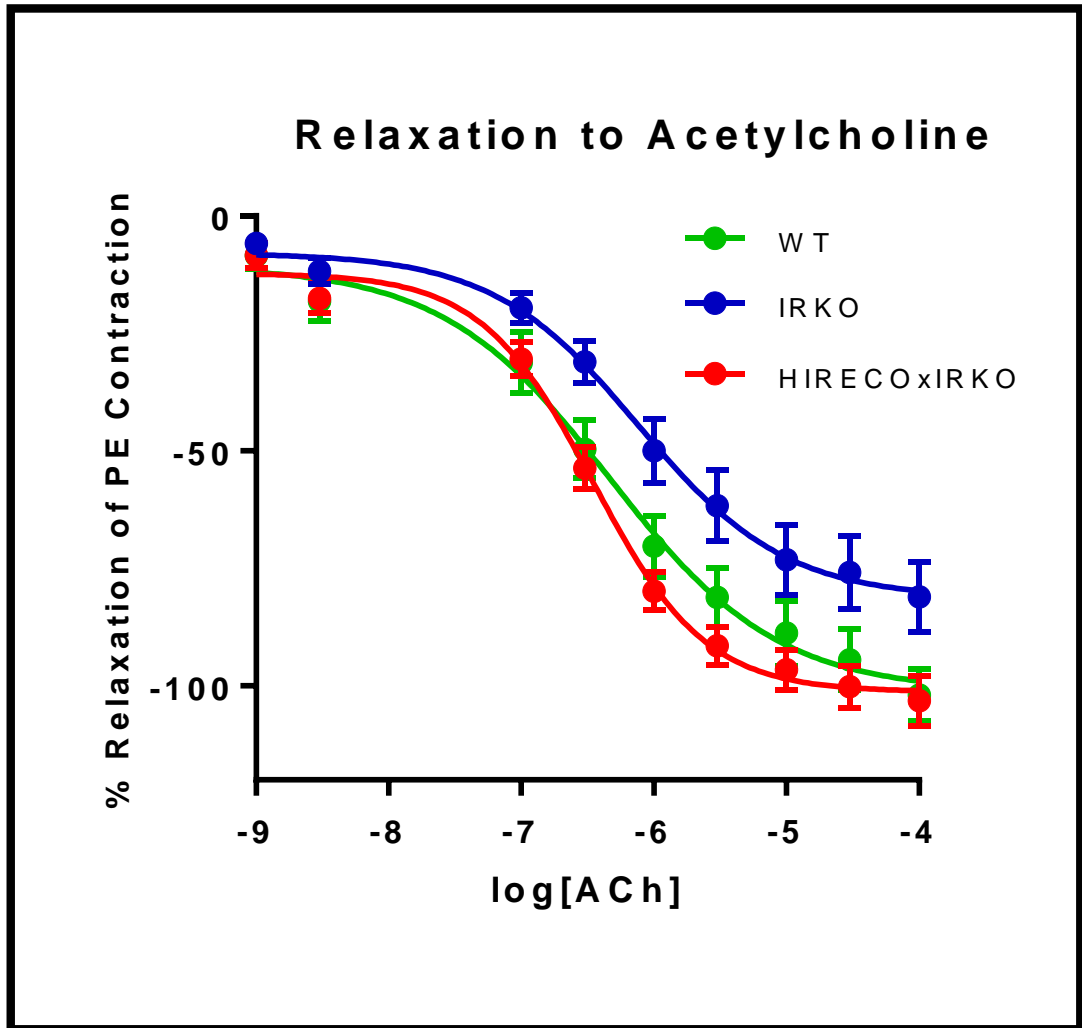
Figure 5-27 Cumulative relaxation of aortic rings to acetylcholine

Aortic rings were prepared as in Figure 5-25. *After pre-constriction with phenylephrine (PE), tension was measured at increasing concentrations of acetylcholine (ACh). (n=7,10,8).*

As well as appraising the degree of divergence in constriction and relaxation curves, one can compare vasomotor responses using the concentration of agonist required to achieve 50% contraction or relaxation (EC_{50}). For PE-mediated vasoconstriction, the mean (SEM) EC_{50} was significantly lower in IRKO rings [6.5×10^{-7} (7.5×10^{-8}) nM]   than in WT [1.1×10^{-6} (1.0×10^{-7}) nM; p<0.01] and HIRECOxIRKO [9.1×10^{-7} (6.6×10^{-8}) nM; p=0.03], demonstrating a greater propensity towards constriction in IRKO and, therefore, endothelial

dysfunction (Figure 5-28). This was corrected to WT levels in the HIRECOxIRKO model (p=0.22). The EC_{50} was not significantly higher for ACh-mediated vasorelaxation in IRKO [8.2×10^{-7} (1.4×10^{-7}) nM] compared with WT [6.4×10^{-7} (2.4×10^{-7}) nM; p=0.49]. However, HIRECOxIRKO rings showed a significantly lower EC_{50} for ACh [3.7×10^{-7} (6.1×10^{-8}) nM; p=0.02], suggesting improved endothelial vasomotor function in these mice (Figure 5-29).
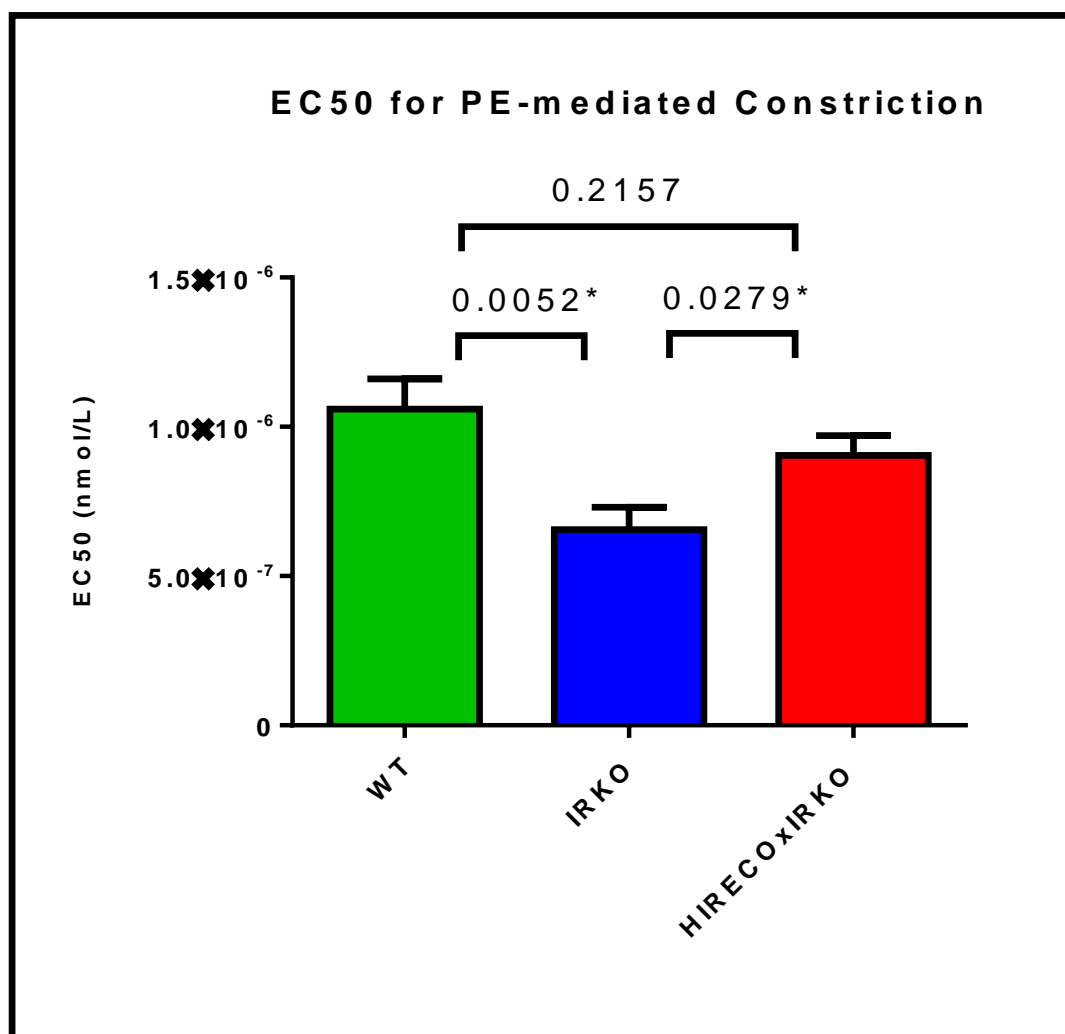
Figure 5-28 Phenylephrine dose required for 50% ring constriction (EC_{50})

PE = phenylephrine. (n=7,10,8).
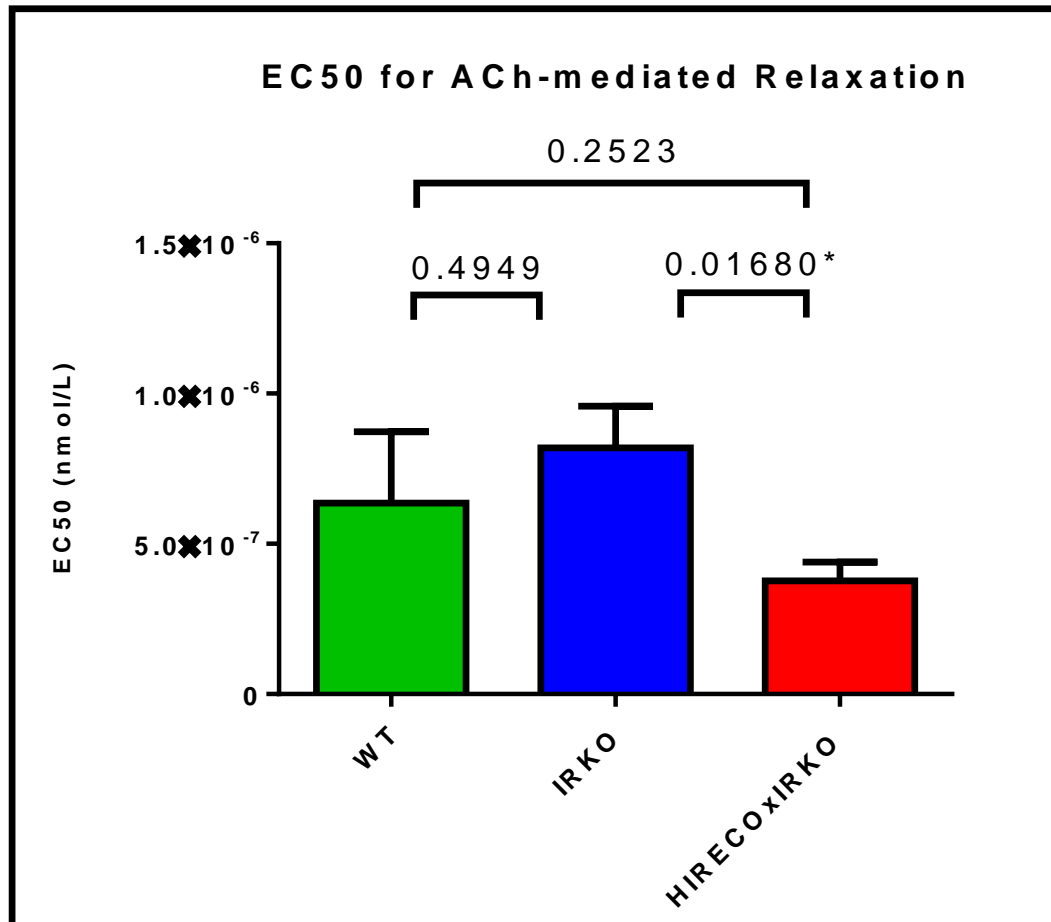
Figure 5-29 Acetylcholine dose required for 50% ring relaxation (EC$_{50}$)

ACh = acetylcholine. (n=7,10,8).

Taken together, the organ bath results corroborate the previously demonstrated finding of endothelial dysfunction in IRKO vasculature, with restoration of PE-mediated vasoconstriction and ACh-mediated vasodilatation in HIRECOxIRKO rings. Furthermore, there was no difference in the behaviour of HIRECOxIRKO compared with WT, suggesting restoration of vasomotor function to WT levels.

Given that NO was implicated in the endothelial dysfunction observed in IRKO [60], we sought to assess the role of NO in the rescue seen in HIRECOxIRKO, by measuring PE-mediated constriction of aortic rings

before and after incubation with L-NMMA. This compound should inhibit the activity of any NOS present and reduce local NO production, resulting in a significant drop in EC_{50}. The lack of such a decrement would suggest reduced NO availability.
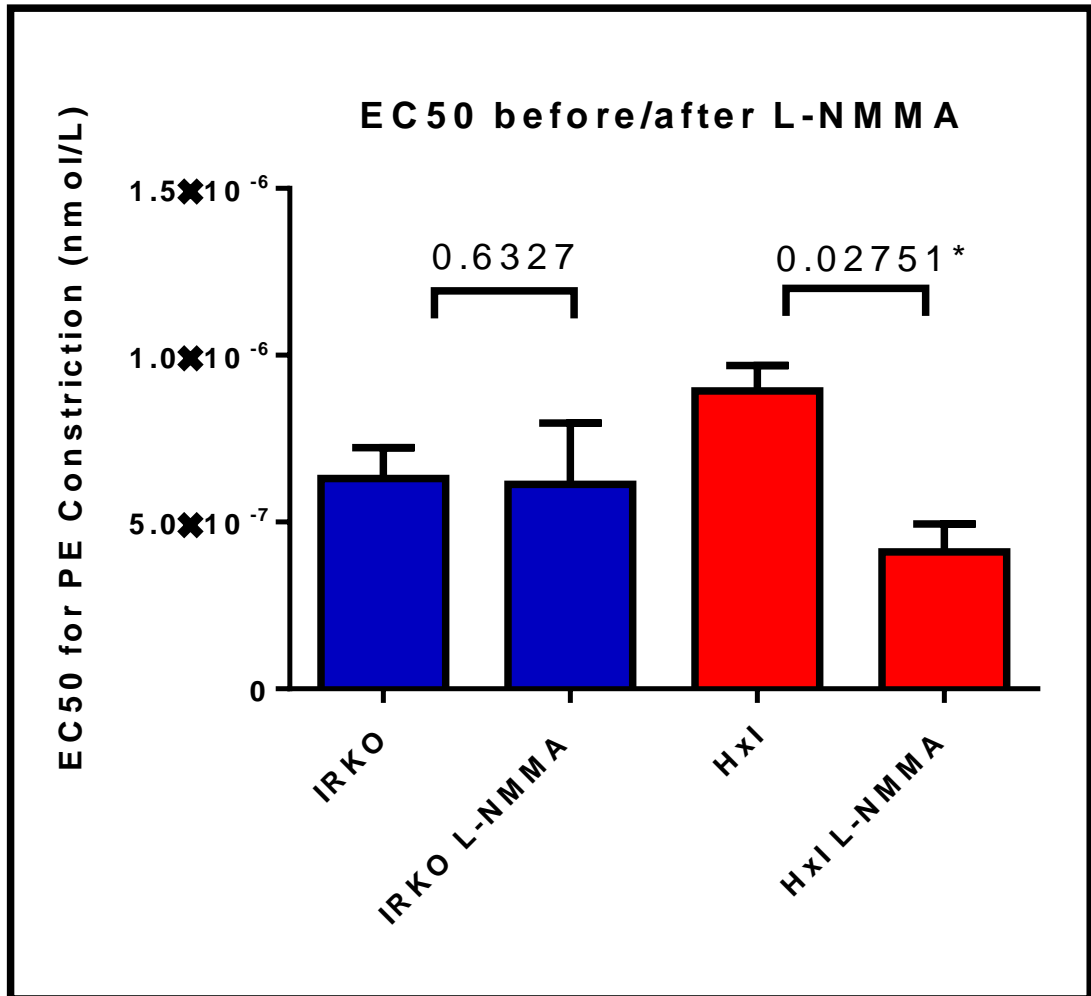
Figure 5-30   Phenylephrine dose for 50% constriction (EC_{50}) after L-NMMA

Aortic rings were prepared as in Figure 5-25. *The constriction response to incremental doses of phenylephrine (PE) was measured before and after a two-hour incubation with levo N-monomethyl arginine (L-NMMA). The EC_{50} for constriction to PE was compared before and after L-NMMA.*

HxI = HIRECOxIRKO. (n=5).

As previously demonstrated, there was no difference in the EC_{50} for PE-mediated constriction in IRKO aortic rings after incubation with L-NMMA, suggesting a lack of NO bioavailability. However, the HIRECOxIRKO rings showed a significant decrement in EC_{50} after incubation with L-NMMA: less PE was required to constrict the rings to 50%, suggesting that these vessels contained bioavailable NO at baseline (Figure 5-30). These findings highlight a potential role for NOS and NO in the rescue of endothelial function in the HIRECOxIRKO model.

5.13 Reactive Oxygen Species

Previous work in IRKO mice has shown increased ROS [115, 123] so it was postulated that a molecular mechanism behind restored endothelial function in HIRECOxIRKO mice could be a reduction in ROS levels. Superoxide concentration was measured in PECs with a fluorescence-based assay using dihydroethidium. Numbers are small and further work is required, but there is a trend towards increased ROS in IRKO [5.9 (1.3) arbitrary units] compared with WT [3.2 (0.6) AU; p=0.08]. HIRECOxIRKO PECs do not appear to generate any less ROS than IRKO [7.1 (2.0) AU; p=0.63] and in fact display significantly raised levels compared with WT (p=0.04). The interim results are presented graphically in Figure 5-31.
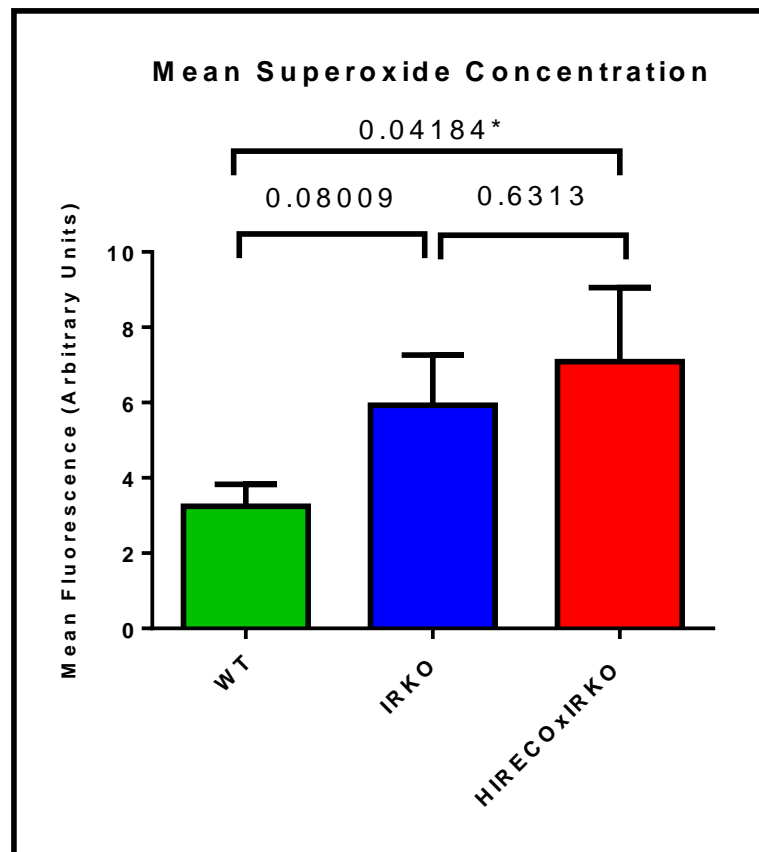
Figure 5-31 Superoxide concentration in endothelial cells

Pulmonary endothelial cells (PEC) at passage 2 were labelled with dihydroethidium in Krebs-HEPES buffer. Fluorescence was measured on a microplate reader after a 20 minute incubation. (n=6,5,3).

Page | 187

5.14 Intracellular Signalling

Several results obtained in this project could be argued to result from increased bioavailability of nitric oxide (NO), perhaps as a result of enhanced insulin signalling in endothelial cells from HIRECOxIRKO mice. In order to interrogate this, Western blots were performed to assess basal and insulin-stimulated expression of Akt and eNOS, both of which are relevant to the PI3K signalling pathway that culminates in generation of NO. Unfortunately, optimisation of this experiment is ongoing and only one set of samples was satisfactorily processed. The preliminary results, displayed in Figure 5-32, suggest that there may be partial rescue of insulin signalling at the Akt level but without a convincing rise in eNOS phosphorylation.
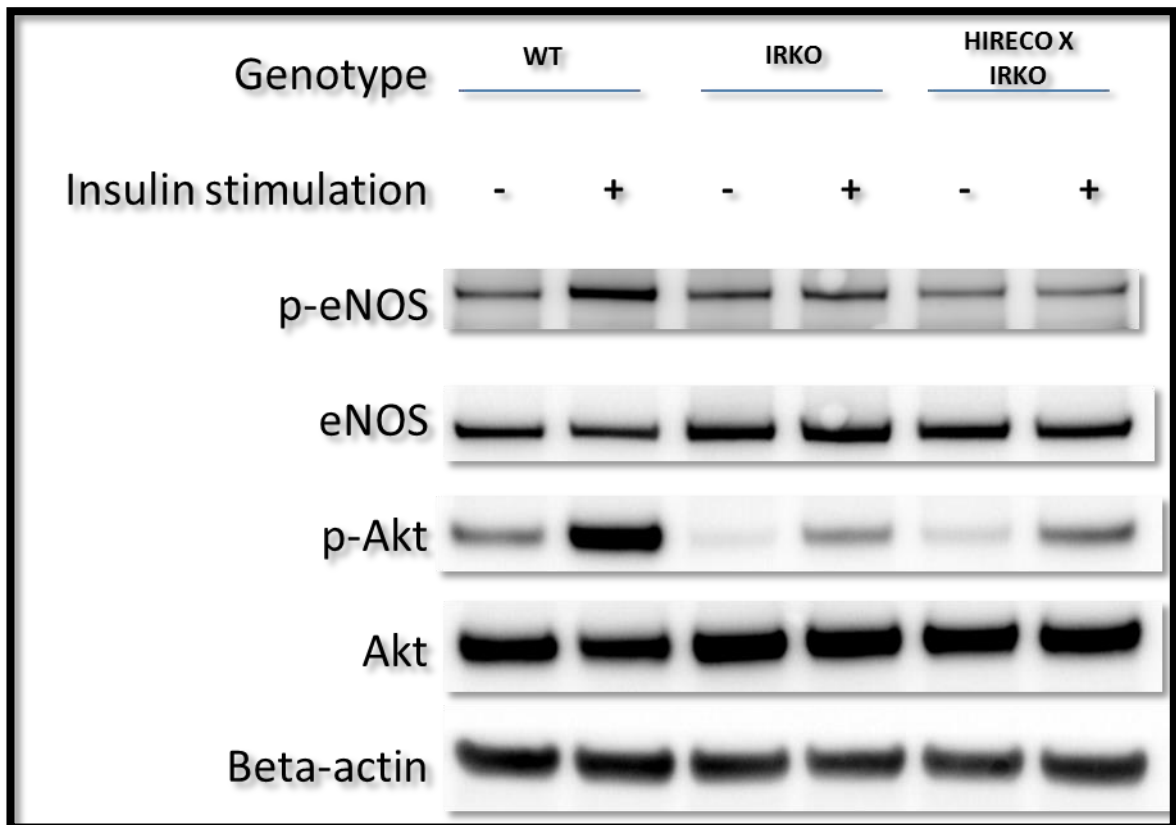
Figure 5-32 Preliminary Western blot showing differential intracellular insulin signalling

eNOS = endothelial nitric oxide synthase; Akt = protein kinase B; prefix "p-" denotes phosphorylated form (serine 1177 for eNOS and serine 473 for Akt). Insulin stimulation with 100nM Actrapid for 15 minutes. (n=1).

Chapter 6 **Discussion**

6.1 **Summary of key findings**

In this study, we have built upon existing literature surrounding the effects of insulin resistance on endothelial function and vascular repair and explored the validity of endothelial insulin sensitisation as a potential therapeutic target. To address this, we created a murine model overexpressing the human isoform of the insulin receptor in endothelial cells, with a systemically insulin resistant background. Using a variety of *in vivo, ex vivo* and *in vitro* methods, we have studied the effects of this manipulation on various elements of vascular biology.

The HIRECOxIRKO mouse has been shown to be a viable model with no gross metabolic differences compared with IRKO littermate controls. Quantitative PCR has confirmed that the human insulin receptor transgene is expressed in the endothelial cells of the HIRECOxIRKO mouse.

In a model of femoral artery wire injury, we have demonstrated that HIRECOxIRKO mice have restored vascular repair to the levels of their WT counterparts. This improvement is not associated with any alteration in EPC numbers or function, but instead is accompanied by enhanced endothelial cell migration to VEGF and, perhaps, increased proliferative capacity.

HIRECOxIRKO mice also have reduced blood pressure compared with IRKO, again to levels similar to WT littermates; in keeping with this, experiments using aortic rings show a reversal of the endothelial dysfunction seen in IRKO vessels. This appears to be related to augmented NO bioavailability, perhaps resulting from enhanced insulin signalling.

6.2 Validation of model and metabolic assessment

6.2.1 Background

Insulin receptor knockout (IRKO) mice are globally haploinsufficient for the insulin receptor and display preserved metabolic parameters [60] with a 30% reduction in insulin signalling [66]; as such, they represent a reasonable approximation to the human metabolic syndrome. Accordingly, they display hypertension and endothelial dysfunction [60], and much of our understanding of vascular disease in the context of insulin resistance *per se* comes from this model as a result. It could be argued that their lack of obesity or hyperlipidaemia [60] makes them less representative of the human metabolic syndrome than perhaps animal models of high fat diet-induced insulin resistance. Conversely, it could be said that the benefit of this relatively undisturbed metabolism is that it allows us to consider the specific contribution of insulin resistance to vascular derangements without introducing the confounding that can arise from other elements of the metabolic syndrome. Despite normal glucoregulation, IRKO mice display endothelial dysfunction and impaired vascular repair after denuding arterial injury, suggesting a key role for perturbed insulin signalling in the causation of vascular disease [60, 164]. The VENIRKO and ESMIRO models help to consolidate our understanding of the endothelium as a key regular of vascular health and demonstrate that limiting insulin resistance to this location is sufficient to result in vasomotor dysfunction, oxidative stress and deranged angiogenesis [113, 114, 123]. These findings lend theoretical validation to the study of the endothelium as a therapeutic target.

6.2.2 Targeting insulin sensitivity to the endothelium

This project was focussed on the study of a mouse with systemic insulin resistance and somewhat preserved endothelial insulin responsiveness. In

order to achieve this combination of insulin sensitivity and resistance, our laboratory group had previously established a colony of HIRECO mice with overexpression of the human insulin receptor targeted to endothelial cells using a Tie-2 promoter. Tie-2 was initially discovered in 1992 as a relatively endothelium-specific receptor tyrosine kinase, though it was identified as being expressed in endothelial precursors as well [183]. The Tie-2 promoter strategy has been used to target the endothelium in the past [184]and various authors have attempted to validate its endothelial specificity by labelling with green fluorescent protein in a selection of tissues; these have suggested predominantly vascular expression, greater in the arterial than in the venous compartment of the circulation [179, 185]. The crossover into mononuclear cells (and therefore EPCs) remains a potential limitation of this strategy, though in this specific project it would not necessarily have a negative impact on the model due to the implication of EPCs as regulators of impaired vascular repair in IRKO mice [164]. Furthermore, our laboratory's previous work (unpublished) on pure HIRECO mice has shown no detectable hIR mRNA in myeloid cells from these mice, suggesting that HIRECOxIRKO monocytes and EPCs are also unlikely to be affected by the insertion of the hIR transgene.

The Tie-2 strategy has been used in our laboratory group to render the endothelium insulin resistant (the ESMIRO mouse; [114]) and to overexpress the insulin like growth factor-1 (IGF-1) receptor in endothelium [186], following other groups' demonstration that targeting the Tie-2 promoter to the Hprt locus results in effective vascular expression of the transgene of interest [187]. We postulated that the sensitisation of endothelial cells to insulin signalling could rescue the vascular impairments seen in systemic insulin resistance, and thus bred HIRECO mice with IRKO to generate the HIRECOxIRKO "double-cross".

6.2.3 Viability of the HIRECOxIRKO model

We established the viability and unaltered growth profile of the HIRECOxIRKO model early in the study. Body weight tended to plateau at around four months in WT, IRKO and HIRECOxIRKO mice and no differences were noted in growth or physical development between the three genotypes over this time period. Similar results were noted in terms of wet organ weight. These were not especially surprising findings, but identified the HIRECOxIRKO model as a viable one in which to perform more detailed phenotyping.

6.2.4 Metabolic assessment

Glucose and insulin tolerance testing confirmed that these mice were not diabetic and in fact displayed similar metabolism to IRKO littermates, allowing us to infer that any differences seen in their vascular parameters were unlikely to result from improved glucose clearance. It was acknowledged that the use of capillary blood glucose measurements is prone to error and therefore we also confirmed that fasting plasma insulin concentrations were similar in IRKO and HIRECOxIRKO using ELISA. In this technique, one can directly measure insulin levels as opposed to using changes in glucose concentration as a surrogate metric for insulin sensitivity. This method has the additional advantage of allowing comparison of study samples against robust standards. Furthermore, specimens for ELISA are plated in duplicate and only those with a low coefficient of variation between replicates are accepted, introducing a level of quality control that is difficult to achieve using the cruder method of capillary glucose measurement. The use of a euglycaemic-hyperinsulinaemic clamp would represent the gold-standard for measuring insulin sensitivity but, as this cannot be performed at our institution, there would need to be a compelling indication for exposing animals to the stresses involved in transport and, indeed, an invasive procedure. We elected not to perform this experiment as no gross

differences had been noted in basic metabolic parameters. A potential further limitation in terms of metabolic phenotyping is that plasma concentrations of free fatty acids and triglycerides were not determined in this project; however, no differences were seen on appraisal of lipids in previous work in IRKO mice [60] so there was no obvious reason to suspect a difference in HIRECOxIRKO. Again, from the perspective of animal welfare, it was deemed prudent to keep blood testing to a minimum as a relatively large volume of whole blood was often only sufficient for one ELISA due to the need to isolate the plasma fraction, and multiple bleeds would have been necessary to investigate a variety of lipid-related parameters. Overall, it was felt that the data presented were sufficiently reassuring to allow us to discount significant metabolic alterations as the causative agents in any improvements noted in vascular endothelial function in HIRECOxIRKO mice.

6.2.5 Endothelial specificity

Finally, we sought to characterise the expression of the human and murine insulin receptors in endothelial cells and other body tissues. The results of quantitative PCR for the human isoform of the insulin receptor (hIR) were reassuring as this was only detectable in lungs and aortae from HIRECOxIRKO mice and could not be found at all in the organs tested from WT or IRKO littermates. When assessing cultured pulmonary endothelial cells (PECs), no hIR mRNA was identified in WT or IRKO, whereas expression was evident in HIRECOxIRKO cells. These findings suggested that the primer used to identify the hIR was sufficiently specific for the human isoform and did not show significant cross-reactivity with the murine receptor (mIR). Additionally, the finding that hIR expression in endothelial cells was essentially limited to HIRECOxIRKO PECs provided some preliminary reassurance that our method for isolating endothelial cells was indeed providing a reasonably pure population. It would be interesting to isolate a population of cells that is essentially devoid of endothelial cells and

quantify hIR mRNA here to confirm a lack of expression in the non-endothelial fragment. However, even this approach could only go some way to demonstrating specificity, unless many distinct cell lineages were assessed. It is also reassuring to note that in pure HIRECO mice, myeloid cells isolated using a CD11b antibody showed no detectable hIR mRNA, suggesting that the cell lineage most likely to be affected by lack of Tie-2 specificity does not suffer from this limitation.

As expected, mRNA expression of the mIR was downregulated in IRKO endothelial cells. This was also the case in HIRECOxIRKO PECs and suggests that insertion of the hIR transgene is unlikely to have caused a large scale alteration in transcription of its murine counterpart. Thus, the insertion of human receptors is likely to have increased the total insulin receptor protein in HIRECOxIRKO compared with what is expressed on IRKO endothelium. Relative quantification of these receptors (or indeed total insulin receptor expression) is not feasible using PCR. A very crude estimate could be made using the mRNA quantity relative to a housekeeping gene such as beta-actin. For example, the relative expression of mIR mRNA in HIRECOxIRKO PECs was observed to be in the order of 0.25 times that of beta-actin, whereas the corresponding RQ for the human receptor was approximately 0.06. On initial appraisal, this may suggest that the insertion of the hIR results in a very slight improvement in total insulin receptor expression in endothelial cells rather than a full restoration to the level of WT. However, this assertion must be regarded with caution. A SYBR green probe was used for hIR quantification whereas a Taqman® probe was used for the mIR. Additionally, there is a reasonably large degree of error in the PCR results, again making it difficult to draw any conclusions beyond the binary appraisal of presence versus absence of the human receptor in HIRECOxIRKO cells.

Future work to ascertain total insulin receptor protein could include the use of Western blotting with densitometry, or quantitative immunofluorescence,

using antibodies that do not differentiate between the murine and human isoforms of the receptor. We are in the process of evaluating anti-insulin receptor antibodies that are in use in our laboratory for this purpose, and aim to perform one or both of these techniques to investigate total receptor protein in endothelial cells once such products and protocols have been sufficiently validated. These experiments may be limited by the fact that there is unlikely to be an antibody that has equal affinity for the human and murine insulin receptors; they may therefore highlight large differences between genotypes simply by virtue of differential affinity for human and murine proteins. An approximation of functional insulin receptor expression may alternatively be gained through detailed comparison of downstream signalling mediators using immunoblotting. Preliminary data using this approach will be discussed in more detail below.

6.2.6 **Summary**

We have established the HIRECOxIRKO mouse as a viable model that can be used to study the impact of endothelial insulin sensitisation in the context of global insulin resistance. Quantitative PCR suggests that the strategy of using a Tie-2 promoter to target the human insulin receptor to endothelial cells is valid in these mice, with no significant detectable hIR in WT or IRKO organs or cells. HIRECOxIRKO mice display broadly similar metabolic parameters to IRKO mice, suggesting that any improvements seen in vascular health are likely to result from restoration of endothelial insulin signalling rather than ameliorations in glucoregulation or insulin sensitivity. With certain caveats, these early data represent sufficient validation of the model to allow further detailed assessment of the vascular phenotype, which will be discussed in the next section.

6.3 Vascular repair

6.3.1 Background

Within the spectrum of insulin resistance and diabetes, several pathological processes can induce vascular injury, including (but not limited to) endothelial cell toxicity from chronic hyperglycaemia, as well as acute events such as atherosclerotic plaque rupture. An appropriate physiological response to injury is critical in mediating effective endothelial healing; this can be studied using models such as femoral arterial wire injury, a technique which causes acute and localised endothelial denudation in animals akin to that seen in humans, and with which our laboratory group is experienced. In previous work from our laboratory, convincing data showed that IRKO mice exhibited delayed vascular repair at several time points up to and including 14 days after wire injury [164]. These data support observations of impaired vascular repair in diabetic mice [163], obese, insulin-resistant rats [151] and even in insulin-sensitive rats exposed to high concentrations of exogenously administered insulin [150]. Diet-induced obesity can also impair vascular function in mice: previous work has described increased oxidative stress and reduced EPC numbers as noted in IRKO mice, associated with impaired angiogenesis after hind limb ischaemia [188]. The phenomenon of reduced vascular repair also appears to be relevant in terms of gross pathological sequelae: loss of endothelial insulin signalling in a mouse model prone to atherosclerosis has been shown to increase atheroma formation [189]. We hypothesised that restoring endothelial insulin sensitivity in the context of global insulin resistance would restore vascular reparative mechanisms, using femoral arterial wire injury as our model. In the current project, we picked a four day time point for analysis because a clear divergence was observed after three days between WT and IRKO mice in the Kahn *et al* study and it was deemed unreasonable to keep mice alive with an injured limb for any longer than necessary, from the perspective of animal welfare.

One of the most exciting results of the current project is the demonstration that HIRECOxIRKO mice display improved vascular repair compared with IRKO littermates; indeed, the degree of recovery observed in HIRECOxIRKO was not significantly different to that documented in WT mice. A major portion of this project was therefore dedicated to trying to understand the mechanisms of enhanced vascular repair in this model and to dissect out the relative contributions of endothelial cells and EPCs in the augmented healing process.

6.3.2 Role of EPCs

Our laboratory group has previously published evidence in favour of the theory that insulin resistance specifically impairs EPC-mediated vascular repair [164]. Numbers of circulating progenitor cells (defined as co-expressing Sca1 and Flk1) were significantly reduced in IRKO mice and the same population of cells displayed reduced mobilisation potential after the intraperitoneal administration of VEGF. Furthermore, culture-derived EPCs were seen in similar quantities in haematopoietic tissues such as bone marrow and spleen, whereas numbers of blood-derived EPCs were significantly lower. Bone marrow lysates from IRKO mice entirely lacked detectable eNOS, which has previously been demonstrated as essential for EPC mobilisation in mice [190] and in humans [165]. Finally, the transfusion of c-kit-positive cells from WT mice could restore post-injury healing to normal WT levels, with only partial recovery when the transfused progenitor cells were derived from IRKO mice. Thus, using various distinct and complementary techniques, Kahn *et al* described a potential pathogenetic mechanism: IRKO mice display a defect in EPC mobilisation despite adequate production in the reticuloendothelial system, with partial recovery after the transfusion of cells with a progenitor phenotype [164]. However, this study did not address the influence of insulin resistance on the function of mature endothelial cells, such as the potential impact on migration and

proliferation; therefore, the findings do not rule out a role for additional disturbances in endothelial cell-mediated repair.

The wider data regarding EPC-mediated versus endothelial cell-mediated dysfunction in insulin resistance are equivocal, as discussed in detail in Chapter 1.4.4. There appears to be little doubt that both the number and *in vitro* function of EPCs are disturbed in the insulin resistance spectrum, both in humans and in various *in vivo* animal studies. These support Kahn *et al* in the assertion that EPC dysfunction represents a relevant determinant of the impaired response to vascular injury [165, 173, 174]. EPCs derived from patients with diabetes have been shown to support re-endothelialisation after carotid artery injury in mice less well than EPCs from healthy volunteers; furthermore, EPCs from diabetic subjects taking rosiglitazone could rescue the deficit, suggesting that insulin sensitisation of these cells can be beneficial in restoring vascular repair [191]. Coupled with these findings is the observation that endothelial cells are terminally differentiated and may therefore not necessarily be expected to participate in very significant degrees of proliferation, whereas EPCs may yet differentiate into mature endothelial cells at sites of injury or at least provide paracrine support for the native endothelium. Conversely, however, other groups have found that mature endothelial cells are more relevant in the process of recovery after injury, with a limited role for EPCs [156]. The reality may be a compromise between the two viewpoints, wherein EPCs are relevant but perhaps do not incorporate into wounded vessels, instead establishing a supportive role and providing a paracrine milieu that favours healing in native endothelial cells, indirectly modulating the response to vascular injury.

Based on the balance of available evidence at the time of planning experiments, we hypothesised that the augmented recovery seen in the HIRECOxIRKO model would be associated with some degree of improvement in the profile of EPCs. However, our experiments using both flow cytometry and early outgrowth EPC culture showed no enhancement in

EPC numbers in the HIRECOxIRKO mouse; this finding gave an early indication that an alternative reparative mechanism was more likely in our model. As well as quantifying early outgrowth EPCs in culture and enumerating CPCs co-expressing Sca1 and Flk1, we appraised the numbers of circulating c-kit-positive cells and found no difference here across the three genotypes. As a result of these preliminary experiments, we elected not to assess CPC mobilisation to VEGF, interrogate bone marrow lysates for eNOS or carry out transfusion studies. The findings may not be surprising in this specific context: as well as the conflicting nature of the data surrounding EPC dysfunction in vascular repair, another possible reason is that an endothelial restricted intervention may not be capable of influencing bone marrow-derived cells. With highly selective expression of the hIR in endothelium, it could be envisaged that transgene insertion did not affect EPCs; therefore, one would not necessarily expect any alteration in their numbers or function in our model. One could argue that increased IR expression in the bone marrow could restore local eNOS production without directly influencing EPCs themselves, thus encouraging more effective EPC mobilisation; however, the lack of EPCs or CPCs in blood in our model suggests that this putative recovery mechanism was also not relevant in the HIRECOxIRKO. Our findings do not necessarily argue against the established role of EPC dysfunction in the pathogenesis of impaired vascular repair in the IRKO model; rather they suggest that multiple mechanisms may be relevant in that pathological setting and that recovery in the context of our specific genetic manipulation is likely to be brought about by alternative phenomena.

These experiments do not, however, fully exclude alterations in EPC biology in the HIRECOxIRKO mouse. Firstly, we only assessed flow cytometrically-defined CPCs and early outgrowth EPCs in this project. Both of these cell types have unclear *in vivo* relevance and, despite their status as useful biomarkers in cardiovascular health, they may not represent the spectrum of endothelial progenitors as a whole. We also cannot fully exclude the

possibility that EPC function, in contrast to abundance, was improved in HIRECOxIRKO mice as we only used one method for modelling this: the effects of conditioned EPC media on endothelial scratch wound healing. This assay was carried out using HUVECs rather than primary murine endothelial cells, which had the advantage of ensuring a high enough yield of macrovascular endothelial cells to use the same donor in all experiments, along with sufficient replicates per scratch to ensure a robust data set. The numbers are relatively low and it would be prudent to perform this experiment using more samples of conditioned media from each genotype before drawing firm conclusions from the data. Furthermore, one could question the ability of EPC-conditioned media from a mouse to influence the healing of a scratch wound made in a human cell line, though Khan *et al* showed reduced tube formation in HUVECs using EPC-conditioned media from mice, lending some degree of validity to the experiment [164]. The relevance of murine paracrine effects on human cells could still be questioned. In order to address this, our data on EPC function could be supplemented by assessing scratch wounds in primary cultured wild-type PECs from mice, exposed to conditioned media derived from mice of all three genotypes. A more complete assessment of the paracrine influence of EPCs on endothelial cells might also include assays of endothelial cell adhesion and proliferation using HUVECs, or indeed PECs, exposed to EPC-conditioned media. Co-culture of endothelial cells with EPCs may also provide some indication as to whether cell-to-cell interactions are important in influencing endothelial repair. Additionally, the cytokine profile in EPC-conditioned media from WT and IRKO mice could be appraised. In the event of IRKO media showing higher concentrations of pro-inflammatory or atherogenic mediators that could be envisaged to interfere with effective vascular healing, the levels of these could be interrogated in HIRECOxIRKO-derived media. Finally, it would also be prudent to look for evidence of human insulin receptor expression in cultured EPCs to rule out the possibility of insufficiently selective transgene targeting by the Tie-2 promoter. This could be performed either on EPC-conditioned media or after lysis of cultured EPCs.

6.3.3 **Role of endothelial cells**

On the basis of these observations, we felt that our hypothesis regarding improved EPC-mediated vascular repair in HIRECOxIRKO had not been confirmed by the data presented. Instead of pursuing further experiments with EPCs, we therefore elected to study primary cultured endothelial cells to look for differences between WT and IRKO and any potential rescue of these defects in the HIRECOxIRKO model. In order to heal injured vasculature, endothelial cells may proliferate more, show greater capacity for migration [192] or a reduced propensity towards apoptosis [193] or necrosis. Pilot data from other projects in our laboratory have shown reduced migration and vascular network formation in IRKO endothelial cells [194] so we opted to begin with these areas of endothelial cell function.

Our laboratory group has previously purified endothelial cells from murine lungs using anti-CD146 magnetic beads [186]. To improve the purity of the endothelial cell fraction achieved using this technique, a novel protocol involving the use of a two-step antibody separation was adopted and optimised for this project (see Chapter 4.12). As demonstrated in Figure 4-11, the population of cells isolated using this two-stage protocol was deemed to show acceptable purity and all assays involving endothelial cells were therefore carried out using this technique. Despite this, it is important to note certain caveats with this protocol. One is that endothelial cells derived from mouse lungs are more likely to represent the microvascular than the macrovascular endothelium. Given that our *in vivo* and *ex vivo* experiments are based around femoral arterial injury and aortic vasomotor function, it could be argued that endothelial cells from large vessels such as the aorta would be more representative of the cellular and molecular phenotypes pertinent to these models. Furthermore, these macrovascular tissues are high-pressure systems as opposed to the low-pressure environment encountered in the lungs, a difference which may influence vascular function and repair [195, 196]. The pulmonary vasculature also displays differences

in terms of ambient oxygen concentrations [195]. However, there is likely to be an overlap between the function of microvascular and macrovascular endothelial cells and it was not felt that they two were sufficiently divergent to preclude the study of PECs. This strategy was supported by the fact that our own previous work, and that of others, tends to demonstrate concomitant derangements in the function of both subsets of endothelium [114, 164, 189]. Moreover, it was not feasible to achieve the endothelial cell numbers required for this project by isolating them from the aorta alone, necessitating derivation of cells from an organ with a high concentration of endothelial cells. Another potential criticism of the two-step separation technique is that cells need to be in culture for a relatively long period before they can be used in experiments. Firstly, the requirement for two antibody separations introduces a delay and an extra passage; secondly, cells take 7-10 days to reach sufficient confluence in a T25 culture vessel for passage at each step. There is a theoretical possibility that repeated passage and prolonged culture could affect cell phenotype; however, we were reassured to see our data replicate prior observations from intact IRKO vessels, such as the extent of murine insulin receptor mRNA reduction, and enhanced superoxide generation.

6.3.4 Endothelial cell migration

With these caveats in mind, two separate assays of cell migration were performed. Initially, the modified Boyden chamber method was used to assess the responses of serum-starved PECs to a VEGF concentration gradient. Whilst VEGF is classically associated with angiogenesis, it also plays a role in the chemotactic component of endothelial cell migration [197, 198] and has been implicated in the response to vascular injury [153]; as such, its effects on PECs were of interest. Consistent with unpublished data from our laboratory group in a pure colony of IRKO mice, the experiments in the current project demonstrated a significant reduction in net migration to

VEGF in IRKO PECs compared with those from WT mice, with recovery to WT levels in HIRECOxIRKO cells.

Little exists in the literature regarding the specific impact of insulin resistance on endothelial cell migration after vascular injury; many studies in this area specifically focus on EPCs. Insulin does appear to encourage endothelial cell migration *in vitro*: a study using human microvascular endothelial cells revealed insulin-induced increases in cell migration *in vitro* using a cloning ring assay [199]. This was found to be dependent on the presence of a functioning insulin receptor and was associated with increased Akt phosphorylation; furthermore, the enhanced migration could be abrogated using a PI3K inhibitor, implicating this specific signalling pathway. One may therefore expect a deficit in endothelial cell migration given that insulin resistance causes specific downregulation of the PI3K pathway; indeed, this signalling cascade has been shown to be important in the migratory response of endothelial cells to VEGF [198]. In particular, Akt1, eNOS and NO are important in mediating the intracellular signalling that results in endothelial cells assuming a migratory and angiogenic phenotype [197, 200], with evidence that migration in the Boyden chamber can be inhibited by adding L-NMMA and thus inhibiting eNOS [201, 202]. It is tempting to speculate that restoration of endothelial insulin signalling could have a beneficial effect on this pathway, perhaps by reinstating a normal chemotactic response to VEGF as observed in our experiments. The hypothesis that NO-dependent migration is improved in the HIRECOxIRKO would also be in keeping with our finding in the organ bath experiments that aortic rings from these mice display evidence of increased NO bioavailability (see Chapter 5.12). It would be interesting to perform a second set of Boyden chamber migration experiments with the inclusion of L-NMMA in some wells: if this abrogated the improved migration seen in HIRECOxIRKO without affecting the results seen in IRKO cells, it would strengthen the case for NO-mediated recovery.

One of the criticisms of the Boyden chamber method as a sole technique for assessing cell migration is that it is an *in vitro* model of a very specific element of the overall process. In reality, endothelial cell migration involves three distinct stages: chemotaxis to a gradient of soluble pro-migratory mediators; haptotaxis towards immobilised ligands such as integrins in the extracellular matrix; and mechanotaxis, resulting from complex spatial rearrangements of the cytoskeletal network of actin filaments [198]. The role of VEGF in migration may also not be critical, as evidenced by the failure of SU1498, an inhibitor of VEGFR-2, to reduce insulin-induced endothelial cell migration [199]. For this reason, we attempted to complement our interrogation of cell migration by using a second technique: the scratch wound assay. It could be argued that this is a more accurate *in vitro* approximation of the contribution of migration to vascular repair as it effectively recreates the macroscopic endothelial denudation that occurs in injury models on a cellular level. Furthermore, the cell migration that closes the scratch wound is not reliant on the exogenous administration of VEGF and instead is likely to draw upon many of the contributory factors that influence the three steps mentioned above. The IncuCyte™ imaging system adds further refinement to the assay. Scratch wound assays can be performed manually using a pipette tip and performing phase-contrast imaging at a certain time point after injuring the cell layer. However, this is clearly an operator-dependent technique and the mechanical scratch induced by the Woundmaker™ represents a more reproducible insult to the cell layer. The real-time imaging possible with the IncuCyte™ further enriches the data set as it allows the determination of a time-course for wound repopulation; an AUC metric can then be used rather than expressing differences in migration at a single time-point. In pilot work, various time-points were appraised and it was felt that AUC analysis over the first 12 hours would allow us to observe differences in migration effectively. A further advantage of the automated imaging software is the calculation of relative wound density: this includes an inbuilt correction for the degree of proliferation observed in cells along the edge of each wound, thus

attempting to reduce the contribution of proliferation to the wound healing observed in the assay.

As such, it is unfortunate that we do not have a complete data set from the scratch wound experiments. The raw numbers suggest a small reduction in relative wound density in IRKO PEC scratch wounds; this is subtle and is not statistically significant, so conclusions should not yet be drawn from this experiment. However, WT and HIRECOxIRKO cells appear to behave similarly and there is a suggestion of slightly improved wound density after 12 hours compared with the IRKO data. As such, it is tempting to speculate that these early data might represent a signal towards a similar result to that of the Boyden chamber experiments. Clearly, these experiments should be completed, and could be refined with the addition of inhibitory factors such as L-NMMA. Additionally, it would be useful to appraise the relative wound density metric independently, to ensure that the impact of proliferation on wound healing has been sufficiently considered in the automated image analysis. This could be done by incubating cells in some wells of each plate with mitomycin C to abrogate proliferation and comparing the migration seen in these wells with that in control wells.

6.3.5 Endothelial cell proliferation

The migration assays therefore suggest a deficit in IRKO endothelial cells, with recovery to WT levels in the HIRECOxIRKO, at least using one of the two methods of assessment. However, another potential mechanism to explain augmented endothelial cell-mediated vascular repair would be if endothelial cells were proliferating more [192]. We appraised this using an *in vitro* assay of EdU uptake which allowed us to image and calculate the percentage of cells undergoing active DNA replication. This assay was relatively simple to perform using fluorescence microscopy with only 20,000 cells per well. In comparison with the traditional bromo-deoxyuridine (BrdU)

assay, use of the EdU probe depends on a simple azide-alkyne reaction, the effects of which are readily detectable in fixed and permeabilised cells instead of having to denature DNA and thus compromise its integrity. Furthermore, BrdU assays rely on an anti-BrdU antibody, which introduces the confounding issue of non-specific binding.

The results of the EdU assay in the current project are somewhat curious. IRKO and WT cells showed no significant differences in rates of proliferation, but HIRECOxIRKO PECs were seen to proliferate significantly more than both other subsets. It is difficult to know how to interpret this and, as such, it would be interesting to assess proliferation using a second technique for confirmation of the robustness of this finding. Cellular proliferation can also be assessed using cell cycle analysis with flow cytometry. This is another *in vitro* assessment, which could be criticised for lacking relevance to the overall animal model. To address this, a further alternative is to label proliferating endothelial cells with EdU *in vivo*; it is anticipated that our laboratory group will take both techniques forward. The finding of increased proliferation in HIRECOxIRKO may be a true phenomenon despite the apparent lack of an accompanying deficit in IRKO cells. Previous investigators have suggested that exogenous insulin does not influence proliferation in human endothelial cells [199], so it is feasible that insulin resistance will have no effect on proliferation. As discussed before, the mechanism for augmented vascular repair in HIRECOxIRKO mice appears not to be EPC-dependent, despite published data suggesting that EPC transfusion can rescue vascular repair in IRKO mice. Therefore, not all beneficial effects seen in HIRECOxIRKO mice or cells necessarily needs to correlate with a reciprocal deficit in the insulin resistance model.

A potential explanation for the discrepant proliferation result lies in the pathway-specific nature of insulin resistance, wherein the PI3K pathway responsible for NO generation is inactivated while the MAPK pathway, which encourages growth and mitogenesis, is unaffected. As a result, one may expect that proliferation would be undisturbed even in the context of insulin

resistance, explaining the lack of a difference between WT and IRKO PECs. However, with greater expression of endothelial insulin receptors, one may expect heightened intracellular signalling in both cascades, which would generate NO in the PI3K arm but also encourage proliferation on the MAPK side. This may explain the higher rate of proliferation seen in HIRECOxIRKO mice and it is therefore important to use alternative methods for analysis of this area of endothelial cell function.

6.3.6 Summary

HIRECOxIRKO mice show improved vascular repair after wire injury than their IRKO littermates, with restoration to the levels seen in WT mice. This does not appear to be related to improved EPC abundance or function in the HIRECOxIRKO mouse. Instead, *in vitro* assessment of endothelial cell function suggests that IRKO cells have reduced migratory capacity to a VEGF gradient, with recovery to WT levels in HIRECOxIRKO PECs. It is too early to comment with certainty on the results of the scratch wound assay, but a similar observation cannot be ruled out. Additionally, HIRECOxIRKO cells appear to proliferate more than those from WT or IRKO mice, which may represent an additional reparative mechanism, despite the lack of an apparent proliferation deficit in IRKO cells. Given that we have not observed any improvement in EPC biology in the HIRECOxIRKO mouse, it is tempting to speculate that enhanced endothelial cell reparative capacity (by way of increased migration, perhaps along with proliferation) represents the primary mechanism for the amelioration noted in vascular repair. Other options include increased cell survival in the HIRECOxIRKO model, but this was not assessed in our project and remains an option for further work.

6.4 Endothelial function

6.4.1 Background

The link between insulin resistance and cardiovascular disease in humans is well established (see Chapter 1.1.2) and work in a variety of murine models has allowed the recreation of a similar phenotype in experimental settings [60, 114, 123]. Previous findings from our laboratory demonstrate that IRKO mice, despite their essentially unperturbed glucoregulation, are hypertensive when compared with WT littermates [60]. Knockout of eNOS has also been demonstrated to result in increased systolic blood pressure [203], while rats can be rendered hypertensive with the use of L-NMMA [204], suggesting a key role for eNOS and NO in maintaining normotension. In addition to effects on blood pressure, IRKO-derived aortic rings showed a loss of insulin-mediated vasodilatation and reduced NO bioavailability in the Wheatcroft *et al* study [60]. Importantly, mice rendered chronically hypertensive via subcutaneous administration of norepinephrine did not show the same differences between genotypes; nor did rings that had undergone endothelial denudation before mounting onto the organ bath apparatus. These findings strengthened the assertion that the vasomotor changes noted were specifically related to endothelial dysfunction. Other investigators have shown increased coronary artery resistance and diminished response to ACh in both high fat-fed mice and those with partial or complete knockout of eNOS [205]. Signalling via the PI3K pathway was implicated in our laboratory's work: IRKO rings lacked the insulin-induced eNOS phosphorylation seen in WT tissue, despite similar quantities of eNOS mRNA and basal eNOS protein being detected in both groups. These molecular findings were recreated in the ESMIRO mouse, also from our laboratory, though these animals were normotensive [114]. Consistent with the demonstration of diminished eNOS phosphorylation, Kahn *et al* also showed a reduction in aortic eNOS activity in the L-citrulline assay. Our group's findings are slightly in contrast with those of Vicent *et al*, who

identified reduced basal eNOS expression in the VENIRKO model [113]. This may be related to the fact that the VENIRKO mouse displays a profound (95%) reduction in insulin receptor mRNA.

These differences notwithstanding, the background data all suggest that impaired endothelial insulin signalling results in a defect at the level of eNOS and the consequent reduction in NO mediates endothelial dysfunction and, in the IRKO mouse, hypertension. In the present study, the hypothesis was that restoration of endothelial insulin signalling would 'rescue' this pathway and result in increased NO bioavailability and reversal of endothelial dysfunction. We sought to use a similar combination of *in vivo*, *ex vivo* and *in vitro* techniques to evaluate this hypothesis.

6.4.2 Vasomotor function

One of the earliest and most interesting findings in the current study was that HIRECOxIRKO mice had significantly lower systolic blood pressure than IRKO littermates, with restoration to the level seen in WT animals. Given that HIRECOxIRKO mice showed no differences in basic morphology or metabolic parameters, this provided an early suggestion that our method for restoring endothelial insulin sensitivity had been successful in reversing the adverse vascular phenotype seen in IRKO. These results were of significant interest for two reasons: firstly, given that ESMIRO and VENIRKO mice do not exhibit hypertension, our finding that IRKO had higher blood pressure than WT was reassuring as it confirmed the arguably contentious earlier haemodynamic data from the IRKO mouse [60]. Secondly, as with the vascular injury experiments, the improvement in blood pressure represented rescue of an important physiological parameter *in vivo* rather than solely in experimental conditions. Ideally, one would wish to take this finding further by measuring NO or quantifying its effects *in vivo*; however, NO levels are

difficult to appraise directly given its volatility. Instead, one could observe the effects of chronic NOS inhibition in the HIRECOxIRKO, and further work could include performing blood pressure measurements in a cohort of mice receiving L-NMMA (versus vehicle) using subcutaneously implanted 'minipumps'. A caveat in the appraisal of arterial pressure in mice is the requirement for fairly large sample sizes in order to detect the small (yet consistent) differences that we have thus far observed. Repeating the experiment post-L-NMMA would necessitate the use of a large quantity of mice and so, in the interests of timing and animal welfare, it was felt prudent to model the process initially using an *ex vivo* organ bath assessment instead. Additionally, the quantification of blood pressure in a conscious animal under restraint is prone to difficulty and perhaps inaccuracy because the measurement can be distressing for the mouse. Attempts were made to minimise this by ensuring at least two habituation sessions prior to recording, as well as performing the experiment at the same time of day to minimise the effects of diurnal variation. The Coda software used also takes 18 recordings per mouse after ten acclimatisation cycles, allowing a mean reading to be calculated over around ten minutes of measurement in an attempt to reduce variability. Intra-arterial blood pressure monitoring is feasible, but the risks of this invasive approach must be offset against the benefits and it was not felt that this was justified in the current project. It was therefore important to consolidate our appraisal of endothelial function using an alternative method, and we elected to perform organ bath experiments using aortic rings for this purpose.

The results from the organ bath experiment were equally exciting: IRKO aortic rings displayed endothelial dysfunction and reduced NO bioavailability, all of which was reversed in the HIRECOxIRKO model. These findings are in keeping with the favourable changes seen in the blood pressure data set and provide further evidence that enhancing endothelial insulin signalling can help to ameliorate the vascular phenotype seen in systemic insulin resistance. The use of acute pharmacological NOS inhibition in these

experiments was also helpful in identifying enhanced NO release as a likely causative factor in the improvements observed. This will be discussed in more depth in the following section but, in brief, we hypothesise that restoration of the PI3K signalling pathway in endothelial cells results in recovery of eNOS activation and thus NO synthesis.

One must appraise the data from the organ bath experiments with a degree of caution given that this is an *ex vivo* technique that is highly operator-dependent. In order to maximise the integrity of aortic tissue, great care was taken not to stretch the vessel during dissection and it was transported and cleaned in Krebs-Henseleit medium to maintain a highly supportive environment. Furthermore, another group member (Mrs Stacey Galloway) collected specimens directly from the animal facility, before dissection of animals was complete, in order to minimise delays in transport. Mrs Galloway's significant experience in performing the remainder of this experiment was an additional method for reducing operator error and variability, and allowed blinding to genotype during experiments. With these measures in place, the technique provided reproducible results and replicated most of the differences previously seen between WT and IRKO.

The method for statistical analysis of organ bath data also varies between investigators. In this project, EC_{50} values were presented as it was felt that a 50% change in constriction or dilatation from baseline was likely to be a reasonable reflection of the levels of fluctuation in vessel tone that occur *in vivo*, in contrast with measuring the concentrations of agonist required for maximal alteration in tension. Equally, some investigators prefer to make serial comparisons of tension at each agonist dose increment but this fails to provide an overall appraisal of differences between genotypes across the spectrum of agonist concentrations; one could argue that the analysis of dose increments is therefore less meaningful. The existence of several methods of analysing data in this experiment makes it harder to compare our findings with those of others. However, the visual appraisal of divergent

dose-response curves appears to be concordant with our statistical analysis of differences in EC_{50} between genotypes. Furthermore, the broad findings of endothelial dysfunction and reduced NO bioavailability in IRKO in the current study are consistent with the results of Wheatcroft *et al* [60], suggesting reproducibility of this phenotype. Therefore, it was felt that the combination of improved vasomotor function in the organ bath and reversal of hypertension represented restoration of endothelial function in the HIRECOxIRKO, most likely due to an increase in NO bioavailability.

6.4.3 Summary

HIRECOxIRKO mice show restoration of the high blood pressure observed in IRKO littermates, with levels similar to those of WT animals. To accompany this *in vivo* finding, the current study has shown recovery of vasomotor function in the HIRECOxIRKO mouse in experiments involving aortic rings. In the latter experiment, HIRECOxIRKO rings displayed restoration of NO bioavailability, suggesting that the mechanism for improved endothelial function and blood pressure was likely to relate to enhanced NO release, possibly as a result of augmented PI3K signalling. In the next section, early data targeted at determining a causative molecular mechanism will be discussed.

6.5 Unifying molecular mechanisms

6.5.1 Background

Previously published data appear to show that the endothelial dysfunction observed in insulin resistance results from reduced NO bioavailability. Our group's findings in aortae from IRKO and ESMIRO mice suggest that eNOS mRNA and basal eNOS protein levels are similar to WT but, in both models, an impairment is seen in eNOS phosphorylation [60, 114]. Consistent with this, IRKO mice also show evidence of reduced aortic eNOS activity [164]. As discussed in the previous section, the VENIRKO mouse shows a slightly different molecular phenotype, in that basal eNOS is reduced in this model [113]. It is well established that NO has a key role in mediating endothelial function in health and it is therefore not surprising that, regardless of the exact mechanism of the deficit in insulin resistance, reduced endothelial NO is implicated in the associated vascular dysfunction. A similar finding has been described in multiple models of obesity-induced insulin resistance [206]. The same impairment also forms an important part of the response to vascular injury, be that due to the essential role of NO in EPC mobilisation or via its contribution to effective migration in native endothelial cells.

Reduced NO bioavailability can result from two broad pathogenetic mechanisms: firstly, reduced expression or activation of eNOS, and secondly, sequestration by reactive oxygen species (ROS). In the context of insulin resistance, there is ample evidence of impaired PI3K signalling resulting in the former, as discussed previously. Oxidative stress has also been demonstrated in animal models encompassing both genetically-induced insulin resistance and that resulting from high fat feeding [114, 115, 123-125]. Taken together, these findings suggest a combination of reduced NO generation and increased sequestration by ROS in the setting of insulin resistance. Similarly, NO release and oxidative stress can both have an

impact on vascular repair and it is likely that the delayed response to injury seen in IRKO mice is again a combination of both factors. Therefore, a key question in this project is the mechanism for enhanced NO bioavailability in the HIRECOxIRKO model. Our hypothesis was that this results from a combination of increased production due to augmentation of the PI3K signalling pathway, and reduction in oxidative stress. Unfortunately, we were not able to complete the relevant experiments in this area, though early data provide some indications.

6.5.2 **Insulin signalling**

Initially, we sought to assess the effects of endothelial insulin sensitisation on intracellular signalling. Unfortunately, only one set of Western blot results was obtained during the time frame in this project; this is a significant shortcoming of this work. Crude appraisal of the blots presented in Chapter 5.14 suggests an appearance compatible with existing knowledge of insulin signalling in IRKO mice, namely the finding of reduced insulin-stimulated phosphorylation of Akt and eNOS. There appears to be a preliminary suggestion that Akt phosphorylation is improved in the HIRECOxIRKO model, though it is impossible to be definitive about this early finding given the single sample. From the blot presented, the increase in insulin-stimulated Akt phosphorylation appears modest and less intense than that observed in WT PECs. If this finding is consistent in future samples then it may suggest partial restoration of downstream insulin signalling. Alternatively, it may be prudent to assess a variety of time points after insulin stimulation or to probe other phosphorylation sites on these molecules. The phosphorylation of eNOS in HIRECOxIRKO appears no different to that seen in IRKO cells but, again, this may simply reflect the fact that this was only assessed at one amino acid residue and at one time point.

Clearly, more replicates need to be processed in order to comment sensibly on levels of total and phosphorylated Akt and eNOS. These data would allow us to determine whether nodes in the PI3K signalling pathway were affected at baseline by the expression of the human insulin receptor in endothelial cells. Furthermore, insulin-stimulated cells could be used to determine the level of insulin sensitivity of each genotype with respect to this signalling cascade. These data could validate the insulin sensitisation strategy on a molecular level, in conjunction with data on insulin receptor concentrations, and also consolidate our understanding of the mechanisms accounting for the beneficial vascular phenotypes seen in HIRECOxIRKO mice. From the perspective of undesirable off-target effects, it would also allow us to appraise the effects of enhancing insulin signalling on Akt, which is important given the oncogenic potential of this signalling node. Any translational use of this model would need to take such effects into consideration.

In addition to assessing phosphorylation of eNOS, it would be prudent to measure the activity of the enzyme. This has previously been performed in our laboratory using the L-citrulline assay, which uses the conversion of carbon-14-labelled L-arginine by NOS to determine L-citrulline generation. Whilst this technique does not allow direct measurement of NO concentrations, it provides a surrogate measure, which is important given that NO is difficult to quantify due to its volatility. Previous work in IRKO mice has shown a loss of augmentation of eNOS activity after stimulating cells with insulin [164]; basal levels in unstimulated cells were not directly compared. It would be important to perform the L-citrulline assay on PECs from all three genotypes in the current project; we hypothesise that HIRECOxIRKO cells will show increased eNOS activity. This may be evident in unstimulated cells, given that eNOS activity is not restricted to times of insulin stimulation. However, the degree of insulin-stimulated eNOS activity could also be compared by incubating PECs with insulin prior to performing the assay. Alternative methods for assessing eNOS and NO exist: for example, the fluorophore diaminofluorescein (DAF) can be used to detect

NO via fluorescence measured using a microplate reader. Should the results of the L-citrulline assay be equivocal, it would be reasonable to consider using a fluorescence-based technique such as this to corroborate any findings.

Western blotting for MAP kinases and other elements of the Shc-Ras-Raf pathway would also be beneficial. One might envisage augmentation of this arm of insulin signalling as a consequence of hIR transgene insertion, and this may in part explain the finding of increased endothelial cell proliferation in the EdU assay as this pathway is pro-mitotic. It would be somewhat surprising if MAPK activity was markedly increased, as one would also expect greater endothelin-1 production as a consequence, and this appears unlikely given that HIRECOxIRKO mice have lower systolic blood pressure than IRKO littermates. It is of course feasible that enhancing insulin sensitivity results in asymmetrical augmentation of the parallel signalling pathways, favouring the PI3K arm which is selectively inhibited in insulin resistance. This could theoretically explain increased proliferation in the absence of higher blood pressure. It would be important to ascertain the degree of MAPK overactivation given the potentially deleterious effects of this on vascular function: as well as producing the vasoconstrictor endothelin-1, the MAPK pathway encourages release of growth factors and this could encourage a pro-atherosclerotic environment.

There may also be cross-talk between various intracellular signalling pathways. One of the more curious findings in our group's organ bath experiments, including those presented in this project, is the relatively modest difference between WT and IRKO aortic rings in terms of acetylcholine-induced vasodilatation. No difference was observed by Wheatcroft et al [60]; in the current study, the relaxation curves appeared divergent but there was no significant difference between WT and IRKO with respect to the EC_{50} for vasodilatation. This may be because the vasodilatation induced by ACh, whilst eNOS dependent, relies on G-protein

coupled receptors and raised cytosolic calcium ion concentration rather than insulin-mediated eNOS activation. It is feasible that this is why significant differences are not noted in IRKO rings. However, if HIRECOxIRKO endothelium is sensitised to insulin and PI3K signalling is indeed enhanced, then there may be simultaneous upregulation of G-protein coupled receptor pathway activity due to co-regulation of these cascades [207]. Similar cross-talk has also been demonstrated for MAP kinases [207], which could partially explain the increased endothelial cell proliferation. Clearly these interactions are complex and detailed interrogation using Western blotting for various mediators would help to increase our understanding of the intracellular effects of hIR transgene insertion.

6.5.3 **Oxidative stress**

As discussed in Chapter 1.3.5, oxidative stress is another potential mechanism for reduced NO bioavailability in the setting of insulin resistance. The superoxide anion reacts with NO to form peroxynitrite, thus reducing the concentration of NO in the cell and encouraging further oxidative stress through the effects of peroxynitrite. Therefore, even if eNOS activity is undisturbed and NO is being produced, the latter can be sequestered by ROS and there is evidence of increased ROS in both the IRKO and ESMIRO models of insulin resistance in the endothelium [114, 123]. We hypothesised that ROS levels may be reduced in HIRECOxIRKO mice and this may contribute to the increase in NO bioavailability in this model. However, the preliminary results of the DHE assay reveal that HIRECOxIRKO have significantly increased superoxide concentrations in PECs compared with WT mice. These experiments are incomplete and numbers should be augmented, but there is a strong suggestion that IRKO mice have increased ROS, in keeping with previous work. This would suggest that, whilst IRKO mice are prone to oxidative stress, enhancing endothelial insulin sensitivity may not reverse this. Clearly, the interim results of an incomplete experiment cannot be used to rule out a role for reduced ROS emphatically, and further

work is warranted. As well as completing the DHE assay, it would be interesting to appraise NOX2 mRNA as this has been demonstrated to be the source of ROS in insulin resistant murine models [114, 123].

6.5.4 **Summary**

The data above are clearly incomplete and, crucially, the project lacks detailed data on intracellular signalling and eNOS activity that would consolidate our understanding of the molecular mechanism behind increased NO bioavailability in the HIRECOxIRKO. The DHE assay, however, provides early data to suggest that there is no gross reduction in superoxide concentration in HIRECOxIRKO PECs, suggesting that diminished oxidative stress is unlikely to be the primary mechanism. If reduced sequestration of NO is not the key difference between IRKO and HIRECOxIRKO then it appears that the rescue of vascular function is occurring at the level of eNOS. It is tempting to postulate that enhancing endothelial insulin sensitivity results in augmented PI3K signalling, resulting in either greater eNOS expression or phosphorylation, or both. If this is correct, one would expect enhanced eNOS activity and this could explain the greater NO bioavailability that appears to be driving improved blood pressure, endothelial function and vascular repair in our model.

6.6 General limitations

As with all exploratory scientific work, the methods utilised have inherent limitations and this must be taken into consideration in our analysis and interpretation of data. I have attempted to highlight specific weaknesses in relevant subsections throughout my discussion. Additionally, various general limitations in this project merit comment.

Firstly, we have used a murine model of insulin resistance, comparing this to a "double-cross" with two genetic manipulations. The phenomenon of insulin resistance in man is complex and it could be argued that a mouse model with a relatively simple receptor knockout strategy cannot fully recapitulate the nuances of this phenotype: for example, IRKO mice lack the obesity and hyperlipidaemia seen in humans with metabolic syndrome [60]. The multi-level insulin resistance seen in man is unlikely to be modelled in the IRKO mouse, nor can we be sure how sensitive we render the endothelium with the HIRECO manipulation. Additionally, the resulting HIRECOxIRKO model has no direct corollary in physiology. However, several experiments on IRKO mice over a number of years have displayed a convincing and consistent vascular phenotype in connection with diverse measures such as blood pressure, endothelial function and vascular repair; meanwhile, the experiments we have performed here clearly could not have been performed in man. Therefore, conceding the general caveat that animal models cannot faithfully mimic a complete disease process in man, we feel that the use of mice has been a reasonable compromise between purely *in vitro* work on one hand and a wholly physiologically relevant model on the other. Equally, larger mammals could theoretically be used but this brings other technical challenges and pragmatic considerations such as longer breeding cycles and time to maturation. Finally, the aim of this project was to appraise the effects of sensitising one tissue (the endothelium) in the setting of systemic insulin resistance and, as this specific configuration cannot be recreated in

man, nor in cell culture conditions, an animal model is a potential way to model the scenario.

The use of an animal model brings another key set of considerations: sample sizes and power calculations. Animal research is underpinned by the "Three Rs" ethical paradigm: reduce, refine and replace. Thus, whilst it would be ideal to ensure several repeats in every experiment, it is important to take a pragmatic view on how many replicates are required in order to answer an exploratory scientific question. Clinical trials are highly dependent on a rationally determined sample size as a clear biologically relevant difference (such as a desired drop in mortality rate with a new drug) can often be defined with accuracy and this can be fed into power calculations. In contrast, the data gathered from this project are expressed as, for example, percentage endothelial regeneration or a blood pressure drop in a mouse, metrics for which a meaningful biological difference is difficult to define. Ideally, results from a small number of mice could be compared as pilot data that would inform a power calculation for more rigorous future study. However, the observed differences are often small and this would likely necessitate the use of prohibitive numbers of mice, both from an ethical and a financial perspective. We instead relied on the achievement of a mathematically significant result in an appropriate statistical test as a preliminary suggestion that a biologically relevant difference had been found. Interestingly, almost every prior finding in the IRKO mouse was recreated in the current project, suggesting a fairly consistent phenotype in this model and, perhaps, reflecting a certain degree of accuracy in our assessment despite the small numbers. Given the hypothesis-generating nature of many of the experiments presented, some of the results should not be viewed as conclusive or definitive, and the findings simply highlight potential differences that can form a foundation for future development. One could argue that this is as dogmatic as one can be about animal research as a whole, and thus whilst it is acknowledged as a criticism of our work, it may not diminish the utility of this research.

The problem of small sample sizes is compounded by the fact that multiple experiments needed to be done on similar organs in this project. Mice are clearly small animals and thus generate relatively small quantities of tissue even when an entire organ is taken from an adult; therefore, an entire aorta per mouse was used for organ bath experiments and more mice needed to be sacrificed when the aorta was used for other work, such as qPCR. For some experiments, such as vascular injury and the aortic ring work, mice needed to be aged in order to reach a size at which surgery or mounting of aortae would be technically feasible. No other experiments were performed on mice reserved for wire injury and, as a result of perfusion with paraformaldehyde at the time of sacrifice, no tissue other than the femoral artery could be used. Similarly, mice sacrificed for organ bath experiments were generally too old for concomitant removal of lungs for PEC culture as the latter set of experiments was optimised in mice aged 4-6 weeks. Thus, despite attempting to reduce mouse use and refine experiments by having experienced operators perform each technique, large overall numbers of mice were required to achieve the relatively small numbers quoted per experiment, and this had implications in terms of trying to increase sample sizes.

One of the consequences of a relatively small sample size is the need to ensure that each data set is as robust and reproducible as it can be. Most of the experiments were designed with this in mind; wherever feasible, several replicates were performed within each condition. For example, up to 18 readings were taken for each blood pressure data point; four aortic rings were mounted per mouse in the organ bath; multiple wells were seeded for each cell culture experiment; and so on. However, the risk of introducing bias in these measurements remains and the methodology could be refined for future work. For example, my analysis of some data sets was not rigorously blinded: mouse IDs were often included in the file name or in the image during analysis. Whilst I did not have a working knowledge of the genotype for a given mouse ID, and I only retrieved this information

retrospectively, a risk of bias was introduced. This could have been reduced by genotyping mice after experiments were complete; however, this was often difficult as it was important to know genotypes for the practical purposes of housing animals and planning broadly equal numbers of each genotype in each individual experiment wherever possible. An alternative strategy would be to create a code for naming files such that analysis was fully blinded and data could later be cross-referenced with mouse IDs and only linked to genotypes as the last step. This is less likely to have had a significant impact on certain results, such as the organ bath work, in which the primary operator was fully blinded and rigorous rules were applied in the inclusion or exclusion of data during analysis. However, appraisals such as the quality of a blood pressure measurement or counting of cells could be more subjectively influenced and blinding, ideally with a second researcher and evaluation of inter-observer agreement, would be a more robust method for performing these analyses.

A further criticism is our reliance on very specific models of vascular disease that do not necessarily recreate the complexity of pathology in man. One of the key sets of data in this project was the vascular injury experiment, a model involving an acute insult to the endothelium, the effects of which were analysed only four days later. These data are interesting in terms of the effects of plaque rupture or stent placement on endothelial injury and repair, though do not provide significant insights into chronic processes such as atherosclerosis, nor do they allow the appraisal of longer term recovery. Similarly, the organ bath experiments are *ex vivo* methods of assessing the immediate response of vasculature to short-acting vasoconstrictors and vasodilators, with only acute pharmacological NOS inhibition. Most of the *in vitro* data simply served to highlight cellular and molecular mechanisms for these basic models. One way to target a more chronic process might be to attempt to breed HIRECOxIRKO mice onto an ApoE$^{-/-}$ background to appraise the effects of our manipulation on atheroma formation. We also tried to circumvent the issue by complementing our vascular injury and

organ bath experiments with the study of longer term measures of vascular biology such as blood pressure. It is felt that the inclusion of several, varied indices of vascular function has therefore provided a data set with broad relevance; as such, we have recreated most of the experiments done in IRKO mice across multiple earlier studies [60, 123, 164] in the HIRECOxIRKO model.

6.7 Future directions

In this project, significant new ground has been covered, as we have commenced the validation of endothelial insulin sensitisation as a therapeutic strategy to address the vascular disease observed in a murine model of global insulin resistance. However, this is early work and much more investigation would be desirable.

The first observation to make is that this is not yet a complete project even within the remit of our initial hypotheses. It will be important to appraise insulin receptor expression in endothelial tissues, as well as to complete the assays of migration and superoxide production that are reported here as interim results. In order to gain mechanistic insights, it will also be crucial to perform more Western blots to probe intracellular signalling and identify the level at which endothelial insulin sensitisation beneficially affects NO production and, thus, vascular function. This may also identify potentially harmful off-target effects of our strategy such as Akt overactivation or increased flux through the MAPK pathway of insulin signalling, which will have implications for translation. Potentially contentious observations such as the increased rates of proliferation in HIRECOxIRKO PECs should be interrogated in more depth using alternative experimental techniques. It would also be prudent to consolidate our understanding of the role of NO in the beneficial effects seen in HIRECOxIRKO mice. This could be done *in vitro* by attempting to reverse the favourable HIRECOxIRKO phenotypes using L-NMMA. It would also be feasible to infuse L-NMMA chronically and repeat key *in vivo* studies such as blood pressure measurement and wire injury after chronic NOS inhibition. Finally, further EPC work such as detailed functional studies would help underline our assertion that improvements in vascular repair are likely to stem from enhanced endothelial cell function rather than rescue of progenitor cell biology.

We have demonstrated rescue of endothelial dysfunction and impaired vascular repair using the HIRECOxIRKO model. However, other vascular aberrances are observed in the context of insulin resistance and the effects of our manipulation could be studied in these areas too. As mentioned above, the effects of endothelial insulin sensitisation on atherosclerosis could be appraised by crossing the HIRECOxIRKO mouse with atheroma-prone, hyperlipidaemic ApoE$^{-/-}$ mice. Similarly, the effects of this intervention on other chronic cardiovascular conditions could theoretically be modelled using IRKO and HIRECOxIRKO mice. Murine models of left anterior descending coronary artery (LAD) occlusion can enhance our understanding of heart failure and there may be merit in examining the interplay between this and insulin resistance. IRKO mice have also been demonstrated to show impairments in *in vitro* measures of angiogenesis [164] and this has been developed significantly in work from our laboratory group [194]. Given the beneficial effects we have observed on the vascular parameters evaluated in the current study, one may hypothesise that the HIRECOxIRKO mouse will display enhancement of angiogenesis as well, and various *in vitro* and *in vivo* studies could be performed to assess this.

Ultimately, the aim of this research is to identify novel therapeutic targets in the management of insulin resistance-associated vascular disease. Our findings represent a decidedly early stage in this process but are an important proof of principle, namely that manipulating insulin sensitivity in the endothelium can be helpful in reversing vascular derangements despite global insulin resistance. With further understanding of this strategy and refinement of our knowledge of its beneficial (and perhaps associated harmful) effects, it is possible that it will become a target for future therapy. Novel methods of drug delivery are being described, and the vascular endothelium, as the first point of contact for intravenously delivered agents, is an attractive prospect [208]. For example, endothelial cells can take up antibodies directed against PECAM-1 and ICAM-1 via endocytosis [209] and even transport antibodies across the cell and direct them towards sub-

endothelial structures [210]. The vascular endothelium could also be targeted by placing drug-eluting stents using percutaneous techniques [208]. In an era of increasing expertise in biotechnology and more nuanced therapeutic approaches, one can envisage the principles underlying this model being translated into clinically meaningful results in time, thus allowing patients with, or at risk of, diabetes to benefit from our work.

6.8 Concluding remarks

Prior to this project being undertaken, it was known that insulin resistance, as part of the constellation of risk factors known as the metabolic syndrome, is a key independent indicator of adverse vascular outcomes in man. The IRKO mouse is one of many murine models of insulin resistance that appears to recapitulate the phenomenon: despite preserved glucoregulation, these mice are hypertensive and exhibit endothelial dysfunction, impaired vascular repair and perturbations in mature endothelial cell and progenitor cell biology.

We sought to validate a therapeutic strategy involving the selective restoration of endothelial insulin sensitivity in the context of global insulin resistance. We hypothesised that this intervention would reverse endothelial dysfunction, normalise blood pressure and improve vascular repair in a model of arterial wire injury. This project has demonstrated that the HIRECOxIRKO is a viable and glucocompetent murine model in which to examine these hypotheses. HIRECOxIRKO mice have restoration of blood pressure and aortic vasomotor function to the levels of WT littermates. Equally, endothelial healing after vascular injury is significantly improved compared with IRKO mice, with data to suggest that this recovery is more likely to be mediated by endothelial cells than by EPCs.

A key determinant of these beneficial vascular phenotypes appears to be increased bioavailability of nitric oxide. Early data from this project appear to suggest that HIRECOxIRKO PECs have similar superoxide levels to those from IRKO mice, suggesting that the improvement in NO is more likely to stem from increased eNOS expression and/or activity than from reduced sequestration by ROS. Much work remains to be done in developing these assertions further. However, the work in this project adds to existing knowledge on the mechanisms behind insulin resistance-associated

vascular disease. Furthermore, it identifies a potential therapeutic target that, to our knowledge, has not been manipulated in this way before. As such, one can envisage the eventual translation of our work to a therapeutic strategy in years to come. In this way, the work within this project could form the basis of novel methods for managing vascular risk in people with insulin resistance and diabetes.

References

1. Wild, S., et al., *Global prevalence of diabetes: estimates for the year 2000 and projections for 2030.* Diabetes Care, 2004. **27**(5): p. 1047-53.

2. IDF. *IDF Diabetes Atlas.* 2013   25 March 2014]; Sixth Edition:[Available   from: http://www.idf.org/sites/default/files/EN_6E_Atlas_Full_0.pdf.

3. Wheatcroft, S.B., et al., *Pathophysiological implications of insulin resistance on vascular endothelial function.* Diabet Med, 2003. **20**(4): p. 255-68.

4. Booth, G.L., et al., *Relation between age and cardiovascular disease in men and women with diabetes compared with non-diabetic people: a population-based retrospective cohort study.* Lancet, 2006. **368**(9529): p. 29-36.

5. Kannel, W.B. and D.L. McGee, *Diabetes and cardiovascular risk factors: the Framingham study.* Circulation, 1979. **59**(1): p. 8-13.

6. Cubbon, R.M., et al., *Temporal trends in mortality of patients with diabetes mellitus suffering acute myocardial infarction: a comparison of over 3000 patients between 1995 and 2003.* Eur Heart J, 2007. **28**(5): p. 540-5.

7. *Intensive blood-glucose control with sulphonylureas or insulin compared with conventional treatment and risk of complications in patients with type 2 diabetes (UKPDS 33). UK Prospective Diabetes Study (UKPDS) Group.* Lancet, 1998. **352**(9131): p. 837-53.

8. Selvin, E., et al., *Meta-analysis: glycosylated hemoglobin and cardiovascular disease in diabetes mellitus.* Ann Intern Med, 2004. **141**(6): p. 421-31.

9. Balkau, B., et al., *High blood glucose concentration is a risk factor for mortality in middle-aged nondiabetic men. 20-year follow-up in the Whitehall Study, the Paris Prospective Study, and the Helsinki Policemen Study.* Diabetes Care, 1998. **21**(3): p. 360-7.

10.	Haffner, S.M., et al., *Cardiovascular risk factors in confirmed prediabetic individuals. Does the clock for coronary heart disease start ticking before the onset of clinical diabetes?* JAMA, 1990. **263**(21): p. 2893-8.

11.	Reaven, G.M., *Role of insulin resistance in human disease (syndrome X): an expanded definition.* Annu Rev Med, 1993. **44**: p. 121-31.

12.	Pyorala, M., et al., *Insulin resistance syndrome predicts the risk of coronary heart disease and stroke in healthy middle-aged men: the 22-year follow-up results of the Helsinki Policemen Study.* Arterioscler Thromb Vasc Biol, 2000. **20**(2): p. 538-44.

13.	Hu, F.B., et al., *Elevated risk of cardiovascular disease prior to clinical diagnosis of type 2 diabetes.* Diabetes Care, 2002. **25**(7): p. 1129-34.

14.	Barr, E.L., et al., *Risk of cardiovascular and all-cause mortality in individuals with diabetes mellitus, impaired fasting glucose, and impaired glucose tolerance: the Australian Diabetes, Obesity, and Lifestyle Study (AusDiab).* Circulation, 2007. **116**(2): p. 151-7.

15.	Reaven, G.M., *Banting lecture 1988. Role of insulin resistance in human disease.* Diabetes, 1988. **37**(12): p. 1595-607.

16.	Cubbon, R.M., et al., *Insulin- and growth factor-resistance impairs vascular regeneration in diabetes mellitus.* Curr Vasc Pharmacol, 2012. **10**(3): p. 271-84.

17.	Holman, R.R., et al., *10-year follow-up of intensive glucose control in type 2 diabetes.* N Engl J Med, 2008. **359**(15): p. 1577-89.

18.	Gerstein, H.C., et al., *Effects of intensive glucose lowering in type 2 diabetes.* N Engl J Med, 2008. **358**(24): p. 2545-59.

19.	Kelly, T.N., et al., *Systematic review: glucose control and cardiovascular disease in type 2 diabetes.* Ann Intern Med, 2009. **151**(6): p. 394-403.

20.	Nathan, D.M. and D.E.R. Group, *The diabetes control and complications trial/epidemiology of diabetes interventions and*

complications study at 30 years: overview. Diabetes Care, 2014. **37**(1): p. 9-16.

21. UKPDS, *Effect of intensive blood-glucose control with metformin on complications in overweight patients with type 2 diabetes (UKPDS 34). UK Prospective Diabetes Study (UKPDS) Group.* Lancet, 1998. **352**(9131): p. 854-65.

22. Home, P.D., et al., *Rosiglitazone evaluated for cardiovascular outcomes in oral agent combination therapy for type 2 diabetes (RECORD): a multicentre, randomised, open-label trial.* Lancet, 2009. **373**(9681): p. 2125-35.

23. Nissen, S.E. and K. Wolski, *Rosiglitazone revisited: an updated meta-analysis of risk for myocardial infarction and cardiovascular mortality.* Arch Intern Med, 2010. **170**(14): p. 1191-1201.

24. Bach, R.G., et al., *Rosiglitazone and outcomes for patients with diabetes mellitus and coronary artery disease in the Bypass Angioplasty Revascularization Investigation 2 Diabetes (BARI 2D) trial.* Circulation, 2013. **128**(8): p. 785-94.

25. Hauner, H., *The mode of action of thiazolidinediones.* Diabetes Metab Res Rev, 2002. **18 Suppl 2**: p. S10-5.

26. Dormandy, J.A., et al., *Secondary prevention of macrovascular events in patients with type 2 diabetes in the PROactive Study (PROspective pioglitAzone Clinical Trial In macroVascular Events): a randomised controlled trial.* Lancet, 2005. **366**(9493): p. 1279-89.

27. NCBI. *INS Insulin.* 10 May 2014 24 January 2014]; Available from: http://www.ncbi.nlm.nih.gov/gene/3630.

28. Bell, G.I., et al., *Sequence of the human insulin gene.* Nature, 1980. **284**(5751): p. 26-32.

29. Czech, M.P. and S. Corvera, *Signaling mechanisms that regulate glucose transport.* J Biol Chem, 1999. **274**(4): p. 1865-8.

30.   Watson, R.T. and J.E. Pessin, *Subcellular compartmentalization and trafficking of the insulin-responsive glucose transporter, GLUT4.* Exp Cell Res, 2001. **271**(1): p. 75-83.

31.   NCBI. *INSR. Insulin Receptor.* 13 May 2014 24 January 2014]; Available from: http://www.ncbi.nlm.nih.gov/gene/3643

32.   Virkamaki, A., K. Ueki, and C.R. Kahn, *Protein-protein interaction in insulin signaling and the molecular mechanisms of insulin resistance.* J Clin Invest, 1999. **103**(7): p. 931-43.

33.   Massague, J., P.F. Pilch, and M.P. Czech, *Electrophoretic resolution of three major insulin receptor structures with unique subunit stoichiometries.* Proc Natl Acad Sci U S A, 1980. **77**(12): p. 7137-41.

34.   McKern, N.M., et al., *Structure of the insulin receptor ectodomain reveals a folded-over conformation.* Nature, 2006. **443**(7108): p. 218-21.

35.   Ebina, Y., et al., *The human insulin receptor cDNA: the structural basis for hormone-activated transmembrane signalling.* Cell, 1985. **40**(4): p. 747-58.

36.   Ward, C.W. and M.C. Lawrence, *Ligand-induced activation of the insulin receptor: a multi-step process involving structural changes in both the ligand and the receptor.* Bioessays, 2009. **31**(4): p. 422-34.

37.   Taniguchi, C.M., B. Emanuelli, and C.R. Kahn, *Critical nodes in signalling pathways: insights into insulin action.* Nat Rev Mol Cell Biol, 2006. **7**(2): p. 85-96.

38.   Kasuga, M., et al., *Insulin stimulates tyrosine phosphorylation of the insulin receptor in a cell-free system.* Nature, 1982. **298**(5875): p. 667-9.

39.   Sun, X.J., et al., *Structure of the insulin receptor substrate IRS-1 defines a unique signal transduction protein.* Nature, 1991. **352**(6330): p. 73-7.

40. Kim, J.A., et al., *Reciprocal relationships between insulin resistance and endothelial dysfunction: molecular and pathophysiological mechanisms.* Circulation, 2006. **113**(15): p. 1888-904.

41. Kubota, N., et al., *Dynamic functional relay between insulin receptor substrate 1 and 2 in hepatic insulin signaling during fasting and feeding.* Cell Metab, 2008. **8**(1): p. 49-64.

42. Tanti, J.F., et al., *Serine/threonine phosphorylation of insulin receptor substrate 1 modulates insulin receptor signaling.* J Biol Chem, 1994. **269**(8): p. 6051-7.

43. Hajduch, E., G.J. Litherland, and H.S. Hundal, *Protein kinase B (PKB/Akt)--a key regulator of glucose transport?* FEBS Lett, 2001. **492**(3): p. 199-203.

44. Andjelkovic, M., et al., *Role of translocation in the activation and function of protein kinase B.* J Biol Chem, 1997. **272**(50): p. 31515-24.

45. Ritchie, S.A., et al., *Insulin-stimulated phosphorylation of endothelial nitric oxide synthase at serine-615 contributes to nitric oxide synthesis.* Biochem J, 2010. **426**(1): p. 85-90.

46. Rask-Madsen, C. and C.R. Kahn, *Tissue-specific insulin signaling, metabolic syndrome, and cardiovascular disease.* Arterioscler Thromb Vasc Biol, 2012. **32**(9): p. 2052-9.

47. Tsuchiya, K., et al., *FoxOs integrate pleiotropic actions of insulin in vascular endothelium to protect mice from atherosclerosis.* Cell Metab, 2012. **15**(3): p. 372-81.

48. Kanai, F., et al., *Insulin-stimulated GLUT4 translocation is relevant to the phosphorylation of IRS-1 and the activity of PI3-kinase.* Biochem Biophys Res Commun, 1993. **195**(2): p. 762-8.

49. Haruta, T., et al., *Insulin-stimulated GLUT4 translocation is mediated by a divergent intracellular signaling pathway.* J Biol Chem, 1995. **270**(47): p. 27991-4.

50. Gatenby, V.K., H. Imrie, and M. Kearney, *The IGF-1 receptor and regulation of nitric oxide bioavailability and insulin signalling in the endothelium.* Pflugers Arch, 2013. **465**(8): p. 1065-74.

51. Krook, A. and S. O'Rahilly, *Mutant insulin receptors in syndromes of insulin resistance.* Baillieres Clin Endocrinol Metab, 1996. **10**(1): p. 97-122.

52. Taylor, S.I., *Lilly Lecture: molecular mechanisms of insulin resistance. Lessons from patients with mutations in the insulin-receptor gene.* Diabetes, 1992. **41**(11): p. 1473-90.

53. White, M.F., et al., *Mutation of the insulin receptor at tyrosine 960 inhibits signal transmission but does not affect its tyrosine kinase activity.* Cell, 1988. **54**(5): p. 641-9.

54. Yoshimasa, Y., et al., *Insulin-resistant diabetes due to a point mutation that prevents insulin proreceptor processing.* Science, 1988. **240**(4853): p. 784-7.

55. Olefsky, J.M., O.G. Kolterman, and J.A. Scarlett, *Insulin action and resistance in obesity and noninsulin-dependent type II diabetes mellitus.* Am J Physiol, 1982. **243**(1): p. E15-30.

56. Freidenberg, G.R., et al., *Reversibility of defective adipocyte insulin receptor kinase activity in non-insulin-dependent diabetes mellitus. Effect of weight loss.* J Clin Invest, 1988. **82**(4): p. 1398-406.

57. Accili, D., et al., *Early neonatal death in mice homozygous for a null allele of the insulin receptor gene.* Nat Genet, 1996. **12**(1): p. 106-9.

58. Joshi, R.L., et al., *Targeted disruption of the insulin receptor gene in the mouse results in neonatal lethality.* EMBO J, 1996. **15**(7): p. 1542-7.

59. Kitamura, T., C.R. Kahn, and D. Accili, *Insulin receptor knockout mice.* Annu Rev Physiol, 2003. **65**: p. 313-32.

60. Wheatcroft, S.B., et al., *Preserved glucoregulation but attenuation of the vascular actions of insulin in mice heterozygous for knockout of the insulin receptor.* Diabetes, 2004. **53**(10): p. 2645-52.

61. Almind, K., et al., *A common amino acid polymorphism in insulin receptor substrate-1 causes impaired insulin signaling. Evidence from transfection studies.* J Clin Invest, 1996. **97**(11): p. 2569-75.

62. Goodyear, L.J., et al., *Insulin receptor phosphorylation, insulin receptor substrate-1 phosphorylation, and phosphatidylinositol 3-kinase activity are decreased in intact skeletal muscle strips from obese subjects.* J Clin Invest, 1995. **95**(5): p. 2195-204.

63. Tamemoto, H., et al., *Insulin resistance and growth retardation in mice lacking insulin receptor substrate-1.* Nature, 1994. **372**(6502): p. 182-6.

64. Withers, D.J., et al., *Disruption of IRS-2 causes type 2 diabetes in mice.* Nature, 1998. **391**(6670): p. 900-4.

65. Bruning, J.C., et al., *Development of a novel polygenic model of NIDDM in mice heterozygous for IR and IRS-1 null alleles.* Cell, 1997. **88**(4): p. 561-72.

66. Kido, Y., et al., *Tissue-specific insulin resistance in mice with mutations in the insulin receptor, IRS-1, and IRS-2.* J Clin Invest, 2000. **105**(2): p. 199-205.

67. Copps, K.D., et al., *Irs1 serine 307 promotes insulin sensitivity in mice.* Cell Metab, 2010. **11**(1): p. 84-92.

68. Hoehn, K.L., et al., *IRS1-independent defects define major nodes of insulin resistance.* Cell Metab, 2008. **7**(5): p. 421-33.

69. Cho, H., et al., *Insulin resistance and a diabetes mellitus-like syndrome in mice lacking the protein kinase Akt2 (PKB beta).* Science, 2001. **292**(5522): p. 1728-31.

70. George, S., et al., *A family with severe insulin resistance and diabetes due to a mutation in AKT2.* Science, 2004. **304**(5675): p. 1325-8.

71. Peraldi, P. and B. Spiegelman, *TNF-alpha and insulin resistance: summary and future prospects.* Mol Cell Biochem, 1998. **182**(1-2): p. 169-75.

72. Assmann, A., et al., *Glucose effects on beta-cell growth and survival require activation of insulin receptors and insulin receptor substrate 2.* Mol Cell Biol, 2009. **29**(11): p. 3219-28.

73. Michael, M.D., et al., *Loss of insulin signaling in hepatocytes leads to severe insulin resistance and progressive hepatic dysfunction.* Mol Cell, 2000. **6**(1): p. 87-97.

74. Biddinger, S.B., et al., *Hepatic insulin resistance is sufficient to produce dyslipidemia and susceptibility to atherosclerosis.* Cell Metab, 2008. **7**(2): p. 125-34.

75. Bluher, M., et al., *Adipose tissue selective insulin receptor knockout protects against obesity and obesity-related glucose intolerance.* Dev Cell, 2002. **3**(1): p. 25-38.

76. Bruning, J.C., et al., *A muscle-specific insulin receptor knockout exhibits features of the metabolic syndrome of NIDDM without altering glucose tolerance.* Mol Cell, 1998. **2**(5): p. 559-69.

77. Lauro, D., et al., *Impaired glucose tolerance in mice with a targeted impairment of insulin action in muscle and adipose tissue.* Nat Genet, 1998. **20**(3): p. 294-8.

78. Esper, R.J., et al., *Endothelial dysfunction: a comprehensive appraisal.* Cardiovasc Diabetol, 2006. **5**: p. 4.

79. Imrie, H., A. Abbas, and M. Kearney, *Insulin resistance, lipotoxicity and endothelial dysfunction.* Biochim Biophys Acta, 2010. **1801**(3): p. 320-6.

80. Fleming, I. and R. Busse, *Signal transduction of eNOS activation.* Cardiovasc Res, 1999. **43**(3): p. 532-41.

81. Furchgott, R.F. and J.V. Zawadzki, *The obligatory role of endothelial cells in the relaxation of arterial smooth muscle by acetylcholine.* Nature, 1980. **288**(5789): p. 373-6.

82. Palmer, R.M., A.G. Ferrige, and S. Moncada, *Nitric oxide release accounts for the biological activity of endothelium-derived relaxing factor.* Nature, 1987. **327**(6122): p. 524-6.

83. Hutchinson, P.J., R.M. Palmer, and S. Moncada, *Comparative pharmacology of EDRF and nitric oxide on vascular strips.* Eur J Pharmacol, 1987. **141**(3): p. 445-51.

84. Andrew, P.J. and B. Mayer, *Enzymatic function of nitric oxide synthases.* Cardiovasc Res, 1999. **43**(3): p. 521-31.

85. Yetik-Anacak, G. and J.D. Catravas, *Nitric oxide and the endothelium: history and impact on cardiovascular disease.* Vascul Pharmacol, 2006. **45**(5): p. 268-76.

86. Zeng, G., et al., *Roles for insulin receptor, PI3-kinase, and Akt in insulin-signaling pathways related to production of nitric oxide in human vascular endothelial cells.* Circulation, 2000. **101**(13): p. 1539-45.

87. Dimmeler, S., et al., *Activation of nitric oxide synthase in endothelial cells by Akt-dependent phosphorylation.* Nature, 1999. **399**(6736): p. 601-5.

88. Liao, J.K., et al., *Regulation of bovine endothelial constitutive nitric oxide synthase by oxygen.* J Clin Invest, 1995. **96**(6): p. 2661-6.

89. Nishida, K., et al., *Molecular cloning and characterization of the constitutive bovine aortic endothelial cell nitric oxide synthase.* J Clin Invest, 1992. **90**(5): p. 2092-6.

90. Shaul, P.W., et al., *Acylation targets emdothelial nitric-oxide synthase to plasmalemmal caveolae.* J Biol Chem, 1996. **271**(11): p. 6518-22.

91. Garcia-Cardena, G., et al., *Targeting of nitric oxide synthase to endothelial cell caveolae via palmitoylation: implications for nitric oxide signaling.* Proc Natl Acad Sci U S A, 1996. **93**(13): p. 6448-53.

92. Ohno, M., et al., *Shear stress elevates endothelial cGMP. Role of a potassium channel and G protein coupling.* Circulation, 1993. **88**(1): p. 193-7.

93. Ju, H., et al., *Direct interaction of endothelial nitric-oxide synthase and caveolin-1 inhibits synthase activity.* J Biol Chem, 1997. **272**(30): p. 18522-5.

94. Arnold, W.P., et al., *Nitric oxide activates guanylate cyclase and increases guanosine 3':5'-cyclic monophosphate levels in various tissue preparations.* Proc Natl Acad Sci U S A, 1977. **74**(8): p. 3203-7.

95. Rees, D.D., R.M. Palmer, and S. Moncada, *Role of endothelium-derived nitric oxide in the regulation of blood pressure.* Proc Natl Acad Sci U S A, 1989. **86**(9): p. 3375-8.

96. Vallance, P., J. Collier, and S. Moncada, *Effects of endothelium-derived nitric oxide on peripheral arteriolar tone in man.* Lancet, 1989. **2**(8670): p. 997-1000.

97. Awolesi, M.A., W.C. Sessa, and B.E. Sumpio, *Cyclic strain upregulates nitric oxide synthase in cultured bovine aortic endothelial cells.* J Clin Invest, 1995. **96**(3): p. 1449-54.

98. Radomski, M.W., R.M. Palmer, and S. Moncada, *Modulation of platelet aggregation by an L-arginine-nitric oxide pathway.* Trends Pharmacol Sci, 1991. **12**(3): p. 87-8.

99. Naseem, K.M., *The role of nitric oxide in cardiovascular diseases.* Mol Aspects Med, 2005. **26**(1-2): p. 33-65.

100. Freedman, J.E., et al., *Deficient platelet-derived nitric oxide and enhanced hemostasis in mice lacking the NOSIII gene.* Circ Res, 1999. **84**(12): p. 1416-21.

101. Kubes, P., M. Suzuki, and D.N. Granger, *Nitric oxide: an endogenous modulator of leukocyte adhesion.* Proc Natl Acad Sci U S A, 1991. **88**(11): p. 4651-5.

102. Ross, R., *Atherosclerosis--an inflammatory disease.* N Engl J Med, 1999. **340**(2): p. 115-26.

103. Gokce, N., et al., *Predictive value of noninvasively determined endothelial dysfunction for long-term cardiovascular events in patients with peripheral vascular disease.* J Am Coll Cardiol, 2003. **41**(10): p. 1769-75.

104. Schachinger, V., M.B. Britten, and A.M. Zeiher, *Prognostic impact of coronary vasodilator dysfunction on adverse long-term outcome of coronary heart disease.* Circulation, 2000. **101**(16): p. 1899-906.

105. Salt, I.P., et al., *High glucose inhibits insulin-stimulated nitric oxide production without reducing endothelial nitric-oxide synthase Ser1177 phosphorylation in human aortic endothelial cells.* J Biol Chem, 2003. **278**(21): p. 18791-7.

106. Jiang, Z.Y., et al., *Characterization of selective resistance to insulin signaling in the vasculature of obese Zucker (fa/fa) rats.* J Clin Invest, 1999. **104**(4): p. 447-57.

107. Cusi, K., et al., *Insulin resistance differentially affects the PI 3-kinase- and MAP kinase-mediated signaling in human muscle.* J Clin Invest, 2000. **105**(3): p. 311-20.

108. Cleland, S.J., et al., *Insulin action is associated with endothelial function in hypertension and type 2 diabetes.* Hypertension, 2000. **35**(1 Pt 2): p. 507-11.

109. Inoue, T., et al., *Insulin resistance affects endothelium-dependent acetylcholine-induced coronary artery response.* Eur Heart J, 2000. **21**(11): p. 895-900.

110. Piatti, P.M., et al., *Relationship between endothelin-1 concentration and metabolic alterations typical of the insulin resistance syndrome.* Metabolism, 2000. **49**(6): p. 748-52.

111. Verma, S., et al., *Endothelin antagonism uncovers insulin-mediated vasorelaxation in vitro and in vivo.* Hypertension, 2001. **37**(2): p. 328-33.

112. Jiang, Z.Y., et al., *Endothelin-1 modulates insulin signaling through phosphatidylinositol 3-kinase pathway in vascular smooth muscle cells.* Diabetes, 1999. **48**(5): p. 1120-30.

113. Vicent, D., et al., *The role of endothelial insulin signaling in the regulation of vascular tone and insulin resistance.* J Clin Invest, 2003. **111**(9): p. 1373-80.

114.   Duncan, E.R., et al., *Effect of endothelium-specific insulin resistance on endothelial function in vivo.* Diabetes, 2008. **57**(12): p. 3307-14.

115.   Duncan, E.R., et al., *Accelerated endothelial dysfunction in mild prediabetic insulin resistance: the early role of reactive oxygen species.* Am J Physiol Endocrinol Metab, 2007. **293**(5): p. E1311-9.

116.   Kim, Y.W. and T.V. Byzova, *Oxidative stress in angiogenesis and vascular disease.* Blood, 2014. **123**(5): p. 625-31.

117.   Cai, H. and D.G. Harrison, *Endothelial dysfunction in cardiovascular diseases: the role of oxidant stress.* Circ Res, 2000. **87**(10): p. 840-4.

118.   Griendling, K.K., D. Sorescu, and M. Ushio-Fukai, *NAD(P)H oxidase: role in cardiovascular biology and disease.* Circ Res, 2000. **86**(5): p. 494-501.

119.   White, C.R., et al., *Superoxide and peroxynitrite in atherosclerosis.* Proc Natl Acad Sci U S A, 1994. **91**(3): p. 1044-8.

120.   Alp, N.J. and K.M. Channon, *Regulation of endothelial nitric oxide synthase by tetrahydrobiopterin in vascular disease.* Arterioscler Thromb Vasc Biol, 2004. **24**(3): p. 413-20.

121.   Zorov, D.B., et al., *Reactive oxygen species (ROS)-induced ROS release: a new phenomenon accompanying induction of the mitochondrial permeability transition in cardiac myocytes.* J Exp Med, 2000. **192**(7): p. 1001-14.

122.   Gage, M.C., et al., *Endothelium-specific insulin resistance leads to accelerated atherosclerosis in areas with disturbed flow patterns: a role for reactive oxygen species.* Atherosclerosis, 2013. **230**(1): p. 131-9.

123.   Sukumar, P., et al., *Nox2 NADPH oxidase has a critical role in insulin resistance-related endothelial cell dysfunction.* Diabetes, 2013. **62**(6): p. 2130-4.

124.   Du, J., et al., *Crucial roles of Nox2-derived oxidative stress in deteriorating the function of insulin receptors and endothelium in*

dietary obesity of middle-aged mice. Br J Pharmacol, 2013. **170**(5): p. 1064-77.

125. Mugge, A., et al., *Chronic treatment with polyethylene-glycolated superoxide dismutase partially restores endothelium-dependent vascular relaxations in cholesterol-fed rabbits.* Circ Res, 1991. **69**(5): p. 1293-300.

126. Guzik, T.J., et al., *Mechanisms of increased vascular superoxide production in human diabetes mellitus: role of NAD(P)H oxidase and endothelial nitric oxide synthase.* Circulation, 2002. **105**(14): p. 1656-62.

127. Fortuno, A., et al., *Phagocytic NADPH oxidase overactivity underlies oxidative stress in metabolic syndrome.* Diabetes, 2006. **55**(1): p. 209-15.

128. Aikawa, M. and P. Libby, *The vulnerable atherosclerotic plaque: pathogenesis and therapeutic approach.* Cardiovasc Pathol, 2004. **13**(3): p. 125-38.

129. Stary, H.C., et al., *A definition of initial, fatty streak, and intermediate lesions of atherosclerosis. A report from the Committee on Vascular Lesions of the Council on Arteriosclerosis, American Heart Association.* Circulation, 1994. **89**(5): p. 2462-78.

130. Pena-Duque, M.A., et al., *Coronary Atherosclerosis and Interventional Cardiology.* Arch Med Res, 2015. **46**(5): p. 372-8.

131. Mondy, J.S., et al., *Platelet-derived growth factor ligand and receptor expression in response to altered blood flow in vivo.* Circ Res, 1997. **81**(3): p. 320-7.

132. Jonasson, L., et al., *Regional accumulations of T cells, macrophages, and smooth muscle cells in the human atherosclerotic plaque.* Arteriosclerosis, 1986. **6**(2): p. 131-8.

133. Barquera, S., et al., *Global Overview of the Epidemiology of Atherosclerotic Cardiovascular Disease.* Arch Med Res, 2015. **46**(5): p. 328-38.

134. Stopeck, A.T., et al., *Cytokine regulation of low density lipoprotein receptor gene transcription in HepG2 cells.* J Biol Chem, 1993. **268**(23): p. 17489-94.

135. Chang, M.Y., et al., *Inhibition of hypercholesterolemia-induced atherosclerosis in the nonhuman primate by probucol. II. Cellular composition and proliferation.* Arterioscler Thromb Vasc Biol, 1995. **15**(10): p. 1631-40.

136. Heart Protection Study Collaborative, G., *MRC/BHF Heart Protection Study of antioxidant vitamin supplementation in 20,536 high-risk individuals: a randomised placebo-controlled trial.* Lancet, 2002. **360**(9326): p. 23-33.

137. Gibbons, G.H., R.E. Pratt, and V.J. Dzau, *Vascular smooth muscle cell hypertrophy vs. hyperplasia. Autocrine transforming growth factor-beta 1 expression determines growth response to angiotensin II.* J Clin Invest, 1992. **90**(2): p. 456-61.

138. Cubbon, R.M., et al., *Importance of insulin resistance to vascular repair and regeneration.* Free Radic Biol Med, 2013. **60**: p. 246-63.

139. Carmeliet, P., *Angiogenesis in life, disease and medicine.* Nature, 2005. **438**(7070): p. 932-6.

140. Swift, M.R. and B.M. Weinstein, *Arterial-venous specification during development.* Circ Res, 2009. **104**(5): p. 576-88.

141. Asahara, T., et al., *Isolation of putative progenitor endothelial cells for angiogenesis.* Science, 1997. **275**(5302): p. 964-7.

142. Vasa, M., et al., *Increase in circulating endothelial progenitor cells by statin therapy in patients with stable coronary artery disease.* Circulation, 2001. **103**(24): p. 2885-90.

143. Rivard, A., et al., *Rescue of diabetes-related impairment of angiogenesis by intramuscular gene therapy with adeno-VEGF.* Am J Pathol, 1999. **154**(2): p. 355-63.

144. Altabas, V., *Diabetes, Endothelial Dysfunction, and Vascular Repair: What Should a Diabetologist Keep His Eye on?* International Journal of Endocrinology, 2015. **2015**: p. 14.

145. Piconi, L., et al., *Constant and intermittent high glucose enhances endothelial cell apoptosis through mitochondrial superoxide overproduction.* Diabetes Metab Res Rev, 2006. **22**(3): p. 198-203.

146. Fuster, V., M. Poon, and J.T. Willerson, *Learning from the transgenic mouse: endothelium, adhesive molecules, and neointimal formation.* Circulation, 1998. **97**(1): p. 16-8.

147. Carmeliet, P., et al., *Vascular wound healing and neointima formation induced by perivascular electric injury in mice.* Am J Pathol, 1997. **150**(2): p. 761-76.

148. Kumar, A. and V. Lindner, *Remodeling with neointima formation in the mouse carotid artery after cessation of blood flow.* Arterioscler Thromb Vasc Biol, 1997. **17**(10): p. 2238-44.

149. Roque, M., et al., *Mouse model of femoral artery denudation injury associated with the rapid accumulation of adhesion molecules on the luminal surface and recruitment of neutrophils.* Arterioscler Thromb Vasc Biol, 2000. **20**(2): p. 335-42.

150. Foster, E., S. Zhang, and A.M. Kahn, *Insulin stimulates arterial neointima formation in normal rats after balloon injury.* Diabetes Obes Metab, 2006. **8**(3): p. 348-51.

151. Park, S.H., et al., *Neointimal hyperplasia after arterial injury is increased in a rat model of non-insulin-dependent diabetes mellitus.* Circulation, 2001. **104**(7): p. 815-9.

152. Hutter, R., et al., *Decreased reendothelialization and increased neointima formation with endostatin overexpression in a mouse model of arterial injury.* Circulation, 2003. **107**(12): p. 1658-63.

153. Hutter, R., et al., *Vascular endothelial growth factor regulates reendothelialization and neointima formation in a mouse model of arterial injury.* Circulation, 2004. **110**(16): p. 2430-5.

154. Foteinos, G., et al., *Rapid endothelial turnover in atherosclerosis-prone areas coincides with stem cell repair in apolipoprotein E-deficient mice.* Circulation, 2008. **117**(14): p. 1856-63.

155. Torsney, E. and Q. Xu, *Resident vascular progenitor cells.* J Mol Cell Cardiol, 2011. **50**(2): p. 304-11.

156. Hagensen, M.K., et al., *Circulating endothelial progenitor cells do not contribute to regeneration of endothelium after murine arterial injury.* Cardiovasc Res, 2012. **93**(2): p. 223-31.

157. Cubbon R, A.A., Mercer B, Yuldasheva N, Skromna A, Makava N, Sengupta A, Ali N, Walker A, Gatenby V, Wheatcroft S, Kearney M, Galloway S, *Vacular regeneration is impaired in the setting of systemic insulin resistance.* Heart, 2014. **100 (suppl 3)**: p. A92.

158. Kornowski, R., et al., *Increased restenosis in diabetes mellitus after coronary interventions is due to exaggerated intimal hyperplasia. A serial intravascular ultrasound study.* Circulation, 1997. **95**(6): p. 1366-9.

159. Indolfi, C., et al., *Effects of balloon injury on neointimal hyperplasia in streptozotocin-induced diabetes and in hyperinsulinemic nondiabetic pancreatic islet-transplanted rats.* Circulation, 2001. **103**(24): p. 2980-6.

160. Breen, D.M., et al., *Insulin inhibits and oral sucrose increases neointimal growth after arterial injury in rats.* J Vasc Res, 2010. **47**(5): p. 412-22.

161. Breen, D.M., et al., *Insulin increases reendothelialization and inhibits cell migration and neointimal growth after arterial injury.* Arterioscler Thromb Vasc Biol, 2009. **29**(7): p. 1060-6.

162. Guo, J., et al., *The effect of insulin to decrease neointimal growth after arterial injury is endothelial nitric oxide synthase-dependent.* Atherosclerosis, 2015. **241**(1): p. 111-20.

163. Ii, M., et al., *Endothelial progenitor thrombospondin-1 mediates diabetes-induced delay in reendothelialization following arterial injury.* Circ Res, 2006. **98**(5): p. 697-704.

164.   Kahn, M.B., et al., *Insulin resistance impairs circulating angiogenic progenitor cell function and delays endothelial regeneration.* Diabetes, 2011. **60**(4): p. 1295-303.

165.   Cubbon, R.M., et al., *Human exercise-induced circulating progenitor cell mobilization is nitric oxide-dependent and is blunted in South Asian men.* Arterioscler Thromb Vasc Biol, 2010. **30**(4): p. 878-84.

166.   Werner, N., et al., *Circulating endothelial progenitor cells and cardiovascular outcomes.* N Engl J Med, 2005. **353**(10): p. 999-1007.

167.   Hirschi, K.K., D.A. Ingram, and M.C. Yoder, *Assessing identity, phenotype, and fate of endothelial progenitor cells.* Arterioscler Thromb Vasc Biol, 2008. **28**(9): p. 1584-95.

168.   Hill, J.M., et al., *Circulating endothelial progenitor cells, vascular function, and cardiovascular risk.* N Engl J Med, 2003. **348**(7): p. 593-600.

169.   Ingram, D.A., et al., *In vitro hyperglycemia or a diabetic intrauterine environment reduces neonatal endothelial colony-forming cell numbers and function.* Diabetes, 2008. **57**(3): p. 724-31.

170.   Seeger, F.H., et al., *p38 mitogen-activated protein kinase downregulates endothelial progenitor cells.* Circulation, 2005. **111**(9): p. 1184-91.

171.   Chen, Y.H., et al., *High glucose impairs early and late endothelial progenitor cells by modifying nitric oxide-related but not oxidative stress-mediated mechanisms.* Diabetes, 2007. **56**(6): p. 1559-68.

172.   Sibal, L., et al., *Circulating endothelial progenitor cells, endothelial function, carotid intima-media thickness and circulating markers of endothelial dysfunction in people with type 1 diabetes without macrovascular disease or microalbuminuria.* Diabetologia, 2009. **52**(8): p. 1464-73.

173.   Cubbon, R.M., et al., *Restoring Akt1 activity in outgrowth endothelial cells from South Asian men rescues vascular reparative potential.* Stem Cells, 2014. **32**(10): p. 2714-23.

174. Desouza, C.V., et al., *Role of inflammation and insulin resistance in endothelial progenitor cell dysfunction.* Diabetes, 2011. **60**(4): p. 1286-94.

175. Fujii, H., et al., *C-reactive protein alters antioxidant defenses and promotes apoptosis in endothelial progenitor cells.* Arterioscler Thromb Vasc Biol, 2006. **26**(11): p. 2476-82.

176. Verma, S., et al., *C-reactive protein attenuates endothelial progenitor cell survival, differentiation, and function: further evidence of a mechanistic link between C-reactive protein and cardiovascular disease.* Circulation, 2004. **109**(17): p. 2058-67.

177. Sun, Y., et al., *Effect of visfatin on the function of endothelial progenitor cells in high-fat-fed obese rats and investigation of its mechanism of action.* Int J Mol Med, 2012. **30**(3): p. 622-8.

178. Endtmann, C., et al., *Angiotensin II impairs endothelial progenitor cell number and function in vitro and in vivo: implications for vascular regeneration.* Hypertension, 2011. **58**(3): p. 394-403.

179. Anghelina, M., L. Moldovan, and N.I. Moldovan, *Preferential activity of Tie2 promoter in arteriolar endothelium.* J Cell Mol Med, 2005. **9**(1): p. 113-21.

180. Viswambharan, H., et al., *D Increasing Insulin Sensitivity in the Endothelium Leads to Reduced Nitric Oxide Bioavailability.* Heart, 2015. **101**(Suppl 4): p. A126-A127.

181. Jin, E., et al., *Differential roles for ETS, CREB, and EGR binding sites in mediating VEGF receptor 1 expression in vivo.* Blood, 2009. **114**(27): p. 5557-66.

182. Sobczak, M., J. Dargatz, and M. Chrzanowska-Wodnicka, *Isolation and culture of pulmonary endothelial cells from neonatal mice.* J Vis Exp, 2010(46).

183. Dumont, D.J., et al., *tek, a novel tyrosine kinase gene located on mouse chromosome 4, is expressed in endothelial cells and their presumptive precursors.* Oncogene, 1992. **7**(8): p. 1471-80.

184.   Kisanuki, Y.Y., et al., *Tie2-Cre transgenic mice: a new model for endothelial cell-lineage analysis in vivo.* Dev Biol, 2001. **230**(2): p. 230-42.

185.   Ohtsuki, S., et al., *Vascular endothelium-selective gene induction by Tie2 promoter/enhancer in the brain and retina of a transgenic rat.* Pharm Res, 2005. **22**(6): p. 852-7.

186.   Imrie, H., et al., *Novel role of the IGF-1 receptor in endothelial function and repair: studies in endothelium-targeted IGF-1 receptor transgenic mice.* Diabetes, 2012. **61**(9): p. 2359-68.

187.   Minami, T., et al., *Ets motifs are necessary for endothelial cell-specific expression of a 723-bp Tie-2 promoter/enhancer in Hprt targeted transgenic mice.* Arterioscler Thromb Vasc Biol, 2003. **23**(11): p. 2041-7.

188.   Kito, T., et al., *Nifedipine ameliorates ischemia-induced revascularization in diet-induced obese mice.* Am J Hypertens, 2012. **25**(4): p. 401-6.

189.   Rask-Madsen, C., et al., *Loss of insulin signaling in vascular endothelial cells accelerates atherosclerosis in apolipoprotein E null mice.* Cell Metab, 2010. **11**(5): p. 379-89.

190.   Aicher, A., et al., *Essential role of endothelial nitric oxide synthase for mobilization of stem and progenitor cells.* Nat Med, 2003. **9**(11): p. 1370-6.

191.   Sorrentino, S.A., et al., *Oxidant stress impairs in vivo reendothelialization capacity of endothelial progenitor cells from patients with type 2 diabetes mellitus: restoration by the peroxisome proliferator-activated receptor-gamma agonist rosiglitazone.* Circulation, 2007. **116**(2): p. 163-73.

192.   Hoeben, A., et al., *Vascular endothelial growth factor and angiogenesis.* Pharmacol Rev, 2004. **56**(4): p. 549-80.

193.   Hermann, C., et al., *Insulin-mediated stimulation of protein kinase Akt: A potent survival signaling cascade for endothelial cells.* Arterioscler Thromb Vasc Biol, 2000. **20**(2): p. 402-9.

194. Cubbon, R., et al., *159 Vascular Regeneration is Impaired in the Setting of Systemic Insulin Resistance.* Heart, 2014. **100**(Suppl 3): p. A92.

195. Shah, D., et al., *Obesity-induced adipokine imbalance impairs mouse pulmonary vascular endothelial function and primes the lung for injury.* Sci Rep, 2015. **5**: p. 11362.

196. Aird, W.C., *Phenotypic heterogeneity of the endothelium: II. Representative vascular beds.* Circ Res, 2007. **100**(2): p. 174-90.

197. Saez, P.J., et al., *Modulation of endothelial cell migration by ER stress and insulin resistance: a role during maternal obesity?* Front Pharmacol, 2014. **5**: p. 189.

198. Lamalice, L., F. Le Boeuf, and J. Huot, *Endothelial cell migration during angiogenesis.* Circ Res, 2007. **100**(6): p. 782-94.

199. Liu, Y., M. Petreaca, and M. Martins-Green, *Cell and molecular mechanisms of insulin-induced angiogenesis.* J Cell Mol Med, 2009. **13**(11-12): p. 4492-504.

200. Lee, M.Y., et al., *Endothelial Akt1 mediates angiogenesis by phosphorylating multiple angiogenic substrates.* Proc Natl Acad Sci U S A, 2014. **111**(35): p. 12865-70.

201. Murohara, T., et al., *Role of endothelial nitric oxide synthase in endothelial cell migration.* Arterioscler Thromb Vasc Biol, 1999. **19**(5): p. 1156-61.

202. Reihill, J.A., M.A. Ewart, and I.P. Salt, *The role of AMP-activated protein kinase in the functional effects of vascular endothelial growth factor-A and -B in human aortic endothelial cells.* Vasc Cell, 2011. **3**: p. 9.

203. Shesely, E.G., et al., *Elevated blood pressures in mice lacking endothelial nitric oxide synthase.* Proc Natl Acad Sci U S A, 1996. **93**(23): p. 13176-81.

204. Baron, A.D., et al., *Insulin resistance after hypertension induced by the nitric oxide synthesis inhibitor L-NMMA in rats.* Am J Physiol, 1995. **269**(4 Pt 1): p. E709-15.

205. Vecoli, C., et al., *Partial deletion of eNOS gene causes hyperinsulinemic state, unbalance of cardiac insulin signaling pathways and coronary dysfunction independently of high fat diet.* PLoS One, 2014. **9**(8): p. e104156.

206. Sansbury, B.E. and B.G. Hill, *Regulation of obesity and insulin resistance by nitric oxide.* Free Radic Biol Med, 2014. **73**: p. 383-99.

207. Natarajan, K. and B.C. Berk, *Crosstalk coregulation mechanisms of G protein-coupled receptors and receptor tyrosine kinases.* Methods Mol Biol, 2006. **332**: p. 51-77.

208. Muzykantov, V.R., *Targeted therapeutics and nanodevices for vascular drug delivery: quo vadis?* IUBMB Life, 2011. **63**(8): p. 583-5.

209. Muro, S., et al., *A novel endocytic pathway induced by clustering endothelial ICAM-1 or PECAM-1.* J Cell Sci, 2003. **116**(Pt 8): p. 1599-609.

210. Oh, P., et al., *Live dynamic imaging of caveolae pumping targeted antibody rapidly and specifically across endothelium in the lung.* Nat Biotechnol, 2007. **25**(3): p. 327-37.